QUANTITATIVE BEHAVIOR OF NON-INTEGRABLE SYSTEMS (IV)

J. BECK, W.W.L. CHEN, AND Y. YANG

ABSTRACT. In this paper, there are two sections. In Section 7, we simplify the eigenvalue-based surplus shortline method for arbitrary finite polysquare surfaces. This makes it substantially simpler to determine the irregularity exponents of some infinite orbits, and quicker to find the escape rate to infinity of some orbits in some infinite models. In Section 8, our primary goal is to extend the surplus shortline method, both this eigenvalue-based version as well as the eigenvalue-free version, for application to a large class of 2-dimensional flat dynamical systems beyond polysquares, including all Veech surfaces, and establish time-quantitative equidistribution and time-quantitative superdensity of some infinite orbits in these new systems.

7. More on the eigenvalue-based shortline method

7.1. **The shortline method and the Edge-cutting Lemma.** Here in part (IV) we assume that the reader is more or less familiar with the earlier parts [2, 3, 4]. The eigenvalue-based surplus shortline method has been developed in the special case of the L-surface in Sections 3–4 in [2, 3].

For a 4-direction billiard flow in a general finite polysquare surface, we can apply *unfolding* introduced in [2] to convert the problem to one concerning a 1-direction geodesic flow in some other finite polysquare surface. We therefore concentrate our attention here on 1-direction geodesic flows in a finite polysquare surface.

We shall show that the surplus shortcut-ancestor process, introduced earlier in [2, 3] in connection with the L-surface, can be adapted to *every* finite polysquare surface with 1-direction geodesic flow. For a quick introduction, we first illustrate the method by applying it to a 1-direction geodesic flow with a particular quadratic irrational slope on the surface S_2 given in the picture on the left in Figure 7.1.1.

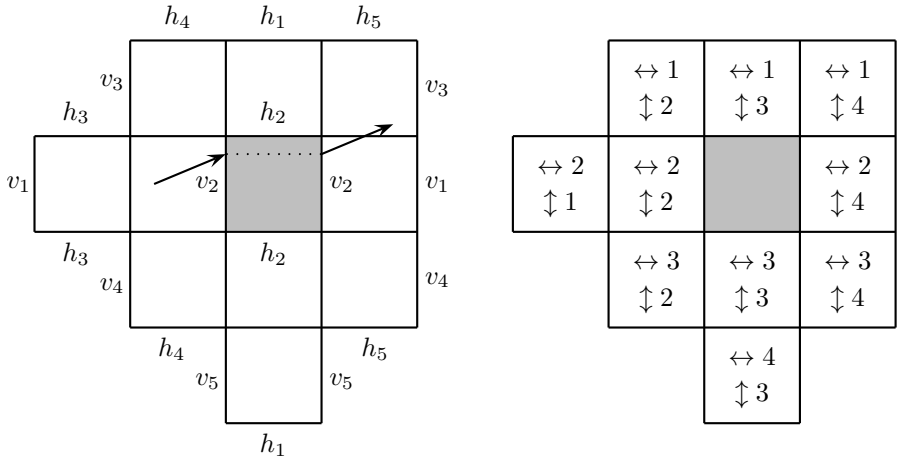

Figure 7.1.1: the surface S_2 with a gap

We shall compute the 2-step transition matrix, and also determine the irregularity exponent for this particular quadratic irrational slope. We shall illustrate the fact

2010 *Mathematics Subject Classification.* 11K38, 37E35.

Key words and phrases. geodesics, billiards, time-quantitative equidistribution, superdensity.

that this 2-step transition matrix is usually "very redundant". This will motivate the so-called Edge-cutting Lemma which we shall formulate later.

We shall consider 1-direction geodesic flow on S_2. Here the boundary pairings come from simple perpendicular translations. The pair of vertical edges v_2 and the pair of horizontal edges h_2 around the missing square represent a slightly less straightforward form of perpendicular translation.

The surface S_2 has 1 vertical street of length 1, 3 vertical streets of length 3, 1 horizontal street of length 1, and 3 horizontal streets of length 3, so the street-LCM is equal to 3. The picture on the right in Figure 7.1.1 shows the streets where, for instance, the entries $\leftrightarrow 2$ and $\updownarrow 4$ in a square indicates that the square face is on the 2-nd horizontal and 4-th vertical street.

To apply the surplus shortline method, we have to restrict our study to slopes α or α^{-1} for which the continued fraction expression of α has the special form

$$\alpha = [3c_0; 3c_1, 3c_2, 3c_3, \ldots] = 3c_0 + \frac{1}{3c_1 + \frac{1}{3c_2 + \frac{1}{3c_3 + \cdots}}}, \tag{7.1.1}$$

where the digits $c_i \geqslant 1$, $i \geqslant 0$, are integers.

For illustration we consider here the simplest slope satisfying (7.1.1), namely

$$\alpha = [3; 3, 3, 3, \ldots] = 3 + \frac{1}{3 + \frac{1}{3 + \frac{1}{3 + \cdots}}} = \frac{3 + \sqrt{13}}{2}, \tag{7.1.2}$$

and its reciprocal α^{-1}. We study the long-term behavior of two particular geodesics $V(t)$ and $H(t)$ on S_2 that start from the origin, which is some chosen vertex of one of the square faces of S_2. Crucially, this guarantees that $V(t)$ and $H(t)$ are *surplus shortlines* of each other. The almost vertical geodesic $V(t)$ has slope α, while the almost horizontal geodesic $H(t)$ has slope α^{-1}. Following Section 3 in [2], we briefly elaborate on the details of the surplus shortline method in this particular case.

We distinguish the 20 types of almost vertical units a_i, $1 \leqslant i \leqslant 20$, in the picture on the left in Figure 7.1.2.

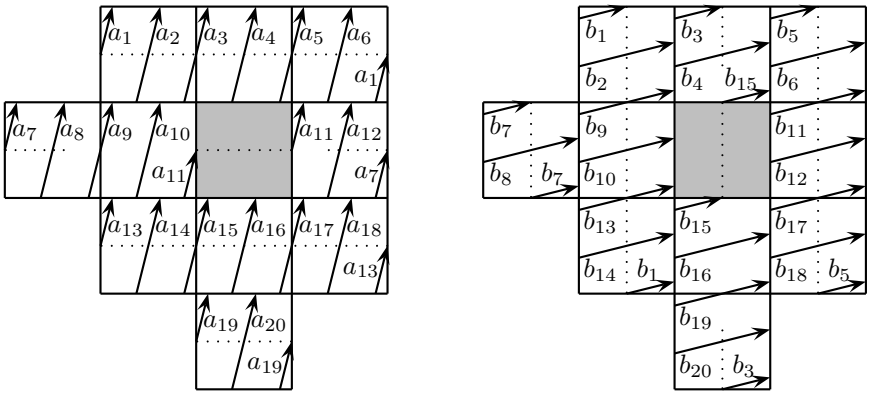

Figure 7.1.2: the 20 types of almost vertical units and the 20 types of almost horizontal units in the surface S_2

We say that each of the almost vertical units

$$a_2, a_4, a_6, a_8, a_{10}, a_{12}, a_{14}, a_{16}, a_{18}, a_{20}$$

is of type $\uparrow$, and starts at the bottom edge of a square face and ends at the top edge of the same square face, while each of the almost vertical units

$$a_1, a_3, a_5, a_7, a_9, a_{11}, a_{13}, a_{15}, a_{17}, a_{19}$$

is of type $\updownarrow$, and starts at the bottom edge of a square face and ends at the top edge of an adjoining square face. Of particular interest is the unit a_{11} which hits the left

edge of the gap at some point and continues from the corresponding point on the identified right edge of the gap.

Similarly, we distinguish the 20 types of almost horizontal units b_j, $1 \leqslant j \leqslant 20$, in the picture on the right in Figure 7.1.2.

Note that the surface S_2 exhibits a 45-degree reflection symmetry. But symmetry is not necessary, and indeed totally irrelevant, for the success of the shortline method. To emphasize this point, we have deliberately used labelling in the picture on the right in Figure 7.1.2 which is not a 45-degree reflection of the labelling in the picture on the left in Figure 7.1.2.

Applying a straightforward adaptation of the surplus shortline method in Section 3 in [2], we can determine the surplus ancestor units of a_i, $1 \leqslant i \leqslant 20$. Similarly, we can determine the surplus ancestor units of b_j, $1 \leqslant j \leqslant 20$.

Consider first the almost vertical unit a_1. It is not difficult to see from Figure 7.1.3, which shows only the top horizontal street of S_2, that a_1 is the shortcut of an almost horizontal detour crossing of the this horizontal street, made up of a fractional almost horizontal unit b_{11}, full almost horizontal units b_2, b_4 and b_6, and then a fractional almost horizontal unit b_1. We apply the Delete-End Rule, meaning that we keep the initial fractional almost horizontal unit b_{11} as a full unit and discard the final fractional almost horizontal unit b_1, and call b_{11}, b_2, b_4, b_6 the ancestor units of a_1.

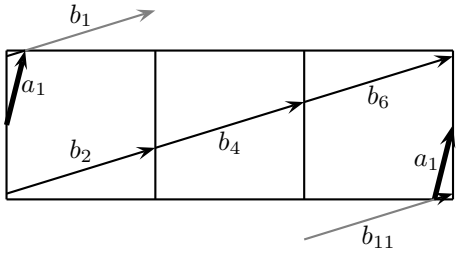

Figure 7.1.3: almost horizontal detour crossing for which a_1 is the shortcut

We do likewise for a_i, $2 \leqslant i \leqslant 20$, and can summarize in the form

$$\begin{aligned}
a_1 &\rightharpoonup b_{11}, b_2, b_4, b_6,\\
a_2 &\rightharpoonup b_9, b_4, b_6,\\
a_3 &\rightharpoonup b_9, b_4, b_6, b_2,\\
&\vdots\\
a_{19} &\rightharpoonup b_3, b_{20}, b_{20}, b_{20},\\
a_{20} &\rightharpoonup b_3, b_{20}, b_{20}.
\end{aligned} \tag{7.1.3}$$

This leads to a transition matrix $M_1(S_2)$, where the i-th row captures the information in the i-th ancestor relation in (7.1.3), with the entry on the j-th column displaying the multiplicity of b_j.

A similar exercise with the roles of the horizontal and vertical interchanged, again using the Delete-End Rule, results in

$$\begin{aligned}
b_1 &\rightharpoonup a_1, a_{14}, a_{10}, a_2,\\
b_2 &\rightharpoonup a_1, a_{14}, a_{10},\\
b_3 &\rightharpoonup a_3, a_{20}, a_{16}, a_4,\\
&\vdots\\
b_{19} &\rightharpoonup a_{19}, a_{16}, a_4, a_{20},\\
b_{20} &\rightharpoonup a_{19}, a_{16}, a_4.
\end{aligned} \tag{7.1.4}$$

This leads to an analogous transition matrix $M_2(S_2)$.

Remark. Instead of using the Delete-End Rule, we may also use the Keep-End Rule, meaning that we keep the final fractional unit as a full unit and discard the initial fractional unit. Both rules are for bookkeeping purposes only, as we do not want to count any unit twice. Depending on which rule we use, (7.1.3) and (7.1.4), and hence also the matrices $M_1(S_1)$ and $M_2(S_2)$, may be a little different, but this will not affect the subsequent argument.

Composition of the two transition matrices arising from (7.1.3)–(7.1.4) leads to the product matrix $M_1(S_2)M_2(S_2)$. The *transpose* of this product matrix happens to be the 20-by-20 matrix

$$M(S_2) = \begin{pmatrix}
1&0&1&1&1&1&0&0&0&0&0&0&0&1&1&0&0&0&0&0\\
0&1&1&0&0&0&1&1&1&1&2&1&1&1&1&1&1&1&0&0\\
1&1&1&0&1&1&0&0&0&0&0&0&0&0&0&0&0&0&1&1\\
0&0&0&1&1&0&0&0&0&0&0&0&0&1&1&1&1&2&1&4&3\\
1&1&1&1&1&0&0&0&0&0&0&0&0&1&0&0&0&0&1&0&0\\
1&0&0&0&0&1&2&1&1&1&1&1&2&1&1&1&1&1&0&0\\
0&0&0&0&0&0&1&1&2&1&1&1&0&0&0&0&0&0&0&0&0\\
0&0&0&0&0&0&2&3&5&2&2&2&0&0&0&0&0&0&0&0&0\\
0&1&1&0&0&0&1&1&1&0&1&1&0&0&0&0&0&0&0&0&0\\
1&1&2&1&1&1&0&0&0&1&1&0&1&1&2&1&1&1&0&0\\
1&0&0&0&0&1&1&1&1&1&1&0&0&0&0&0&0&0&0&0&0\\
2&1&1&1&1&1&1&0&0&0&0&1&2&1&1&1&1&1&0&0\\
0&0&0&0&0&0&0&0&0&1&1&0&1&0&1&1&1&1&0&0\\
1&1&2&1&1&1&1&1&1&1&2&1&0&1&1&0&0&0&0&0\\
0&0&0&1&1&0&0&0&0&0&0&0&1&1&1&0&1&1&0&0\\
1&1&1&1&2&1&0&0&0&0&0&0&0&0&0&0&1&1&0&4&3\\
0&0&0&0&0&0&1&0&0&0&0&1&1&1&1&1&1&1&0&0&0\\
2&1&1&1&1&1&2&1&1&1&1&1&1&0&0&0&0&1&0&0\\
0&0&0&0&0&0&0&0&0&0&0&0&0&0&0&0&1&1&0&3&2\\
1&1&1&1&2&1&0&0&0&0&0&0&1&1&1&1&2&1&1&1
\end{pmatrix}. \tag{7.1.5}$$

We use the transpose, because in the Edge-cutting Lemma, to be formulated later, we are interested in eigenvectors as column vectors of $M(S_2)$. And it helps that MATLAB, like any other linear algebra computer program, automatically computes right or column eigenvectors.

We start with the 3 eigenvalues of (7.1.5) with the largest absolute values. By MATLAB, the largest eigenvalue is

$$\lambda_1 = \lambda_1(M(S_2)) = \frac{11+3\sqrt{13}}{2} = \left(\frac{3+\sqrt{13}}{2}\right)^2 = \alpha^2, \tag{7.1.6}$$

in view of (7.1.2), with corresponding eigenvector

$$\begin{aligned}\mathbf{v}_1 = \mathbf{v}_1(M(S_2)) &= (v_1(1), v_1(2), v_1(3), \ldots, v_1(20))^T\\ &= (c,1,c,1,c,1,c,1,c,1,c,1,c,1,c,1,c,1,c,1)^T,\end{aligned} \tag{7.1.7}$$

where

$$c = \frac{\sqrt{13}-1}{6}.$$

The second largest eigenvalue is

$$\lambda_2 = \lambda_2(M(S_2)) = 3+2\sqrt{2} = (1+\sqrt{2})^2, \tag{7.1.8}$$

with corresponding eigenvector

$$\begin{aligned}\mathbf{v}_2 &= \mathbf{v}_2(M(S_2)) = (v_2(1), v_2(2), v_2(3), \ldots, v_2(20))^T \\ &= (c_1, c_2, c_1, c_3, c_1, c_2, c_4, c_5, c_4, c_6, c_4, c_6, c_1, c_2, c_1, c_3, c_1, c_2, c_7, 1)^T, \end{aligned} \tag{7.1.9}$$

where

$$\begin{aligned} c_1 &= \frac{2\sqrt{2}+1}{14}, \quad c_2 = -\frac{5\sqrt{2}+6}{14}, \quad c_3 = \frac{10\sqrt{2}+19}{14}, \quad c_4 = -\frac{4\sqrt{2}+2}{7}, \\ c_5 &= -\frac{5\sqrt{2}+13}{7}, \quad c_6 = \frac{5\sqrt{2}-1}{14}, \quad c_7 = \frac{6\sqrt{2}+3}{7}. \end{aligned}$$

The third largest eigenvalue is

$$\lambda_3 = \lambda_3(M(S_2)) = \frac{3+\sqrt{5}}{2}, \tag{7.1.10}$$

with corresponding eigenvector

$$\begin{aligned}\mathbf{v}_3 &= \mathbf{v}_3(M(S_2)) = (v_3(1), v_3(2), v_3(3), \ldots, v_3(20))^T \\ &= (c_1^*, c_2^*, c_1^*, c_3^*, c_1^*, c_2^*, c_4^*, c_5^*, c_4^*, c_6^*, c_4^*, c_6^*, c_1^*, c_2^*, c_1^*, c_3^*, c_1^*, c_2^*, c_7^*, 1)^T, \end{aligned} \tag{7.1.11}$$

where

$$\begin{aligned} c_1^* &= \frac{\sqrt{5}+5}{10}, \quad c_2^* = \frac{\sqrt{5}}{5}, \quad c_3^* = -\frac{2\sqrt{5}+5}{5}, \quad c_4^* = -c_1^*, \\ c_5^* &= -\frac{4\sqrt{5}+5}{5}, \quad c_6^* = -c_3^*, \quad c_7^* = -\frac{3\sqrt{5}+15}{10}. \end{aligned}$$

There are 3 other eigenvalues which are the algebraic conjugates of λ_i, $1 \leqslant i \leqslant 3$, and these are between 0 and 1. There are 14 other eigenvalues with absolute value 1. We shall see that λ_i, $1 \leqslant i \leqslant 3$, are the only relevant eigenvalues of $M(S_2)$, and the other 17 eigenvalues are irrelevant. We comment that the Jordan normal form of the matrix $M(S_2)$ is simple, as the matrix has 20 different eigenvectors.

The irregularity exponent of this special slope α given by (7.1.2) is, by definition, equal to

$$\kappa_0(\alpha) = \frac{\log|\lambda_2|}{\log|\lambda_1|} = \frac{\log(1+\sqrt{2})}{\log\frac{3+\sqrt{13}}{2}}.$$

Before discussing the substantial redundancy and repetition of the coordinates in (7.1.7), (7.1.9) and (7.1.11), we make a short detour and state two general theorems.

What we are doing here with the surface S_2 and have done with the L-surface in [2, 3] can be adapted for any finite polysquare surface, and we shall give some details in the next section. In particular, we obtain the following result.

Theorem 7.1.1. *Let $\mathcal{P}$ be a finite polysquare surface, and let* $\mathrm{LCM}(\mathcal{P})$ *denote the street-LCM, i.e., the least common multiple of the lengths of the horizontal and vertical streets of $\mathcal{P}$. Consider a* 1*-direction geodesic flow, with a quadratic irrational slope where the ordinary continued fraction digits are all divisible by* $\mathrm{LCM}(\mathcal{P})$.

Using the eigenvalue-based version of the surplus shortline method developed in [2, 3]*, we can explicitly compute the irregularity exponent for such a slope.*

Combining the irregularity exponent with the method of zigzagging introduced in Section 3.3 in [2]*, we can also describe, for a geodesic flow on $\mathcal{P}$ with such a slope, the time-quantitative behavior of the edge-cutting and face-crossing numbers, as well as equidistribution relative to all convex sets.*

We remark that for the slopes in Theorem 7.1.1, Theorem 6.4.1 in [4] applies, and guarantees superdensity.

In fact, Theorem 6.4.1 establishes superdensity for *more* slopes than those for which Theorem 7.1.1 provides the explicit values of the irregularity exponents. On top of the arithmetic condition "divisible by the street-LCM", for superdensity in Theorem 6.4.1, we need the boundedness of the continued fraction digits given by badly approximable slopes. On the other hand, we need in Theorem 7.1.1 the stronger condition of periodicity of the tail of the sequence of continued fraction digits, so that the slope is a quadratic irrational.

The irregularity exponent can be computed from the two eigenvalues with the largest absolute values of an appropriate $2d \times 2d$ matrix, where d is the number of square faces of the polysquare surface $\mathcal{P}$.

Since for every non-integrable polysquare surface the street-LCM is at least 2, the *surplus* shortline method does not have a chance of determining the irregularity exponent for every quadratic irrational slope.

The reason why in the special case of the L-surface we are able to determine the irregularity exponent for every quadratic irrational slope is two-fold. First, the street-LCM is equal to 2. More importantly, we combine the surplus and deficit versions of the shortline method according to the $\pm$-even type continued fraction expansion of the slope.

If the street-LCM of a polysquare region/surface is equal to 2, then we call it a 2-*polysquare* region/surface. One such region with the simplest boundary identification via perpendicular translation is called a 2-*polysquare snake*. The special class of 2-polysquare snakes is surprisingly large, and Figure 7.1.4 gives an example.

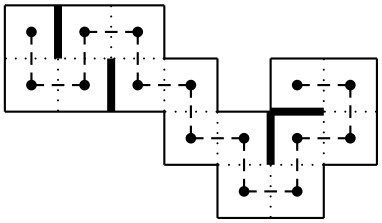

Figure 7.1.4: 2-polysquare snake with capitals and its strictly alternating path

We can easily characterize every 2-polysquare snake by making use of the simple graph-theoretic term of "path".

Given a 2-polysquare snake, we can put a point at the center of every square face of the underlying polysquare, and call it the "capital of the square face". Two capitals are joined by a dashed line-segment if and only if the corresponding square faces share a common edge. Then we obtain a non self-intersecting strictly alternating h-v-path (or v-h-path) of the capitals, where "h" stands for a horizontal edge of unit length and "v" stands for a vertical edge of unit length. The term "strictly alternating" means that h is always preceded and followed by v, and v is always preceded and followed by h, unless the path stops.

We also have the converse, that every non self-intersecting strictly alternating h-v-path (or v-h-path) corresponds to a 2-polysquare snake. Indeed, we cover every vertex of the path with a unit size square such that the vertex is the capital of the square, and we may place some extra walls, denoted by boldface line-segments, if necessary.

It can be shown that the special treatment of the L-surface in [2, 3] can be adapted to *every* 2-polysquare surface. The idea is similar to that for the L-surface. We combine the surplus and deficit versions of the eigenvalue-based shortline method according to the $\pm$-even type continued fraction expansion of the slope.

Theorem 7.1.2. *Let $\mathcal{P}$ be a finite 2-polysquare surface. Then the LCM-divisibility condition in Theorem 7.1.1 may be dropped, so that Theorem 7.1.1 can be extended to every quadratic irrational slope.*

To explain the substantial redundancy or repetition of the coordinates in the eigenvectors (7.1.7), (7.1.9) and (7.1.11), the trick is to visualize and represent the surface S_2 in Figure 7.1.1 as the *period* of a doubly periodic infinite polysquare surface $S_2(\infty)$ in Figure 7.1.5 below.

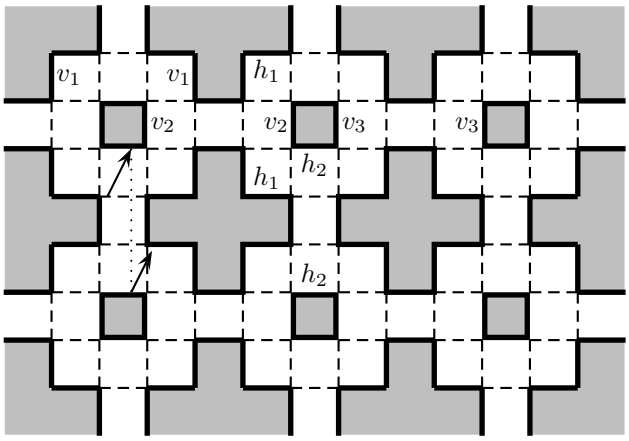

Figure 7.1.5: the doubly periodic polysquare surface $S_2(\infty)$

The infinite polysquare surface $S_2(\infty)$ is essentially a square lattice of copies of S_2 with a noticeable difference – observe carefully the edge pairings in $S_2(\infty)$. For convenience, we say that S_2 is the period surface of $S_2(\infty)$.

Following the surplus shortline method, we study two special geodesics on the infinite polysquare surface $S_2(\infty)$. The first geodesic $V_*(t)$, $t \geqslant 0$, starts from the origin, namely a vertex of one of the square faces, and has slope α defined in (7.1.2). The second geodesic $H_*(t)$, $t \geqslant 0$, also starts from the origin and has reciprocal slope α^{-1}. Note that the projections of $V_*(t)$ and $H_*(t)$ on the period surface S_2 give back the geodesics $V(t)$ and $H(t)$ defined earlier.

A particle traveling on the almost vertical geodesic $V_*(t)$, $t \geqslant 0$, of the doubly periodic infinite surface $S_2(\infty)$ moves from one copy of the period S_2 to another copy of S_2, back and forth, up and down, and generally wanders around.

Note that in $S_2(\infty)$, each copy of S_2 has 4 immediate neighbors: we shall refer to them as the North, South, East and West neighbors. Traveling along the geodesic $V_*(t)$, $t \geqslant 0$, is somewhat similar to a symmetric random walk on the 2-dimensional doubly periodic lattice $\mathbb{Z}^2$. Escaping from a copy of S_2 to the North means following a unit of type a_3 or a_4 in Figure 7.1.2, while escaping to the South means a following a unit of type a_{15} or a_{16}. Similarly, escaping to the East means following a unit of type a_7, while escaping to the West means following a unit of type a_{11}.

To describe an arbitrary finite segment of the geodesic $V_*(t)$, $t \geqslant 0$, of slope α on the infinite polysquare surface $S_2(\infty)$, it suffices to consider its projection on the period surface S_2. The difference between number of North-escapes and the number of South-escapes gives the vertical change on $S_2(\infty)$, while the difference between the number of East-escapes and the number of West-escapes gives the horizontal change on $S_2(\infty)$. This is how we can determine the *escape rate to infinity* of the special geodesic $V_*(t)$, $t \geqslant 0$, on $S_2(\infty)$ from the behavior of its projection $V(t)$, $t \geqslant 0$, on the period surface S_2.

Since the two special geodesics $V(t)$ and $H(t)$ are surplus *shortlines* of each other on the period surface S_2, the time evolution of $V(t)$, $t \geqslant 0$, of slope α and starting from the origin is described by powers of the 2-step transition matrix $M(S_2)$ given by

(7.1.5). Since $M(S_2)$ is diagonalizable, it is particularly easy to express the number of types of units by using the relevant eigenvalues and their eigenvectors. Since the number of types of units is expressed as a linear combination of the *powers* of the eigenvalues, in case of large powers the contribution of the *irrelevant* eigenvalues is clearly negligible.

Recall that escaping to the North means following a unit of type a_3 or a_4 in Figure 7.1.2, and escaping to the South means following a unit of type a_{15} or a_{16}. It follows that for the vertical change, we need to know the 3-rd, 4-th, 15-th and 16-th coordinates of the relevant eigenvectors $\mathbf{v}_i$, $i = 1, 2, 3$, in (7.1.7), (7.1.9) and (7.1.11). Escaping to the East means following a unit of type a_7, and escaping to the West means following a unit of type a_{11}. It follows that for the horizontal change, we need to know the 7-th and 11-th coordinates of the relevant eigenvectors.

Recall that $v_i(j)$ denotes the j-th coordinate of $\mathbf{v}_i$, $i = 1, 2, 3$ and $j = 1, 2, \ldots, 20$. It is easily seen from (7.1.7), (7.1.9) and (7.1.11) that

$$v_i(3) + v_i(4) = v_i(15) + v_i(16), \quad i = 1, 2, 3, \tag{7.1.12}$$

and

$$v_i(7) = v_i(11), \quad i = 1, 2, 3. \tag{7.1.13}$$

The reader may perhaps find (7.1.12)–(7.1.13) a surprising coincidence. However, there is a simple explanation why these equalities must hold. The underlying reason is the fact that the geodesic $V_*(t)$, $t \geqslant 0$, of $S_2(\infty)$ satisfies the condition of Theorem 6.5.1 and exhibits super-slow logarithmic escape rate to infinity; see the Remark after the proof of Theorem 6.5.1 in Section 6.5 of [4]. Meanwhile, a violation of (7.1.12)–(7.1.13) would imply a power-size escape rate to infinity, exponentially larger than logarithmic escape rate to infinity.

Remark. The equalities (7.1.12)–(7.1.13) remain true even if in obtaining (7.1.3)–(7.1.4) we replace the Delete-End Rule by the Keep-End Rule, or mix the two rules arbitrarily. It follows from the fact that the *relevant* eigenvalues and eigenvectors remain the same under these changes.

The Edge-cutting Lemma, which we shall formulate later, is simply a far-reaching generalization of the equalities (7.1.12)–(7.1.13).

It can be seen from (7.1.7), (7.1.9) and (7.1.11) that (7.1.13) can be extended to include the 9-th coordinate, so that

$$v_i(7) = v_i(9) = v_i(11), \quad i = 1, 2, 3. \tag{7.1.14}$$

Note from Figure 7.1.2 that the entries in (7.1.14) represent almost vertical units of type $\nmid$ on the second horizontal street of S_2, of length 3. For the first horizontal street and the third horizontal street, both also of length 3, we have respectively the analogs

$$v_i(1) = v_i(3) = v_i(5), \quad i = 1, 2, 3, \tag{7.1.15}$$

and

$$v_i(13) = v_i(15) = v_i(17), \quad i = 1, 2, 3, \tag{7.1.16}$$

both of which hold, as can be seen from (7.1.7), (7.1.9) and (7.1.11).

It can also be seen from (7.1.7), (7.1.9) and (7.1.11) that (7.1.12) can be extended to

$$v_i(3) + v_i(4) = v_i(15) + v_i(16) = v_i(19) + v_i(20), \quad i = 1, 2, 3. \tag{7.1.17}$$

Note from Figure 7.1.2 that the entries in (7.1.17) represent almost vertical units of type $\uparrow$ or $\nmid$ on the third vertical street of S_2, of length 3. Note that we have chosen almost vertical units of type $\nmid$ that intersect the left edge of each square face. In view of (7.1.15) and (7.1.16), it would have made no difference if we had chosen instead any that intersects the right edge of the same square face. For the

second vertical street and the fourth vertical street, both also of length 3, we have respectively the analogs

$$v_i(1) + v_i(2) = v_i(9) + v_i(10) = v_i(13) + v_i(14), \quad i = 1, 2, 3, \tag{7.1.18}$$

and

$$v_i(5) + v_i(6) = v_i(11) + v_i(12) = v_i(17) + v_i(18), \quad i = 1, 2, 3, \tag{7.1.19}$$

both of which hold, as can be seen from (7.1.7), (7.1.9) and (7.1.11).

The Edge-cutting Lemma basically says that for *any* finite polysquare surface with 1-direction geodesic flow, analogs of the equalities (7.1.14)–(7.1.19) hold. Section 7.2 contains a proof of this fact. In fact, we prove more, see Theorem 7.2.2.

We conclude this section by giving a simple proof of the Edge-cutting Lemma in the simplest special case of the L-surface. We include it, because this simple proof already illustrates quite well the method we use in Section 7.2.

We go back to Section 3 in [2], to the L-surface with a 1-direction geodesic flow with slope $\alpha = 1 + \sqrt{2}$. Figure 7.1.6 below shows the edges of the L-surface as well as the almost vertical units.

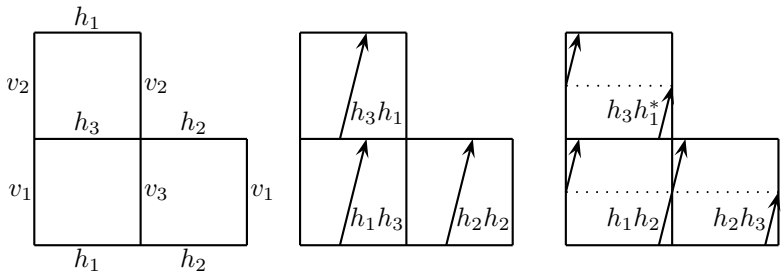

Figure 7.1.6: the L-surface and almost vertical units

Corresponding to the matrix $M(S_2)$ for the polysquare surface S_2, we have the 2-step transition matrix

$$M = M_2^T M_1^T = \begin{pmatrix} 2 & 1 & 1 & 1 & 0 & 0 \\ 1 & 1 & 0 & 0 & 2 & 3 \\ 1 & 1 & 2 & 3 & 0 & 0 \\ 1 & 1 & 1 & 2 & 0 & 0 \\ 2 & 1 & 1 & 1 & 1 & 1 \\ 0 & 0 & 0 & 0 & 2 & 3 \end{pmatrix}. \tag{7.1.20}$$

In (7.1.20), we have used the lexicographic order for the almost vertical units

$$h_1h_2, h_1h_3, h_2h_2, h_2h_3, h_3h_1, h_3h_1^*. \tag{7.1.21}$$

The L-surface has precisely one vertical and one horizontal street of length greater than 1. If $\mathbf{v} = (v_1, v_2, v_3, v_4, v_5, v_6)$ is a relevant eigenvector of M, then the coordinates correspond to the 6 almost vertical units in (7.1.21). It follows that the L-surface analog of the equalities (7.1.14)–(7.1.16) is

$$v_1 = v_4, \tag{7.1.22}$$

and the L-surface analog of the inequalities (7.1.17)–(7.1.19) is

$$v_1 + v_2 = v_5 + v_6. \tag{7.1.23}$$

These two equations together give an invariant subspace of the matrix M. To see this, suppose that

$$M\mathbf{v}^T = \mathbf{w}^T = (w_1, w_2, w_3, w_4, w_5, w_6)^T.$$

Then

$$\begin{aligned}
w_1 &= 2v_1 + v_2 + v_3 + v_4,\\
w_2 &= v_1 + v_2 + 2v_5 + 3v_6,\\
w_3 &= v_1 + v_2 + 2v_3 + 3v_4,\\
w_4 &= v_1 + v_2 + v_3 + 2v_4,\\
w_5 &= 2v_1 + v_2 + v_3 + v_4 + v_5 + v_6,\\
w_6 &= 2v_5 + 3v_6.
\end{aligned}$$

It is easy to see that $w_1 = w_4$ follows from $v_1 = v_4$. On the other hand, we have

$$\begin{aligned}
w_1 + w_2 &= 3v_1 + 2v_2 + v_3 + v_4 + 2v_5 + 3v_6,\\
w_5 + w_6 &= 2v_1 + v_2 + v_3 + v_4 + 3v_5 + 4v_6,
\end{aligned}$$

so that

$$(w_1 + w_2) - (w_5 + w_6) = (v_1 + v_2) - (v_5 + v_6),$$

and so $w_1 + w_2 = w_5 + w_6$ follows from $v_1 + v_2 = v_5 + v_6$.

The 2-step transition matrix M has 6 eigenvalues and 6 independent eigenvectors in $\mathbb{R}^6$. The eigenvalues, in order of decreasing absolute value, are

$$\begin{aligned}
&\lambda_1 = 3 + 2\sqrt{2}, \quad \lambda_2 = \frac{3+\sqrt{5}}{2}, \quad \lambda_3 = 1,\\
&\lambda_4 = 1, \quad \lambda_5 = \frac{3-\sqrt{5}}{2}, \quad \lambda_6 = 3 - 2\sqrt{2}.
\end{aligned} \tag{7.1.24}$$

Suppose that the corresponding eigenvectors of M are respectively $\mathbf{v}_i$, $1 \leqslant i \leqslant 6$. Then

$$\begin{aligned}
\lambda_1 &\to \mathbf{v}_1 = (1, \sqrt{2}, \sqrt{2}, 1, \sqrt{2}, 1)^T,\\
\lambda_2 &\to \mathbf{v}_2 = \left(-\frac{1}{2}, \frac{\sqrt{5}+3}{4}, -\frac{\sqrt{5}}{2}, -\frac{1}{2}, \frac{\sqrt{5}-3}{4}, 1\right)^T,\\
\lambda_3 &\to \mathbf{v}_3 = (0, -1, 1, 0, 0, 0)^T,\\
\lambda_4 &\to \mathbf{v}_4 = (-1, 1, 0, 0, -1, 1)^T,\\
\lambda_5 &\to \mathbf{v}_5 = \left(-\frac{1}{2}, -\frac{\sqrt{5}-3}{4}, \frac{\sqrt{5}}{2}, -\frac{1}{2}, -\frac{\sqrt{5}+3}{4}, 1\right)^T,\\
\lambda_6 &\to \mathbf{v}_6 = (1, -\sqrt{2}, -\sqrt{2}, 1, -\sqrt{2}, 1)^T.
\end{aligned}$$

Note now that the 4-dimensional invariant subspace of the matrix M given by the equations (7.1.22) and (7.1.23) contains the eigenvectors $\mathbf{v}_1$ and $\mathbf{v}_2$ corresponding to the two relevant eigenvalues λ_1 and λ_2. It also contains the eigenvectors $\mathbf{v}_5$ and $\mathbf{v}_6$ of the two conjugate eigenvalues λ_5 and λ_6.

This simple example illustrates what we call an *invariant subspace* argument. In the next section we use a similar but more sophisticated version of this to prove the Edge-cutting Lemma and more.

Finally observe that the Edge-cutting Lemma has the following vague intuitive meaning. If the surplus shortline method works for a 1-direction geodesic flow of a finite polysquare surface with some fixed slope, then the edge-cutting numbers of the edges in the *same* street are "nearly the same". We shall clarify this later.

7.2. **Reducing the 2-step transition matrix: the street-spreading matrix.** We see from the examples in Section 7.1 that the 2-step transition matrix of the shortline method is quite redundant. Here we elaborate on this. What we are interested in is the long-term behavior of the geodesics, and when the shortline method works, it suffices to consider the relevant eigenvalues, those with absolute value greater than 1, and the corresponding eigenvectors. For example, while the 2-step transition matrix $M(S_2)$ in (7.1.5) has 20 eigenvalues, only 3 of them are relevant. Moreover, each of the corresponding 20-dimensional eigenvectors (7.1.7), (7.1.9) and (7.1.11) has at most 8 distinct coordinates, with some multiplicities.

Accordingly, we introduce a general reduction process that, roughly speaking, eliminates the irrelevant part of the 2-step transition matrix M. We shall give a recipe of how we can read out the relevant eigenvalues and their eigenvectors from a smaller matrix called the *street-spreading matrix*.

We consider a vector space W with basis made up of all the distinct types of almost vertical units of $\mathcal{P}$, of dimension equal to twice the number of distinct square faces of $\mathcal{P}$. We shall show that the equations in the Edge-cutting Lemma define a subspace of W, and we want to show that this subspace is M-invariant and contains all the relevant eigenvectors. Thus the basic idea is to find such a *relevant* M-invariant subspace, and a convenient basis of it, leading to the usually substantially smaller street-spreading matrix. A proof of the Edge-cutting Lemma will come as a byproduct of the reduction process. Theorem 7.2.2, the main result, will be formulated towards the end of this section.

The Shortcut-Ancestor Process. Let $\mathcal{P}$ be a given finite polysquare surface, with d square faces. Let m be any fixed integer multiple of the lengths of the horizontal streets of $\mathcal{P}$, and let n be any fixed integer multiple of the lengths of the vertical streets of $\mathcal{P}$.

We adopt the following convention.

A typical square face of $\mathcal{P}$, on the i-th horizontal street and j-th vertical street, is denoted by $S_{i,j}$. For any fixed i, there is a finite set J_i of indices j such that $j \in J_i$ if and only if $S_{i,j} \subset \mathcal{P}$, so that

$$\bigcup_{j \in J_i} S_{i,j}$$

is the i-th horizontal street of $\mathcal{P}$. For any fixed j, there is a finite set I_j of indices i such that $i \in I_j$ if and only if $S_{i,j} \subset \mathcal{P}$, so that

$$\bigcup_{i \in I_j} S_{i,j}$$

is the j-th vertical street of $\mathcal{P}$.

Remark. Our convention here is an over-simplification of the general situation, as it is in fact possible for two or more distinct square faces of a polysquare surface to lie on the same horizontal street and the same vertical street simultaneously. We have chosen to adopt the present simplification and convention here as the notation is somewhat simpler and rather convenient, and enough to enable us to study many of the polysquare surfaces of interest. In general, the notation $S_{i,j}$ does not allow us to distinguish between two distinct square faces that may lie on the i-th horizontal street and the j-th vertical street, and we shall have to introduce an extra parameter to enable us to identify individual square faces of the polysquare surface in question.

Indeed, the first occasion in this paper where our notation becomes inadequate is at the end of Section 8.2 when we discuss the regular octagon surface, and we shall deal with the problem on a case by case basis when it arises.

We consider two types of almost vertical units in $S_{i,j}$. Both types start from the bottom edge of $S_{i,j}$. However, type $\uparrow_{i,j}$ ends on the top edge of $S_{i,j}$, whereas type $\updownarrow_{i,j}$ exits $S_{i,j}$ through the right edge. We also consider two types of almost horizontal units in $S_{i,j}$. Both types end on the right edge of $S_{i,j}$. However, type $\rightarrow_{i,j}$ starts from the left edge of $S_{i,j}$, whereas type $\twoheadrightarrow_{i,j}$ enters $S_{i,j}$ through the bottom edge.

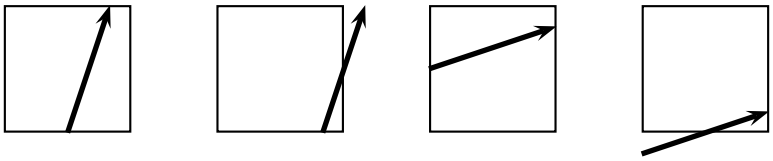

Figure 7.2.1: the square face $S_{i,j}$, with units of types $\uparrow_{i,j}, \updownarrow_{i,j}, \rightarrow_{i,j}, \twoheadrightarrow_{i,j}$

We now consider a 1-direction almost vertical geodesic V_0 on $\mathcal{P}$, starting at a vertex of $\mathcal{P}$ and with slope

$$\alpha = [n; m, n, m, \ldots] = n + \frac{1}{m + \frac{1}{n + \frac{1}{m + \cdots}}}, \tag{7.2.1}$$

so that $n \leqslant \alpha < n + 1$. The geodesic V_0 is made up of almost vertical units of type $\uparrow_{i,j}$ and $\updownarrow_{i,j}$, all with slope α. Thus we may consider a vector space W, with basis

$$\mathscr{W} = \{\uparrow_{i,j}, \updownarrow_{i,j} : S_{i,j} \subset \mathcal{P}\}. \tag{7.2.2}$$

The shortline of V_0 is a 1-direction almost horizontal geodesic H_0 on $\mathcal{P}$, starting at the same vertex of $\mathcal{P}$ and with slope α_1^{-1}, where

$$\alpha_1 = [m; n, m, \ldots] = m + \frac{1}{n + \frac{1}{m + \cdots}},$$

so that $m \leqslant \alpha_1 < m + 1$. The geodesic H_0 is made up of almost horizontal units of type $\rightarrow_{i,j}$ and $\twoheadrightarrow_{i,j}$, all with slope α_1^{-1}. Thus we may consider a vector space W', with basis

$$\mathscr{W}' = \{\rightarrow_{i,j}, \twoheadrightarrow_{i,j} : S_{i,j} \subset \mathcal{P}\}.$$

The shortline of H_0 is the original 1-direction almost vertical geodesic V_0 on $\mathcal{P}$, with slope α. Thus we return to the vector space W, with basis $\mathscr{W}$.

Remark. Note that V_0 and H_0 are mutual shortlines. Note the special property of α, that its continued fraction expansion has period 2.

Our task is to start with $\mathscr{W}$ and identify the 2-step ancestors in $\mathscr{W}$ of each of the almost vertical units. Let ANC denote one step of this ancestor process.

Step 1. We consider each of the almost vertical units in $\mathscr{W}$, and determine its ancestors in $\mathscr{W}'$ using the Delete-End Rule, in the same spirit as in (7.1.3). This leads to a transition matrix M_1, where each row captures the information concerning the ancestors of a particular almost vertical unit, with the columns displaying the multiplicities of the individual ancestor almost horizontal units. Indeed, M_1^T is the matrix for this ancestor process $\mathscr{W} \to \mathscr{W}'$, where the coefficient vectors are taken as column vectors. Note that M_1^T is a $2d \times 2d$ matrix.

Thus for every i_0, j_0 such that $S_{i_0,j_0} \subset \mathcal{P}$, using the Delete-End Rule, we have the ancestor relationships

$$\mathrm{ANC}(\{\uparrow_{i_0,j_0}\}) = \{\twoheadrightarrow_{i_0,j_0}\} \cup \{\rightarrow_{i_0,j} \colon j \in J_{i_0}^*\} \setminus \{\rightarrow_{i_0,j_0}\}, \tag{7.2.3}$$

$$\mathrm{ANC}(\{\updownarrow_{i_0,j_0}\}) = \{\twoheadrightarrow_{i_0,j_0}\} \cup \{\rightarrow_{i_0,j} \colon j \in J_{i_0}^*\}, \tag{7.2.4}$$

where the $*$ in $J_{i_0}^*$ denotes that each edge of J_{i_0} is counted with multiplicity $m|J_{i_0}|^{-1}$, where $|J_{i_0}|$ denotes the number of distinct elements of the set J_{i_0}. We also adopt the convention that unions and complements are taken with appropriate multiplicities.

Step 2. We consider each of the almost horizontal units in $\mathscr{W}'$, and determine its ancestors in $\mathscr{W}$ using the Keep-End Rule, so not quite in the same spirit as in (7.1.4). This leads to a transition matrix M_2, where each row captures the information concerning the ancestors of a particular almost horizontal unit, with the columns displaying the multiplicities of the individual ancestor almost vertical units. Indeed, M_2^T is the matrix for this ancestor process $\mathscr{W}' \to \mathscr{W}$, where the coefficient vectors are taken as column vectors. Note that M_2^T is a $2d \times 2d$ matrix.

Thus for every i_1, j_1 such that $S_{i_1,j_1} \subset \mathcal{P}$, using the Keep-End Rule, we have the ancestor relationships

$$\mathrm{ANC}(\{\rightarrow_{i_1,j_1}\}) = \{\upmapsto_{i_1,j_1}\} \cup \{\uparrow_{i,j_1} \colon i \in I_{j_1}^*\} \setminus \{\uparrow_{i_1,j_1}\}, \tag{7.2.5}$$

$$\mathrm{ANC}(\{\mapsto_{i_1,j_1}\}) = \{\upmapsto_{i_1,j_1}\} \cup \{\uparrow_{i,j_1} \colon i \in I_{j_1}^*\}, \tag{7.2.6}$$

where the $*$ in $I_{j_1}^*$ denotes that each edge of I_{j_1} is counted with multiplicity $n|I_{j_1}|^{-1}$, where $|I_{j_1}|$ denotes the number of distinct elements of the set I_{j_1}. We also adopt the convention that unions and complements are taken with appropriate multiplicities.

Step 3. Finally, we combine the two steps and end up with a 2-step transition matrix $M = (M_1 M_2)^T$, of size $2d \times 2d$, in the same spirit as in (7.1.5). Thus combining the ancestor relationships (7.2.3)–(7.2.6), we deduce that

$$\begin{aligned}
&\mathrm{ANC}(\mathrm{ANC}(\{\uparrow_{i_0,j_0}\})) \\
&\quad = \big(\{\upmapsto_{i_0,j_0}\} \cup \{\uparrow_{i,j_0} \colon i \in I_{j_0}^*\}\big) \\
&\qquad \cup \big(\{\upmapsto_{i_0,j} : j \in J_{i_0}^*\} \cup \{\uparrow_{i,j} \colon j \in J_{i_0}^*, i \in I_j^*\} \setminus \{\uparrow_{i_0,j} \colon j \in J_{i_0}^*\}\big) \\
&\qquad \setminus \big(\{\upmapsto_{i_0,j_0}\} \cup \{\uparrow_{i,j_0} \colon i \in I_{j_0}^*\} \setminus \{\uparrow_{i_0,j_0}\}\big) \\
&\quad = \{\uparrow_{i_0,j_0}\} \cup \{\uparrow_{i,j} \colon j \in J_{i_0}^*, i \in I_j^*\} \cup \{\upmapsto_{i_0,j} : j \in J_{i_0}^*\} \setminus \{\uparrow_{i_0,j} \colon j \in J_{i_0}^*\},
\end{aligned} \tag{7.2.7}$$

$$\begin{aligned}
&\mathrm{ANC}(\mathrm{ANC}(\{\upmapsto_{i_0,j_0}\})) \\
&\quad = \big(\{\upmapsto_{i_0,j_0}\} \cup \{\uparrow_{i,j_0} \colon i \in I_{j_0}^*\}\big) \\
&\qquad \cup \big(\{\upmapsto_{i_0,j} : j \in J_{i_0}^*\} \cup \{\uparrow_{i,j} \colon j \in J_{i_0}^*, i \in I_j^*\} \setminus \{\uparrow_{i_0,j} \colon j \in J_{i_0}^*\}\big) \\
&\quad = \{\upmapsto_{i_0,j_0}\} \cup \{\uparrow_{i,j} \colon j \in J_{i_0}^*, i \in I_j^*\} \\
&\qquad \cup \{\uparrow_{i,j_0} \colon i \in I_{j_0}^*\} \cup \{\upmapsto_{i_0,j} : j \in J_{i_0}^*\} \setminus \{\uparrow_{i_0,j} \colon j \in J_{i_0}^*\}.
\end{aligned} \tag{7.2.8}$$

Remark. We choose this particular convention regarding the Delete-End Rule and Keep-End Rule, as it makes the matrix reduction particularly simple. For instance, if we use this particular convention for the surface S_2, then in the 2-step transition matrix M, the 14 eigenvalues of absolute value 1 are all the same and equal to 1. Indeed, we shall give a good reason later, when we discuss a simpler approach to the process, why they are all equal to 1.

Suppose that $\lambda_1, \ldots, \lambda_s$ are the eigenvalues of the 2-step transition matrix M, with multiplicities $d_1, \ldots, d_s$ respectively, and where $|\lambda_1| \geqslant \ldots \geqslant |\lambda_s|$. Then clearly $d_1 + \ldots + d_s = 2d$. Furthermore, the space $\mathbb{C}^{2d}$ can be decomposed into a direct sum

$$\mathbb{C}^{2d} = W_1 \oplus \ldots \oplus W_s,$$

where each W_i, $i = 1, \ldots, s$, is an M-invariant subspace of $\mathbb{C}^{2d}$ and also contains an eigenvector Ψ_i corresponding to the eigenvalue λ_i. If $d_i = 1$, then Ψ_i generates W_i and gives rise to a basis of W_i. If $d_i > 1$, then we can find a basis $\Psi_{i,j}$, $j = 1, \ldots, d_i$, of W_i, with $\Psi_i = \Psi_{i,1}$. Thus the collection

$$\Psi_{i,j}, \quad i = 1, \ldots, s, \quad j = 1, \ldots, d_i,$$

gives rise to a basis of $\mathbb{C}^{2d}$.

The almost vertical geodesic V_0 starts at a vertex of $\mathcal{P}$, and it starts with a finite succession of almost vertical units. Let $\mathbf{w}_0$ denote the column coefficient vector

of this finite collection of units with respect to the basis $\mathscr{W}$. Then we can find coefficients $c_{i,j} \in \mathbb{C}$, $i = 1, \ldots, s$, $j = 1, \ldots, d_i$, such that

$$\mathbf{w}_0 = \sum_{i=1}^{s} \sum_{j=1}^{d_i} c_{i,j} \Psi_{i,j}. \tag{7.2.9}$$

Suppose that $\mathbf{w}_r = M^r \mathbf{w}_0$. Then

$$\mathbf{w}_r = \sum_{i=1}^{s} \sum_{j=1}^{d_i} c_{i,j} M^r \Psi_{i,j}. \tag{7.2.10}$$

We shall consider the special case where for every eigenvalue λ_i of M with $|\lambda_i| > 1$, the M-invariant subspace W_i has a basis consisting entirely of eigenvectors of M with eigenvalue λ_i. Let λ_i, $i = 1, \ldots, s_0$, be these eigenvalues. Then

$$\Psi_{i,j}, \quad i = 1, \ldots, s_0, \quad j = 1, \ldots, d_i,$$

are all eigenvectors of M. Furthermore, $|\lambda_i| \leqslant 1$, $i = s_0 + 1, \ldots, s$.

In this case, we have

$$\mathbf{w}_r = \sum_{i=1}^{s_0} \sum_{j=1}^{d_i} c_{i,j} \lambda_i^r \Psi_{i,j} + O(r^{D-1}), \tag{7.2.11}$$

where $D = \max\{d_1, \ldots, d_s\}$, and the error term $O(r^{D-1})$ gives an upper bound on the absolute value of the coordinates of the missing vectors. To see this, note that the matrix M is similar to a matrix of the form

$$\begin{pmatrix} J(\tau_1, e_1) & & \\ & \ddots & \\ & & J(\tau_u, e_u) \end{pmatrix},$$

where a typical Jordan block $J = J(\tau, e)$ is an $e \times e$ matrix of the form

$$J(\tau, e) = \begin{pmatrix} \tau & 1 & & \\ & \ddots & \ddots & \\ & & \ddots & 1 \\ & & & \tau \end{pmatrix},$$

where every entry on the diagonal is equal to an eigenvalue τ of M, every entry on the superdiagonal is equal to 1, and every other entry is equal to 0.

The contribution to the error term in (7.2.11) comes from those eigenvalues of M with absolute value at most 1. These are related to Jordan blocks $J = J(\tau, e)$ with $|\tau| \leqslant 1$ and $e \leqslant D$. The matrix J^r is $e \times e$ and upper-triangular, and the entry on row i and column j, with $j \geqslant i$, is given by

$$\binom{r}{j-i} \tau^{r-(j-i)},$$

where the binomial coefficient is equal to 0 if $j - i > r$. The bound $O(r^{D-1})$ follows on observing that

$$\binom{r}{j-i} \leqslant r^{e-1} \leqslant r^{D-1} \quad \text{and} \quad |\tau^{r-(j-i)}| \leqslant 1.$$

Important Remark. It is crucial to bring those eigenvalues with the largest absolute values into play. The coefficient in (7.2.11) of the eigenvector corresponding to the largest eigenvalue is non-zero, since the left hand side of (7.2.11) contains terms of order of magnitude λ_1^r. For the coefficient of the eigenvector corresponding to the second largest eigenvalue, this is less obvious. The trick here is to start with

an almost vertical unit from the chosen vertex. If the coefficient corresponding to the second eigenvector is non-zero, then we have a *good* initial vector $\mathbf{w}_0$. If the coefficient is zero, then we add the next unit, and keep on doing so but stop as soon as we get a non-zero coefficient. Take this as our starting succession of almost vertical units, and use the corresponding *good* $\mathbf{w}_0$. This process must stop after bounded time, depending only on $\mathcal{P}$ and the slope α, as soon every basis element in $\mathscr{W}$ will come into play. Of the $2d$ types of almost vertical units, it is clear that at least one of them gives rise to a non-zero coefficient.

Finding a Relevant M-invariant Subspace and the Edge-cutting Lemma. The above method in rather laborious. Finding the eigenvalues and eigenvectors of the 2-step transition matrix M, of size $2d \times 2d$, is not a very pleasant task.

It is clear that the expression (7.2.11) is dominated by the terms arising from those eigenvalues λ_i, $i = 1, \ldots, s$, with absolute values exceeding 1. We call these the relevant eigenvalues, and the remaining eigenvalues make little to no contribution. We next seek a simpler way of finding these relevant eigenvalues and their corresponding eigenvectors.

For any set $\mathscr{S}$ of almost vertical units in $\mathcal{P}$, counted with multiplicity, let $[\mathscr{S}]$ denote the column coefficient vector of $\mathscr{S}$ with respect to the basis $\mathscr{W}$. Note that $[\mathscr{S}] \in \mathbb{C}^{2d}$, where d is the number of square faces of $\mathcal{P}$.

As the matrix M is the transition matrix of the 2-step ancestor process with respect to the basis $\mathscr{W}$, (7.2.7) and (7.2.8) can be rewritten in the form

$$\begin{aligned}(M-I)[\{\uparrow_{i_0,j_0}\}] &= [\{\uparrow_{i,j}\colon j \in J^*_{i_0}, i \in I^*_j\}] \\ &\quad + [\{\updownarrow_{i_0,j} : j \in J^*_{i_0}\}] - [\{\uparrow_{i_0,j}\colon j \in J^*_{i_0}\}], \qquad (7.2.12)\\ (M-I)[\{\updownarrow_{i_0,j_0}\}] &= [\{\uparrow_{i,j}\colon j \in J^*_{i_0}, i \in I^*_j\}] + [\{\uparrow_{i,j_0}\colon i \in I^*_{j_0}\}] \\ &\quad + [\{\updownarrow_{i_0,j} : j \in J^*_{i_0}\}] - [\{\uparrow_{i_0,j}\colon j \in J^*_{i_0}\}]. \qquad (7.2.13)\end{aligned}$$

Write

$$\begin{aligned}\mathbf{u}_{i_0} &= [\{\uparrow_{i,j}\colon j \in J^*_{i_0}, i \in I^*_j\}], \qquad (7.2.14)\\ \mathbf{v}_{i_0} &= [\{\updownarrow_{i_0,j} : j \in J^*_{i_0}\}] - [\{\uparrow_{i_0,j}\colon j \in J^*_{i_0}\}], \qquad (7.2.15)\\ \mathbf{z}_{j_0} &= [\{\uparrow_{i,j_0}\colon i \in I^*_{j_0}\}]. \qquad (7.2.16)\end{aligned}$$

Then $\mathbf{u}_{i_0}, \mathbf{v}_{i_0}, \mathbf{z}_{j_0} \in \mathbb{C}^{2d}$, and (7.2.12) and (7.2.13) can be expressed in the form

$$\begin{aligned}(M-I)[\{\uparrow_{i_0,j_0}\}] &= \mathbf{u}_{i_0} + \mathbf{v}_{i_0}, \qquad (7.2.17)\\ (M-I)[\{\updownarrow_{i_0,j_0}\}] &= \mathbf{u}_{i_0} + \mathbf{v}_{i_0} + \mathbf{z}_{j_0}. \qquad (7.2.18)\end{aligned}$$

Motivated by the equations (7.2.17) and (7.2.18), we consider $\mathrm{Im}(M-I)$, the image of the matrix $M-I$ in $\mathbb{C}^{2d}$. Note that this is an M-invariant subspace of $\mathbb{C}^{2d}$. Indeed, for every vector $\mathbf{w} \in \mathbb{C}^{2d}$, we have

$$M((M-I)\mathbf{w}) = (M^2 - M)\mathbf{w} = (M-I)(M\mathbf{w}) = (M-I)\mathbf{w}'$$

where $\mathbf{w}' \in \mathbb{C}^{2d}$ satisfies $\mathbf{w}' = M\mathbf{w}$. It is clear from the equations (7.2.17) and (7.2.18) that the subspace $\mathrm{Im}(M-I)$ is generated by the elements of the form

$$\mathbf{u}_{i_0}, \mathbf{v}_{i_0}, \mathbf{z}_{j_0} \in \mathrm{Im}(M-I) \subset \mathbb{C}^{2d}. \qquad (7.2.19)$$

Lemma 7.2.1. *All eigenvectors corresponding to relevant eigenvalues of M belong to the subspace* $\mathrm{Im}(M-I) \subset \mathbb{C}^{2d}$.

Proof. Suppose that $\mathbf{w} \in \mathbb{C}^{2d}$ satisfies $M\mathbf{w} = \lambda\mathbf{w}$ with $|\lambda| > 1$. Then

$$(\lambda - 1)\mathbf{w} = (M-I)\mathbf{w} \in \mathrm{Im}(M-I),$$

so that $\mathbf{w} \in \mathrm{Im}(M-I)$. □

Theorem 7.2.1 ("edge-cutting lemma"). *Let $\mathcal{P}$ be a finite polysquare surface. Let m be any fixed integer multiple of the lengths of the horizontal streets of $\mathcal{P}$, and let n be any fixed integer multiple of the lengths of the vertical streets of $\mathcal{P}$. Consider a 1-direction almost vertical geodesic V_0 on $\mathcal{P}$, with slope α given by* (7.2.1). *Let M denote the transition matrix of the 2-step ancestor process with respect to the basis $\mathscr{W}$, where $\mathscr{W}$ is given by* (7.2.2). *Then the following hold:*

(i) *For any two distinct almost vertical units $\updownarrow_{i_0,j_1}$ in a square face S_{i_0,j_1} and $\updownarrow_{i_0,j_2}$ in a square face S_{i_0,j_2} on the same horizontal street of $\mathcal{P}$ and every eigenvector corresponding to a relevant eigenvalue of M, the two entries in the eigenvector corresponding to $\updownarrow_{i_0,j_1}$ and $\updownarrow_{i_0,j_2}$ are equal.*

(ii) *For any two distinct pairs of almost vertical units $\uparrow_{i_1,j_0}, \updownarrow_{i_1,j_0}$ in a square face S_{i_1,j_0} and $\uparrow_{i_2,j_0}, \updownarrow_{i_2,j_0}$ in a square face S_{i_2,j_0} on the same vertical street of $\mathcal{P}$ and every eigenvector corresponding to a relevant eigenvalue of M, the sum of the two entries in the eigenvector corresponding to $\uparrow_{i_1,j_0}, \updownarrow_{i_1,j_0}$ in the square face S_{i_1,j_0} is equal to the sum of the two entries in the eigenvector corresponding to $\uparrow_{i_2,j_0}, \updownarrow_{i_2,j_0}$ in the square face S_{i_2,j_0}.*

Proof. In view of Lemma 7.2.1, it is enough to concentrate our attention on the subspace $\mathrm{Im}(M-I)$. Since this subspace is generated by the vectors in (7.2.19), it suffices to check that these generating vectors all satisfy (i) and (ii). Our argument is reduced to a simple case study.

Note that $\mathbf{u}_{i_0}$ does not involve units of type $\updownarrow_{i,j}$, so (i) holds by default. On the other hand, $\mathbf{u}_{i_0}$ satisfies (ii), due to cyclic vertical symmetry. A similar argument applies to $\mathbf{z}_{j_0}$.

On the other hand, $\mathbf{v}_{i_0}$ satisfies (i), due to cyclic horizontal symmetry. Clearly it also satisfies (ii), as the count for each $\updownarrow_{i_0,j}$ cancels the count for $\uparrow_{i_0,j}$.

This completes the proof of the Edge-cutting Lemma. □

An Important Subspace. Let $h = h(\mathcal{P})$ and $v = v(\mathcal{P})$ denote respectively the number of horizontal and vertical streets in $\mathcal{P}$.

Let $\mathcal{V}$ be the subspace of $\mathbb{C}^{2d}$ generated by $\mathbf{u}_i, \mathbf{v}_i$, $1 \leqslant i \leqslant h$, defined in (7.2.14) and (7.2.15), so that the dimension of $\mathcal{V}$ is at most $2h$.

Lemma 7.2.2. *We have* $\mathrm{Im}((M-I)^2) \subset \mathcal{V}$.

Proof. Since $\mathrm{Im}((M-I)^2) = (M-I)(\mathrm{Im}(M-I))$, and the subspace $\mathrm{Im}(M-I)$ is generated by the vectors in (7.2.19), it suffices to show that

$$(M-I)\mathbf{u}_{i_0} \in \mathcal{V}, \quad (M-I)\mathbf{v}_{i_0} \in \mathcal{V}, \quad (M-I)\mathbf{z}_{j_0} \in \mathcal{V}. \tag{7.2.20}$$

From (7.2.14) and (7.2.16), it is clear that both $\mathbf{u}_{i_0}$ and $\mathbf{z}_{j_0}$ involve only the almost vertical units of various types $\uparrow_{i,j}$, so it follows from (7.2.17) that the first and third statements in (7.2.20) hold. On the other hand, it follows from (7.2.14)–(7.2.18) that

$$(M-I)\mathbf{v}_{i_0} = \sum_{j \in J^*_{i_0}} \mathbf{z}_j = [\{\uparrow_{i,j} \colon i \in I^*_j, j \in J^*_{i_0}\}] = \mathbf{u}_{i_0}, \tag{7.2.21}$$

and the second statement in (7.2.20) follows immediately. □

By definition $\mathcal{V}$ is a subspace of $\mathrm{Im}(M-I)$. Thus the following lemma is an extension of Lemma 7.2.1.

Lemma 7.2.3. *The vector space $\mathcal{V}$ is an M-invariant subspace of $\mathbb{C}^{2d}$, and contains the eigenvectors corresponding to each of the eigenvalues $\lambda \neq 1$ of M.*

Proof. To prove that $\mathcal{V}$ is M-invariant, it suffices to check that

$$M\mathbf{u}_i \in \mathcal{V} \quad \text{and} \quad M\mathbf{v}_i \in \mathcal{V}.$$

This is trivial, since we know from (7.2.20) that $(M-I)\mathbf{u}_i \in \mathcal{V}$ and $(M-I)\mathbf{v}_i \in \mathcal{V}$. Next suppose that $\mathbf{w} \in \mathbb{C}^{2d}$ satisfies $M\mathbf{w} = \lambda\mathbf{w}$ for some $\lambda \neq 1$. Then

$$(\lambda-1)^2\mathbf{w} = (M-I)^2\mathbf{w} \in \mathrm{Im}((M-I)^2),$$

so that $\mathbf{w} \in \mathrm{Im}((M-I)^2) \subset \mathcal{V}$, where in the last step we have used Lemma 7.2.2. □

Next we study how the matrix M acts on $\mathcal{V}$. First of all, the equation (7.2.21) implies

$$M\mathbf{v}_i = \mathbf{u}_i + \mathbf{v}_i. \tag{7.2.22}$$

We already know that $M\mathbf{u}_i \in \mathcal{V}$, so that $M\mathbf{u}_i$ is a linear combination of the vectors $\mathbf{u}_i, \mathbf{v}_i$, $1 \leqslant i \leqslant h$. Next we shall find these coefficients explicitly, but this process is much more complicated than (7.2.22), as the coefficients depend heavily on the combinatorial arrangement of the square faces on the given polysquare surface $\mathcal{P}$. In fact, they depend on the given triple $(\mathcal{P}; m, n)$. This will eventually lead us to the desired $h \times h$ *street-spreading matrix* $\mathbf{S} = \mathbf{S}(\mathcal{P}; m, n)$ which contains all the "relevant information".

Combining (7.2.14) and (7.2.17), one can determine the desired coefficients by using a particular algorithm. The abstract/formal definition of this algorithm in the general case is somewhat complicated. As with most algorithms, the best way to learn it is to study a few concrete examples with figures. We strongly recommend the reader to study the next two examples, after which the abstract/formal definition becomes almost self-explanatory.

Algorithm to Find the Street-spreading Matrix. The algorithm can easily be summarized in a nutshell: *spread the horizontal streets vertically.* We illustrate part of the recipe by two examples.

Example 7.2.1. Consider again the polysquare surface S_2, given in Figure 7.1.1, and consider a 1-direction geodesic starting from some vertex of S_2 with slope α given by (7.2.1) with $m = n = 3$.

We shall number the horizontal streets from top to bottom, and the vertical streets from left to right.

Consider the first horizontal street at the top, corresponding to $\mathbf{u}_1$. We now use (7.2.14), and since $J_1^* = \{2, 3, 4\}$, it follows that $\mathbf{u}_1$ concerns almost vertical units of type $\uparrow$ on the vertical streets $2, 3, 4$. In other words, we start with the first horizontal street, and spread along every vertical street that intersects this horizontal street. The picture on the left in Figure 7.2.2 shows a listing of all the almost vertical units of type $\uparrow$ along these vertical streets. Applying (7.2.17), we have

$$\begin{aligned}(M-I)\mathbf{u}_1 &= (M-I)[\{\uparrow_{1,2}, \uparrow_{1,3}, \uparrow_{1,4}\}] + (M-I)[\{\uparrow_{2,2}, \uparrow_{2,4}\}] \\ &\quad + (M-I)[\{\uparrow_{3,2}, \uparrow_{3,3}, \uparrow_{3,4}\}] + (M-I)[\{\uparrow_{4,3}\}] \\ &= 3(\mathbf{u}_1 + \mathbf{v}_1) + 2(\mathbf{u}_2 + \mathbf{v}_2) + 3(\mathbf{u}_3 + \mathbf{v}_3) + (\mathbf{u}_4 + \mathbf{v}_4). \end{aligned} \tag{7.2.23}$$

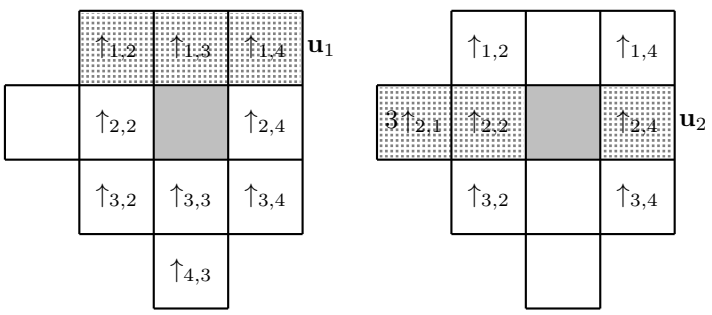

Figure 7.2.2: S_2 with $m = n = 3$: almost vertical units of type $\uparrow$ in $\mathbf{u}_1, \mathbf{u}_2$

For the second horizontal street, corresponding to $\mathbf{u}_2$, highlighted in the picture on the right in Figure 7.2.2, we have $J_2^* = \{1, 2, 4\}$, and a similar argument gives

$$\begin{aligned}(M-I)\mathbf{u}_2 &= (M-I)[\{\uparrow_{1,2}, \uparrow_{1,4}\}] + (M-I)[\{\uparrow_{2,1}, \uparrow_{2,1}, \uparrow_{2,1}, \uparrow_{2,2}, \uparrow_{2,4}\}] \\ &\quad + (M-I)[\{\uparrow_{3,2}, \uparrow_{3,4}\}] \\ &= 2(\mathbf{u}_1 + \mathbf{v}_1) + 5(\mathbf{u}_2 + \mathbf{v}_2) + 2(\mathbf{u}_3 + \mathbf{v}_3). \end{aligned} \tag{7.2.24}$$

The multiple 3 for $\uparrow_{2,1}$ in the square face $S_{2,1}$ comes from the fact that $I_1^* = \{2, 2, 2\}$, since $n = 3$ but the vertical street has length 1.

For the third horizontal street, corresponding to $\mathbf{u}_3$, highlighted in the picture on the left in Figure 7.2.3, we have $J_3^* = \{2, 3, 4\}$, and a similar argument gives

$$\begin{aligned}(M-I)\mathbf{u}_3 &= (M-I)[\{\uparrow_{1,2}, \uparrow_{1,3}, \uparrow_{1,4}\}] + (M-I)[\{\uparrow_{2,2}, \uparrow_{2,4}\}] \\ &\quad + (M-I)[\{\uparrow_{3,2}, \uparrow_{3,3}, \uparrow_{3,4}\}] + (M-I)[\{\uparrow_{4,3}\}] \\ &= 3(\mathbf{u}_1 + \mathbf{v}_1) + 2(\mathbf{u}_2 + \mathbf{v}_2) + 3(\mathbf{u}_3 + \mathbf{v}_3) + (\mathbf{u}_4 + \mathbf{v}_4). \end{aligned} \tag{7.2.25}$$

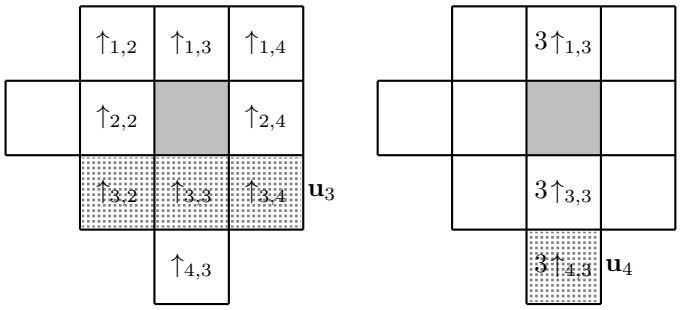

Figure 7.2.3: S_2 with $m = n = 3$: almost vertical units of type $\uparrow$ in $\mathbf{u}_3, \mathbf{u}_4$

For the fourth horizontal street, corresponding to $\mathbf{u}_4$, highlighted in the picture on the right in Figure 7.2.3, we have $J_4^* = \{3, 3, 3\}$, and a similar argument gives

$$\begin{aligned}(M-I)\mathbf{u}_4 &= (M-I)[\{\uparrow_{1,3}, \uparrow_{1,3}, \uparrow_{1,3}\}] + (M-I)[\{\uparrow_{3,3}, \uparrow_{3,3}, \uparrow_{3,3}\}] \\ &\quad + (M-I)[\{\uparrow_{4,3}, \uparrow_{4,3}, \uparrow_{4,3}\}] \\ &= 3(\mathbf{u}_1 + \mathbf{v}_1) + 3(\mathbf{u}_3 + \mathbf{v}_3) + 3(\mathbf{u}_4 + \mathbf{v}_4). \end{aligned} \tag{7.2.26}$$

We now define the street-spreading matrix by

$$\mathbf{S} = \begin{pmatrix} 3 & 2 & 3 & 3 \\ 2 & 5 & 2 & 0 \\ 3 & 2 & 3 & 3 \\ 1 & 0 & 1 & 3 \end{pmatrix}, \tag{7.2.27}$$

where the j-th column comes from the coefficients of $(\mathbf{u}_i + \mathbf{v}_i)$, $i = 1, 2, 3, 4$, in the expression for $(M-I)\mathbf{u}_j$, $j = 1, 2, 3, 4$, as given by (7.2.23)–(7.2.26).

Combining (7.2.22) and (7.2.23)–(7.2.26), we obtain

$$\begin{aligned} M\mathbf{u}_1 &= 3(\mathbf{u}_1 + \mathbf{v}_1) + 2(\mathbf{u}_2 + \mathbf{v}_2) + 3(\mathbf{u}_3 + \mathbf{v}_3) + (\mathbf{u}_4 + \mathbf{v}_4) + \mathbf{u}_1, \\ M\mathbf{u}_2 &= 2(\mathbf{u}_1 + \mathbf{v}_1) + 5(\mathbf{u}_2 + \mathbf{v}_2) + 2(\mathbf{u}_3 + \mathbf{v}_3) + \mathbf{u}_2, \\ M\mathbf{u}_3 &= 3(\mathbf{u}_1 + \mathbf{v}_1) + 2(\mathbf{u}_2 + \mathbf{v}_2) + 3(\mathbf{u}_3 + \mathbf{v}_3) + (\mathbf{u}_4 + \mathbf{v}_4) + \mathbf{u}_3, \\ M\mathbf{u}_4 &= 3(\mathbf{u}_1 + \mathbf{v}_1) + 3(\mathbf{u}_3 + \mathbf{v}_3) + 3(\mathbf{u}_4 + \mathbf{v}_4) + \mathbf{u}_4, \\ M\mathbf{v}_1 &= \mathbf{u}_1 + \mathbf{v}_1, \\ M\mathbf{v}_2 &= \mathbf{u}_2 + \mathbf{v}_2, \\ M\mathbf{v}_3 &= \mathbf{u}_3 + \mathbf{v}_3, \\ M\mathbf{v}_4 &= \mathbf{u}_4 + \mathbf{v}_4. \end{aligned}$$

For any $\mathbf{w} \in \mathcal{V}$, if we write

$$\mathbf{w} = a_1\mathbf{u}_1 + a_2\mathbf{u}_2 + a_3\mathbf{u}_3 + a_4\mathbf{u}_4 + b_1\mathbf{v}_1 + b_2\mathbf{v}_2 + b_3\mathbf{v}_3 + b_4\mathbf{v}_4,$$

and

$$M\mathbf{w} = c_1\mathbf{u}_1 + c_2\mathbf{u}_2 + c_3\mathbf{u}_3 + c_4\mathbf{u}_4 + d_1\mathbf{v}_1 + d_2\mathbf{v}_2 + d_3\mathbf{v}_3 + d_4\mathbf{v}_4,$$

then

$$\begin{pmatrix} c_1 \\ c_2 \\ c_3 \\ c_4 \\ d_1 \\ d_2 \\ d_3 \\ d_4 \end{pmatrix} = \begin{pmatrix} 4 & 2 & 3 & 3 & 1 & 0 & 0 & 0 \\ 2 & 6 & 2 & 0 & 0 & 1 & 0 & 0 \\ 3 & 2 & 4 & 3 & 0 & 0 & 1 & 0 \\ 1 & 0 & 1 & 4 & 0 & 0 & 0 & 1 \\ 3 & 2 & 3 & 3 & 1 & 0 & 0 & 0 \\ 2 & 5 & 2 & 0 & 0 & 1 & 0 & 0 \\ 3 & 2 & 3 & 3 & 0 & 0 & 1 & 0 \\ 1 & 0 & 1 & 3 & 0 & 0 & 0 & 1 \end{pmatrix} \begin{pmatrix} a_1 \\ a_2 \\ a_3 \\ a_4 \\ b_1 \\ b_2 \\ b_3 \\ b_4 \end{pmatrix},$$

so the 8×8 matrix in question is

$$M|_{\mathcal{V}} = \begin{pmatrix} \mathbf{S} + I & I \\ \mathbf{S} & I \end{pmatrix}.$$

We shall return to this example later.

Example 7.2.2. Consider the polysquare surface S_3, given in Figure 7.2.4.

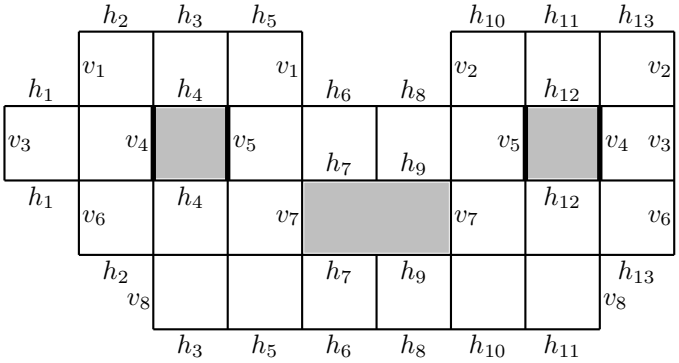

Figure 7.2.4: S_3 with edge pairings

This has 6 horizontal streets of lengths $3, 3, 3, 4, 6, 6$, and 9 vertical streets of lengths $1, 3, 3, 4, 2, 2, 4, 3, 3$, as illustrated in Figure 7.2.5 where, for instance, $\leftrightarrow 4$ and $\updownarrow 6$ in a square face indicates that this square face is part of the 4-th horizontal street and the 6-th vertical street.

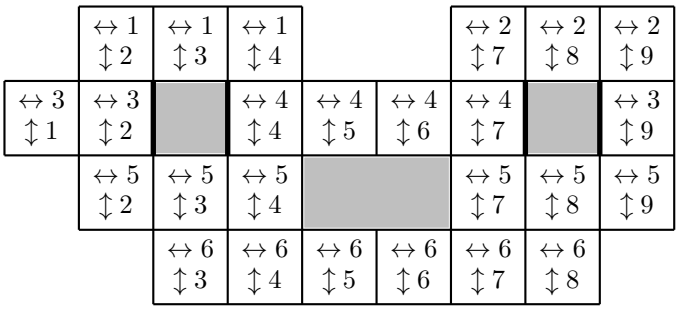

Figure 7.2.5: the horizontal and vertical streets of S_3

Consider a 1-direction geodesic starting from some vertex of the polysquare surface S_3 with slope α given by (7.2.1) with $m = n = 12$.

The polysquare surface S_3 has 25 square faces, so any 2-step transition matrix M has size 50×50, making it an onerous task to find any eigenvalue, even with the help of MATLAB. It is clearly much simpler to find the 6×6 street-spreading matrix.

First of all, we define the vectors $\mathbf{u}_i, \mathbf{v}_i$, $i = 1, 2, 3, 4, 5, 6$, according to (7.2.14) and (7.2.15).

Consider the horizontal street corresponding to $\mathbf{u}_1$, as highlighted in the left half of Figure 7.2.6. We see that

$$J_1 = \{2, 3, 4\} \quad \text{and} \quad J_1^* = \{2, 2, 2, 2, 3, 3, 3, 3, 4, 4, 4, 4\},$$

since $m = 12$, and $\mathbf{u}_1$ concerns almost vertical units on the vertical streets $2, 3, 4$. In other words, we start with the first horizontal street, and spread along every vertical street that intersects this horizontal street. The left half of Figure 7.2.6 shows a listing of all the almost vertical units of type $\uparrow$ along these vertical streets. Applying (7.2.17), we have

$$\begin{aligned}(M-I)\mathbf{u}_1 &= (M-I)[\{16\uparrow_{1,2}, 16\uparrow_{1,3}, 12\uparrow_{1,4}\}] \\ &\quad + (M-I)[\{16\uparrow_{3,2}\}] + (M-I)[\{12\uparrow_{4,4}\}] \\ &\quad + (M-I)[\{16\uparrow_{5,2}, 16\uparrow_{5,3}, 12\uparrow_{5,4}\}] + (M-I)[\{16\uparrow_{6,3}, 12\uparrow_{6,4}\}] \\ &= 44(\mathbf{u}_1+\mathbf{v}_1) + 16(\mathbf{u}_3+\mathbf{v}_3) + 12(\mathbf{u}_4+\mathbf{v}_4) \\ &\quad + 44(\mathbf{u}_5+\mathbf{v}_5) + 28(\mathbf{u}_6+\mathbf{v}_6). \end{aligned} \tag{7.2.28}$$

We need to explain the multiples in Figure 7.2.6. Observe the horizontal street corresponding to $\mathbf{u}_1$ consists of 3 square faces. As $m = 12$, the correct multiplicity is $12/3 = 4$. On the other hand, the vertical street containing the square face $S_{1,4}$ consists of 4 square faces. As $n = 12$, the correct multiplicity is $12/4 = 3$. Thus the multiple for that square face is 3×4.

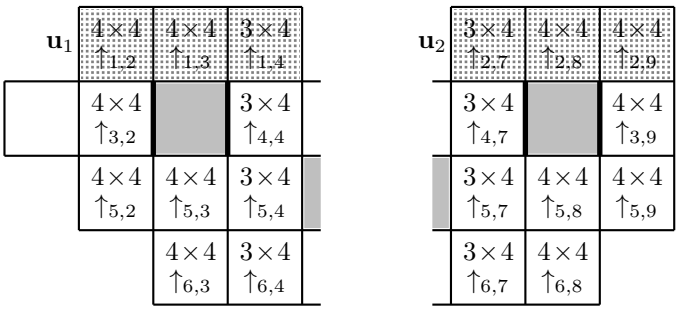

Figure 7.2.6: S_3 with $m = n = 12$: almost vertical units of type $\uparrow$ in $\mathbf{u}_1, \mathbf{u}_2$

Remark. We always have $|I_j^*| = n$ for every $j = 1, \ldots, v$, and $|J_i^*| = m$ for every $i = 1, \ldots, h$. The first of these corresponds to the fact that every almost vertical detour crossing of V_0 travels a vertical distance between n and $n+1$. The second of these corresponds to the fact that every almost horizontal detour crossing of H_0 travels a horizontal distance between m and $m+1$.

With $J_2^* = \{7, 7, 7, 7, 8, 8, 8, 8, 9, 9, 9, 9\}$, for the horizontal street corresponding to $\mathbf{u}_2$, as highlighted in the right half of Figure 7.2.6, a similar argument gives

$$\begin{aligned}(M-I)\mathbf{u}_2 &= 44(\mathbf{u}_2+\mathbf{v}_2) + 16(\mathbf{u}_3+\mathbf{v}_3) + 12(\mathbf{u}_4+\mathbf{v}_4) \\ &\quad + 44(\mathbf{u}_5+\mathbf{v}_5) + 28(\mathbf{u}_6+\mathbf{v}_6). \end{aligned} \tag{7.2.29}$$

With $J_3^* = \{1, 1, 1, 1, 2, 2, 2, 2, 9, 9, 9, 9\}$, for the horizontal street corresponding to $\mathbf{u}_3$, as highlighted in Figure 7.2.7, a similar argument gives

$$(M-I)\mathbf{u}_3 = 16(\mathbf{u}_1+\mathbf{v}_1) + 16(\mathbf{u}_2+\mathbf{v}_2) + 80(\mathbf{u}_3+\mathbf{v}_3) + 32(\mathbf{u}_5+\mathbf{v}_5). \tag{7.2.30}$$

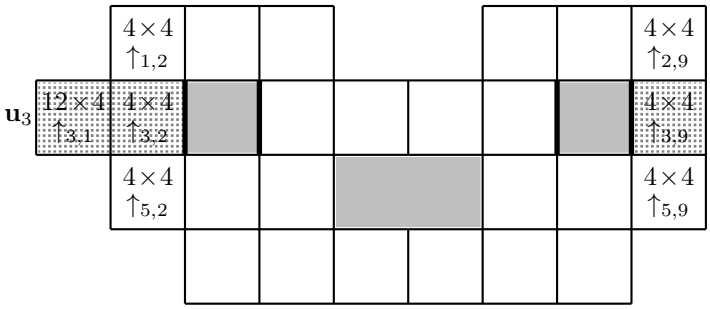

Figure 7.2.7: S_3 with $m = n = 12$: almost vertical units of type $\uparrow$ in $\mathbf{u}_3$

With $J_4^* = \{4, 4, 4, 5, 5, 5, 6, 6, 6, 7, 7, 7\}$, for the horizontal street corresponding to $\mathbf{u}_4$, as highlighted in Figure 7.2.8, a similar argument gives

$$(M - I)\mathbf{u}_4 = 9(\mathbf{u}_1 + \mathbf{v}_1) + 9(\mathbf{u}_2 + \mathbf{v}_2) + 54(\mathbf{u}_4 + \mathbf{v}_4) + 18(\mathbf{u}_5 + \mathbf{v}_5) + 54(\mathbf{u}_6 + \mathbf{v}_6). \tag{7.2.31}$$

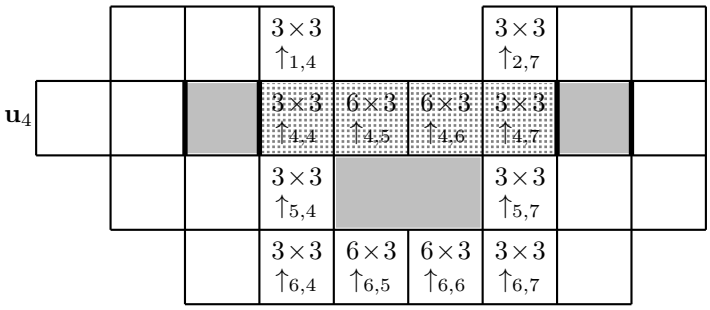

Figure 7.2.8: S_3 with $m = n = 12$: almost vertical units of type $\uparrow$ in $\mathbf{u}_4$

With $J_5^* = \{2, 2, 3, 3, 4, 4, 7, 7, 8, 8, 9, 9\}$, for the horizontal street corresponding to $\mathbf{u}_5$, as highlighted in Figure 7.2.9, a similar argument gives

$$(M - I)\mathbf{u}_5 = 22(\mathbf{u}_1 + \mathbf{v}_1) + 22(\mathbf{u}_2 + \mathbf{v}_2) + 16(\mathbf{u}_3 + \mathbf{v}_3) + 12(\mathbf{u}_4 + \mathbf{v}_4) + 44(\mathbf{u}_5 + \mathbf{v}_5) + 28(\mathbf{u}_6 + \mathbf{v}_6). \tag{7.2.32}$$

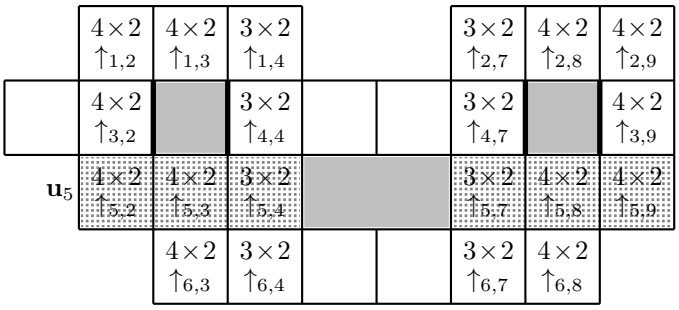

Figure 7.2.9: S_3 with $m = n = 12$: almost vertical units of type $\uparrow$ in $\mathbf{u}_5$

With $J_6^* = \{3, 3, 4, 4, 5, 5, 6, 6, 7, 7, 8, 8\}$, for the horizontal street corresponding to $\mathbf{u}_6$, as highlighted in Figure 7.2.10, a similar argument gives

$$(M - I)\mathbf{u}_6 = 14(\mathbf{u}_1 + \mathbf{v}_1) + 14(\mathbf{u}_2 + \mathbf{v}_2) + 36(\mathbf{u}_4 + \mathbf{v}_4) + 28(\mathbf{u}_5 + \mathbf{v}_5) + 52(\mathbf{u}_6 + \mathbf{v}_6). \tag{7.2.33}$$

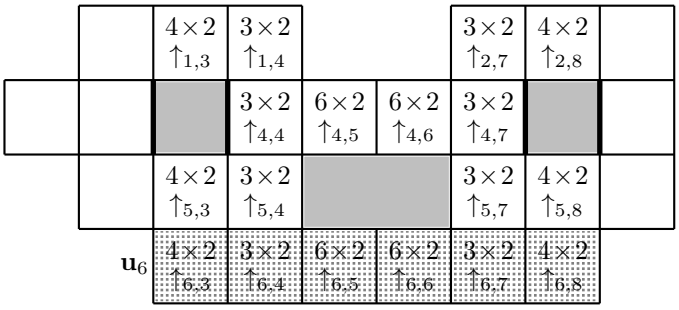

Figure 7.2.10: S_3 with $m = n = 12$: almost vertical units of type $\uparrow$ in $\mathbf{u}_6$

We now define the street-spreading matrix by

$$\mathbf{S} = \begin{pmatrix} 44 & 0 & 16 & 9 & 22 & 14 \\ 0 & 44 & 16 & 9 & 22 & 14 \\ 16 & 16 & 80 & 0 & 16 & 0 \\ 12 & 12 & 0 & 54 & 12 & 36 \\ 44 & 44 & 32 & 18 & 44 & 28 \\ 28 & 28 & 0 & 54 & 28 & 52 \end{pmatrix},$$

where the j-th column comes from the coefficients of $(\mathbf{u}_i + \mathbf{v}_i)$, $i = 1, 2, 3, 4, 5, 6$, in the expression for $(M - I)\mathbf{u}_j$, $j = 1, 2, 3, 4, 5, 6$, as given by (7.2.28)–(7.2.33).

Theorem 7.2.2. *Let $\mathcal{P}$ be a finite polysquare surface with d square faces. Assume that $h \leqslant v$, where h is the number of horizontal streets in $\mathcal{P}$ and v is the number of vertical streets in $\mathcal{P}$. Let m be any fixed integer multiple of the lengths of the horizontal streets of $\mathcal{P}$, and let n be any fixed integer multiple of the lengths of the vertical streets of $\mathcal{P}$.*

Consider a 1-direction almost vertical geodesic V_0 on $\mathcal{P}$, with slope α given by (7.2.1)*. Let M denote the transition matrix of the 2-step ancestor process with respect to the basis $\mathscr{W}$, where $\mathscr{W}$ is given by* (7.2.2) *. Then all the relevant eigenvalues of M and their corresponding eigenvectors can be determined as follows:*

(i) *Let $\mathcal{V}$ denote the subspace of $\mathbb{C}^{2d}$ generated by $\mathbf{u}_i, \mathbf{v}_i$, $i = 1, \ldots, h$, given by* (7.2.14) *and* (7.2.15)*. Then $\mathcal{V}$ in an M-invariant subspace of $\mathbb{C}^{2d}$, and contains the eigenvectors corresponding to all the relevant eigenvalues of M. Furthermore, there exist non-negative integers $s_{i,j}$, $i, j = 1, \ldots, h$, such that for every $j = 1, \ldots, h$,*

$$(M - I)\mathbf{u}_j = \sum_{i=1}^{h} s_{i,j}(\mathbf{u}_i + \mathbf{v}_i), \tag{7.2.34}$$

and

$$M\mathbf{v}_j = \mathbf{u}_j + \mathbf{v}_j. \tag{7.2.35}$$

(ii) *Consider the street-spreading matrix*

$$\mathbf{S} = \begin{pmatrix} s_{1,1} & \cdots & s_{1,h} \\ \vdots & & \vdots \\ s_{h,1} & \cdots & s_{h,h} \end{pmatrix}, \tag{7.2.36}$$

as well as the matrix

$$M|_{\mathcal{V}} = \begin{pmatrix} \mathbf{S} + I & I \\ \mathbf{S} & I \end{pmatrix}. \tag{7.2.37}$$

Suppose that τ is an eigenvalue of $\mathbf{S}$ with eigenvector ψ, so that $\mathbf{S}\psi = \tau\psi$. Then

$$\lambda(\tau; \pm) = 1 + \frac{\tau \pm \sqrt{\tau^2 + 4\tau}}{2} \tag{7.2.38}$$

are two eigenvalues of $M|_{\mathcal{V}}$ with product equal to 1*, with corresponding eigenvectors*

$$\Psi(\tau;\pm) = \left(\psi, \frac{-\tau \pm \sqrt{\tau^2+4\tau}}{2}\psi\right)^T \in \mathbb{C}^{2h}. \tag{7.2.39}$$

In particular, the h eigenvalues of $\mathbf{S}$ give rise to $2h$ eigenvalues of $M|_{\mathcal{V}}$.

(iii) *If $\Psi(\tau;\pm) = (a_1, a_2, a_3, a_4, b_1, b_2, b_3, b_4)^T$ is an eigenvector corresponding to an eigenvalue $\lambda(\tau;\pm)$ of $M|_{\mathcal{V}}$, then $\lambda(\tau;\pm)$ is an eigenvalue of M with eigenvector*

$$\mathbf{w} = \sum_{i=1}^{h} a_i \mathbf{u}_i + \sum_{i=1}^{h} b_i \mathbf{v}_i. \tag{7.2.40}$$

Remark. The assumption that the number $h = h(\mathcal{P})$ of horizontal streets is less than or equal to the number $v = v(\mathcal{P})$ of vertical streets, *i.e.*, $h \leqslant v$, is one for convenience, as the street-spreading matrix is smaller. For any polysquare surface $\mathcal{P}$ where $h \geqslant v$, we can always interchange the horizontal and vertical directions.

Proof of Theorem 7.2.2. (i) In view of Lemma 7.2.3, it remains to establish (7.2.34) and (7.2.35). For (7.2.34), note from (7.2.14) that each $\mathbf{u}_j$ involves only units of type $\uparrow$, and so (7.2.34) follows immediately from (7.2.17), on observing that $\mathbf{u}_i, \mathbf{v}_i$, $i = 1, \ldots, h$, generate $\mathcal{V}$. On the other hand, (7.2.35) follows immediately from (7.2.21).

(ii) Suppose that Ψ is a column eigenvector corresponding to an eigenvalue λ of $M|_{\mathcal{V}}$. From (7.2.37), it is clear that $M|_{\mathcal{V}}$ can be reduced to the matrix

$$\begin{pmatrix} I & 0 \\ \mathbf{S} & I \end{pmatrix}$$

by elementary row operations. The determinant of this matrix is clearly equal to 1. It follows that $\det(M|_{\mathcal{V}}) = 1$, and so $\lambda \neq 0$. We can write

$$\Psi = (\psi, \psi^*)^T, \tag{7.2.41}$$

where ψ and ψ^* are both column vectors with h entries. Then

$$M|_{\mathcal{V}}\Psi = \begin{pmatrix} \mathbf{S}+I & I \\ \mathbf{S} & I \end{pmatrix} \begin{pmatrix} \psi \\ \psi^* \end{pmatrix} = \lambda \begin{pmatrix} \psi \\ \psi^* \end{pmatrix},$$

and so

$$\begin{aligned} \mathbf{S}\psi + \psi + \psi^* &= \lambda\psi, \\ \mathbf{S}\psi + \psi^* &= \lambda\psi^*. \end{aligned} \tag{7.2.42}$$

Subtracting the second equation in (7.2.42) from the first, we obtain $\psi = \lambda(\psi - \psi^*)$, and so

$$\psi^* = \frac{\lambda - 1}{\lambda}\psi. \tag{7.2.43}$$

Substituting this into the first equation in (7.2.42), we obtain

$$\mathbf{S}\psi = \left(\lambda - \frac{2\lambda - 1}{\lambda}\right)\psi,$$

so that

$$\tau = \lambda - \frac{2\lambda - 1}{\lambda}$$

is an eigenvalue of $\mathbf{S}$ with eigenvector ψ. This is equivalent to

$$\lambda = 1 + \frac{\tau \pm \sqrt{\tau^2+4\tau}}{2}. \tag{7.2.44}$$

This proves that any eigenvalue λ of $M|_{\mathcal{V}}$ is obtained from an eigenvalue τ of $\mathbf{S}$ by (7.2.44), and establishes (7.2.38). Finally, note that

$$\frac{\lambda-1}{\lambda} = 1 - \frac{1}{\lambda} = 1 - \left(1 + \frac{\tau \mp \sqrt{\tau^2+4\tau}}{2}\right) = \frac{-\tau \pm \sqrt{\tau^2+4\tau}}{2}.$$

In view of (7.2.41) and (7.2.43), this establishes (7.2.39).

(iii) Suppose that $(a_1, \ldots, a_h, b_1, \ldots, b_h)^T$ is an eigenvector corresponding to an eigenvalue λ of $M|_{\mathcal{V}}$. Let the vector $\mathbf{w}$ be given by (7.2.40). Then

$$M\mathbf{w} = \sum_{i=1}^{h} c_i \mathbf{u}_i + \sum_{i=1}^{h} d_i \mathbf{v}_i, \tag{7.2.45}$$

where the coefficients are related by

$$(c_1, \ldots, c_h, d_1, \ldots, d_h)^T = M|_{\mathcal{V}}(a_1, \ldots, a_h, b_1, \ldots, b_h)^T.$$

It is clear that

$$(c_1, \ldots, c_h, d_1, \ldots, d_h)^T = \lambda(a_1, \ldots, a_h, b_1, \ldots, b_h)^T,$$

and so it follows from (7.2.40) and (7.2.45) that $M\mathbf{w} = \lambda\mathbf{w}$, so that λ is an eigenvalue of M with eigenvector $\mathbf{w}$. □

Continuation of Example 7.2.1. Recall from (7.1.6), (7.1.8) and (7.1.10) that the relevant eigenvalues of $M(S_2)$ are

$$\lambda_1 = \frac{11+3\sqrt{13}}{2}, \quad \lambda_2 = 3+2\sqrt{2}, \quad \lambda_3 = \frac{3+\sqrt{5}}{2},$$

obtained by tedious calculation using MATLAB. Let us instead retrieve the same information using the street-spreading matrix $\mathbf{S}$ given by (7.2.27).

The eigenvalues of $\mathbf{S}$ are $\tau_1 = 9$, $\tau_2 = 4$, $\tau_3 = 1$ and $\tau_4 = 0$. Using (7.2.38), the corresponding eigenvalues of M are

$$\lambda(9;\pm) = \frac{11 \pm 3\sqrt{13}}{2}, \quad \lambda(4;\pm) = 3 \pm 2\sqrt{2}, \quad \lambda(1;\pm) = \frac{3 \pm \sqrt{5}}{2}, \quad \lambda(0;\pm) = 1.$$

Note that in view of Lemma 7.2.3, $\lambda(9;\pm)$, $\lambda(4;\pm)$ and $\lambda(1;\pm)$ are the only eigenvalues of M that are not equal to 1. Thus the multiplicity of the eigenvalue 1 is 14, as we have claimed earlier in the Remark following (7.2.8).

Example 7.2.3. Consider again the L-surface, given in Figure 7.1.6, and consider a 1-direction geodesic starting from some vertex of the L-surface with slope α given by (7.2.1) with $m = n = 2$. It is easy to see from Figure 7.2.11 that

$$(M-I)\mathbf{u}_1 = 2(\mathbf{u}_1 + \mathbf{v}_1) + 2(\mathbf{u}_2 + \mathbf{v}_2), \tag{7.2.46}$$

$$(M-I)\mathbf{u}_2 = (\mathbf{u}_1 + \mathbf{v}_1) + 3(\mathbf{u}_2 + \mathbf{v}_2). \tag{7.2.47}$$

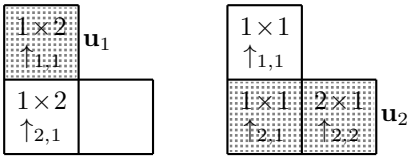

Figure 7.2.11: L-surface with $m = n = 2$: almost vertical units of type $\uparrow$ in $\mathbf{u}_1, \mathbf{u}_2$

It follows from (7.2.46)–(7.2.47) that the street-spreading matrix is given by

$$\mathbf{S} = \begin{pmatrix} 2 & 1 \\ 2 & 3 \end{pmatrix},$$

with eigenvalues $\tau_1 = 4$ and $\tau_2 = 1$. Using (7.2.38) leads to the eigenvalues

$$\lambda(4;\pm) = 3 \pm 2\sqrt{2} \quad \text{and} \quad \lambda(1;\pm) = \frac{3 \pm \sqrt{5}}{2},$$

including those given in (7.1.24) with absolute values greater than 1.

Example 7.2.4. It is not difficult to show that geodesic flow on the surface of the unit cube is equivalent to 1-direction geodesic flow on the polysquare surface $\mathcal{P}$ as shown in Figure 7.2.12 that represents the 4-copy version of the cube surface.

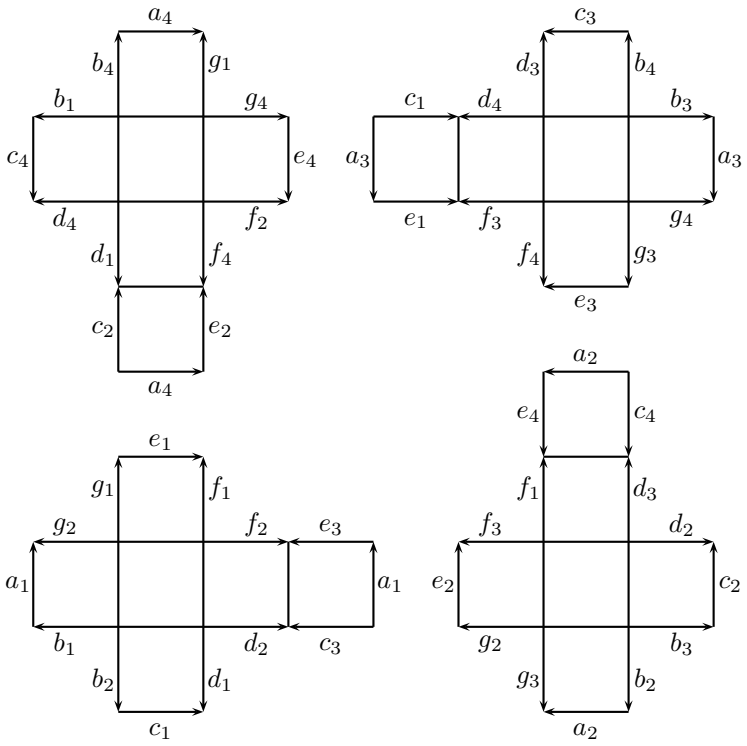

Figure 7.2.12: 4-copy version of the surface of the unit cube

Note that $\mathcal{P}$ has 6 horizontal streets and 6 vertical streets, all of length 4, as shown in Figure 7.2.13, where, for instance, $\leftrightarrow 4$ and $\updownarrow 6$ in a square face indicates that this square face is part of the 4-th horizontal street and 6-th vertical street.

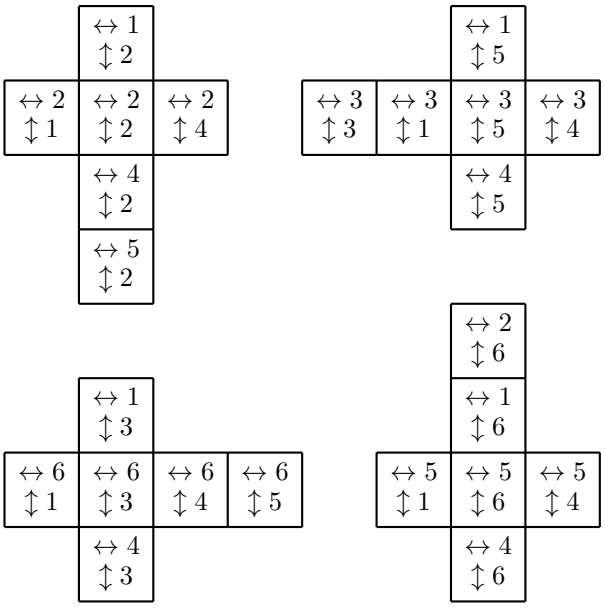

Figure 7.2.13: 4-copy version of the surface of the unit cube

Figures 7.2.12 and 7.2.13 are not very convenient for us to visualize the horizontal and vertical streets clearly. We can re-draw these two figures, and attempt to arrange the square faces in an array where each row represents a horizontal street and each column represents a vertical street. In Figure 7.2.14, we do precisely this, where for $i, j = 1, \ldots, 6$, the i-th row represents the i-th horizontal street and the j-th column represents the j-th vertical street as shown in Figure 7.2.13. Note that this exercise is somewhat cumbersome and requires very careful edge identifications as illustrated. We include the details here for the sake of completeness, and comment that the edge identifications are not required in the process for the determination of the street-spreading matrix.

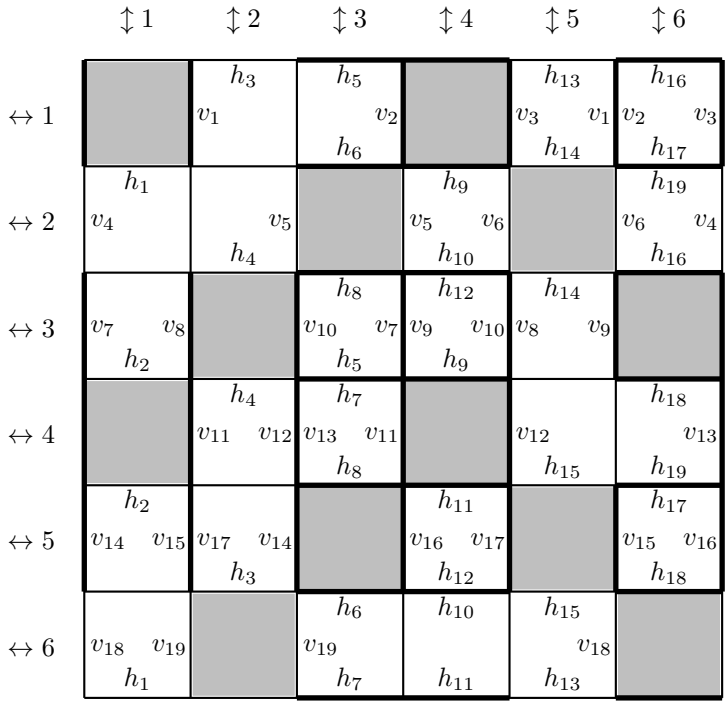

Figure 7.2.14: 4-copy version of the surface of the unit cube with square faces arranged in an array

Consider now a 1-direction geodesic on the polysquare surface $\mathcal{P}$ starting from some vertex of $\mathcal{P}$ with slope α given by (7.2.1) with $m = n = 4$.

The polysquare surface $\mathcal{P}$ has 24 square faces, so any 2-step transition matrix M has size 48×48. It is much simpler to find the 6×6 street-spreading matrix.

As before, we define the matrices $\mathbf{u}_i, \mathbf{v}_i$, $i = 1, \ldots, 6$, according to (7.2.14) and (7.2.15).

Consider the horizontal street corresponding to $\mathbf{u}_1$, and also the horizontal street corresponding to $\mathbf{u}_4$, as highlighted in the picture on the left in Figure 7.2.15. We see that $J_1^* = J_4^* = \{2, 3, 5, 6\}$, and both $\mathbf{u}_1$ and $\mathbf{u}_4$ concern almost vertical units on the vertical streets $2, 3, 5, 6$. Applying (7.2.17), we have

$$\begin{aligned}
(M-I)\mathbf{u}_1 &= (M-I)\mathbf{u}_4 \\
&= (M-I)[\{\uparrow_{1,2}, \uparrow_{1,3}, \uparrow_{1,5}, \uparrow_{1,6}\}] + (M-I)[\{\uparrow_{2,2}, \uparrow_{2,6}\}] \\
&\quad + (M-I)[\{\uparrow_{3,3}, \uparrow_{3,5}\}] + (M-I)[\{\uparrow_{4,2}, \uparrow_{4,3}, \uparrow_{4,5}, \uparrow_{4,6}\}] \\
&\quad + (M-I)[\{\uparrow_{5,2}, \uparrow_{5,6}\}] + (M-I)[\{\uparrow_{6,3}, \uparrow_{6,5}\}] \\
&= 4(\mathbf{u}_1 + \mathbf{v}_1) + 2(\mathbf{u}_2 + \mathbf{v}_2) + 2(\mathbf{u}_3 + \mathbf{v}_3) \\
&\quad + 4(\mathbf{u}_4 + \mathbf{v}_4) + 2(\mathbf{u}_5 + \mathbf{v}_5) + 2(\mathbf{u}_6 + \mathbf{v}_6). \qquad (7.2.48)
\end{aligned}$$

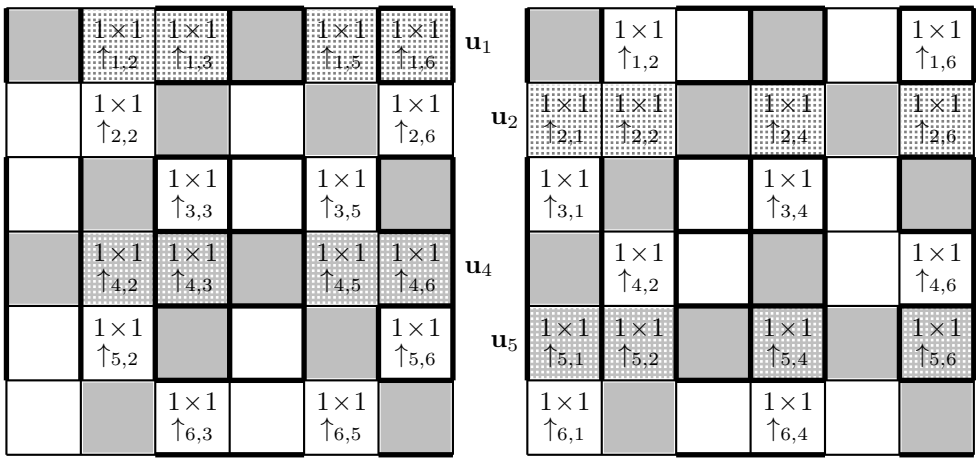

Figure 7.2.15: $\mathcal{P}$ with $m = n = 4$: almost vertical units of type $\uparrow$ in $\mathbf{u}_1\mathbf{u}_2, \mathbf{u}_4, \mathbf{u}_5$

With $J_2^* = J_5^* = \{1, 2, 4, 6\}$, for the horizontal street corresponding to $\mathbf{u}_2$, and also the horizontal street corresponding to $\mathbf{u}_5$, as highlighted in the picture on the right in Figure 7.2.15, a similar argument gives

$$\begin{aligned}(M - I)\mathbf{u}_2 &= (M - I)\mathbf{u}_5 \\ &= 2(\mathbf{u}_1 + \mathbf{v}_1) + 4(\mathbf{u}_2 + \mathbf{v}_2) + 2(\mathbf{u}_3 + \mathbf{v}_3) \\ &\quad + 2(\mathbf{u}_4 + \mathbf{v}_4) + 4(\mathbf{u}_5 + \mathbf{v}_5) + 2(\mathbf{u}_6 + \mathbf{v}_6). \end{aligned} \tag{7.2.49}$$

With $J_3^* = J_6^* = \{1, 3, 4, 5\}$, for the horizontal street corresponding to $\mathbf{u}_3$, and also the horizontal street corresponding to $\mathbf{u}_6$, as highlighted in Figure 7.2.16, a similar argument gives

$$\begin{aligned}(M - I)\mathbf{u}_3 &= (M - I)\mathbf{u}_6 \\ &= 2(\mathbf{u}_1 + \mathbf{v}_1) + 2(\mathbf{u}_2 + \mathbf{v}_2) + 4(\mathbf{u}_3 + \mathbf{v}_3) \\ &\quad + 2(\mathbf{u}_4 + \mathbf{v}_4) + 2(\mathbf{u}_5 + \mathbf{v}_5) + 4(\mathbf{u}_6 + \mathbf{v}_6). \end{aligned} \tag{7.2.50}$$

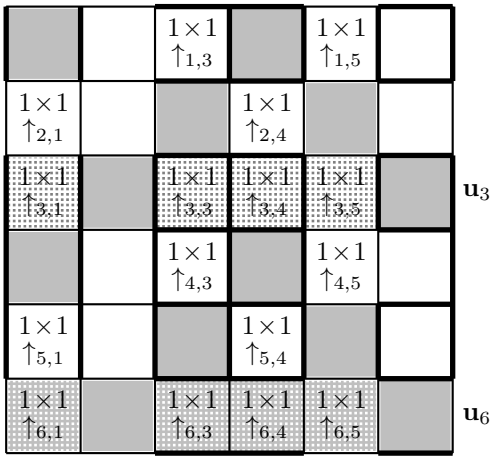

Figure 7.2.16: $\mathcal{P}$ with $m = n = 4$: almost vertical units of type $\uparrow$ in $\mathbf{u}_3, \mathbf{u}_6$

It follows from (7.2.48)–(7.2.50) that the street-spreading matrix is given by

$$\mathbf{S} = \begin{pmatrix} 4 & 2 & 2 & 4 & 2 & 2 \\ 2 & 4 & 2 & 2 & 4 & 2 \\ 2 & 2 & 4 & 2 & 2 & 4 \\ 4 & 2 & 2 & 4 & 2 & 2 \\ 2 & 4 & 2 & 2 & 4 & 2 \\ 2 & 2 & 4 & 2 & 2 & 4 \end{pmatrix},$$

with eigenvalues $\tau_1 = 16$, $\tau_2 = \tau_3 = 4$ and $\tau_4 = \tau_5 = \tau_6 = 0$. Using (7.2.38), the corresponding eigenvalues of M are

$$\lambda(16;\pm) = 9 \pm 4\sqrt{5}, \quad \lambda(4;\pm) = 3 \pm 2\sqrt{2}, \quad \lambda(0;\pm) = 1,$$

with the appropriate multiplicities. The two largest eigenvalues of M are therefore

$$\lambda_1 = 9 + 4\sqrt{5} = (2+\sqrt{5})^2 \quad \text{and} \quad \lambda_2 = 3 + 2\sqrt{2} = (1+\sqrt{2})^2.$$

Furthermore, the multiplicity of the eigenvalue 1 is 42.

Note that

$$2 + \sqrt{5} = [4; 4, 4, 4, \ldots] \quad \text{and} \quad 1 + \sqrt{2} = [2; 2, 2, 2, \ldots]$$

exhibit "digit-halving" in their continued fraction expansions, and are also the two largest eigenvalues of the 1-step transition matrix of a 1-direction geodesic of slope $\alpha = 2 + \sqrt{5}$ on the L-surface; see Section 4.1 in [3].

We comment that digit-halving is still exhibited if α is defined by (7.2.1) with $m = n = 4k$ for any positive integers k. In this general case, the largest eigenvalue is the square of $[4k; 4k, 4k, 4k, \ldots]$, and the second largest eigenvalue is the square of $[2k; 2k, 2k, 2k, \ldots]$.

We complete this section by considering two consequences of Theorem 7.2.2. The first one is fairly straightforward.

Corollary 7.2.1. *The determinant of the* 2*-step transition matrix* M *is equal to* 1.

Proof. We have shown earlier that $\det(M|_{\mathcal{V}}) = 1$.

Let $p(x)$ be the characteristic polynomial of $M|_{\mathcal{V}}$. In view of Theorem 7.2.2, it is clear that the characteristic polynomial of M is equal to $p(x)q(x)$, where $q(x)$ has degree $2d - 2h$ and its roots are all the eigenvalues of M that are not eigenvalues of $M|_{\mathcal{V}}$. In view of Lemma 7.2.3, we have $q(x) = (x-1)^{2d-2h}$. On the other hand, it follows from (7.2.38) that

$$p(x) = \prod_{i=1}^{h} (x - \lambda(\tau_i;+))(x - \lambda(\tau_i;-)),$$

where $\tau_1, \ldots, \tau_h$ are the eigenvalues of $\mathbf{S}$, and $\lambda(\tau_i;+)\lambda(\tau_i;-) = 1$, $i = 1, \ldots, h$.

Clearly the determinant of M is equal to $p(0)q(0) = 1$. □

To motivate the second consequence, we start with the L-surface, and obtain a new polysquare surface with 6 smaller square faces, each of area 1/2. The trick is to draw two diagonals on each of the 3 square faces of the L-surface. We use the boundary pairing in the picture on the right in Figure 7.2.17, which gives the so-called *diagonal subdivision surface* of the L-surface, or DS-L-surface. Of course the genus remains the same; namely, 2. Rotating this picture on the right anticlockwise by 45 degrees and resizing, the DS-L-surface becomes a polysquare surface in the standard horizontal-vertical position. It is easy to see that the DS-L-surface has only one horizontal street, which has length 6 and is defined by the cycle $1, 2, 3, 4, 6, 5$. It also has only one vertical street, defined by the cycle $1, 5, 6, 2, 3, 4$. So the street size multiple of the DS-L-surface is equal to 6.

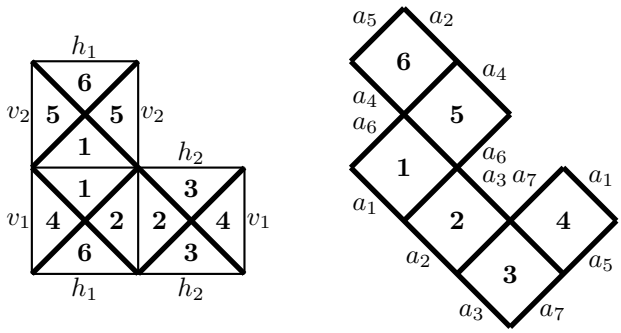

Figure 7.2.17: L-surface and DS-L-surface

Now Theorem 5.5.1 in [3] says that, applying the surplus shortline method to this particular *one-street surface*, we obtain infinitely many explicit slopes with the property that a 1-direction geodesic with any such slope is *superuniform*.

Theorem 5.5.1 is obtained by using Theorem 5.3.1 in [3], the main result for the L-surface in that paper, with an exceptionally long proof. So the mysterious connection between a concrete one-street surface and superuniformity in Theorem 5.5.1 may seem at first sight a very deep, perhaps accidental result. However, nothing is further from the truth. There is a general connection between one-street surfaces and superuniformity, and it is an easy consequence of Theorem 7.2.2. Indeed, we simply need the condition that the polysquare surface has only one horizontal street (or one vertical street), but no restriction about the perpendicular direction. Then the street-spreading matrix $\mathbf{S}$ is a 1×1 matrix which gives rise to the largest eigenvalue of the 2-step transition matrix M. It follows that the second largest eigenvalue is irrelevant, which implies that the surplus shortline method provides explicit quadratic irrational slopes for which the geodesic is superuniform.

If a polysquare surface has only one horizontal street, or only one vertical street, then we call it a *one-street polysquare surface*. Thus we just proved the following result.

Corollary 7.2.2. *For every one-street polysquare surface, there exist infinitely many explicit quadratic irrational slopes such that every* 1*-direction geodesic with any such slope is superuniform.*

We complete this section by showing that one-street polysquare surfaces are not rare. The idea is based on a a far-reaching generalization of the DS-L-surface.

Recall the 2-polysquare snake surface in Figure 7.1.4. Snake surfaces are not restricted to 2-polysquare surfaces, as illustrated in Figure 7.2.18.

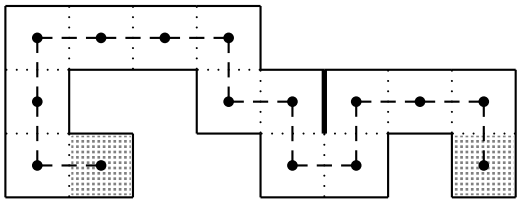

Figure 7.2.18: a snake surface

More precisely, let $\mathcal{P}$ be a finite polysquare surface. We put a point at the center of every square face of $\mathcal{P}$, and call it the "capital of the square face". Consider the *neighbor graph* of $\mathcal{P}$, where the *vertices* are the capitals, and where two capitals are joined by an *edge* of the graph if the corresponding square faces share a common edge. If the neighbor graph of $\mathcal{P}$ is a "path", with no branching, then $\mathcal{P}$ is called a snake surface, as shown in Figure 7.2.18. If the neighbor graph of $\mathcal{P}$ is a "tree", then $\mathcal{P}$ is called a polysquare-tree surface, as shown in Figure 7.2.18 and 7.2.19.

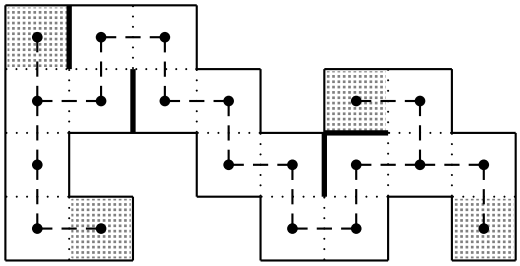

Figure 7.2.19: a polysquare-tree surface

Given any graph, the number of edges at a vertex is called the *degree* of the vertex. In a path, the degree of every vertex is 2, except at the two end-vertices where the degree is 1. In a tree we may have higher degrees. For example, the neighbor tree of the polysquare-tree surface in Figure 7.2.19 has two vertices of degree 3.

One-street polysquare surfaces are not rare, because the diagonal subdivision of every polysquare-tree surface has only one street.

The proof goes by induction on the number of square faces in the polysquare. The inductive step is based on the elementary result in graph theory that every tree has a vertex of degree 1. Indeed, it is easy to see that a tree with n vertices has precisely $n-1$ edges, and that the sum of the degrees is twice the number of edges. Since the sum of the degrees is $2(n-1)$, this implies that there must be a vertex with degree less than 2, and so must be equal to 1.

In terms of the polysquare-tree region, this result in graph theory means that there is always a square face with 3 sides not shared with neighboring square faces. Let us call them end square faces. We have highlighted these end square faces in Figures 7.2.18 and 7.2.19.

Figure 7.2.20 shows the smaller polysquare-tree surface which is obtained from the polysquare-tree surface in Figure 7.2.19 by removing one of the end square faces. By the induction hypothesis, the diagonal subdivision of this smaller polysquare-tree surface is a one-street surface, labelled by the numbers 1 to 38.

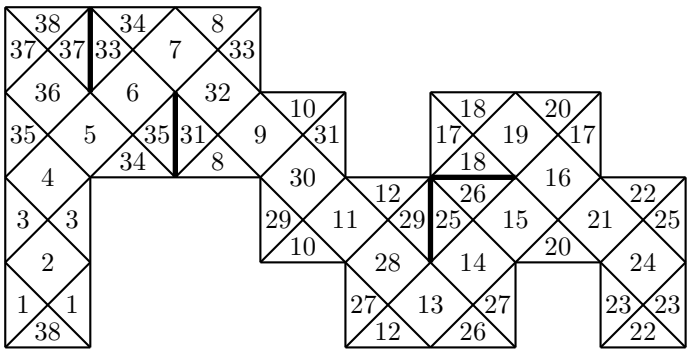

Figure 7.2.20: removing an end square face

Note that we carefully start the labelling from a common edge shared with the removed end square face, and keep moving in the north-east direction. Adding back the removed end square face, Figure 7.2.21 shows an explicit one-street in the original polysquare-street surface, where the consecutive squares along the street are labelled with the consecutive integers from 1 to 40.

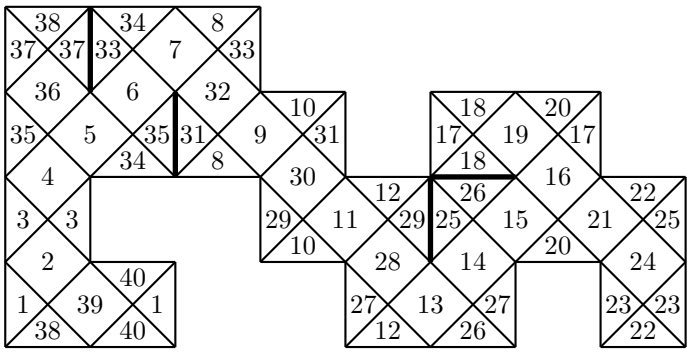

Figure 7.2.21: extension of the labelling

Note that the labelling in Figure 7.2.21 is obtained as a trivial extension of the labelling in Figure 7.2.20 by including 39 and 40. This completes the inductive step.

We cannot entirely drop the tree condition for the neighbor graph, as cycles may spoil the argument. Consider the two polysquare cycles in Figure 7.2.22.

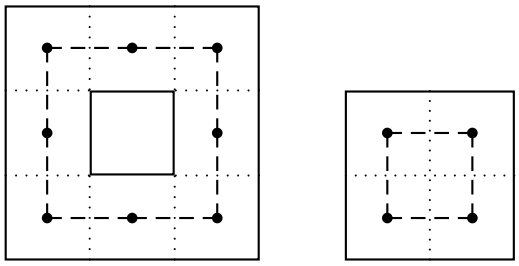

Figure 7.2.22: two polysquare-cycles

Neither of these polysquare-cycles leads to a one-street diagonal decomposition surface, as can be shown in Figure 7.2.23.

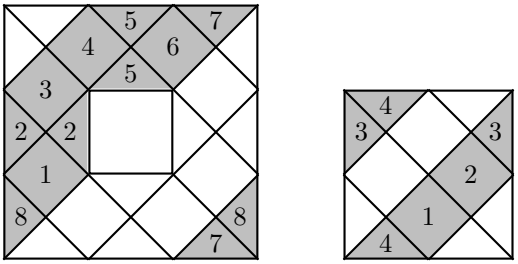

Figure 7.2.23: diagonal decomposition of two polysquare-cycles

In the picture on the left, we have a tilted street of length 8, covering only half the tilted square faces of the polysquare. In the picture on the right, we have a tilted street of length 4, again covering only half the tilted square faces of the polysquare.

7.3. **Application of Theorem 7.2.2: super-fast escape to infinity.** Our goal in this section is to find explicit quadratic irrational slopes which give rise to orbits that exhibit *super-fast* escape rate to infinity. More precisely, given any $\varepsilon > 0$, we shall find explicit quadratic irrational slopes such that for any orbit with any such slope, there exists an infinite sequence T_n, $n \geqslant 1$, such that $T_n \to \infty$ as $n \to \infty$, and the diameter of the initial segment of length T_n of the orbit exceeds $c_0 T_n^{1-\varepsilon}$, where c_0 is an absolute constant depending only on the given special slope.

Orbits in integrable polysquare systems behave in the same way for all quadratic irrational slopes. In complete contrast, orbits in infinite non-integrable polysquare systems may behave in completely different ways for different quadratic irrational slopes. We may have the full spectrum from super-slow to super-fast escape rate to infinity.

Example 7.3.1. We return to the problem of billiard in the ∞-L-strip region shown in Figure 7.3.1. In Theorem 6.7.2 in [4], it is shown that there are infinitely many quadratic irrational slopes such that a billiard orbit starting from a corner point with such a slope is dense on the ∞-L-strip region and also exhibits *super-slow* logarithmic escape rate to infinity. In particular, any initial segment of such an orbit of length T, $T \geqslant 2$, has distance at most $c_0 \log T$ from the starting point, where c_0 is an absolute constant depending only on the given special slope.

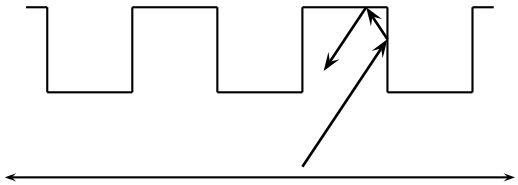

Figure 7.3.1: billiard in the ∞-L-strip region

As illustrated in Figure 7.3.2, the L-shape is the building block of the ∞-L-strip region.

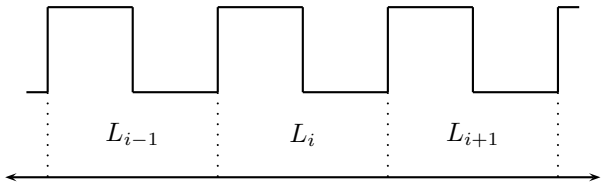

Figure 7.3.2: the ∞-L-strip region with its building blocks

The trick of "unfolding" reduces the problem of billiard on the ∞-L-strip region, a 4-direction flow, to the problem of a 1-direction geodesic flow on an appropriate infinite polysquare surface. We call this surface the 1-*direction billiard surface of the* ∞-*L-strip*, and denote it by $\mathrm{Bil}(\infty; 1)$.

To describe $\mathrm{Bil}(\infty; 1)$, we first "unfold" each of the L-shapes L_i by reflecting it horizontally and vertically to obtain 4 reflected copies and then put them together to form a 4-copy-L_i. We then obtain $\mathrm{Bil}(\infty; 1)$ by gluing together the infinitely many copies of these 4-copy-L_i.

Clearly there is billiard flow from each L-shape L_i to its two immediate neighbours L_{i-1} and L_{i+1}. We therefore need to identify corresponding edges of these 4-copy versions very carefully. A simple examination will convince the reader that the edge identifications can be as illustrated in Figure 7.3.3.

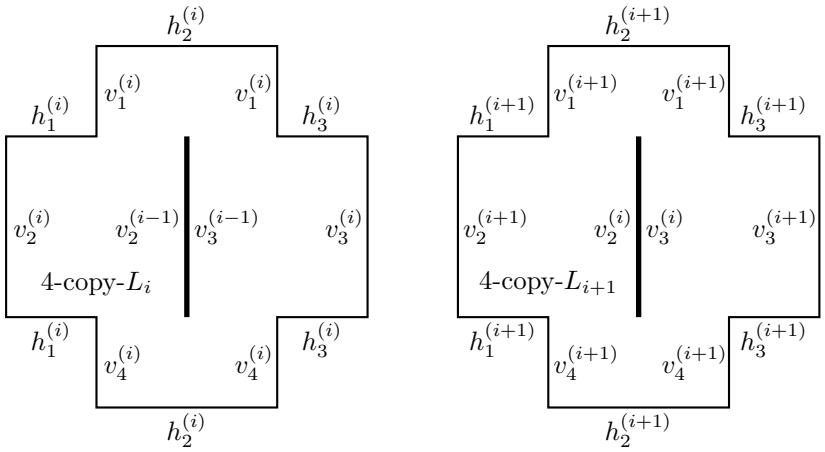

Figure 7.3.3: 4-copy-L_i and 4-copy-L_{i+1} together with edge identifications

Note that a 1-direction geodesic on $\mathrm{Bil}(\infty; 1)$ that goes from the vertical edge $v_2^{(i+1)}$ to the vertical edge $v_2^{(i)}$ corresponds to a billiard path going from L_{i+1} to L_i,

whereas a 1-direction geodesic on Bil(∞; 1) that goes from the vertical edge $v_3^{(i-1)}$ to the vertical edge $v_3^{(i)}$ corresponds to a billiard path going from L_i to L_{i+1}.

Thus the motion of the infinite L-strip billiard can be described in terms of 1-direction geodesic flow on a finite polysquare surface $\mathcal{P}$, the *period-surface* of Bil(∞; 1), illustrated in Figure 7.3.4, where we have rotated by 90 degrees in the anticlockwise direction. Clearly $\mathcal{P}$ has 12 square faces, 4 horizontal streets and 6 vertical streets, labelled according to the picture on the right where, for instance, the information $\leftrightarrow 3$ and $\updownarrow 5$ in a square face indicates that this square face is on the 3-rd horizontal street and the 5-th vertical street. Note that the anticlockwise rotation by 90 degrees makes the application of Theorem 7.2.2 more convenient.

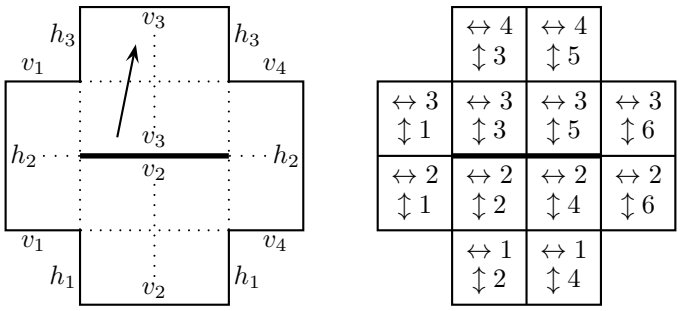

Figure 7.3.4: the period surface $\mathcal{P}$ of Bil(∞; 1)

The boundary identification in $\mathcal{P}$ is clearly the simplest perpendicular translation. Consider a 1-direction geodesic in $\mathcal{P}$ with slope given by the arrow in the picture on the left in Figure 7.3.4. If such a geodesic hits the edge v_3 at the top, then it jumps down vertically to the identified edge v_3 in the middle. In terms of the ∞-L-strip billiard this means precisely that the billiard moves from L_i to L_{i+1}, *i.e.*, "moving right". If such a geodesic hits the edge v_2 in the middle, then it jumps down vertically to the identified edge v_2 at the bottom. In terms of the ∞-L-strip billiard this means precisely that the billiard moves from L_i to L_{i-1}, *i.e.*, "moving left". Thus by counting the number of edge cuttings for v_2 and for v_3, we know the total number of steps moving to the left and the total number of steps moving to the right. Taking the difference of these two numbers, we then know precisely which particular constituent L-shape happens to contain the billiard at a given moment.

Now the edge cutting numbers are expressed in terms of *powers* of the relevant eigenvalues of the 2-step transition matrix corresponding to the given quadratic irrational slope. It makes it plausible to guess that the *irregularity exponent* of the period-surface $\mathcal{P}$ gives the escape rate to infinity for the infinite L-strip billiard, as long as the shortline method works. Next we expand on this and justify this intuition.

We need to choose the parameters m and n, which have to be integer multiples of the lengths of the horizontal and vertical streets respectively. For this period surface, the horizontal streets have length 2 or 4, while the vertical streets all have length 2. Thus we let $m = 4k$ and $n = 2k$, where $k \geqslant 1$ is any integer. Consequently, we let

$$\alpha_k = [2k; 4k, 2k, 4k, \ldots] = k + \frac{\sqrt{4k^2+2}}{2}. \tag{7.3.1}$$

Since the period-surface $\mathcal{P}$ has 12 squares, the original shortline method leads to a 24×24 2-step transition matrix M. To find the relevant eigenvalues and eigenvectors of such a large matrix directly is clearly rather inconvenient.

Instead we apply Theorem 7.2.2, which leads to a much smaller 4×4 street-spreading matrix $\mathbf{S}$ defined by (7.2.36). We follow the notation in Section 7.2. We consider the M-invariant subspace $\mathcal{V}$ generated by the 8 vectors $\mathbf{u}_i, \mathbf{v}_i$, $i = 1, 2, 3, 4$,

defined by (7.2.14) and (7.2.15). The relevant eigenvalues of M are then eigenvalues of the matrix $M|_{\mathcal{V}}$, defined by (7.2.37).

Consider the horizontal street corresponding to $\mathbf{u}_1$, as highlighted in the picture on the left in Figure 7.3.5. Clearly $J_1 = \{2, 4\}$. Using (7.2.17), we have

$$\begin{aligned}(M-I)\mathbf{u}_1 &= (M-I)[\{2k^2 \uparrow_{1,2}, 2k^2 \uparrow_{1,4}\}] + (M-I)[\{2k^2 \uparrow_{2,2}, 2k^2 \uparrow_{2,4}\}] \\ &= 4k^2(\mathbf{u}_1 + \mathbf{v}_1) + 4k^2(\mathbf{u}_2 + \mathbf{v}_2). \end{aligned} \tag{7.3.2}$$

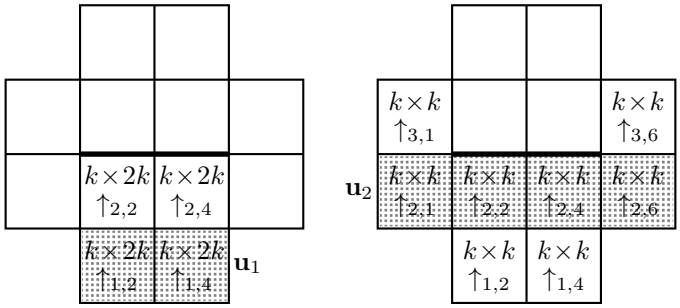

Figure 7.3.5: almost vertical units of type $\uparrow$ in $\mathbf{u}_1$ and $\mathbf{u}_2$

With $J_2 = \{1, 2, 4, 6\}$, for the horizontal street corresponding to $\mathbf{u}_2$, as highlighted in the picture on the right in Figure 7.3.5, a similar argument gives

$$(M-I)\mathbf{u}_2 = 2k^2(\mathbf{u}_1 + \mathbf{v}_1) + 4k^2(\mathbf{u}_2 + \mathbf{v}_2) + 2k^2(\mathbf{u}_3 + \mathbf{v}_3). \tag{7.3.3}$$

With $J_3 = \{1, 3, 5, 6\}$, for the horizontal street corresponding to $\mathbf{u}_3$, as highlighted in the picture on the left in Figure 7.3.6, a similar argument gives

$$(M-I)\mathbf{u}_3 = 2k^2(\mathbf{u}_2 + \mathbf{v}_2) + 4k^2(\mathbf{u}_3 + \mathbf{v}_3) + 2k^2(\mathbf{u}_4 + \mathbf{v}_4). \tag{7.3.4}$$

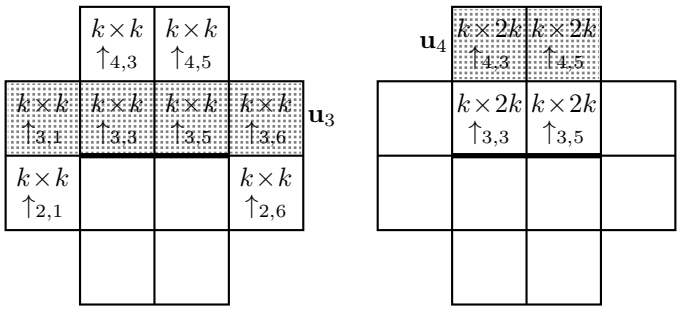

Figure 7.3.6: almost vertical units of type $\uparrow$ in $\mathbf{u}_3$ and $\mathbf{u}_4$

With $J_4 = \{3, 5\}$, for the horizontal street corresponding to $\mathbf{u}_3$, as highlighted in the picture on the right in Figure 7.3.6, a similar argument gives

$$(M-I)\mathbf{u}_4 = 4k^2(\mathbf{u}_3 + \mathbf{v}_3) + 4k^2(\mathbf{u}_4 + \mathbf{v}_4). \tag{7.3.5}$$

It follows from (7.3.2)–(7.3.5) that the street-spreading matrix is given by

$$\mathbf{S} = \begin{pmatrix} 4k^2 & 2k^2 & 0 & 0 \\ 4k^2 & 4k^2 & 2k^2 & 0 \\ 0 & 2k^2 & 4k^2 & 4k^2 \\ 0 & 0 & 2k^2 & 4k^2 \end{pmatrix} = k^2 \begin{pmatrix} 4 & 2 & 0 & 0 \\ 4 & 4 & 2 & 0 \\ 0 & 2 & 4 & 4 \\ 0 & 0 & 2 & 4 \end{pmatrix}.$$

This has eigenvalues and corresponding eigenvectors

$$\begin{aligned} \tau_1 &= 8k^2, \quad \psi_1 = (1, 2, 2, 1)^T, \\ \tau_2 &= 6k^2, \quad \psi_2 = (1, 1, -1, -1)^T, \\ \tau_3 &= 2k^2, \quad \psi_3 = (1, -1, -1, 1)^T, \\ \tau_4 &= 0, \quad \psi_4 = (1, -2, 2, -1)^T. \end{aligned}$$

Using the formula (7.2.38), we obtain corresponding eigenvalues of $M|_{\mathcal{V}}$ given by

$$\begin{aligned}
\lambda(\tau_1;\pm) &= 1 + \frac{8k^2 \pm \sqrt{64k^4+32k^2}}{2} = 1 + 4k^2 \pm 2k\sqrt{4k^2+2},\\
\lambda(\tau_2;\pm) &= 1 + \frac{6k^2 \pm \sqrt{36k^4+24k^2}}{2} = 1 + 3k^2 \pm k\sqrt{9k^2+6},\\
\lambda(\tau_3;\pm) &= 1 + \frac{2k^2 \pm \sqrt{4k^4+8k^2}}{2} = 1 + k^2 \pm k\sqrt{k^2+2},\\
\lambda(\tau_4;\pm) &= 1.
\end{aligned}$$

The three relevant eigenvalues of $M|_{\mathcal{V}}$ and corresponding eigenvectors are therefore

$$\lambda_1 = 1 + 4k^2 + 2k\sqrt{4k^2+2}, \quad \Psi_1 = (1,2,2,1,b_{11},b_{12},b_{13},b_{14})^T, \tag{7.3.6}$$

$$\lambda_2 = 1 + 3k^2 + k\sqrt{9k^2+6}, \quad \Psi_2 = (1,1,-1,-1,b_{21},b_{22},b_{23},b_{24})^T, \tag{7.3.7}$$

$$\lambda_3 = 1 + k^2 + k\sqrt{k^2+2}, \quad \Psi_3 = (1,-1,-1,1,b_{31},b_{32},b_{33},b_{34})^T,$$

where the values of b_{ij}, $i = 1,2,3$, $j = 1,2,3,4$, can be calculated using (7.2.39).

Recall that by counting the number of edge cuttings for v_2 and for v_3, we know the total number of steps of the billiard orbit moving to the left and the total number of steps of the billiard orbit moving to the right. The difference between these two numbers then gives us information on the movement of the billiard orbit.

We now proceed to find the edge-cutting numbers of v_2 and v_3.

The eigenvector of M corresponding to the eigenvector Ψ_1 of $M|_{\mathcal{V}}$ is given by

$$\mathbf{u}_1 + 2\mathbf{u}_2 + 2\mathbf{u}_3 + \mathbf{u}_4 + b_{11}\mathbf{v}_1 + b_{12}\mathbf{v}_2 + b_{13}\mathbf{v}_3 + b_{14}\mathbf{v}_4.$$

We first identity the number of almost vertical units counted here that cut the edge v_2; see Figure 7.3.4. Concerning the contribution from those units counted by $\mathbf{u}_1$, it is clear from the picture on the left in Figure 7.3.5 that we have $2k^2$ units of type $\uparrow_{2,2}$ and $2k^2$ units of type $\uparrow_{2,4}$, making a total of $4k^2$. Concerning the contribution from those units counted by $\mathbf{u}_2$, it is clear from the picture on the right in Figure 7.3.5 that we have k^2 units of type $\uparrow_{2,2}$ and k^2 units of type $\uparrow_{2,4}$, making a total of $2k^2$. Concerning the contribution from those units counted by $\mathbf{u}_3$ and $\mathbf{u}_4$, it is clear from Figure 7.3.6 that there is none. To study the contribution from those units counted by $\mathbf{v}_1, \ldots, \mathbf{v}_4$, we appeal to (7.2.15) and Figure 7.2.1. There is clearly no contribution from $\mathbf{v}_1, \mathbf{v}_3, \mathbf{v}_4$, while for $\mathbf{v}_2$, we have positive contributions from $\upharpoonleft_{2,1}$ and $\upharpoonleft_{2,2}$, and negative contributions from $\uparrow_{2,2}$ and $\uparrow_{2,4}$, each counted with the multiplicity of J_2^*, and so there is perfect cancellation. Thus for the edge v_2, we have a total count of $4k^2 + 2(2k^2) = 8k^2$.

We next identity the number of almost vertical units counted here that cut the edge v_3; see Figure 7.3.4. Concerning the contribution from those units counted by $\mathbf{u}_1$ and $\mathbf{u}_2$, it is clear from Figure 7.3.5 that there is none. Concerning the contribution from those units counted by $\mathbf{u}_3$, it is clear from the picture on the left in Figure 7.3.6 that we have k^2 units of type $\uparrow_{4,3}$ and k^2 units of type $\uparrow_{4,5}$, making a total of $2k^2$. Concerning the contribution from those units counted by $\mathbf{u}_4$, it is clear from the picture on the right in Figure 7.3.6 that we have $2k^2$ units of type $\uparrow_{4,3}$ and $2k^2$ units of type $\uparrow_{4,5}$, making a total of $4k^2$. There is clearly no contribution from $\mathbf{v}_1, \mathbf{v}_2, \mathbf{v}_3$, while for $\mathbf{v}_4$, we have positive contributions from $\upharpoonleft_{4,3}$ and $\upharpoonleft_{4,5}$, and negative contributions from $\uparrow_{4,3}$ and $\uparrow_{4,5}$, each counted with the multiplicity of J_4^*, and so there is perfect cancellation. Thus for the edge v_3, we have a total count of $2(2k^2) + 4k^2 = 8k^2$.

Since the two counts are the same, it follows that the eigenvalue λ_1 does not contribute to the difference between the edge-cutting numbers of v_2 and v_3.

Remark. The perfect cancellation is not surprising at all. Indeed, the high powers corresponding to the largest eigenvalue represents the *main term* of the problem. Any lack of cancellation here would violate the uniformity of the geodesic. With a quadratic irrational slope, this would specifically violate the Gutkin–Veech theorem [9, 16, 18] that guarantees uniformity of any 1-direction geodesic in any polysquare surface with irrational slope. See also [5, 6].

The eigenvector of M corresponding to the eigenvector Ψ_2 of $M|_{\mathcal{V}}$ is given by

$$\mathbf{u}_1 + \mathbf{u}_2 - \mathbf{u}_3 - \mathbf{u}_4 + b_{21}\mathbf{v}_1 + b_{22}\mathbf{v}_2 + b_{23}\mathbf{v}_3 + b_{24}\mathbf{v}_4.$$

We first identity the number of almost vertical units counted here that cut the edge v_2. Recall that the contribution from $\mathbf{u}_1$ and $\mathbf{u}_2$ are $4k^2$ and $2k^2$ respectively, while there is no contribution from $\mathbf{u}_3$ and $\mathbf{u}_4$, and also no contribution from $\mathbf{v}_1, \ldots, \mathbf{v}_4$. Thus for the edge v_2, we have a total count of $4k^2 + 2k^2 = 6k^2$. We next identity the number of almost vertical units counted here that cut the edge v_3. Recall that the contribution from $\mathbf{u}_3$ and $\mathbf{u}_4$ are $2k^2$ and $4k^2$ respectively, while there is no contribution from $\mathbf{u}_1$ and $\mathbf{u}_2$, and also no contribution from $\mathbf{v}_1, \ldots, \mathbf{v}_4$. Thus for the edge v_3, we have a total count of $-2k^2 - 4k^2 = -6k^2$.

The difference, in absolute value, is therefore $12k^2$. Let $c_2 = c_{2,1}$ in (7.2.11). Then it follows that the second eigenvalue λ_2 contributes $12c_2\lambda_2^r k^2$ to the difference between the edge-cutting numbers of v_2 and v_3.

So the deviation from the starting point comes from the second largest eigenvalue, and this has the order of magnitude λ_2^r compared to the order of magnitude λ_1^r of the main term. Choosing $T = \lambda_1^r$, we have $\lambda_2^r \asymp T^{\kappa_0}$, where

$$\kappa_0 = \kappa_0(k) = \frac{\log \lambda_2}{\log \lambda_1} = \frac{2\log k + \log 6}{2\log k + \log 8} + o(1), \tag{7.3.8}$$

in view of (7.3.6)–(7.3.7), is the irregularity exponent of a 1-direction geodesic of slope (7.3.1) on the period-surface in Figure 7.3.4.

Clearly $\kappa_0 = \kappa_0(k) \to 1$ as $k \to \infty$. So we have just established $T^{\kappa_0} = T^{1-\varepsilon}$ size *super-fast escape rate to infinity* for the infinite L-strip billiard with the explicit class of quadratic irrational slopes in (7.3.1) where the parameter $k \geqslant 1$ is any integer.

It is easy to see that the irregularity exponent $\kappa_0 = \kappa_0(k)$ in (7.3.8) is *precisely* the escape rate to infinity of this infinite billiard. Indeed, the escape rate to infinity cannot be larger than the expression (7.3.8) coming from the two largest eigenvalues.

Example 7.3.2. Consider the Ehrenfest wind-tree model with $a = b = 1/2$, rescaled so that we have square faces of unit area. Consider a 4-direction billiard trajectory in the infinite region in Figure 7.3.7. Here the building block of this infinite polysquare surface is an L-shape.

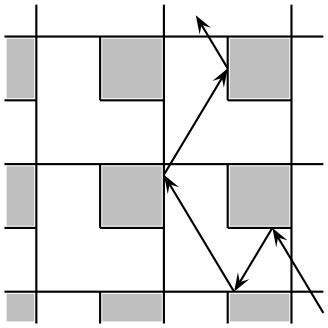

Figure 7.3.7: Ehrenfest wind-tree billiard model

As usual, this infinite billiard model is equivalent to a 1-direction geodesic flow on an infinite polysquare surface that we denote by $\mathrm{Bil}(\infty; 2)$, with the index 2 here indicating that this is double periodic. To construct $\mathrm{Bil}(\infty; 2)$, we take one

of the L-shape building blocks, and unfold the 4-direction billiard flow on it to a 1-direction geodesic flow on a 4-copy version of it, obtained by reflecting horizontally and vertically. Note that each 4-copy L-shape has a right-neighbor, a left-neighbor, a down-neighbor and an up-neighbor in $\mathrm{Bil}(\infty;2)$, and we need appropriate edge identification which amount to to a more complicated version of Figure 7.3.3. The *period-surface* $\mathrm{Bil}(2)$ of $\mathrm{Bil}(\infty;2)$ is shown in the picture on the left in Figure 7.3.8.

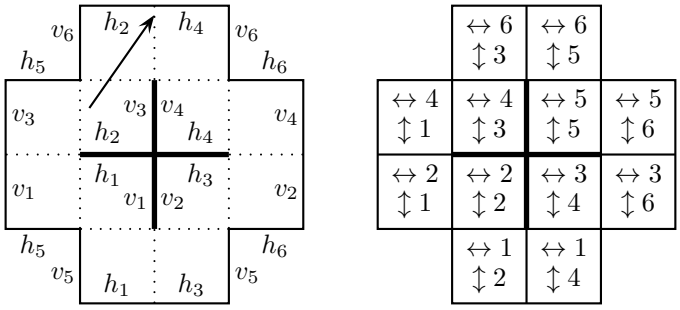

Figure 7.3.8: the period surface $\mathrm{Bil}(2)$ of $\mathrm{Bil}(\infty;2)$

The horizontal and vertical streets of $\mathrm{Bil}(2)$ are indicated in the picture on the right in Figure 7.3.8 where, for instance, the entries $\leftrightarrow 3$ and $\updownarrow 4$ in a square face indicates that the square face is on the 3-rd horizontal street and the 4-th vertical street. It is easy to see that $\mathrm{Bil}(2)$ has 6 horizontal streets and 6 vertical streets.

The boundary identification in $\mathrm{Bil}(2)$ is clearly the simplest perpendicular translation. Consider a 1-direction geodesic in $\mathrm{Bil}(2)$ with slope given by the arrow in the picture on the left in Figure 7.3.8. If such a geodesic hits the edge h_2 or h_4 at the top, then it jumps down vertically to the identified edge h_2 or h_4 in the middle. In terms of the Ehrenfest wind-tree billiard this means precisely that the billiard moves from one L-shape to the next above, *i.e.*, "moving up". If such a geodesic hits the edge h_1 or h_3 in the middle, then it jumps down vertically to the identified edge h_1 or h_3 at the bottom. In terms of the Ehrenfest wind-tree billiard this means precisely that the billiard moves from one L-shape to the next below, *i.e.*, "moving down". Thus by counting the number of edge cuttings for h_2, h_4 and for h_1, h_3, we know the total number of steps moving up and the total number of steps moving down. Taking the difference of these two numbers, we then know precisely the vertical location of the billiard at a given moment.

We need to choose the parameters m and n, which have to be integer multiples of the lengths of the horizontal and vertical streets respectively. For this period surface, the horizontal and vertical streets all have length 2. Thus we let $m = 2k$ and $n = 2k$, where $k \geqslant 1$ is any integer. Consequently, we let

$$\alpha_k = [2k; 2k, 2k, 2k, \ldots] = k + \sqrt{k^2+1}. \tag{7.3.9}$$

We apply Theorem 7.2.2, leading to a 6×6 street-spreading matrix $\mathbf{S}$ defined by (7.2.36). We follow the notation in Section 7.2. We consider the M-invariant subspace $\mathcal{V}$ generated by the 12 vectors $\mathbf{u}_i, \mathbf{v}_i$, $i = 1, \ldots, 6$, defined by (7.2.14) and (7.2.15). The relevant eigenvalues of M are then eigenvalues of the matrix $M|_{\mathcal{V}}$, defined by (7.2.37).

Consider the horizontal street corresponding to $\mathbf{u}_1$, as highlighted in the picture on the left in Figure 7.3.9. Clearly $J_1 = \{2, 4\}$. Using (7.2.17), we have

$$\begin{aligned}(M-I)\mathbf{u}_1 &= (M-I)[\{k^2 \uparrow_{1,2}, k^2 \uparrow_{1,4}\}] + (M-I)[\{k^2 \uparrow_{2,2}, k^2 \uparrow_{3,4}\}] \\ &= 2k^2(\mathbf{u}_1 + \mathbf{v}_1) + k^2(\mathbf{u}_2 + \mathbf{v}_2) + k^2(\mathbf{u}_3 + \mathbf{v}_3). \end{aligned} \tag{7.3.10}$$

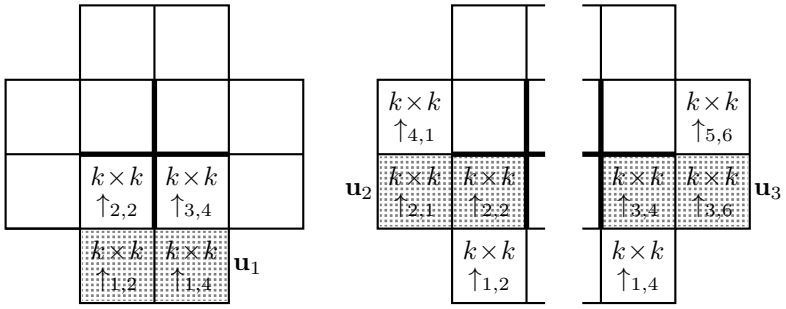

Figure 7.3.9: almost vertical units of type $\uparrow$ in $\mathbf{u}_1, \mathbf{u}_2, \mathbf{u}_3$

With $J_2 = \{1, 2\}$, for the horizontal street corresponding to $\mathbf{u}_2$, as highlighted in the picture in the middle in Figure 7.3.9, a similar argument gives

$$(M - I)\mathbf{u}_2 = k^2(\mathbf{u}_1 + \mathbf{v}_1) + 2k^2(\mathbf{u}_2 + \mathbf{v}_2) + k^2(\mathbf{u}_4 + \mathbf{v}_4). \tag{7.3.11}$$

With $J_3 = \{4, 6\}$, for the horizontal street corresponding to $\mathbf{u}_3$, as highlighted in the picture on the right in Figure 7.3.9, a similar argument gives

$$(M - I)\mathbf{u}_3 = k^2(\mathbf{u}_1 + \mathbf{v}_1) + 2k^2(\mathbf{u}_3 + \mathbf{v}_3) + k^2(\mathbf{u}_5 + \mathbf{v}_5). \tag{7.3.12}$$

With $J_4 = \{1, 3\}$, for the horizontal street corresponding to $\mathbf{u}_4$, as highlighted in the picture on the left in Figure 7.3.10, a similar argument gives

$$(M - I)\mathbf{u}_4 = k^2(\mathbf{u}_2 + \mathbf{v}_2) + 2k^2(\mathbf{u}_4 + \mathbf{v}_4) + k^2(\mathbf{u}_6 + \mathbf{v}_6). \tag{7.3.13}$$

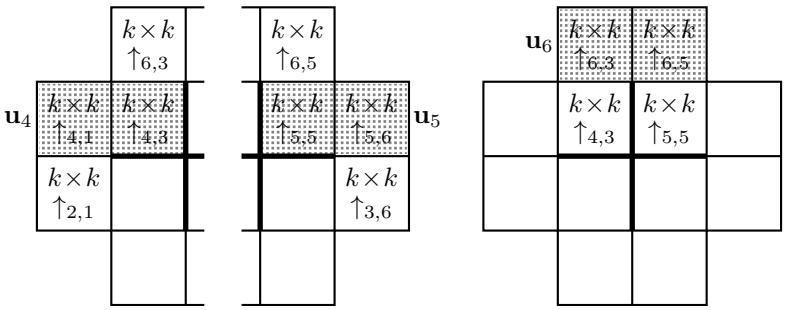

Figure 7.3.10: almost vertical units of type $\uparrow$ in $\mathbf{u}_4, \mathbf{u}_5, \mathbf{u}_6$

With $J_5 = \{5, 6\}$, for the horizontal street corresponding to $\mathbf{u}_5$, as highlighted in the picture in the middle in Figure 7.3.10, a similar argument gives

$$(M - I)\mathbf{u}_5 = k^2(\mathbf{u}_3 + \mathbf{v}_3) + 2k^2(\mathbf{u}_5 + \mathbf{v}_5) + k^2(\mathbf{u}_6 + \mathbf{v}_6). \tag{7.3.14}$$

With $J_6 = \{3, 5\}$, for the horizontal street corresponding to $\mathbf{u}_5$, as highlighted in the picture in the middle in Figure 7.3.10, a similar argument gives

$$(M - I)\mathbf{u}_6 = k^2(\mathbf{u}_4 + \mathbf{v}_4) + k^2(\mathbf{u}_5 + \mathbf{v}_5) + 2k^2(\mathbf{u}_6 + \mathbf{v}_6). \tag{7.3.15}$$

It follows from (7.3.10)–(7.3.15) that the street-spreading matrix is given by

$$\mathbf{S} = \begin{pmatrix} 2k^2 & k^2 & k^2 & 0 & 0 & 0 \\ k^2 & 2k^2 & 0 & k^2 & 0 & 0 \\ k^2 & 0 & 2k^2 & 0 & k^2 & 0 \\ 0 & k^2 & 0 & 2k^2 & 0 & k^2 \\ 0 & 0 & k^2 & 0 & 2k^2 & k^2 \\ 0 & 0 & 0 & k^2 & k^2 & 2k^2 \end{pmatrix} = k^2 \begin{pmatrix} 2 & 1 & 1 & 0 & 0 & 0 \\ 1 & 2 & 0 & 1 & 0 & 0 \\ 1 & 0 & 2 & 0 & 1 & 0 \\ 0 & 1 & 0 & 2 & 0 & 1 \\ 0 & 0 & 1 & 0 & 2 & 1 \\ 0 & 0 & 0 & 1 & 1 & 2 \end{pmatrix}.$$

This has non-zero eigenvalues and corresponding eigenvectors

$$\begin{aligned}
\tau_1 = 4k^2, &\quad \psi_1 = (1,1,1,1,1,1)^T,\\
\tau_2 = 3k^2, &\quad \psi_{2,1} = (-1,0,-1,1,0,1)^T,\\
&\quad \psi_{2,2} = (0,-1,1,-1,1,0)^T,\\
\tau_3 = k^2, &\quad \psi_{3,1} = (1,0,-1,-1,0,1)^T,\\
&\quad \psi_{3,2} = (0,1,-1,-1,1,0)^T,\\
\tau_4 = 0, &\quad \psi_4 = (-1,1,1,-1,-1,1)^T.
\end{aligned}$$

Using the formula (7.2.38), we obtain corresponding eigenvalues of $M|_{\mathcal{V}}$ given by

$$\begin{aligned}
\lambda(\tau_1;\pm) &= 1 + \frac{4k^2 \pm \sqrt{16k^4+16k^2}}{2} = 1 + 2k^2 \pm 2k\sqrt{k^2+1},\\
\lambda(\tau_2;\pm) &= 1 + \frac{3k^2 \pm \sqrt{9k^4+12k^2}}{2} = 1 + \frac{3k^2}{2} \pm \frac{k\sqrt{9k^2+12}}{2},\\
\lambda(\tau_3;\pm) &= 1 + \frac{k^2 \pm \sqrt{k^4+4k^2}}{2} = 1 + \frac{k^2}{2} \pm \frac{k\sqrt{k^2+4}}{2}.\\
\lambda(\tau_4;\pm) &= 1.
\end{aligned}$$

The three relevant eigenvalues of $M|_{\mathcal{V}}$ and corresponding eigenvectors are therefore

$$\lambda_1 = 1 + 2k^2 + 2k\sqrt{k^2+1}, \quad \Psi_1 = (1,1,1,1,1,1,b_{11},\dots,b_{16})^T, \tag{7.3.16}$$

$$\begin{aligned}
\lambda_2 = 1 + \frac{3k^2}{2} + \frac{k\sqrt{9k^2+12}}{2}, &\quad \Psi_{2,1} = (-1,0,-1,1,0,1,b_{21}^{(1)},\dots,b_{26}^{(1)})^T, \qquad (7.3.17)\\
&\quad \Psi_{2,2} = (0,-1,1,-1,1,0,b_{21}^{(2)},\dots,b_{26}^{(2)})^T,\\
\lambda_3 = 1 + \frac{k^2}{2} + \frac{k\sqrt{k^2+4}}{2}, &\quad \Psi_{3,1} = (1,0,-1,-1,0,1,b_{31}^{(1)},\dots,b_{36}^{(1)})^T,\\
&\quad \Psi_{3,2} = (0,1,-1,-1,1,0,b_{31}^{(2)},\dots,b_{36}^{(2)})^T,
\end{aligned}$$

where the values of $b_{1j}, b_{2j}^{(1)}, b_{2j}^{(2)}, b_{3j}^{(1)}, b_{3j}^{(2)}$, $j = 1,\dots,6$, can all be calculated using (7.2.39).

We now proceed to find the edge-cutting numbers of h_2, h_4 and h_1, h_3.

As in Example 7.3.1, the eigenvalue λ_1 does not contribute to their difference, as any lack of cancellation would violate the Gutkin–Veech theorem that guarantees uniformity.

The eigenvector of M corresponding to the eigenvector $\Psi_{2,1}$ of $M|_{\mathcal{V}}$ is given by

$$-\mathbf{u}_1 - \mathbf{u}_3 + \mathbf{u}_4 + \mathbf{u}_6 - b_{21}^{(1)}\mathbf{v}_1 - b_{23}^{(1)}\mathbf{v}_3 + b_{24}^{(1)}\mathbf{v}_4 + b_{26}^{(1)}\mathbf{v}_6. \tag{7.3.18}$$

The eigenvector of M corresponding to the eigenvector $\Psi_{2,2}$ of $M|_{\mathcal{V}}$ is given by

$$-\mathbf{u}_2 + \mathbf{u}_3 - \mathbf{u}_4 + \mathbf{u}_5 - b_{22}^{(2)}\mathbf{v}_2 + b_{23}^{(2)}\mathbf{v}_3 - b_{24}^{(2)}\mathbf{v}_4 + b_{25}^{(2)}\mathbf{v}_5. \tag{7.3.19}$$

We first identity the number of almost vertical units counted here that cut the edges h_2 and h_4; see Figure 7.3.8. The count from each of $\mathbf{u}_i$, $i = 1,\dots,6$ are

$$\begin{aligned}
&\mathbf{u}_1 \mapsto 0, \qquad \mathbf{u}_2 \mapsto 0, \qquad \mathbf{u}_3 \mapsto 0,\\
&\mathbf{u}_4 \mapsto k^2, \qquad \mathbf{u}_5 \mapsto k^2, \qquad \mathbf{u}_6 \mapsto 2k^2.
\end{aligned}$$

On the other hand, it is easy to show that the total contribution from $\mathbf{v}_i$, $i = 1,\dots,6$ is 0. Thus corresponding to the eigenvector $\Psi_{2,1}$ and (7.3.18), the total count is $3k^2$. Corresponding to the eigenvector $\Psi_{2,2}$ and (7.3.19), the total count is 0.

We next identity the number of almost vertical units counted here that cut the edges h_1 and h_3; see Figure 7.3.8. The count from each of $\mathbf{u}_i$, $i = 1, \ldots, 6$ are

$$\begin{array}{lll} \mathbf{u}_1 \mapsto 2k^2, & \mathbf{u}_2 \mapsto k^2, & \mathbf{u}_3 \mapsto k^2, \\ \mathbf{u}_4 \mapsto 0, & \mathbf{u}_5 \mapsto 0, & \mathbf{u}_6 \mapsto 0. \end{array}$$

Like before, the total contribution from $\mathbf{v}_i$, $i = 1, \ldots, 6$ is 0. Thus corresponding to the eigenvector $\Psi_{2,1}$ and (7.3.18), the total count is $-3k^2$. Corresponding to the eigenvector $\Psi_{2,2}$ and (7.3.19), the total count is 0.

It follows that the second eigenvalue λ_2 contributes $6c_{2,1}\lambda_2^r k^2$ to the difference between the edge-cuttings numbers of h_2, h_4 and h_1, h_3.

So the deviation from the starting point comes from the second largest eigenvalue, and this has the order of magnitude λ_2^r compared to the order of magnitude λ_1^r of the main term. Choosing $T = \lambda_1^r$, we have $\lambda_2^r \asymp T^{\kappa_0}$, where

$$\kappa_0 = \kappa_0(k) = \frac{\log \lambda_2}{\log \lambda_1} = \frac{2\log k + \log 3}{2\log k + \log 4} + o(1), \tag{7.3.20}$$

in view of (7.3.16)–(7.3.17), is the irregularity exponent of a 1-direction geodesic of slope (7.3.9) on the period-surface in Figure 7.3.8.

Clearly $\kappa_0 = \kappa_0(k) \to 1$ as $k \to \infty$. So we have just established $T^{\kappa_0} = T^{1-\varepsilon}$ size *super-fast escape rate to infinity* for the infinite L-strip billiard with the explicit class of quadratic irrational slopes in (7.3.9) where the parameter $k \geqslant 1$ is any integer.

It is easy to see that the irregularity exponent $\kappa_0 = \kappa_0(k)$ in (7.3.20) is *precisely* the escape rate to infinity of this infinite billiard. Indeed, the escape rate to infinity cannot be larger than the expression (7.3.20) coming from the two largest eigenvalues.

This example also highlights that different quadratic irrational slopes can lead to 1-direction geodesics that exhibit vastly different escape rates to infinity. To explain this, we shall consider an infinite polysquare surface $\mathcal{P}$ where there is an absolute bound ℓ such that the length of any horizontal or vertical street of $\mathcal{P}$ is at most ℓ. This is called an ℓ-square-maze, and 1-direction geodesics on square-mazes are studied in Theorem 6.5.1 in [4].

The problem connected to the Ehrenfest wind-tree model billiard with $a = b = 1/2$ that we have considered here leads to a problem of 1-direction geodesic flow on $\mathrm{Bil}(\infty; 2)$. Now $\mathrm{Bil}(\infty; 2)$ has infinite horizontal and vertical streets, so is not a square-maze. However, if we consider "streets" in $\mathrm{Bil}(\infty; 2)$ at 45 degrees to the horizontal and vertical axes, then the situation becomes very different. First of all, observe such a street in the Ehrenfest wind-tree model billiard as shown in Figure 7.3.11.

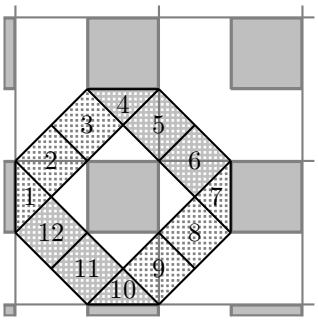

Figure 7.3.11: a diagonal street in the Ehrenfest wind-tree model billiard

The street indicated is contained in 4 constituent L-shapes. If we consider the analogous problem of 1-direction geodesic flow in $\mathrm{Bil}(\infty; 2)$, then the image of this street is shown in Figure 7.3.12, made up of the 4-copy versions of these 4 constituent

L-shapes. We have in fact shown that Bil$(\infty; 2)$ rotated by 45 degrees becomes a square-maze where every horizontal and vertical street has length 12.

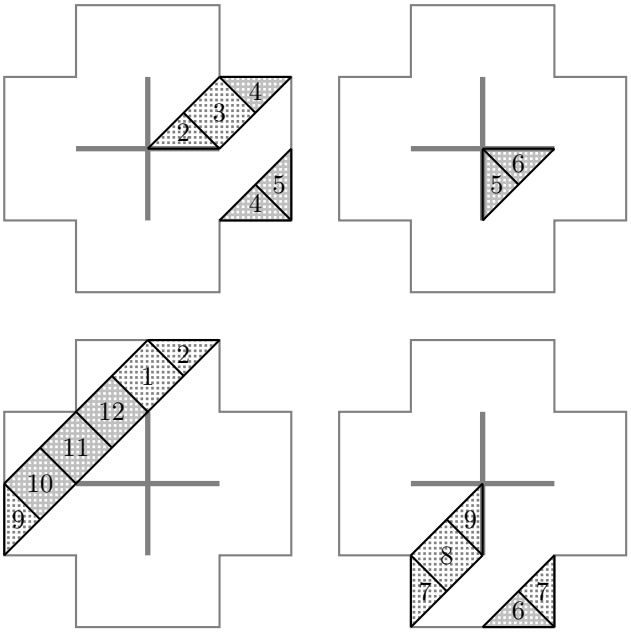

Figure 7.3.12: a 45-degree street of length 12 in Bil$(\infty; 2)$

Theorem 6.5.1 in [4] asserts that for an ℓ-square-maze, there are infinitely many numbers α of the form

$$\alpha = [a; a, a, a, \ldots] = a + \frac{1}{a + \frac{1}{a + \frac{1}{a + \cdots}}},$$

where $a \geqslant \ell!$ is divisible by $\ell!$, such that there exist 1-direction geodesics with slope α that exhibit time-quantitative density and super-slow logarithmic escape rate to infinity. For a square-maze where every street has length precisely ℓ, the condition on a can be relaxed to include all integers $a \geqslant \ell$ that are divisible by ℓ.

It follows that for the rotated Bil$(\infty; 2)$, there exist infinitely many numbers α_k of the form

$$\alpha_k = [12k; 12k, 12k, 12k, \ldots] = 12k + \frac{1}{12k + \frac{1}{12k + \frac{1}{12k + \cdots}}}, \tag{7.3.21}$$

where $k \geqslant 1$ is an integer, such that there exist 1-direction geodesics with slope α_k that exhibit super-slow logarithmic escape rate to infinity.

Now note that slopes α_k of the form (7.3.21) make up a subset of those slopes α_k of the form (7.3.9). It follows that slopes α_k of the form (7.3.21) give rise to 1-direction geodesics on Bil$(\infty; 2)$ that exhibit super-fast escape rate to infinity.

It is easy to show that a line with slope α_k, after a clockwise rotation of 45 degrees, now has slope equal to

$$\alpha_k^* = \frac{\alpha_k - 1}{\alpha_k + 1}. \tag{7.3.22}$$

Thus we have shown that there are infinitely many numbers α_k of the form (7.3.21) such that there exist 1-direction geodesics of slope α_k in Bil$(\infty; 2)$ that exhibit super-fast escape rate to infinity, and also 1-direction geodesics of slope α_k^* in Bil$(\infty; 2)$ that exhibit super-slow logarithmic escape rate to infinity. Note that in view of (7.3.21) and (7.3.22), both α_k and α_k^* are quadratic irrationals.

7.4. **More on the escape rate to infinity.** In this section, we consider some more complicated infinite billiards.

Example 7.4.1. Consider "C-wall" obstacles, as shown in Figure 7.4.1.

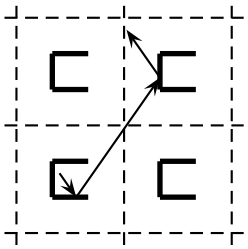

Figure 7.4.1: infinite billiard with double periodic C-shaped walls

More precisely, the building block of this infinite polysquare region is a 3×3 square, with walls on three sides of the middle square face as shown.

As usual, this infinite billiard model is equivalent to a 1-direction geodesic flow on an infinite polysquare surface that we denote by $\mathrm{Bil}(\infty; 2; \mathrm{C})$. Here the index 2 indicates that this is double periodic, and the letter C refers to the common shape of the obstacles. To construct $\mathrm{Bil}(\infty; 2; \mathrm{C})$, we take one of the building blocks, and unfold the 4-direction billiard flow on it to a 1-direction geodesic flow on a 4-copy version of it, obtained by reflecting horizontally and vertically. Note that each 4-copy version has a right-neighbor, a left-neighbor, a down-neighbor and an up-neighbor in $\mathrm{Bil}(\infty; 2; \mathrm{C})$, and we need appropriate edge identification for gluing them together.

The *period-surface* $\mathrm{Bil}(2; \mathrm{C})$ of $\mathrm{Bil}(\infty; 2; \mathrm{C})$ is shown in the picture on the left in Figure 7.4.2. The horizontal and vertical streets of $\mathrm{Bil}(2; \mathrm{C})$ are indicated in the picture on the right in Figure 7.4.2 where, for instance, the entries $\leftrightarrow 3$ and $\updownarrow 5$ in a square face indicates that the square face is on the 3-rd horizontal street and the 5-th vertical street. It is easy to see that $\mathrm{Bil}(2; \mathrm{C})$ has 8 horizontal streets of length 3, and 2 horizontal streets of length 6. It also has 8 vertical streets of length 3, 2 vertical streets of length 4, and 2 vertical streets of length 2. Thus the street-LCM is equal to 12.

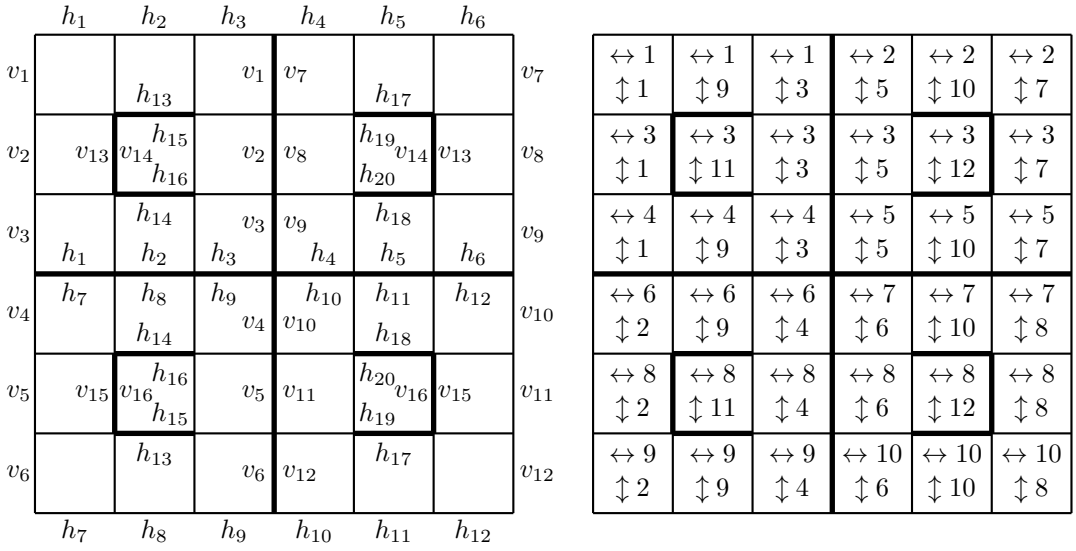

Figure 7.4.2: the period surface $\mathrm{Bil}(2; \mathrm{C})$ of $\mathrm{Bil}(\infty; 2; \mathrm{C})$

We shall consider an almost vertical geodesic V_0 in $\mathrm{Bil}(2; \mathrm{C})$ with slope α given by (7.2.1) with $m = n = 12$. As $\mathrm{Bil}(2; \mathrm{C})$ has 36 square faces, the 2-step transition

matrix M is 72×72 which is mildly inconvenient. Instead, we shall determine the street-spreading matrix $\mathbf{S}$ which, at size 10×10, is considerably smaller.

We follow the notation in Section 7.2. We consider the M-invariant subspace $\mathcal{V}$ generated by the 20 vectors $\mathbf{u}_i, \mathbf{v}_i$, $i = 1, \ldots, 10$, defined by (7.2.14) and (7.2.15). The relevant eigenvalues of M are then eigenvalues of the matrix $M|_{\mathcal{V}}$, defined by (7.2.37).

For $\mathbf{u}_1, \mathbf{u}_2, \mathbf{u}_4, \mathbf{u}_5$, Figure 7.4.3 describes the situation. With $J_1 = J_4 = \{1, 3, 9\}$ and $J_2 = J_5 = \{5, 7, 10\}$, for the horizontal streets corresponding to $\mathbf{u}_1, \mathbf{u}_2, \mathbf{u}_4, \mathbf{u}_5$, we have, using (7.2.17),

$$\begin{aligned}
(M-I)\mathbf{u}_1 &= (M-I)\mathbf{u}_4 \\
&= (M-I)[\{16 \uparrow_{1,1}, 16 \uparrow_{1,3}, 12 \uparrow_{1,9}\}] + (M-I)[\{16 \uparrow_{3,1}, 16 \uparrow_{3,3}\}] \\
&\quad + (M-I)[\{16 \uparrow_{4,1}, 16 \uparrow_{4,3}, 12 \uparrow_{4,9}\}] + (M-I)[\{12 \uparrow_{6,9}\}] \\
&\quad + (M-I)[\{12 \uparrow_{9,9}\}] \\
&= 44(\mathbf{u}_1 + \mathbf{v}_1) + 32(\mathbf{u}_3 + \mathbf{v}_3) + 44(\mathbf{u}_4 + \mathbf{v}_4) \\
&\quad + 12(\mathbf{u}_6 + \mathbf{v}_6) + 12(\mathbf{u}_9 + \mathbf{v}_9), \qquad (7.4.1) \\
(M-I)\mathbf{u}_2 &= (M-I)\mathbf{u}_5 \\
&= 44(\mathbf{u}_2 + \mathbf{v}_2) + 32(\mathbf{u}_3 + \mathbf{v}_3) + 44(\mathbf{u}_5 + \mathbf{v}_5) \\
&\quad + 12(\mathbf{u}_7 + \mathbf{v}_7) + 12(\mathbf{u}_{10} + \mathbf{v}_{10}). \qquad (7.4.2)
\end{aligned}$$

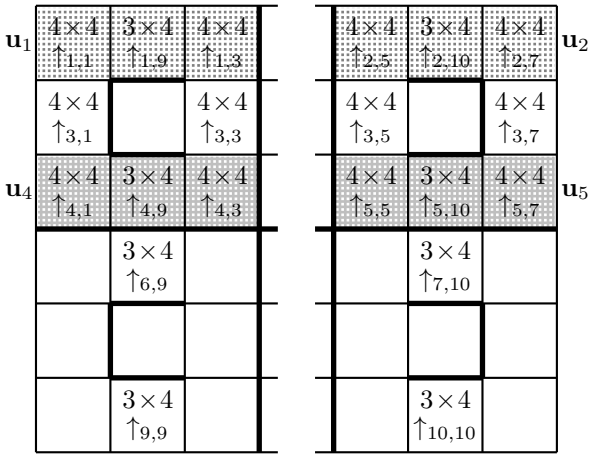

Figure 7.4.3: almost vertical units of type $\uparrow$ in $\mathbf{u}_1, \mathbf{u}_2, \mathbf{u}_4, \mathbf{u}_5$

For $\mathbf{u}_6, \mathbf{u}_7, \mathbf{u}_9, \mathbf{u}_{10}$, Figure 7.4.4 describes the situation. With $J_6 = J_9 = \{2, 4, 9\}$ and $J_7 = J_{10} = \{6, 8, 10\}$, for the horizontal streets corresponding to $\mathbf{u}_6, \mathbf{u}_7, \mathbf{u}_9, \mathbf{u}_{10}$, we have

$$\begin{aligned}
(M-I)\mathbf{u}_6 &= (M-I)\mathbf{u}_9 \\
&= 12(\mathbf{u}_1 + \mathbf{v}_1) + 12(\mathbf{u}_4 + \mathbf{v}_4) + 44(\mathbf{u}_6 + \mathbf{v}_6) \\
&\quad + 32(\mathbf{u}_8 + \mathbf{v}_8) + 44(\mathbf{u}_9 + \mathbf{v}_9), \qquad (7.4.3) \\
(M-I)\mathbf{u}_7 &= (M-I)\mathbf{u}_{10} \\
&= 12(\mathbf{u}_2 + \mathbf{v}_2) + 12(\mathbf{u}_5 + \mathbf{v}_5) + 44(\mathbf{u}_7 + \mathbf{v}_7) \\
&\quad + 32(\mathbf{u}_8 + \mathbf{v}_8) + 44(\mathbf{u}_{10} + \mathbf{v}_{10}). \qquad (7.4.4)
\end{aligned}$$

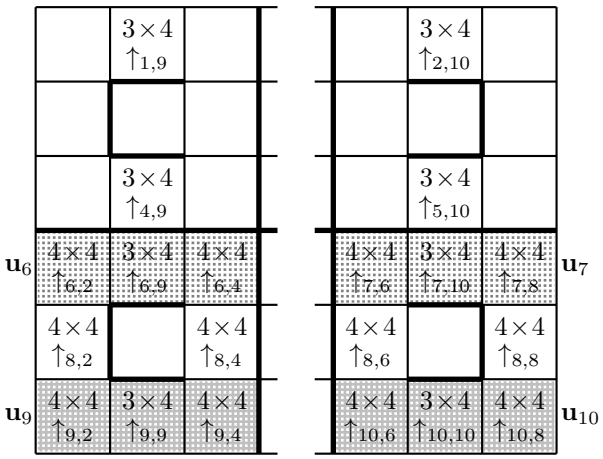

Figure 7.4.4: almost vertical units of type ↑ in $\mathbf{u}_6, \mathbf{u}_7, \mathbf{u}_9, \mathbf{u}_{10}$

For $\mathbf{u}_3, \mathbf{u}_8$, Figure 7.4.5 describes the situation. With $J_3 = \{1, 3, 5, 7, 11, 12\}$ and $J_8 = \{2, 4, 6, 8, 11, 12\}$, for the horizontal streets corresponding to $\mathbf{u}_3, \mathbf{u}_8$, we have

$$\begin{aligned}(M - I)\mathbf{u}_3 &= 16(\mathbf{u}_1 + \mathbf{v}_1) + 16(\mathbf{u}_2 + \mathbf{v}_2) + 56(\mathbf{u}_3 + \mathbf{v}_3) \\ &\quad + 16(\mathbf{u}_4 + \mathbf{v}_4) + 16(\mathbf{u}_5 + \mathbf{v}_5) + 24(\mathbf{u}_8 + \mathbf{v}_8), \qquad (7.4.5)\\ (M - I)\mathbf{u}_8 &= 24(\mathbf{u}_3 + \mathbf{v}_3) + 16(\mathbf{u}_6 + \mathbf{v}_6) + 16(\mathbf{u}_7 + \mathbf{v}_7) \\ &\quad + 56(\mathbf{u}_8 + \mathbf{v}_8) + 16(\mathbf{u}_9 + \mathbf{v}_9) + 16(\mathbf{u}_{10} + \mathbf{v}_{10}). \qquad (7.4.6)\end{aligned}$$

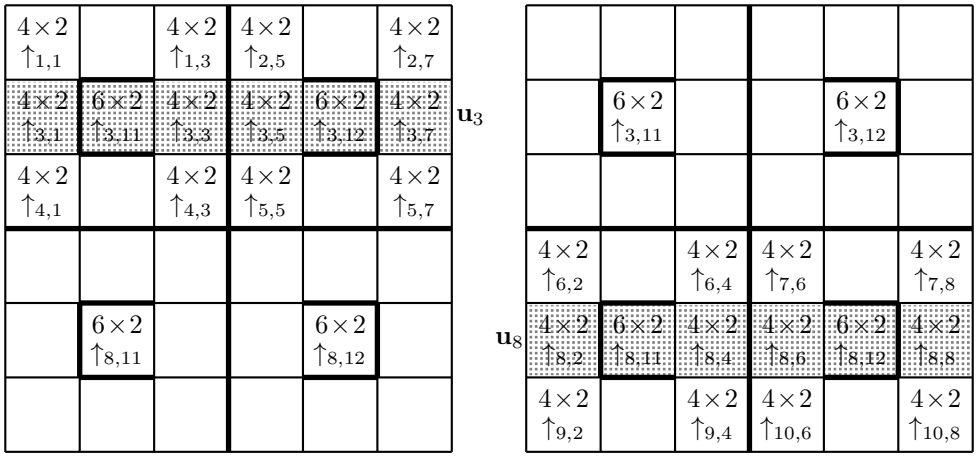

Figure 7.4.5: almost vertical units of type ↑ in $\mathbf{u}_3, \mathbf{u}_8$

It follows from (7.4.1)–(7.4.6) that the street-spreading matrix is given by

$$\mathbf{S} = \begin{pmatrix} 44 & 0 & 16 & 44 & 0 & 12 & 0 & 0 & 12 & 0 \\ 0 & 44 & 16 & 0 & 44 & 0 & 12 & 0 & 0 & 12 \\ 32 & 32 & 56 & 32 & 32 & 0 & 0 & 24 & 0 & 0 \\ 44 & 0 & 16 & 44 & 0 & 12 & 0 & 0 & 12 & 0 \\ 0 & 44 & 16 & 0 & 44 & 0 & 12 & 0 & 0 & 12 \\ 12 & 0 & 0 & 12 & 0 & 44 & 0 & 16 & 44 & 0 \\ 0 & 12 & 0 & 0 & 12 & 0 & 44 & 16 & 0 & 44 \\ 0 & 0 & 24 & 0 & 0 & 32 & 32 & 56 & 32 & 32 \\ 12 & 0 & 0 & 12 & 0 & 44 & 0 & 16 & 44 & 0 \\ 0 & 12 & 0 & 0 & 12 & 0 & 44 & 16 & 0 & 44 \end{pmatrix}. \qquad (7.4.7)$$

This has non-zero eigenvalues and corresponding eigenvectors given by

$$\begin{aligned}
\tau_1 &= 144, \quad \psi_1 = (1,1,2,1,1,1,1,2,1,1)^T,\\
\tau_2 &= 112, \quad \psi_2 = (-1,1,0,-1,1,-1,1,0,-1,1)^T,\\
\tau_3 &= 96, \quad \psi_3 = (-1,-1,-2,-1,-1,1,1,2,1,1)^T,\\
\tau_4 &= 64, \quad \psi_4 = (1,-1,0,1,-1,-1,1,0,-1,1)^T,\\
\tau_5 &= 48, \quad \psi_5 = (1,1,-4,1,1,1,1,-4,1,1)^T.
\end{aligned}$$

Note that the street-spreading matrix $\mathbf{S}$ given by (7.4.7) corresponds to the choice of parameters $m = n = 12$. Switching to $m = n = 12k$, where $k \geqslant 1$ is any integer, we obtain the new street-spreading matrix $\mathbf{S}(k) = k^2\mathbf{S}$ simply by multiplying the matrix $\mathbf{S}$ by k^2. Then of course the eigenvalues are also multiplied by k^2, but the eigenvectors remain the same. Naturally the 2-step transition matrix M is modified to $M(k)$.

We next determine some of the eigenvalues of $M(k)$ using (7.2.38). The largest eigenvalue of $M(k)|_{\mathcal{V}}$ is

$$\lambda_1(k) = 1 + \frac{\tau_1 k^2 + \sqrt{\tau_1^2 k^4 + 4\tau_1 k^2}}{2} = 1 + 72k^2 + 12k\sqrt{36k^2+1}, \tag{7.4.8}$$

while the second largest eigenvalue of $M(k)|_{\mathcal{V}}$ is

$$\lambda_2(k) = 1 + \frac{\tau_2 k^2 + \sqrt{\tau_2^2 k^4 + 4\tau_2 k^2}}{2} = 1 + 56k^2 + 4k\sqrt{196k^2+7}, \tag{7.4.9}$$

with eigenvector of the form

$$\Psi_2 = (-1,1,0,-1,1,-1,1,0,-1,1,-\tau_2^*,\tau_2^*,0,-\tau_2^*,\tau_2^*,-\tau_2^*,\tau_2^*,0,-\tau_2^*,\tau_2^*)^T,$$

where

$$\tau_2^* = \frac{-\tau_2 k^2 + \sqrt{\tau_2^2 k^4 + 4\tau_2 k^2}}{2} = 4k\sqrt{196k^2+7} - 56k^2.$$

Let us return to Figures 7.4.1 and 7.4.2. It is clear that the billiard moves to the up-neighbor if the 1-direction geodesic hits any of the edges $h_1, \ldots, h_6$, and moves to the down-neighbor if the 1-direction geodesic hits any of the edges $h_7, \ldots, h_{12}$. It is also clear that the billiard moves to the right-neighbor if the 1-direction geodesic hits any of the edges $v_7, \ldots, v_{12}$, and moves to the left-neighbor if the 1-direction geodesic hits any of the edges $v_1, \ldots, v_6$.

We now proceed to find the edge-cutting numbers of $h_1, \ldots, h_6$ and $h_7, \ldots, h_{12}$.

As in the example in Section 7.3, the eigenvalue λ_1 does not contribute to their difference, as any lack of cancellation would violate the Gutkin–Veech theorem that guarantees uniformity.

The eigenvector of $M(k)$ corresponding to the eigenvector Ψ_2 of $M(k)|_{\mathcal{V}}$ is given by

$$\begin{aligned}
&-\mathbf{u}_1 + \mathbf{u}_2 - \mathbf{u}_4 + \mathbf{u}_5 - \mathbf{u}_6 + \mathbf{u}_7 - \mathbf{u}_9 + \mathbf{u}_{10}\\
&\quad - \tau_2^*\mathbf{v}_1 + \tau_2^*\mathbf{v}_2 - \tau_2^*\mathbf{v}_4 + \tau_2^*\mathbf{v}_5 - \tau_2^*\mathbf{v}_6 + \tau_2^*\mathbf{v}_7 - \tau_2^*\mathbf{v}_9 + \tau_2^*\mathbf{v}_{10}.
\end{aligned} \tag{7.4.10}$$

We first identity the number of almost vertical units counted here that cut the edges $h_1, \ldots, h_6$; see Figure 7.4.2. The counts from $\mathbf{u}_i$, $i = 1, \ldots, 10$, are

$$\begin{aligned}
&\mathbf{u}_1 \mapsto 44k^2, \quad \mathbf{u}_2 \mapsto 44k^2, \quad \mathbf{u}_3 \mapsto 32k^2, \quad \mathbf{u}_4 \mapsto 44k^2, \quad \mathbf{u}_5 \mapsto 44k^2,\\
&\mathbf{u}_6 \mapsto 12k^2, \quad \mathbf{u}_7 \mapsto 12k^2, \quad \mathbf{u}_8 \mapsto 0, \quad \mathbf{u}_9 \mapsto 12k^2, \quad \mathbf{u}_{10} \mapsto 12k^2.
\end{aligned} \tag{7.4.11}$$

On the other hand, it is not difficult to show that each of $\mathbf{v}_1, \ldots \mathbf{v}_{10}$ contributes precisely zero. Thus for the edges $h_1, \ldots, h_6$, we have a total count of

$$-44k^2 + 44k^2 - 44k^2 + 44k^2 - 12k^2 + 12k^2 - 12k^2 + 12k^2 = 0.$$

We next identity the number of almost vertical units counted here that cut the edges $h_7, \ldots, h_{12}$; see Figure 7.4.2. The counts from $\mathbf{u}_i$, $i = 1, \ldots, 10$, are

$$\begin{array}{lllll} \mathbf{u}_1 \mapsto 12k^2, & \mathbf{u}_2 \mapsto 12k^2, & \mathbf{u}_3 \mapsto 0, & \mathbf{u}_4 \mapsto 12k^2, & \mathbf{u}_5 \mapsto 12k^2, \\ \mathbf{u}_6 \mapsto 44k^2, & \mathbf{u}_7 \mapsto 44k^2, & \mathbf{u}_8 \mapsto 32k^2, & \mathbf{u}_9 \mapsto 44k^2, & \mathbf{u}_{10} \mapsto 44k^2. \end{array} \tag{7.4.12}$$

Again, it is not difficult to show that each of $\mathbf{v}_1, \ldots \mathbf{v}_{10}$ contributes precisely zero. Thus for the edges $h_7, \ldots, h_{12}$, we have a total count of

$$-12k^2 + 12k^2 - 12k^2 + 12k^2 - 44k^2 + 44k^2 - 44k^2 + 44k^2 = 0.$$

Thus there is perfect cancellation in the vertical direction.

We next proceed to find the edge-cutting numbers of $v_1, \ldots, v_6$ and $v_7, \ldots, v_{12}$; see Figure 7.4.2.

Again, the eigenvalue λ_1 does not contribute to their difference, as any lack of cancellation would violate the Gutkin–Veech theorem that guarantees uniformity. So we concentrate our attention on the contribution from the eigenvector Ψ_2 of $M|_{\mathcal{V}}$. Here, note that none of $\mathbf{u}_1, \ldots, \mathbf{u}_{10}$ makes any non-zero contribution, as only units of type $\nmid$ can contribute to the count. For the contributions from $\mathbf{v}_1, \ldots, \mathbf{v}_{10}$, we use (7.2.15).

We first identity the number of almost vertical units counted in (7.4.10) that cut the edges $v_1, \ldots, v_6$; see Figure 7.4.2. Since $\mathbf{v}_3$ and $\mathbf{v}_8$ do not feature in (7.4.10), it is not necessary to any counting for them. Clearly we have a count of $4k$ for each of $\mathbf{v}_1, \mathbf{v}_4, \mathbf{v}_6, \mathbf{v}_9$, and none for the rest, making a total of $-16\tau_2^* k$.

We next identity the number of almost vertical units counted in (7.4.10) that cut the edges $v_7, \ldots, v_{12}$; see Figure 7.4.2. Clearly we have a count of $4k$ for each of $\mathbf{v}_2, \mathbf{v}_5, \mathbf{v}_7, \mathbf{v}_{10}$, and none for the rest, making a total of $16\tau_2^* k$.

The difference, in absolute value, is therefore $32\tau_2^* k$. Let $c_2 = c_{2,1}$ in (7.2.9) and (7.2.10). It follows that the second eigenvalue $\lambda_2(k)$ contributes $32c_2\tau_2^*\lambda_2^r(k)k$ to the difference between the edge-cuttings numbers of $v_1, \ldots, v_6$ and $v_7, \ldots, v_{12}$.

So the *horizontal* deviation from the starting point comes from the second largest eigenvalue, with order of magnitude λ_2^r compared to the order of magnitude λ_1^r of the main term. Choosing $T = \lambda_1^r$, we have $\lambda_2^r \asymp T^{\kappa_0}$, where

$$\kappa_0 = \kappa_0(k) = \frac{\log \lambda_2}{\log \lambda_1} = \frac{2\log k + \log 112}{2\log k + \log 144} + o(1), \tag{7.4.13}$$

in view of (7.4.8)–(7.4.9), is the irregularity exponent of a 1-direction geodesic of slope

$$\alpha_k = [12k; 12k, 12k, 12k, \ldots] = 6k + \sqrt{36k^2 + 1} = \sqrt{\lambda_1(k)} \tag{7.4.14}$$

on the period-surface Bil(2; C) in Figure 7.4.2.

Clearly $\kappa_0 = \kappa_0(k) \to 1$ as $k \to \infty$. So we have just established $T^{\kappa_0} = T^{1-\varepsilon}$ size *super-fast escape rate to infinity* for this infinite billiard with the explicit class of quadratic irrational slopes in (7.4.14) where the parameter $k \geqslant 1$ is any integer.

It is easy to see that the irregularity exponent $\kappa_0 = \kappa_0(k)$ in (7.4.13) is *precisely* the escape rate to infinity of this infinite billiard. The escape rate to infinity cannot be larger than the expression (7.4.13) coming from the two largest eigenvalues.

Note that this super-fast escape rate to infinity comes from horizontal deviation. As observed earlier, we have perfect cancellation in the vertical direction for the two largest eigenvalues. So let us investigate what the third eigenvalue gives.

The third largest eigenvalue of $M(k)|_{\mathcal{V}}$ is

$$\lambda_3(k) = 1 + \frac{\tau_3 k^2 + \sqrt{\tau_3^2 k^4 + 4\tau_3 k^2}}{2} = 1 + 48k^2 + 4k\sqrt{144k^2 + 6},$$

with eigenvector of the form

$$\Psi_3 = (-1,-1,-2,-1,-1,1,1,2,1,1,-\tau_3^*,-\tau_3^*,-2\tau_3^*,-\tau_3^*,-\tau_3^*,\tau_3^*,\tau_3^*,2\tau_3^*,\tau_3^*,\tau_3^*)^T,$$

where

$$\tau_3^* = \frac{-\tau_3 k^2 + \sqrt{\tau_3^2 k^4 + 4\tau_3 k^2}}{2} = 4k\sqrt{144k^2+6} - 48k^2.$$

The eigenvector of $M(k)$ corresponding to the eigenvector Ψ_3 of $M(k)|_{\mathcal{V}}$ is given by

$$\begin{aligned} &-\mathbf{u}_1 - \mathbf{u}_2 - 2\mathbf{u}_3 - \mathbf{u}_4 - \mathbf{u}_5 + \mathbf{u}_6 + \mathbf{u}_7 + 2\mathbf{u}_8 + \mathbf{u}_9 + \mathbf{u}_{10} \\ &\quad - \tau_3^*\mathbf{v}_1 - \tau_3^*\mathbf{v}_2 - 2\tau_3^*\mathbf{v}_3 - \tau_3^*\mathbf{v}_4 - \tau_3^*\mathbf{v}_5 \\ &\quad + \tau_3^*\mathbf{v}_6 + \tau_3^*\mathbf{v}_7 + 2\tau_3^*\mathbf{v}_8 + \tau_3^*\mathbf{v}_9 + \tau_3^*\mathbf{v}_{10}. \end{aligned}$$

We first identity the number of almost vertical units counted here that cut the edges $h_1,\ldots,h_6$; see Figure 7.4.2. The counts from $\mathbf{u}_i$, $i=1,\ldots,10$, are given by (7.4.11). Again, it is not difficult to show that each of $\mathbf{v}_1,\ldots\mathbf{v}_{10}$ contributes precisely zero. Thus for the edges $h_1,\ldots,h_6$, we have a total count of

$$-44k^2 - 44k^2 - 64k^2 - 44k^2 - 44k^2 + 12k^2 + 12k^2 + 12k^2 + 12k^2 = -196k^2.$$

We next identity the number of almost vertical units counted here that cut the edges $h_7,\ldots,h_{12}$; see Figure 7.4.2. The counts from $\mathbf{u}_i$, $i=1,\ldots,10$, are given by (7.4.12). Again, it is not difficult to show that each of $\mathbf{v}_1,\ldots\mathbf{v}_{10}$ contributes precisely zero. Thus for the edges $h_7,\ldots,h_{12}$, we have a total count of

$$-12k^2 - 12k^2 - 12k^2 - 12k^2 + 44k^2 + 44k^2 + 64k^2 + 44k^2 + 44k^2 = 196k^2.$$

The difference, in absolute value, is therefore $392\tau_3^*k^2$. Let $c_3 = c_{3,1}$ in (7.2.9) and (7.2.10). It follows that the third eigenvalue $\lambda_3(k)$ contributes $392c_3\tau_3^*\lambda_3^r(k)k^2$ to the difference between the edge-cuttings numbers of $h_1,\ldots,h_6$ and $h_7,\ldots,h_{12}$.

So the *vertical* deviation from the starting point comes from the third largest eigenvalue, with order of magnitude λ_3^r compared to the order of magnitude λ_1^r of the main term.

Example 7.4.2. Consider the Ehrenfest wind-tree model with $a=b=1/3$, rescaled so that we have square faces of unit area. Consider a 4-direction billiard trajectory in the infinite region in Figure 7.4.6. Here the building block of this infinite polysquare surface is a 3×3 square, with walls on all sides of the middle square face as shown.

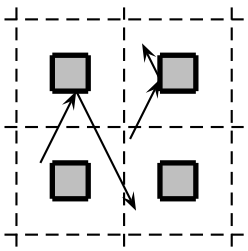

Figure 7.4.6: Ehrenfest wind-tree billiard model

As usual, this infinite billiard model is equivalent to a 1-direction geodesic flow on an infinite polysquare surface that we denote by $\mathrm{Bil}(\infty;2;\mathrm{W})$. Here the index 2 indicates that this is double periodic, and the letter W refers to the wind-tree model. To construct $\mathrm{Bil}(\infty;2;\mathrm{W})$, we take one of the building blocks, and unfold the 4-direction billiard flow on it to a 1-direction geodesic flow on a 4-copy version of it, obtained by reflecting horizontally and vertically. Note that each copy of the period surface has a right-neighbor, a left-neighbor, a down-neighbor and an up-neighbor in $\mathrm{Bil}(\infty;2;\mathrm{W})$, and we need appropriate edge identification for gluing them together.

The *period-surface* Bil(2; W) of Bil(∞; 2; W) is shown in the picture on the left in Figure 7.4.7. The horizontal and vertical streets of Bil(2; W) are indicated in the picture on the right in Figure 7.4.7 where, for instance, the entries $\leftrightarrow 3$ and $\updownarrow 5$ in a square face indicates that the square face is on the 3-rd horizontal street and the 5-th vertical street. It is easy to see that Bil(2; W) has 10 horizontal streets, of which 8 are of length 3 and 2 are of length 4. It also has 10 vertical streets, of which 8 are of length 3 and 2 are of length 4.

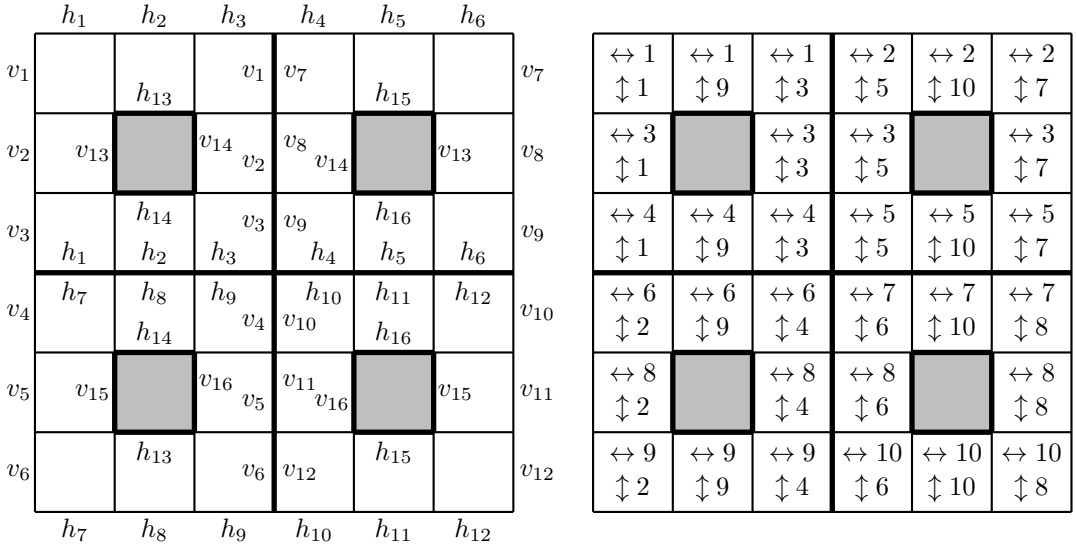

Figure 7.4.7: the period surface Bil(2; W) of Bil(∞; 2; W)

Consider now a 1-direction geodesic starting from some vertex of Bil(2; W) with slope α given by (7.2.1) with $m = n = 12$.

For $\mathbf{u}_1, \mathbf{u}_2, \mathbf{u}_4, \mathbf{u}_5$, Figure 7.4.8 describes the situation. With $J_1 = J_4 = \{1, 3, 9\}$ and $J_2 = J_5 = \{5, 7, 10\}$, for the horizontal streets corresponding to $\mathbf{u}_1, \mathbf{u}_2, \mathbf{u}_4, \mathbf{u}_5$, we have

$$\begin{aligned}(M - I)\mathbf{u}_1 &= (M - I)\mathbf{u}_4 \\ &= 44(\mathbf{u}_1 + \mathbf{v}_1) + 32(\mathbf{u}_3 + \mathbf{v}_3) + 44(\mathbf{u}_4 + \mathbf{v}_4) \\ &\quad + 12(\mathbf{u}_6 + \mathbf{v}_6) + 12(\mathbf{u}_9 + \mathbf{v}_9), \qquad (7.4.15) \\ (M - I)\mathbf{u}_2 &= (M - I)\mathbf{u}_5 \\ &= 44(\mathbf{u}_2 + \mathbf{v}_2) + 32(\mathbf{u}_3 + \mathbf{v}_3) + 44(\mathbf{u}_5 + \mathbf{v}_5) \\ &\quad + 12(\mathbf{u}_7 + \mathbf{v}_7) + 12(\mathbf{u}_{10} + \mathbf{v}_{10}). \qquad (7.4.16)\end{aligned}$$

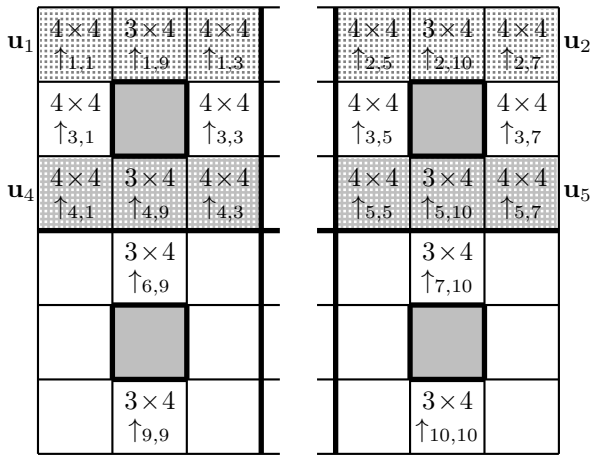

Figure 7.4.8: almost vertical of type $\uparrow$ in $\mathbf{u}_1, \mathbf{u}_2, \mathbf{u}_4, \mathbf{u}_5$

For $\mathbf{u}_6, \mathbf{u}_7, \mathbf{u}_9, \mathbf{u}_{10}$, Figure 7.4.9 describes the situation. With $J_6 = J_9 = \{2, 4, 9\}$ and $J_7 = J_{10} = \{6, 8, 10\}$, for the horizontal streets corresponding to $\mathbf{u}_6, \mathbf{u}_7, \mathbf{u}_9, \mathbf{u}_{10}$, we have

$$\begin{aligned}(M-I)\mathbf{u}_6 &= (M-I)\mathbf{u}_9 \\ &= 12(\mathbf{u}_1+\mathbf{v}_1)+12(\mathbf{u}_4+\mathbf{v}_4)+44(\mathbf{u}_6+\mathbf{v}_6) \\ &\quad +32(\mathbf{u}_8+\mathbf{v}_8)+44(\mathbf{u}_9+\mathbf{v}_9), \qquad (7.4.17)\\ (M-I)\mathbf{u}_7 &= (M-I)\mathbf{u}_{10} \\ &= 12(\mathbf{u}_2+\mathbf{v}_2)+12(\mathbf{u}_5+\mathbf{v}_5)+44(\mathbf{u}_7+\mathbf{v}_7) \\ &\quad +32(\mathbf{u}_8+\mathbf{v}_8)+44(\mathbf{u}_{10}+\mathbf{v}_{10}). \qquad (7.4.18)\end{aligned}$$

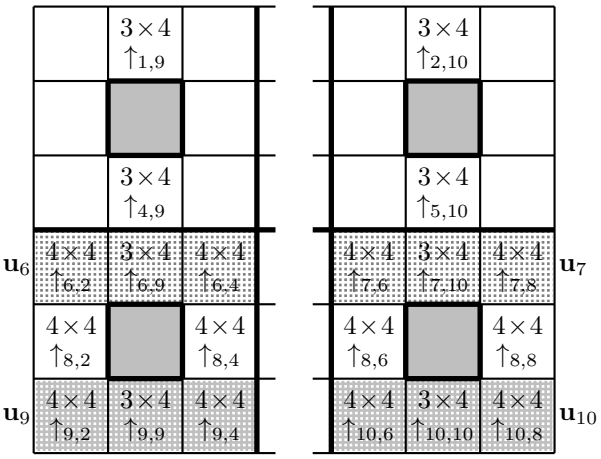

Figure 7.4.9: almost vertical of type ↑ in $\mathbf{u}_6, \mathbf{u}_7, \mathbf{u}_9, \mathbf{u}_{10}$

For $\mathbf{u}_3, \mathbf{u}_8$, Figure 7.4.10 describes the situation. Noting that $J_3 = \{1, 3, 5, 7\}$ and $J_8 = \{2, 4, 6, 8\}$, for the horizontal streets corresponding to $\mathbf{u}_3, \mathbf{u}_8$, we have

$$\begin{aligned}(M-I)\mathbf{u}_3 &= 24(\mathbf{u}_1+\mathbf{v}_1)+24(\mathbf{u}_2+\mathbf{v}_2)+48(\mathbf{u}_3+\mathbf{v}_3) \\ &\quad +24(\mathbf{u}_4+\mathbf{v}_4)+24(\mathbf{u}_5+\mathbf{v}_5), \qquad (7.4.19)\\ (M-I)\mathbf{u}_8 &= 24(\mathbf{u}_6+\mathbf{v}_6)+24(\mathbf{u}_7+\mathbf{v}_7)+48(\mathbf{u}_8+\mathbf{v}_8) \\ &\quad +24(\mathbf{u}_9+\mathbf{v}_9)+24(\mathbf{u}_{10}+\mathbf{v}_{10}). \qquad (7.4.20)\end{aligned}$$

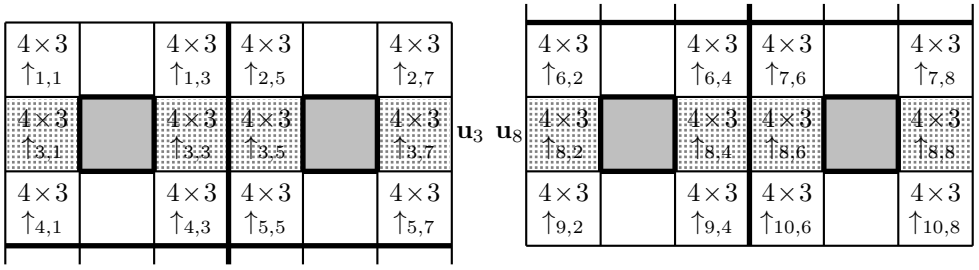

Figure 7.4.10: almost vertical of type ↑ in $\mathbf{u}_3$

It follows from (7.4.15)–(7.4.20) that the street-spreading matrix is given by

$$\mathbf{S} = \begin{pmatrix} 44 & 0 & 24 & 44 & 0 & 12 & 0 & 0 & 12 & 0 \\ 0 & 44 & 24 & 0 & 44 & 0 & 12 & 0 & 0 & 12 \\ 32 & 32 & 48 & 32 & 32 & 0 & 0 & 0 & 0 & 0 \\ 44 & 0 & 24 & 44 & 0 & 12 & 0 & 0 & 12 & 0 \\ 0 & 44 & 24 & 0 & 44 & 0 & 12 & 0 & 0 & 12 \\ 12 & 0 & 0 & 12 & 0 & 44 & 0 & 24 & 44 & 0 \\ 0 & 12 & 0 & 0 & 12 & 0 & 44 & 24 & 0 & 44 \\ 0 & 0 & 0 & 0 & 0 & 32 & 32 & 48 & 32 & 32 \\ 12 & 0 & 0 & 12 & 0 & 44 & 0 & 24 & 44 & 0 \\ 0 & 12 & 0 & 0 & 12 & 0 & 44 & 24 & 0 & 44 \end{pmatrix}. \tag{7.4.21}$$

This has non-zero eigenvalues and corresponding eigenvectors given by

$$\begin{aligned} \tau_1 = 144, &\quad \psi_1 = (3,3,4,3,3,3,3,4,3,3)^T, \\ \tau_2 = 112, &\quad \psi_{2,1} = (0,-1,-1,0,-1,1,0,1,1,0)^T, \\ &\quad \psi_{2,2} = (-1,0,-1,-1,0,0,1,1,0,1)^T, \\ \tau_3 = 64, &\quad \psi_3 = (1,-1,0,1,-1,-1,1,0,-1,1)^T, \\ \tau_4 = 16, &\quad \psi_4 = (1,1,-4,1,1,1,1,-4,1,1)^T. \end{aligned}$$

Note that the street-spreading matrix $\mathbf{S}$ given by (7.4.21) corresponds to the choice of parameters $m = n = 12$. Switching to $m = n = 12k$, where $k \geqslant 1$ is any integer, we obtain the new street-spreading matrix $\mathbf{S}(k) = k^2\mathbf{S}$ simply by multiplying the matrix $\mathbf{S}$ by k^2. Then of course the eigenvalues are also multiplied by k^2, but the eigenvectors remain the same. Naturally the 2-step transition matrix M is modified to $M(k)$.

We next determine some of the eigenvalues of $M(k)$ using (7.2.38). The largest eigenvalue of $M(k)$ is

$$\lambda_1(k) = 1 + \frac{\tau_1 k^2 + \sqrt{\tau_1^2 k^4 + 4\tau_1 k^2}}{2} = 1 + 72k^2 + 12k\sqrt{36k^2+1}, \tag{7.4.22}$$

while the second largest eigenvalue of $M(k)$ is

$$\lambda_2(k) = 1 + \frac{\tau_2 k^2 + \sqrt{\tau_2^2 k^4 + 4\tau_2 k^2}}{2} = 1 + 56k^2 + 4k\sqrt{196k^2+7}, \tag{7.4.23}$$

with eigenvectors of the form

$$\begin{aligned} \Psi_{2,1} &= (0,-1,-1,0,-1,1,0,1,1,0,0,-\tau_2^*,-\tau_2^*,0,-\tau_2^*,\tau_2^*,0,\tau_2^*,\tau_2^*,0)^T, \\ \Psi_{2,2} &= (-1,0,-1,-1,0,0,1,1,0,1,-\tau_2^*,0,-\tau_2^*,-\tau_2^*,0,0,\tau_2^*,\tau_2^*,0,\tau_2^*)^T, \end{aligned}$$

where

$$\tau_2^* = \frac{-\tau_2 k^2 + \sqrt{\tau_2^2 k^4 + 4\tau_2 k^2}}{2} = 4k\sqrt{196k^2+7} - 56k^2.$$

Let us return to Figures 7.4.6 and 7.4.7. It is clear that the billiard moves to the up-neighbour if the 1-direction geodesic hits any of the edges $h_1, \ldots, h_6$, and moves to the down-neighbor if the 1-direction geodesic hits any of the edges $h_7, \ldots, h_{12}$. It is also clear that the billiard moves to the right-neighbor if the 1-direction geodesic hits any of the edges $v_7, \ldots, v_{12}$, and moves to the left-neighbor if the 1-direction geodesic hits any of the edges $v_1, \ldots, v_6$.

We now proceed to find the edge-cutting numbers of $h_1, \ldots, h_6$ and $h_7, \ldots, h_{12}$. As before, it is easily shown that each of $\mathbf{v}_1, \ldots \mathbf{v}_{10}$ contributes precisely zero.

As in Examples 7.3.1 and 7.3.2, the eigenvalue λ_1 does not contribute to their difference, as any lack of cancellation would violate the Gutkin–Veech theorem that guarantees uniformity.

The eigenvector of $M(k)$ corresponding to the eigenvector $\Psi_{2,1}$ of $M|_{\mathcal{V}}$ is given by

$$\begin{aligned} &- \mathbf{u}_2 - \mathbf{u}_3 - \mathbf{u}_5 + \mathbf{u}_6 + \mathbf{u}_8 + \mathbf{u}_9 \\ &\quad - \tau_2^* \mathbf{v}_2 - \tau_2^* \mathbf{v}_3 - \tau_2^* \mathbf{v}_5 + \tau_2^* \mathbf{v}_6 + \tau_2^* \mathbf{v}_8 + \tau_2^* \mathbf{v}_9. \end{aligned} \tag{7.4.24}$$

The eigenvector of $M(k)$ corresponding to the eigenvector $\Psi_{2,2}$ of $M|_{\mathcal{V}}$ is given by

$$\begin{aligned} &- \mathbf{u}_1 - \mathbf{u}_3 - \mathbf{u}_4 + \mathbf{u}_7 + \mathbf{u}_8 + \mathbf{u}_{10} \\ &\quad - \tau_2^* \mathbf{v}_1 - \tau_2^* \mathbf{v}_3 - \tau_2^* \mathbf{v}_4 + \tau_2^* \mathbf{v}_7 + \tau_2^* \mathbf{v}_8 + \tau_2^* \mathbf{v}_{10}. \end{aligned} \tag{7.4.25}$$

We first identity the number of almost vertical units counted here that cut the edges $h_1, \ldots, h_6$; see Figure 7.4.7. The counts from $\mathbf{u}_i$, $i = 1, \ldots, 10$, are

$$\begin{array}{lllll} \mathbf{u}_1 \mapsto 44k^2, & \mathbf{u}_2 \mapsto 44k^2, & \mathbf{u}_3 \mapsto 48k^2, & \mathbf{u}_4 \mapsto 44k^2, & \mathbf{u}_5 \mapsto 44k^2, \\ \mathbf{u}_6 \mapsto 12k^2, & \mathbf{u}_7 \mapsto 12k^2, & \mathbf{u}_8 \mapsto 0, & \mathbf{u}_9 \mapsto 12k^2, & \mathbf{u}_{10} \mapsto 12k^2. \end{array}$$

Thus corresponding to the eigenvector $\Psi_{2,1}$ and (7.4.24), the total count is $-112k^2$. Corresponding to the eigenvector $\Psi_{2,2}$ and (7.4.25), the total count is also $-112k^2$.

We next identity the number of almost vertical units counted here that cut the edges $h_7, \ldots, h_{12}$; see Figure 7.4.7. The counts from $\mathbf{u}_i$, $i = 1, \ldots, 10$, are

$$\begin{array}{lllll} \mathbf{u}_1 \mapsto 12k^2, & \mathbf{u}_2 \mapsto 12k^2, & \mathbf{u}_3 \mapsto 0, & \mathbf{u}_4 \mapsto 12k^2, & \mathbf{u}_5 \mapsto 12k^2, \\ \mathbf{u}_6 \mapsto 44k^2, & \mathbf{u}_7 \mapsto 44k^2, & \mathbf{u}_8 \mapsto 48k^2, & \mathbf{u}_9 \mapsto 44k^2, & \mathbf{u}_{10} \mapsto 44k^2. \end{array}$$

Thus corresponding to the eigenvector $\Psi_{2,1}$ and (7.4.24), the total count is $112k^2$. Corresponding to the eigenvector $\Psi_{2,2}$ and (7.4.25), the total count is also $112k^2$.

The difference, in absolute value, is therefore $224k^2$ in each case. It follows that the second eigenvalue $\lambda_2(k)$ contributes $224(c_{2,1} + c_{2,2})\lambda_2^r(k)k^2$ to the difference between the edge-cuttings numbers of $h_1, \ldots, h_6$ and $h_7, \ldots, h_{12}$.

Naturally, we can choose a starting vector $\mathbf{w}_0$ for the geodesic in question such that $c_{2,1} + c_{2,2} \neq 0$. This is clearly possible, since $c_{2,1} + c_{2,2} = 0$ always would violate the linear independence of the eigenvectors $\Psi_{2,1}$ and $\Psi_{2,2}$.

So the deviation from the starting point comes from the second largest eigenvalue, with order of magnitude λ_2^r compared to the order of magnitude λ_1^r of the main term. Choosing $T = \lambda_1^r$, we have $\lambda_2^r \asymp T^{\kappa_0}$, where

$$\kappa_0 = \kappa_0(k) = \frac{\log \lambda_2}{\log \lambda_1} = \frac{2 \log k + \log 112}{2 \log k + \log 144} + o(1), \tag{7.4.26}$$

in view of (7.4.22)–(7.4.23), is the irregularity exponent of a 1-direction geodesic of slope

$$\alpha_k = [12k; 12k, 12k, 12k, \ldots] = 6k + \sqrt{36k^2 + 1} = \sqrt{\lambda_1(k)} \tag{7.4.27}$$

on the period-surface Bil(2; W) in Figure 7.4.8.

Again $\kappa_0 = \kappa_0(k) \to 1$ as $k \to \infty$. So we have just established $T^{\kappa_0} = T^{1-\varepsilon}$ size *super-fast escape rate to infinity* for this infinite billiard with the explicit class of quadratic irrational slopes in (7.4.27) where the parameter $k \geqslant 1$ is any integer.

It is easy to see that the irregularity exponent $\kappa_0 = \kappa_0(k)$ in (7.4.26) is *precisely* the escape rate to infinity of this infinite billiard. The escape rate to infinity cannot be larger than the expression (7.4.26) coming from the two largest eigenvalues.

In view of the examples in Sections 7.3–7.4 so far, it seems plausible to conjecture that every periodic infinite polysquare billiard with at least one *infinite street* exhibits super-fast escape rate to infinity for some concrete infinite class of quadratic irrational slopes. It would be nice to prove this conjecture in general.

We complete this section with a hybrid example.

Example 7.4.3. Our final example is modified from the Ehrenfest wind-tree model. Consider a 2-direction billiard trajectory in the region in Figure 7.4.11. Here the building block of this infinite polysquare surface is a 3×3 square, with the middle square missing and with two vertical walls. Note that there is no billiard in the vertical direction, so this is a hybrid problem. The trajectory keeps on going up vertically, or going down vertically, one way but not both.

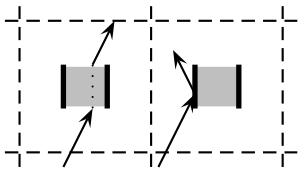

Figure 7.4.11: a hybrid model

As usual, this infinite hybrid model is equivalent to a 1-direction geodesic flow on an infinite polysquare surface that we denote by $\mathrm{Bil}(\infty; 2; \mathrm{H})$. Here the index 2 indicates that this is double periodic, and the letter H refers to the hybrid model. To construct $\mathrm{Bil}(\infty; 2; \mathrm{H})$, we take one of the building blocks, and unfold the 2-direction billiard flow on it to a 1-direction geodesic flow on a 2-copy version of it, obtained by reflecting vertically. Note that each 2-copy version has a right-neighbor, a left-neighbor, a down-neighbor and an up-neighbor in $\mathrm{Bil}(\infty; 2; \mathrm{H})$, and we need appropriate edge identification for gluing them together.

The *period-surface* $\mathrm{Bil}(2; \mathrm{H})$ of $\mathrm{Bil}(\infty; 2; \mathrm{H})$ is shown in the picture on the left in Figure 7.4.12.

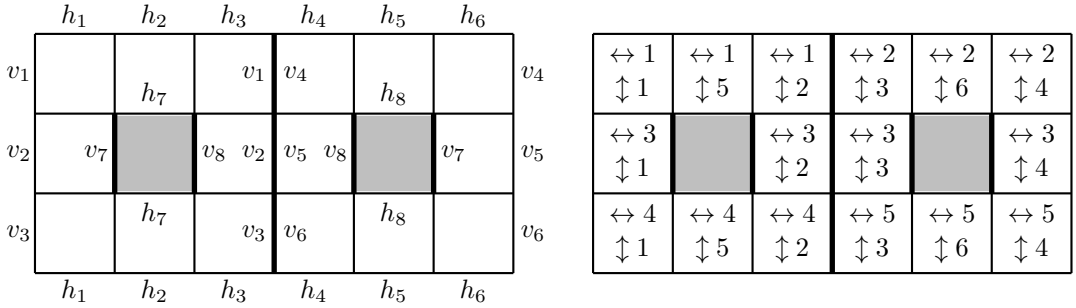

Figure 7.4.12: the period surface $\mathrm{Bil}(2; \mathrm{H})$ of $\mathrm{Bil}(\infty; 2; \mathrm{H})$

The horizontal and vertical streets of $\mathrm{Bil}(2; \mathrm{H})$ are indicated in the picture on the right in Figure 7.4.12 where, for instance, the entries $\leftrightarrow 3$ and $\updownarrow 4$ in a square face indicates that the square face is on the 3-rd horizontal street and the 4-th vertical street. It is easy to see that $\mathrm{Bil}(2; \mathrm{H})$ has 5 horizontal streets, of which 4 are of length 3 and 1 is of length 4. It also has 6 vertical streets, of which 4 are of length 3 and 2 are of length 2.

Consider now a 1-direction geodesic starting from some vertex of $\mathrm{Bil}(2; H)$ with slope α given by (7.2.1) with $m = n = 12$.

For $\mathbf{u}_1, \mathbf{u}_2, \mathbf{u}_4, \mathbf{u}_5$, Figure 7.4.13 describes the situation. With $J_1 = J_4 = \{1, 2, 5\}$ and $J_2 = J_5 = \{3, 4, 6\}$, for the horizontal streets corresponding to $\mathbf{u}_1, \mathbf{u}_2, \mathbf{u}_4, \mathbf{u}_5$, we have

$$\begin{aligned}(M - I)\mathbf{u}_1 &= (M - I)\mathbf{u}_4 \\ &= 56(\mathbf{u}_1 + \mathbf{v}_1) + 32(\mathbf{u}_3 + \mathbf{v}_3) + 56(\mathbf{u}_4 + \mathbf{v}_4) \qquad (7.4.28) \\ (M - I)\mathbf{u}_2 &= (M - I)\mathbf{u}_5 \\ &= 56(\mathbf{u}_2 + \mathbf{v}_2) + 32(\mathbf{u}_3 + \mathbf{v}_3) + 56(\mathbf{u}_5 + \mathbf{v}_5). \qquad (7.4.29)\end{aligned}$$

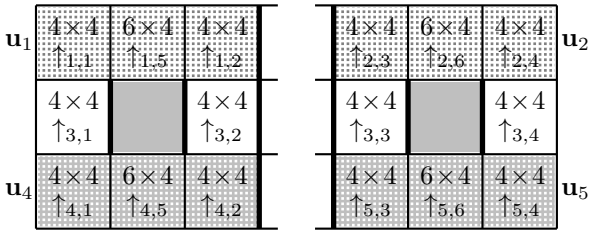

Figure 7.4.13: almost vertical units of type ↑ in $\mathbf{u}_1, \mathbf{u}_2, \mathbf{u}_4, \mathbf{u}_5$

For $\mathbf{u}_3$, Figure 7.4.14 describes the situation. With $J_3 = \{1, 2, 3, 4\}$, for the horizontal street corresponding to $\mathbf{u}_3$, we have

$$(M - I)\mathbf{u}_3 = 24(\mathbf{u}_1 + \mathbf{v}_1) + 24(\mathbf{u}_2 + \mathbf{v}_2) + 48(\mathbf{u}_3 + \mathbf{v}_3) + 24(\mathbf{u}_4 + \mathbf{v}_4) + 24(\mathbf{u}_5 + \mathbf{v}_5). \tag{7.4.30}$$

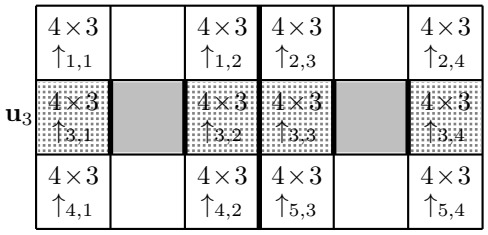

Figure 7.4.14: almost vertical units of type ↑ in $\mathbf{u}_3$

It follows from (7.4.28)–(7.4.30) that the street-spreading matrix is given by

$$\mathbf{S} = \begin{pmatrix} 56 & 0 & 24 & 56 & 0 \\ 0 & 56 & 24 & 0 & 56 \\ 32 & 32 & 48 & 32 & 32 \\ 56 & 0 & 24 & 56 & 0 \\ 0 & 56 & 24 & 0 & 56 \end{pmatrix}. \tag{7.4.31}$$

This has non-zero eigenvalues and corresponding eigenvectors given by

$$\tau_1 = 144, \quad \psi_1 = (3, 3, 4, 3, 3)^T,$$
$$\tau_2 = 112, \quad \psi_2 = (-1, 1, 0, -1, 1)^T,$$
$$\tau_3 = 16, \quad \psi_3 = (1, 1, -4, 1, 1)^T.$$

Note that the street-spreading matrix $\mathbf{S}$ given by (7.4.31) corresponds to the choice of parameters $m = n = 12$. Switching to $m = n = 12k$, where $k \geqslant 1$ is any integer, we obtain the new street-spreading matrix $\mathbf{S}(k) = k^2\mathbf{S}$ simply by multiplying the matrix $\mathbf{S}$ by k^2. Then of course the eigenvalues are also multiplied by k^2, but the eigenvectors remain the same. Naturally the 2-step transition matrix M is modified to $M(k)$.

We next determine some of the eigenvalues of $M(k)$ using (7.2.38). The largest eigenvalue of $M(k)$ is

$$\lambda_1(k) = 1 + \frac{\tau_1 k^2 + \sqrt{\tau_1^2 k^4 + 4\tau_1 k^2}}{2} = 1 + 72k^2 + 12k\sqrt{36k^2 + 1},$$

while the second largest eigenvalue of $M(k)$ is

$$\lambda_2(k) = 1 + \frac{\tau_2 k^2 + \sqrt{\tau_2^2 k^4 + 4\tau_2 k^2}}{2} = 1 + 56k^2 + 4k\sqrt{196k^2 + 7},$$

with eigenvector of the form

$$\Psi_2 = (-1, 1, 0, -1, 1, -\tau_2^*, \tau_2^*, 0, -\tau_2^*, \tau_2^*)^T,$$

where

$$\tau_2^* = \frac{-\tau_2 k^2 + \sqrt{\tau_2^2 k^4 + 4\tau_2 k^2}}{2} = 4k\sqrt{196k^2+7} - 56k^2.$$

As observed earlier, there is no billiard in the vertical direction, so we now proceed to study its horizontal behaviour. We thus proceed to find the edge-cutting numbers of v_1, v_2, v_3 and v_4, v_5, v_6; see Figure 7.4.12.

It can be shown that the eigenvalue λ_1 does not contribute to their difference, although the Gutkin–Veech theorem does not apply here. So we concentrate our attention on the contribution from the eigenvector Ψ_2 of $M|_{\mathcal{V}}$.

The eigenvector of $M(k)$ corresponding to the eigenvector Ψ_2 of $M|_{\mathcal{V}}$ is given by

$$-\mathbf{u}_1 + \mathbf{u}_2 - \mathbf{u}_4 + \mathbf{u}_5 - \tau_2^*\mathbf{v}_1 + \tau_2^*\mathbf{v}_2 - \tau_2^*\mathbf{v}_4 + \tau_2^*\mathbf{v}_5. \tag{7.4.32}$$

Here, note that none of $\mathbf{u}_1, \ldots, \mathbf{u}_5$ makes any non-zero contribution, as only units of type $\dagger$ can contribute to the count. For the contributions from $\mathbf{v}_1, \ldots, \mathbf{v}_5$, we use (7.2.15).

We first identity the number of almost vertical units counted in (7.4.32) that cut the edges v_1, v_2, v_3; see Figure 7.4.12. Since $\mathbf{v}_3$ does not feature in (7.4.32), it is not necessary to any counting for it. Clearly we have a count of $4k$ for each of $\mathbf{v}_1, \mathbf{v}_4$, and none for $\mathbf{v}_2, \mathbf{v}_5$, making a total of $-8\tau_2^* k$.

We next identity the number of almost vertical units counted in (7.4.32) that cut the edges v_4, v_5, v_6; see Figure 7.4.12. Clearly we have a count of $4k$ for each of $\mathbf{v}_2, \mathbf{v}_5$, and none for $\mathbf{v}_1, \mathbf{v}_4$, making a total of $8\tau_2^* k$.

The difference, in absolute value, is therefore $16\tau_2^* k$. Thus the second eigenvalue $\lambda_2(k)$ contributes $16c_2\tau_2^*\lambda_2^r(k)k$ to the difference between the edge-cuttings numbers of v_1, v_2, v_3 and v_4, v_5, v_6.

Again the *horizontal* deviation from the starting point comes from the second largest eigenvalue, with order of magnitude λ_2^r compared to the order of magnitude λ_1^r of the main term.

7.5. **Geodesics with arbitrary starting points.** In Sections 7.3 and 7.4, we have exhibited examples of 1-direction geodesics in infinite polysquare surfaces that start from a vertex and which exhibit super-fast escape rate to infinity. In Example 7.3.2, we have also shown that there are 1-direction geodesics in square-mazes that start from a vertex and which exhibit super-slow escape rate to infinity.

We now describe a method by which we can relax the restriction that the starting point of the geodesic has to be a vertex of a polysquare, so that only the angle α of the geodesic matters, and can still establish results on the escape rate to infinity as before.

Note, first of all, that a 1-direction geodesic *modulo one* is equivalent to a torus line in the unit square. To help us visualize the situation even more clearly, we can replace the unit square by $\mathbb{R}^2$ and the torus line by a line on $\mathbb{R}^2$.

Next, note that we are considering slopes α that are badly approximable numbers. Such numbers satisfy the following two properties.

Property A. *Suppose that α is badly approximable. Then there exists a constant $C^* = C^*(\alpha) > 0$ such that for every real number $\ell \geqslant 1$, every segment of length ℓ of a straight line of slope α has distance at most C^*/ℓ from the nearest integer lattice point in $\mathbb{Z}^2$.*

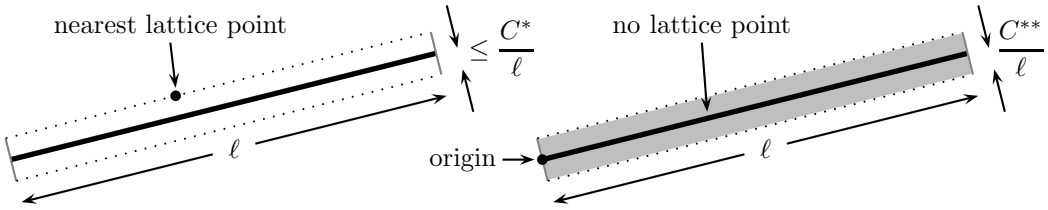

Figure 7.5.1: illustrating Property A and Property B

Property B. *Suppose that α is badly approximable. Then there exists a constant $C^{**} = C^{**}(\alpha) > 0$ such that for any real number $\ell \geqslant 1$, any tilted rectangle with one side starting from the origin, with slope α and length ℓ, and with the perpendicular side of length C^{**}/ℓ, does not contain any integer lattice point in $\mathbb{Z}^2$ except the origin.*

The idea is to consider geodesics that are parallel to our given geodesic and which share some of its characteristics.

Consider the initial segment $L(S;t)$, $0 \leqslant t \leqslant T$, with $T \geqslant 2$, of a 1-direction geodesic L of slope α, starting at a point S, not necessarily a vertex of a polysquare surface $\mathcal{P}$, as shown in the top half of Figure 7.5.2. Let $Q = Q(T) = L(S;t_0)$ denote the point on this segment which is closest to a vertex of $\mathcal{P}$, and let V be this closest vertex. Using Property A, we see that the distance between Q and V is at most C^*/T.

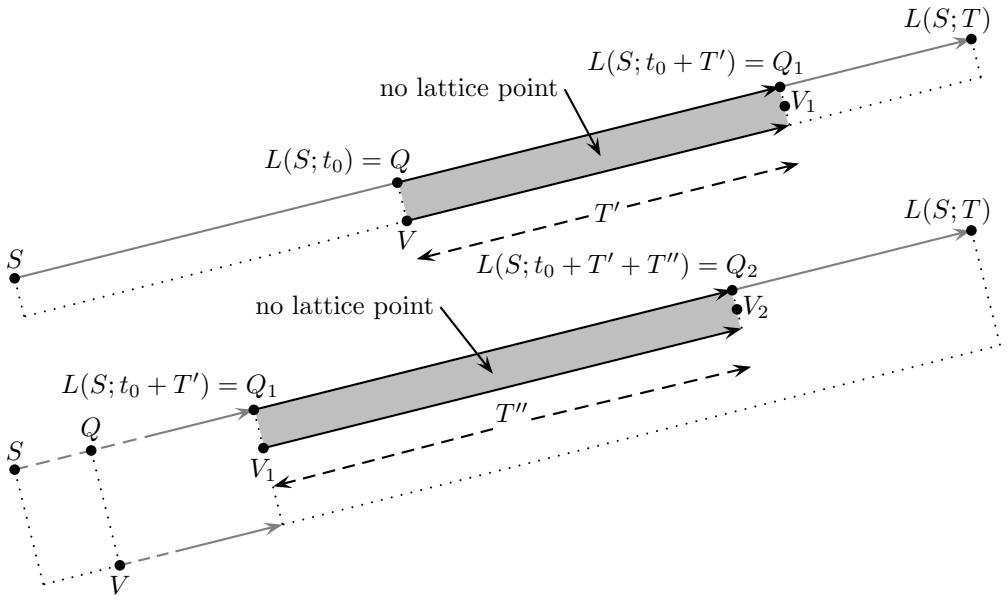

Figure 7.5.2: using parallel geodesics

Starting from the vertex V, we draw a new geodesic L' of slope α, in the same forward direction as L. Consider the longest vertex-free rectangle between L and L'. Using Property B, we see that the side of this rectangle parallel to L has length

$$T' \geqslant \frac{C^{**}}{C^*} T. \tag{7.5.1}$$

Suppose that $T \leqslant t_0 + T'$. Then the segment $L(S;t)$, $t_0 \leqslant t \leqslant T$, of L remains close to the segment $L'(V;t)$, $0 \leqslant t \leqslant T - t_0$, of the new geodesic L', since the rectangle between them does not contain any vertex of $\mathcal{P}$ apart from V and another vertex at the far end if $T = t_0 + T'$.

Suppose that $T > t_0 + T'$. Then the segment $L(S;t)$, $t_0 \leqslant t \leqslant t_0 + T'$, of L remains close to the segment $L'(V;t)$, $0 \leqslant t \leqslant T'$, of the new geodesic L', since the rectangle

between them does not contain any vertex of $\mathcal{P}$ apart from at the two ends. Since this rectangle is the longest vertex-free rectangle that we can draw, clearly there is another vertex V_1 of $\mathcal{P}$ at the far end. We now repeat the argument.

Starting from the vertex V_1, we draw a new geodesic L'' of slope α, in the same forward direction as L. Consider the longest vertex-free rectangle between L and L'', as shown in the bottom half of Figure 7.5.2. Using Property B, we see that the side of this rectangle parallel to L has length

$$T'' \geqslant \frac{C^{**}}{C^*} T. \tag{7.5.2}$$

Suppose that $t_0+T' < T \leqslant t_0+T'+T''$. Then the segment $L(S;t)$, $t_0+T' \leqslant t \leqslant T$, of L remains close to the segment $L''(V_1;t)$, $0 \leqslant t \leqslant T - t_0 - T'$, of the new geodesic L'', since the rectangle between them does not contain any vertex of $\mathcal{P}$ apart from V_1 and another vertex at the far end if $T = t_0 + T' + T''$.

Suppose that $T > t_0+T'+T''$. Then the segment $L(S;t)$, $t_0+T' \leqslant t \leqslant t_0+T'+T''$, of L remains close to the segment $L''(V_1;t)$, $0 \leqslant t \leqslant T''$, of the new geodesic L'', since the rectangle between them does not contain any vertex of $\mathcal{P}$ apart from at the two ends. Since this rectangle is the longest vertex-free rectangle that we can draw, clearly there is another vertex V_2 of $\mathcal{P}$ at the far end. We now repeat the argument again.

Clearly the argument must stop after a finite number of steps, in view of estimates such as (7.5.1) and (7.5.2) and their analogs. In particular it must stop after at most C^*/C^{**} steps.

Note that we have moved forward from the point Q to the point $L(S;T)$. Clearly a similar argument applies when we move backward from the point Q to the starting point $S = L(S;0)$.

What we have shown is that the finite geodesic $L(S;t)$, $0 \leqslant t \leqslant T$, can be broken up into a finite number of parts, each of which remains close to a parallel finite geodesic of the same length that starts from a vertex of the polysquare surface $\mathcal{P}$.

We can now use this observation to study escape rates to infinity.

Suppose that we have established that for a polysquare surface $\mathcal{P}$, the escape rate to infinity for a 1-direction geodesic L of slope α that starts at a vertex of $\mathcal{P}$ is $O(f(T))$ as a function of time T, where f is an increasing function satisfying $f(t) \to \infty$ as $t \to \infty$. This means that the diameter of the finite geodesic $L(t)$, $0 \leqslant t \leqslant T$, is $O(f(T))$. Consider now a 1-direction geodesic $L(S;t)$, $0 \leqslant t \leqslant T$, of slope α and starting point S that is not necessarily a vertex of $\mathcal{P}$. We now break $L(S;t)$, $0 \leqslant t \leqslant T$, into a finite number of parts as described above, and note that each part remains close to a parallel finite geodesic that starts at a vertex of $\mathcal{P}$ and has length at most T. The diameter of each of these parallel finite geodesics is $O(f(T))$. It follows that the diameter of $L(S;t)$, $0 \leqslant t \leqslant T$, is also $O(f(T))$.

For super-slow logarithmic escape rate to infinity, we have $f(T) = \log T$. For super-fast escape rate to infinity as in the examples in Sections 7.3 and 7.4, we have $f(T) = T^{\kappa_0}$.

To exhibit fluctuations of the required order of magnitude in the escape rate to infinity, we have a similar approach but with a slightly different first step.

Let $n \geqslant 2$ be an arbitrarily large but fixed integer. Consider a 1-direction geodesic $L(S;t)$, $t \geqslant 0$, on a polysquare surface $\mathcal{P}$ that starts from an arbitrary point with slope α. Suppose that t_0 is the first value of $t \geqslant 0$ such that $L(S;t_0)$ has perpendicular distance at most $1/n$ from a vertex of $\mathcal{P}$, as shown in Figure 7.5.3.

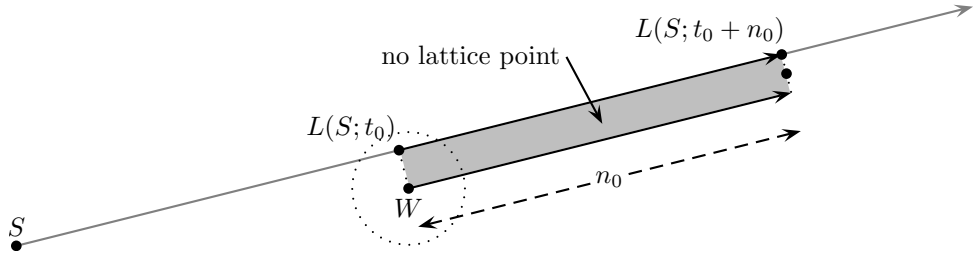

Figure 7.5.3: using parallel geodesics

In view of Property A, we know that $0 \leqslant t_0 \leqslant C^* n$.

Suppose that the vertex of $\mathcal{P}$ in question is W. Starting from this vertex W, we draw a new geodesic L' of slope α, in the same forward direction as L. Consider the longest vertex-free rectangle between L and L'. Using Property B, we see that the side of this rectangle parallel to L has length

$$n_0 \geqslant C^{**} n. \tag{7.5.3}$$

Furthermore, the segment $L(S;t)$, $t_0 \leqslant t \leqslant t_0+n_0$, of L remains close to the segment $L'(W;t)$, $0 \leqslant t \leqslant n_0$, of the new geodesic L', since the rectangle between them does not contain any vertex of $\mathcal{P}$ apart from at the two ends.

Suppose now that fluctuations of size $C_1 T^{\kappa_0}$ are exhibited for geodesics of slope α and length T that start from a vertex of $\mathcal{P}$. Then $L'(W;t)$, $0 \leqslant t \leqslant n_0$, and hence also $L(S;t)$, $t_0 \leqslant t \leqslant t_0 + n_0$, exhibits fluctuations of size

$$C_1 n_0^{\kappa_0} \geqslant C_2 n^{\kappa_0},$$

in view of (7.5.3). If the distance between S and $L(S;t_0)$ exceeds

$$\frac{1}{2} C_2 n^{\kappa_0}, \tag{7.5.4}$$

then $L(S;t)$, $0 \leqslant t \leqslant t_0$, has diameter at least equal to (7.5.4). Otherwise $L(S;t)$, $0 \leqslant t \leqslant t_0 + n_0$, has diameter at least equal to

$$C_2 n^{\kappa_0} - \frac{1}{2} C_2 n^{\kappa_0} = \frac{1}{2} C_2 n^{\kappa_0}.$$

8. Beyond polysquare surfaces

8.1. **Street-rational polyrectangle surfaces.** For polysquare surfaces, we have developed two very different versions of the shortline method. Using the eigenvalue-based version of the method, we can prove time-quantitative uniformity in terms of the irregularity exponent, as in [2, 3] and Section 7 of the present paper. Using the eigenvalue-free version of the method, we can prove time-quantitative density, including superdensity in some cases, as in [4].

The purpose of this section is to show that both versions of the shortline method can be extended to the class of *street-rational polyrectangle surfaces*, a class which includes all polysquare surfaces but goes far beyond. The first example of this larger class comes from right triangle billiard with angle $\pi/8$. This is perhaps the simplest non-integrable right triangle billiard. The standard trick of "unfolding" implies that this billiard can be described in terms of a 1-direction geodesic flow on the *regular octagon surface*, as shown in Figure 8.1.1.

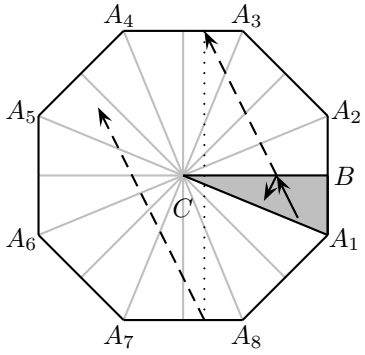

Figure 8.1.1: right triangle billiard with angle $\pi/8$, and geodesic flow on the regular octagon surface via unfolding

The definition of the *regular octagon surface* is rather straightforward. We identify the opposite parallel boundary edges by translation. Thus the four identified pairs are

$$(A_1A_2, A_6A_5), \quad (A_2A_3, A_7A_6), \quad (A_3A_4, A_8A_7), \quad (A_4A_5, A_1A_8).$$

Thus a 1-direction geodesic flow on the regular octagon surface, a compact orientable surface, is a 16-fold covering of the right triangle billiard with angle $\pi/8$, in much the same way as a torus line flow on a 2×2 square is a 4-fold covering of the square billiard. Needless to say, the regular octagon surface looks completely different from a polysquare surface.

In Figure 8.1.1, the point C represents the center of the octagon. The right triangle A_1BC has angle $\pi/8$ at C. Reflecting the A_1BC billiard across the side CB is the first step in the unfolding process, and leads to the triangle A_1A_2C. There are three more steps. Reflecting A_1A_2C across the side CA_2 leads to a polygon $A_1A_2A_3C$. Reflecting $A_1A_2A_3C$ across the side CA_3 leads to a polygon $A_1A_2A_3A_4A_5C$. Finally, reflecting $A_1A_2A_3A_4A_5C$ across the side CA_5 leads to the whole octagon.

Non-integrability is clear from the unfolding, since the vertices of the octagon are split-singularities of the geodesic flow on the surface.

Of course the same elegant construction works for any right triangle billiard with angle π/k where $k \geqslant 4$ is *even*. Unfolding will then convert the billiard orbit to a 1-direction geodesic flow on the *regular k-gon surface*, defined by identifying parallel boundary edges of the k-gon by translation. These are non-integrable systems for every even integer $k \geqslant 8$, so the regular octagon is the simplest such system.

Remark. Consider the regular k-gon surface with even $k \geqslant 4$. If k is divisible by 4, then the boundary identification gives 1 vertex, $k/2$ edges, and 1 region, so Euler's formula

$$2 - 2g = \chi = V - E + R = 1 - (k/2) + 1$$

gives $g = k/4$. If k is not divisible by 4, then the boundary identification gives 2 vertices, $k/2$ edges, and 1 region, so Euler's formula

$$2 - 2g = \chi = V - E + R = 2 - (k/2) + 1$$

gives $g = (k-2)/4$. Thus the regular k-gon surface with even k has genus 1 when $k = 4, 6$. This is consistent with the well known fact that we can tile the plane with squares or regular hexagons, but not with any other regular polygons with an even number of sides.

Let us return to the regular octagon surface. While it looks completely different from a polysquare surface, there is a hidden similarity. The regular octagon surface is in fact equivalent to a *polyrectangle surface*; see Figure 8.1.2.

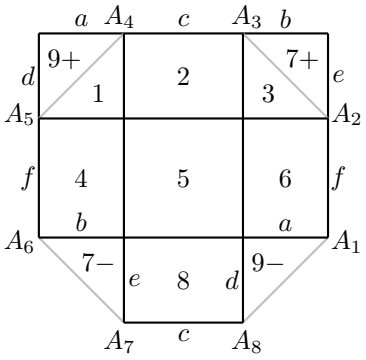

Figure 8.1.2: the regular octagon surface seen as a polyrectangle surface

The edge A_2A_3 is identified with the edge A_7A_6. This allows us to replace the triangle labelled 7− by the triangle labelled 7+, with the two horizontal edges b identified and the two vertical edges e identified. Likewise, the edge A_4A_5 is identified with the edge A_1A_8. This allows us to replace the triangle labelled 9− by the triangle labelled 9+, with the two horizontal edges a identified and the two vertical edges d identified. Thus the regular octagon surface becomes a polyrectangle surface consisting of 7 rectangles, labelled

$$(1, 9+), 2, (3, 7+), 4, 5, 6, 8.$$

With the edge identification, this polyrectangle surface has 2 horizontal streets

$$(1, 9+), 2, (3, 7+), 8 \quad \text{and} \quad 4, 5, 6,$$

as well as 2 vertical streets

$$(1, 9+), 4, (3, 7+), 6 \quad \text{and} \quad 2, 5, 8.$$

The two identified edges e also allows us to replace the rectangle 8 at the bottom in Figure 8.1.2, indicated by 8− in Figure 8.1.3, by a rectangle on the top right indicated by 8+.

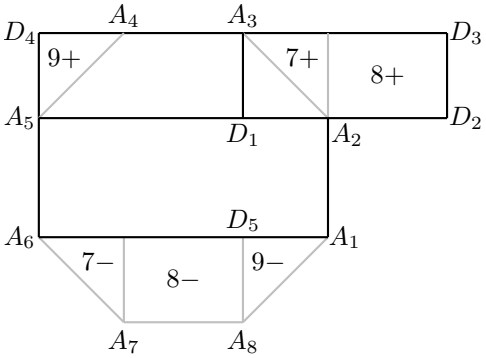

Figure 8.1.3: street decomposition into similar rectangles

Figures 8.1.2 and 8.1.3 justify the claim that the regular octagon surface is in fact a *polyrectangle surface*. Furthermore, we have a second crucial property of the regular octagon surface, that the three rectangles

$$D_4A_5D_1A_3, \quad A_3D_1D_2D_3, \quad A_5A_6A_1A_2$$

are similar. To see this, assume, without loss of generality, that $\text{length}(A_3D_1) = 1$, so that each edge of the regular octagon has length $\sqrt{2}$. Then

$$\frac{\text{length}(A_5D_1)}{\text{length}(A_3D_1)} = \frac{\text{length}(D_1D_2)}{\text{length}(D_3D_2)} = 1 + \sqrt{2}, \tag{8.1.1}$$

and

$$\frac{\text{length}(A_6A_1)}{\text{length}(A_2A_1)} = \frac{2+\sqrt{2}}{\sqrt{2}} = 1+\sqrt{2}. \tag{8.1.2}$$

We also have

$$\frac{\text{length}(A_5D_2)}{\text{length}(D_3D_2)} = 2(1+\sqrt{2}). \tag{8.1.3}$$

Note that (8.1.3) shows that the cotangent of the diagonal A_5D_3 of the horizontal street $D_4A_5D_2D_3$ is equal to $2(1+\sqrt{2})$, while (8.1.2) shows that the cotangent of the diagonal A_6A_2 of the horizontal street $A_5A_6A_1A_2$ is equal to $1+\sqrt{2}$. We can draw similar conclusions for the vertical streets.

Remark. The equality of the ratios in (8.1.1) and (8.1.2) can also be established by using the well known geometric property of the circle very often known as the "chord-angle relation" and which states that if we fix any chord with endpoints P, Q on a circle, then the angle PRQ remains the same for any point R on the same circular arc PQ. Since A_1A_2 and A_2A_3 are two chords of the same length, the angles $A_1A_6A_2$ and $A_2A_5A_3$ are equal.

The ratio of the cotangents of the diagonals of the horizontal streets, and similarly, the ratio of the cotangents of the diagonals of the vertical streets, is *rational*. Thus we refer to the regular octagon surface as a *street-rational polyrectangle surface*.

Remark. Consider a horizontal street on a finite polyrectangle surface $\mathcal{P}$. The width of this street, *i.e.* the perpendicular distance between its top and bottom horizontal edges, may not be equal to 1. Let us expand or contract this street to obtain a similar copy where the width is now equal to 1. Then we call the length of this expanded or contracted horizontal street the *normalized length* of the horizontal street. Some authors also use the terms *modulus* and *cylinder* in place of the terms *normalized length* and *street*. We can also think of this as the cotangent of the (angle that the) diagonals (make with the direction) of the horizontal street. For a finite street-rational polyrectangle surface $\mathcal{P}$, there clearly exists a smallest real number h^* which is an integer multiple of the normalized length of every horizontal street. We call h^* the *normalized horizontal street-LCM* of $\mathcal{P}$. Analogous to this, we denote by v^* the *normalized vertical street-LCM* of $\mathcal{P}$.

To have a suitable version of the surplus shortline method on a street-rational polyrectangle surface $\mathcal{P}$, we must consider slopes of the form

$$\alpha = v^*a_0 + \cfrac{1}{h^*a_1 + \cfrac{1}{v^*a_2 + \cfrac{1}{h^*a_3 + \cdots}}}, \tag{8.1.4}$$

where $a_0, a_1, a_2, a_3, \ldots$ are positive integers.

Note that h^* plays the analogous role of an integer which is the least integer multiple of the lengths of the horizontal streets in a polysquare surface, and v^* plays the analogous role of an integer which is the least integer multiple of the lengths of the vertical streets in a polysquare surface. We can view the expression (8.1.4) as an extension of the concept of continued fraction expansion. For the success of the surplus shortline method in a street-rational polyrectangle surface, we require these "digits" to be integer multiples of h^* and v^* as relevant.

Note that it is not necessary that h^* and v^* are rational multiples of each other, so there may not be a quantity that corresponds to the street-LCM of a finite polysquare surface.

Indeed, we have the two key ingredients needed for the success of the shortline method. Working with a *polyrectangle* automatically gives rise to the horizontal

and vertical directions, vital for the shortline method which is an alternating process between two directions, while *street-rationality* guarantees that the concept of *shortline* is well defined.

Thus the eigenvalue-free version of the shortline method developed in Sections 6.2 and 6.4 in [4] also works for street-rational polyrectangle surfaces, and establishes superdensity of the right triangle billiard with angle $\pi/8$ for some special slopes.

The normalized lengths of the streets, or the cotangents of the diagonals of the streets, of the regular octagon surface represented as a street-rational polyrectangle surface are $2(1+\sqrt{2})$ and $1+\sqrt{2}$, so that $h^* = v^* = 2(1+\sqrt{2})$. Thus we consider the special slopes of the form

$$\alpha = 2(1+\sqrt{2})a_0 + \frac{1}{2(1+\sqrt{2})a_1 + \frac{1}{2(1+\sqrt{2})a_2+\cdots}}, \tag{8.1.5}$$

and their reciprocals α^{-1}, where $a_i \geqslant 1$, $i \geqslant 0$, is an infinite sequence of positive integers *bounded from above*.

The choice (8.1.5) represents the analog of those badly approximable slopes for which the eigenvalue-free version of the shortline method works in the case of polysquare surfaces.

Figure 8.1.4 illustrates some almost horizontal detour crossings and their almost vertical shortcuts.

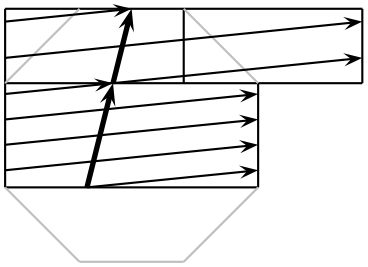

Figure 8.1.4: almost horizontal detour crossings
and their almost vertical shortcuts

By a straightforward adaptation of the proof of Theorems 6.1.1 and 6.4.1 to the street-rational polyrectangle surface in Figures 8.1.2–8.1.4 that represents the regular octagon surface, we obtain the following result concerning the right triangle billiard with angle $\pi/8$.

Theorem 8.1.1. (i) *Consider the right triangle with angle $\pi/8$. Let $\alpha > 1$ be a real number of the form* (8.1.5)*. Then any half-infinite billiard orbit in the right triangle with angle $\pi/8$ with initial slope α exhibits superdensity.*

Figures 8.1.2–8.1.4 are based on the parallel decomposition of the regular octagon into 3 parts as shown in the picture on the left in Figure 8.1.5. The picture on the right shows a different decomposition into 4 parts.

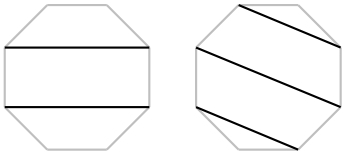

Figure 8.1.5: parallel decompositions of the regular octagon

Figure 8.1.6 illustrates the representation of the regular octagon surface as a street-rational polyrectangle surface, based on this second decomposition. The 4 rectangles are similar. Since A_3A_4 and A_4A_5 are two chords of the same length, the angles $A_3A_2A_4$ and $A_4A_1A_5$ are equal.

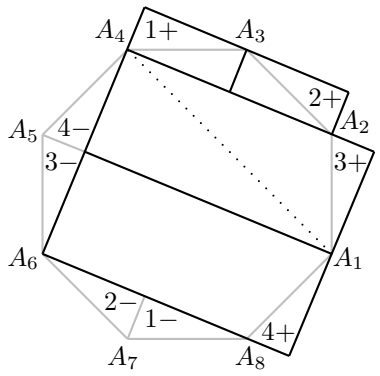

Figure 8.1.6: another street decomposition into similar rectangles

It is not difficult to see that this polyrectangle surface, suitably rotated, has 2 horizontal streets and 2 vertical streets. For instance, in one of these two directions, one street comprises the two smaller rectangles, and the other street comprises the two larger rectangles. Furthermore, it can be checked that the normalized lengths of the streets are equal to $2(1 + \sqrt{2})$, so we can consider slopes of the form (8.1.5) for the suitably rotated copy of this polyrectangle surface. This leads to *new* explicit slopes such that any half-infinite orbit with such an initial slope in the right triangle billiard with angle $\pi/8$ exhibits superdensity.

It can be shown that the same method works for the right triangle billiard with angle π/k, where $k \geqslant 8$ is an even integer. Again we use the elementary fact that the vertices of a regular k-gon are all on a circle, and *street-rationality* comes from the "chord-angle relation" on this circle. We leave the details to the reader.

Theorem 8.1.1. (ii) *Let $k \geqslant 8$ be an even integer, and consider the right-triangle with angle π/k. There exist infinitely many slopes, depending on k, such that any half-infinite billiard orbit in the right triangle with angle π/k with such an initial slope exhibits superdensity.*

(iii) *In general, consider an arbitrary finite street-rational polyrectangle surface $\mathcal{P}$. There exist infinitely many slopes, depending on $\mathcal{P}$, such that any half-infinite 1-direction geodesic on $\mathcal{P}$ having such a slope exhibits superdensity.*

(iv) *As in Theorem 7.1.1, for many of these slopes we can explicitly compute the irregularity exponent. Combining the irregularity exponent with the method of zigzagging introduced in Section 3.3 in* [2]*, we can also describe, for a geodesic flow on $\mathcal{P}$ with such a slope, the time-quantitative behavior of the edge-cutting and face-crossing numbers, as well as equidistribution relative to all convex sets.*

In the course on the next few sections, we shall emphasize on parts (iii) and (iv) by giving a few examples; see Theorems 8.3.1 and Theorems 8.4.1–8.4.3.

Remark. This paper is not about ergodic theory. Instead, we focus on the time-quantitative evolution of individual orbits instead of geodesic *flow* as a whole. Nevertheless, it is very interesting to point out a substantial difference between geodesic flow on a polysquare surface and geodesic flow on a regular k-gon surface with even $k \geqslant 8$. From the viewpoint of ergodic theory these two flows are very different. The latter is *weakly mixing* in almost every direction, while the former is *not* weakly mixing in any direction; see [1].

Our main point is that, despite this big difference between the two flows, the shortline method works *equally well* for individual orbits in either case.

However, whereas for a polysquare surface, a geodesic *modulo one* is equivalent to a torus line in the unit square, there is no corresponding analog for the street-rational polyrectangle surface corresponding to the regular octagon surface.

In the next section, we illustrate the proof of part (iv) in a special case that reflects the whole difficulty of the general case.

8.2. **Computing the irregularity exponent for the octagon surface.** We now apply the eigenvalue-based version of the shortline method on the regular octagon surface, and compute the irregularity exponent of 1-direction geodesics with certain slopes. In particular, we consider special slopes of the form

$$\alpha = 2(1+\sqrt{2})a_0 + \cfrac{1}{2(1+\sqrt{2})a_1 + \frac{1}{2(1+\sqrt{2})a_2+\cdots}}, \tag{8.2.1}$$

where $a_i \geqslant 1$, $i \geqslant 0$, form a sequence of integers which is eventually periodic. This last requirement distinguishes (8.2.1) from (8.1.5).

Since the common ratio of the vertical and horizontal sides of the rectangles in Figure 8.1.4 is $1+\sqrt{2}$, the shortline of a geodesic on the regular octagon surface with slope α given by (8.2.1) has slope α_1^{-1}, where

$$\alpha_1 = 2(1+\sqrt{2})a_1 + \cfrac{1}{2(1+\sqrt{2})a_2 + \frac{1}{2(1+\sqrt{2})a_3+\cdots}},$$

and the shortline of this shortline has slope

$$\alpha_2 = 2(1+\sqrt{2})a_2 + \cfrac{1}{2(1+\sqrt{2})a_3 + \frac{1}{2(1+\sqrt{2})a_4+\cdots}},$$

and so on. Note that for $\alpha, \alpha_1, \alpha_2, \ldots$, the usual shift of digits $a_0, a_1, a_2, \ldots$ applies.

Theorem 8.2.1. *Consider* 1*-direction geodesic flow on the regular octagon surface with slope* α *given by* (8.2.1)*. If the sequence* $a_0, a_1, a_2, \ldots$ *has period* $k_1, k_2, \ldots, k_r$ *eventually, then the irregularity exponent of the geodesic with slope* α *is equal to*

$$\frac{\log|\lambda|}{\log|\Lambda|},$$

where λ *is the eigenvalue with the larger absolute value of the product matrix*

$$\prod_{i=1}^{r} \begin{pmatrix} -2(\sqrt{2}-1)k_i & 1 \\ 1 & 0 \end{pmatrix},$$

and Λ *is the eigenvalue with the larger absolute value of the product matrix*

$$\prod_{i=1}^{r} \begin{pmatrix} 2(1+\sqrt{2})k_i & 1 \\ 1 & 0 \end{pmatrix}.$$

Alternatively, we have the product formula

$$\Lambda = \prod_{i=1}^{r} \beta_i,$$

where for every $i = 1, \ldots, r$,

$$\beta_i = 2(1+\sqrt{2})k_i + \cfrac{1}{2(1+\sqrt{2})k_{i+1} + \frac{1}{2(1+\sqrt{2})k_{i+2}+\cdots}},$$

corresponding to the periodic sequence

$$k_i, k_{i+1}, k_{i+2}, \ldots, k_r, k_1, k_2, \ldots, k_r, \ldots.$$

Remark. If the sequence $a_0, a_1, a_2, \ldots$ has period k_1, k_2 eventually, of length 2, then it is possible to use the street-spreading matrix in the same spirit as in Theorem 7.2.2, noting that the method there works even for street-rational polyrectangle surfaces. But here the period can be arbitrarily long.

Proof of Theorem 8.2.1. We apply an adaptation of the original eigenvalue-based version of the surplus shortline method developed in Sections 3 and 4 in [2, 3].

First of all, we note that the regular octagon region, viewed as a street-rational polyrectangle surface as in Figures 8.1.2–8.1.4, has 7 horizontal and 7 vertical edges, some with identified pairs, as shown in Figure 8.2.1.

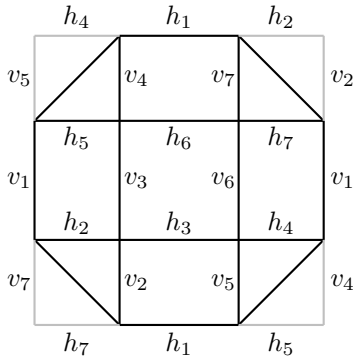

Figure 8.2.1: horizontal and vertical edges of the regular octagon surface viewed as a street-rational polyrectangle surface

We distinguish the 14 types of almost vertical units

$$h_1h_3, h_1h_4, h_2h_5, h_2h_6, h_3h_6, h_3h_7, h_4h_5, h_4h_7, h_5h_1, h_5h_4, h_6h_1, h_6h_2, h_7h_2, h_7h_3,$$

as shown in Figure 8.2.2.

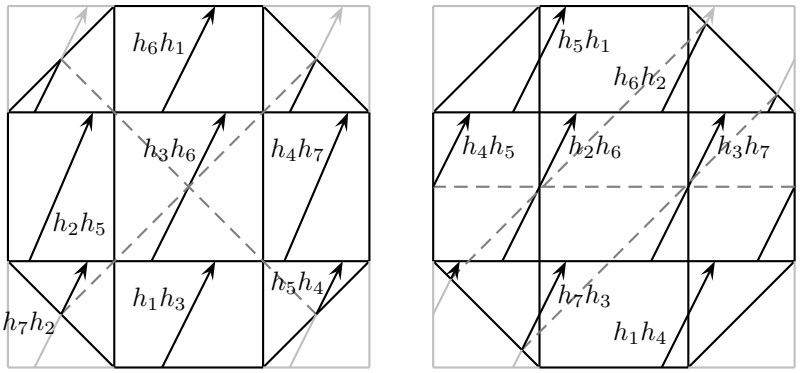

Figure 8.2.2: almost vertical units of the regular octagon surface

We distinguish the 14 types of almost horizontal units

$$v_1v_3, v_1v_4, v_2v_5, v_2v_6, v_3v_6, v_3v_7, v_4v_5, v_4v_7, v_5v_1, v_5v_4, v_6v_1, v_6v_2, v_7v_2, v_7v_3,$$

as shown in Figure 8.2.3.

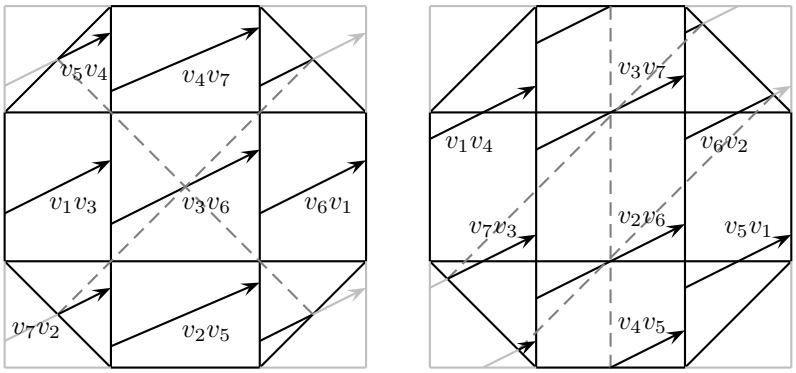

Figure 8.2.3: almost horizontal units of the regular octagon surface

Consider first the almost vertical unit h_1h_3. It is not difficult to see from Figures 8.2.2 and 8.2.3 that h_1h_3 is the shortcut of an almost horizontal detour crossing of

a horizontal street, made up of a fractional almost horizontal unit v_4v_5, full almost horizontal units v_5v_4, v_4v_7, v_7v_2, then $(k-1)$ copies of full almost horizontal units $v_2v_5, v_5v_4, v_4v_7, v_7v_2$, and finally a fractional almost horizontal unit v_2v_6. This can be summarized by

$$h_1h_3 \to v_4v_5, v_5v_4, v_4v_7, v_7v_2, (v_2v_5, v_5v_4, v_4v_7, v_7v_2)^{k-1}, v_2v_6,$$

where $k \geqslant 1$ is the branching parameter. For bookkeeping purposes, we next apply the Delete-End Rule, keep the initial fractional almost horizontal unit v_4v_5 as a full unit, discard the final fractional almost horizontal unit v_2v_6, and call these units the ancestor units of h_1h_3. Repeating the same exercise on the other 13 almost vertical units, we can summarize this ancestor process by

$$h_1h_3 \rightharpoonup v_4v_5, k \times v_5v_4, k \times v_4v_7, k \times v_7v_2, (k-1) \times v_2v_5, \tag{8.2.2}$$
$$h_1h_4 \rightharpoonup v_4v_5, k \times v_5v_4, k \times v_4v_7, k \times v_7v_2, k \times v_2v_5, \tag{8.2.3}$$
$$h_2h_5 \rightharpoonup v_7v_3, 2k \times v_3v_6, 2k \times v_6v_1, (2k-1) \times v_1v_3, \tag{8.2.4}$$
$$h_2h_6 \rightharpoonup v_7v_3, 2k \times v_3v_6, 2k \times v_6v_1, 2k \times v_1v_3, \tag{8.2.5}$$
$$h_3h_6 \rightharpoonup v_2v_6, 2k \times v_6v_1, 2k \times v_1v_3, (2k-1) \times v_3v_6, \tag{8.2.6}$$
$$h_3h_7 \rightharpoonup v_2v_6, 2k \times v_6v_1, 2k \times v_1v_3, 2k \times v_3v_6, \tag{8.2.7}$$
$$h_4h_5 \rightharpoonup v_5v_1, 2k \times v_1v_3, 2k \times v_3v_6, 2k \times v_6v_1, \tag{8.2.8}$$
$$h_4h_7 \rightharpoonup v_5v_1, 2k \times v_1v_3, 2k \times v_3v_6, (2k-1) \times v_6v_1, \tag{8.2.9}$$
$$h_5h_1 \rightharpoonup v_1v_4, k \times v_4v_7, k \times v_7v_2, k \times v_2v_5, k \times v_5v_4, \tag{8.2.10}$$
$$h_5h_4 \rightharpoonup v_1v_4, k \times v_4v_7, k \times v_7v_2, k \times v_2v_5, (k-1) \times v_5v_4, \tag{8.2.11}$$
$$h_6h_1 \rightharpoonup v_3v_7, k \times v_7v_2, k \times v_2v_5, k \times v_5v_4, (k-1) \times v_4v_7, \tag{8.2.12}$$
$$h_6h_2 \rightharpoonup v_3v_7, k \times v_7v_2, k \times v_2v_5, k \times v_5v_4, k \times v_4v_7, \tag{8.2.13}$$
$$h_7h_2 \rightharpoonup v_6v_2, k \times v_2v_5, k \times v_5v_4, k \times v_4v_7, (k-1) \times v_7v_2, \tag{8.2.14}$$
$$h_7h_3 \rightharpoonup v_6v_2, k \times v_2v_5, k \times v_5v_4, k \times v_4v_7, k \times v_7v_2, \tag{8.2.15}$$

These lead to a 14×14 transition matrix

$$M(k) = \begin{pmatrix} M_{1,1}(k) & M_{1,2}(k) \\ M_{2,1}(k) & M_{2,2}(k) \end{pmatrix},$$

where any particular row captures the information in the ancestor relation of the almost vertical unit in question by displaying the multiplicities of each of its ancestor almost horizontal units. We have

$$M_{1,1}(k) = \begin{array}{c} \\ h_1h_3 \\ h_1h_4 \\ h_2h_5 \\ h_2h_6 \\ h_3h_6 \\ h_3h_7 \\ h_4h_5 \end{array} \begin{array}{c} \begin{array}{ccccccc} v_1v_3 & v_1v_4 & v_2v_5 & v_2v_6 & v_3v_6 & v_3v_7 & v_4v_5 \end{array} \\ \begin{pmatrix} 0 & 0 & k-1 & 0 & 0 & 0 & 1 \\ 0 & 0 & k & 0 & 0 & 0 & 1 \\ 2k-1 & 0 & 0 & 0 & 2k & 0 & 0 \\ 2k & 0 & 0 & 0 & 2k & 0 & 0 \\ 2k & 0 & 0 & 1 & 2k-1 & 0 & 0 \\ 2k & 0 & 0 & 1 & 2k & 0 & 0 \\ 2k & 0 & 0 & 0 & 2k & 0 & 0 \end{pmatrix} \end{array},$$

$$M_{1,2}(k) = \begin{array}{c} \\ h_1h_3 \\ h_1h_4 \\ h_2h_5 \\ h_2h_6 \\ h_3h_6 \\ h_3h_7 \\ h_4h_5 \end{array} \begin{array}{c} \begin{array}{ccccccc} v_4v_7 & v_5v_1 & v_5v_4 & v_6v_1 & v_6v_2 & v_7v_2 & v_7v_3 \end{array} \\ \begin{pmatrix} k & 0 & k & 0 & 0 & k & 0 \\ k & 0 & k & 0 & 0 & k & 0 \\ 0 & 0 & 0 & 2k & 0 & 0 & 1 \\ 0 & 0 & 0 & 2k & 0 & 0 & 1 \\ 0 & 0 & 0 & 2k & 0 & 0 & 0 \\ 0 & 0 & 0 & 2k & 0 & 0 & 0 \\ 0 & 1 & 0 & 2k & 0 & 0 & 0 \end{pmatrix} \end{array},$$

$$M_{2,1}(k) = \begin{array}{c} \\ h_4h_7 \\ h_5h_1 \\ h_5h_4 \\ h_6h_1 \\ h_6h_2 \\ h_7h_2 \\ h_7h_3 \end{array} \begin{array}{c} \begin{array}{ccccccc} v_1v_3 & v_1v_4 & v_2v_5 & v_2v_6 & v_3v_6 & v_3v_7 & v_4v_5 \end{array} \\ \begin{pmatrix} 2k & 0 & 0 & 0 & 2k & 0 & 0 \\ 0 & 1 & k & 0 & 0 & 0 & 0 \\ 0 & 1 & k & 0 & 0 & 0 & 0 \\ 0 & 0 & k & 0 & 0 & 1 & 0 \\ 0 & 0 & k & 0 & 0 & 1 & 0 \\ 0 & 0 & k & 0 & 0 & 0 & 0 \\ 0 & 0 & k & 0 & 0 & 0 & 0 \end{pmatrix} \end{array},$$

and

$$M_{2,2}(k) = \begin{array}{c} \\ h_4h_7 \\ h_5h_1 \\ h_5h_4 \\ h_6h_1 \\ h_6h_2 \\ h_7h_2 \\ h_7h_3 \end{array} \begin{array}{c} \begin{array}{ccccccc} v_4v_7 & v_5v_1 & v_5v_4 & v_6v_1 & v_6v_2 & v_7v_2 & v_7v_3 \end{array} \\ \begin{pmatrix} 0 & 1 & 0 & 2k-1 & 0 & 0 & 0 \\ k & 0 & k & 0 & 0 & k & 0 \\ k & 0 & k-1 & 0 & 0 & k & 0 \\ k-1 & 0 & k & 0 & 0 & k & 0 \\ k & 0 & k & 0 & 0 & k & 0 \\ k & 0 & k & 0 & 1 & k-1 & 0 \\ k & 0 & k & 0 & 1 & k & 0 \end{pmatrix} \end{array}.$$

Similarly, we can study the ancestor relation of each of the almost horizontal units, again using the Delete-End Rule, and obtain the analogs of (8.2.2)–(8.2.15). These will lead to another 14×14 transition matrix. Since we have listed the almost vertical units and almost horizontal units in lexicographical order, these two 14×14 transition matrices are the same.

Of the 14 eigenvalues of $M(k)$, there are 10 irrelevant ones of the form ± 1, $\pm \mathrm{i}$ and $(-1 \pm \sqrt{3}\mathrm{i})/2$. The more interesting ones are

$$(1+\sqrt{2})k \pm \left((1+\sqrt{2})^2k^2+1\right)^{1/2}, \quad (1-\sqrt{2})k \pm \left((1-\sqrt{2})^2k^2+1\right)^{1/2}.$$

Clearly the eigenvalue with the largest absolute value is

$$\Lambda = (1+\sqrt{2})k + \left((1+\sqrt{2})^2k^2+1\right)^{1/2}, \tag{8.2.16}$$

and the eigenvalue with the second largest absolute value is

$$\lambda = -(\sqrt{2}-1)k - \left((\sqrt{2}-1)^2k^2+1\right)^{1/2}. \tag{8.2.17}$$

The other two eigenvalues among these four are also irrelevant.

We shall show that the transition matrix $M(k)$ has a conjugate with the form

$$P^{-1}M(k)P = \begin{pmatrix} T & ? \\ 0 & A(k) \end{pmatrix}, \tag{8.2.18}$$

where T is a 10×10 triangular matrix with main diagonal entries

$$1, -1, -1, -1, -\mathrm{i}, \mathrm{i}, -1, 1, \frac{-1-\sqrt{3}\mathrm{i}}{2}, \frac{-1+\sqrt{3}\mathrm{i}}{2}, \tag{8.2.19}$$

in this order, the entries of T below the main diagonal are all zero, and

$$A(k) = \begin{pmatrix} 2(1+\sqrt{2})k & 1 & ? & ? \\ 1 & 0 & ? & ? \\ 0 & 0 & -2(\sqrt{2}-1)k & 1 \\ 0 & 0 & 1 & 0 \end{pmatrix}. \tag{8.2.20}$$

The description of the matrix $M(k)$ by (8.2.18)–(8.2.20) is extremely convenient. It reduces the necessary eigenvalue computation of arbitrary products

$$\prod_{i=1}^{r} M(k_i)$$

of 14×14 matrices with different values of the branching parameter k_i to the much simpler eigenvalue computation of products

$$\prod_{i=1}^{r} \begin{pmatrix} 2(1+\sqrt{2})k_i & 1 \\ 1 & 0 \end{pmatrix} \quad \text{and} \quad \prod_{i=1}^{r} \begin{pmatrix} -2(\sqrt{2}-1)k_i & 1 \\ 1 & 0 \end{pmatrix}$$

of 2×2 matrices, as the remaining eigenvalues ± 1, $\pm \mathrm{i}$ and $(-1\pm\sqrt{3}\mathrm{i})/2$ are irrelevant.

We now outline the routine deduction of (8.2.18)–(8.2.20).

We first make use of the fact that $M(k)$ has 6 eigenvectors that are independent of the branching parameter k. Together with the eigenvalues, they are

$$\begin{aligned}
\lambda_1 = 1, &\quad \mathbf{v}_1 = (-1,0,1,0,0,0,0,-1,0,0,1,0,0,0)^T, \\
\lambda_2 = -1, &\quad \mathbf{v}_2 = (-1,0,-1,0,1,0,0,0,0,1,0,0,0,0)^T, \\
\lambda_3 = -1, &\quad \mathbf{v}_3 = (-1,0,-1,0,0,0,0,1,0,0,1,0,0,0)^T, \\
\lambda_4 = -1, &\quad \mathbf{v}_4 = (-1,0,-1,0,1,0,0,0,0,0,0,0,1,0)^T, \\
\lambda_5 = -\mathrm{i}, &\quad \mathbf{v}_5 = (1,0,\mathrm{i},2\mathrm{i},-1+\mathrm{i},-2,0,-1,0,0,-\mathrm{i},-2\mathrm{i},1-\mathrm{i},2)^T, \\
\lambda_6 = \mathrm{i}, &\quad \mathbf{v}_6 = (1,0,-\mathrm{i},-2\mathrm{i},-1-\mathrm{i},-2,0,-1,0,0,\mathrm{i},2\mathrm{i},1+\mathrm{i},2)^T.
\end{aligned}$$

This observation allows us to apply a "partial diagonalization" trick first discussed in Lemma 4.1.1 in [3]. Let Q be a 14×14 invertible matrix such that the first 6 columns are $\mathbf{v}_1, \ldots, \mathbf{v}_6$. Then for every $1 \leqslant i \leqslant 6$, the i-th column of the conjugate $Q^{-1}M(k)Q$ has the special form that its i-th element is λ_i, and the remaining elements are all zero. A concrete choice of Q gives

$$Q^{-1}M(k)Q = \begin{pmatrix} D_6 & ? \\ 0 & M_8(k) \end{pmatrix},$$

where D_6 is a 6×6 diagonal matrix with diagonal entries $\lambda_1, \ldots \lambda_6$, and

$$M_8(k) = \begin{pmatrix}
-\frac{1}{4}-\frac{\sqrt{3}\mathrm{i}}{4} & \frac{1}{4}-\frac{\sqrt{3}\mathrm{i}}{4} & -\frac{\sqrt{3}\mathrm{i}}{12} & \frac{1}{4}-\frac{\sqrt{3}k\mathrm{i}}{6} & \frac{1}{4}-\frac{\sqrt{3}k\mathrm{i}}{6} & 0 & 0 & 0 \\
\frac{1}{4}+\frac{\sqrt{3}\mathrm{i}}{4} & -\frac{1}{4}+\frac{\sqrt{3}\mathrm{i}}{4} & \frac{\sqrt{3}\mathrm{i}}{12} & \frac{1}{4}+\frac{\sqrt{3}k\mathrm{i}}{6} & \frac{1}{4}+\frac{\sqrt{3}k\mathrm{i}}{6} & 0 & 0 & 0 \\
-2k-\frac{3+3\sqrt{3}\mathrm{i}}{2} & -2k-\frac{3-3\sqrt{3}\mathrm{i}}{2} & \frac{1}{2} & 2k-\frac{3}{2} & k-\frac{5}{2} & 0 & k & 0 \\
-6k-\frac{7+3\sqrt{3}\mathrm{i}}{2} & -6k-\frac{7-3\sqrt{3}\mathrm{i}}{2} & \frac{1}{2} & 6k+\frac{3}{2} & 3k+\frac{3}{2} & 0 & 3k & 0 \\
2k-\frac{3+3\sqrt{3}\mathrm{i}}{2} & 2k-\frac{3-3\sqrt{3}\mathrm{i}}{2} & -\frac{1}{2} & -2k-\frac{3}{2} & -k-\frac{3}{2} & 0 & -k & 0 \\
-2k & -2k & 0 & 3k & 2k & 0 & k & 1 \\
2k-\frac{7+3\sqrt{3}\mathrm{i}}{2} & 2k-\frac{7-3\sqrt{3}\mathrm{i}}{2} & \frac{1}{2} & -\frac{5}{2} & k-\frac{5}{2} & 1 & -k-1 & 1 \\
-2k & -2k & 0 & 3k & 2k & 1 & k & 0
\end{pmatrix}.$$

We next make use of the fact that $M_8(k)$ has 4 eigenvectors that are independent of the branching parameter k. Together with the eigenvalues, they are

$$\begin{aligned}
\tau_1 = -1, &\quad \mathbf{w}_1 = (0,0,0,0,0,-1,0,1)^T,\\
\tau_2 = 1, &\quad \mathbf{w}_2 = \left(\frac{\sqrt{3}\mathrm{i}}{18}, -\frac{\sqrt{3}\mathrm{i}}{18}, -1, -1, 1, 1, 1, 1\right)^T,\\
\tau_3 = -\frac{1+\sqrt{3}\mathrm{i}}{2}, &\quad \mathbf{w}_3 = \left(\frac{1}{6}, -\frac{1}{6}, 1, -1, 1, 0, 1, 0\right)^T,\\
\tau_4 = -\frac{1-\sqrt{3}\mathrm{i}}{2}, &\quad \mathbf{w}_4 = \left(-\frac{1}{6}, \frac{1}{6}, 1, -1, 1, 0, 1, 0\right)^T.
\end{aligned}$$

We apply the same "partial diagonalization" trick. Let R be an 8×8 invertible matrix such that the first 4 columns are $\mathbf{w}_1, \ldots, \mathbf{w}_4$. Then for every $1 \leqslant i \leqslant 4$, the i-th column of the conjugate $R^{-1}M_8(k)R$ has the special form that its i-th element is τ_i, and the remaining elements are all zero. A concrete choice of R gives

$$R^{-1}M_8(k)R = \begin{pmatrix} D_4 & ? \\ 0 & M_4(k) \end{pmatrix},$$

where D_4 is a 4×4 diagonal matrix with diagonal entries $\tau_1, \ldots, \tau_4$, and

$$M_4(k) = \begin{pmatrix} 6k-2 & 2-4k & 2k & 0 \\ 6k-\frac{3}{2} & 2-4k & 2k & 0 \\ 8k-1 & 1-4k & 2k-1 & 1 \\ 14k-\frac{3}{2} & 1-8k & 4k & 1 \end{pmatrix}.$$

Finally, one more routine conjugation turns $M_4(k)$ into $A(k)$ in (8.2.20). This completes the deduction of (8.2.18)–(8.2.20).

One can derive Theorem 8.2.1 from (8.2.18)–(8.2.20) in the usual way; we leave it to the reader. □

To complete this section, we shall compute the eigenvalues of the 2-step transition matrix M of the regular octagon surface.

With Figure 8.1.2 in mind, we view the regular octagon surface as a polyrectangle surface with 7 rectangle faces, as shown in Figure 8.2.4. Here the horizontal streets are $1, 2, 3, 8$ and $4, 5, 6$, while the vertical streets are $1, 4, 3, 6$ and $2, 5, 8$. Note here that two distinct rectangle faces can fall into the same horizontal and the same vertical street simultaneously, for instance, faces $2, 8$ or faces $4, 6$, so we shall adapt our notation from that used in earlier street-spreading matrix determination.

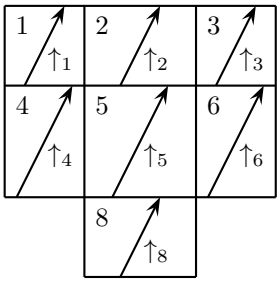

Figure 8.2.4: the regular octagon surfaces and almost vertical units of type ↑

We also show the almost vertical units of type ↑ in the polyrectangle surface. We have not shown the almost vertical units of type ↟ here.

Let

$$J_1 = \{1, 2, 3, 8\} \quad \text{and} \quad J_2 = \{4, 5, 6\}$$

denote the horizontal streets, and let

$$I_1 = I_3 = I_4 = I_6 = \{1, 3, 4, 6\} \quad \text{and} \quad I_2 = I_5 = I_8 = \{2, 5, 8\}$$

denote the vertical streets.

For simplicity, we consider only the special case with branching parameter $k = 1$, so that we are considering a slope of the form

$$\alpha = 2(1 + \sqrt{2}) + \frac{1}{2(1 + \sqrt{2}) + \frac{1}{2(1+\sqrt{2})+\cdots}}.$$

Corresponding to (7.2.14), we define the column matrices

$$\mathbf{u}_1 = [\{\uparrow_s\colon j \in J_1^*, s \in I_j^*\}] \quad \text{and} \quad \mathbf{u}_2 = [\{\uparrow_s\colon j \in J_2^*, s \in I_j^*\}]. \tag{8.2.21}$$

Here J_1^*, J_2^* and I_j^* denote that the edges are counted with multiplicity.

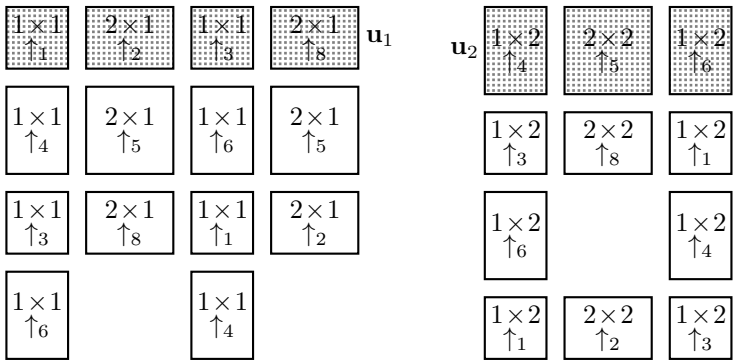

Figure 8.2.5: almost vertical units of type ↑ in $\mathbf{u}_1$ and $\mathbf{u}_2$

The horizontal street J_1 has length $2(1+\sqrt{2})$ and width 1, so has normalized length $2(1 + \sqrt{2})$. Since the normalized length is precisely the value of the digit $2(1 + \sqrt{2})$ of α, this means that an almost horizontal detour crossing of slope α^{-1} travels along this street essentially once, giving rise to a single count and $J_1^* = \{1, 2, 3, 8\}$. On the other hand, the horizontal street J_2 has smaller length $2+\sqrt{2}$ but greater width $\sqrt{2}$, and so has normalized length $1 + \sqrt{2}$. Thus an almost horizontal detour crossing of slope α^{-1} travels along the horizontal street J_2 essentially twice, giving rise to a double count and $J_2^* = \{4, 5, 6, 4, 5, 6\}$.

A similar argument now gives

$$I_1^* = I_3^* = I_4^* = I_6^* = \{1, 3, 4, 6\} \quad \text{and} \quad I_2^* = I_5^* = I_8^* = \{2, 5, 8, 2, 5, 8\}.$$

We also define the column matrices $\mathbf{v}_1$ and $\mathbf{v}_2$ analogous to (7.2.15), but their details are not important. Also, analogous to (7.2.17), we have

$$(M - I)[\{\uparrow_s\}] = \begin{cases} \mathbf{u}_1 + \mathbf{v}_1, & \text{if } s \in J_1, \\ \mathbf{u}_2 + \mathbf{v}_2, & \text{if } s \in J_2. \end{cases} \tag{8.2.22}$$

We now combine (8.2.21) and (8.2.22). For the horizontal street corresponding to $\mathbf{u}_1$, as highlighted in the picture on the left in Figure 8.2.5, we have

$$\begin{aligned} (M - I)\mathbf{u}_1 &= (M - I)[\{2 \uparrow_1, 4 \uparrow_2, 2 \uparrow_3, 4 \uparrow_8\}] \\ &\quad + (M - I)[\{2 \uparrow_4, 4 \uparrow_5, 2 \uparrow_6\}] \\ &= 12(\mathbf{u}_1 + \mathbf{v}_1) + 8(\mathbf{u}_2 + \mathbf{v}_2). \end{aligned} \tag{8.2.23}$$

For the horizontal street corresponding to $\mathbf{u}_2$, as highlighted in the picture on the right in Figure 8.2.5, we have

$$\begin{aligned}(M-I)\mathbf{u}_2 &= (M-I)[\{4\uparrow_1, 4\uparrow_2, 4\uparrow_3, 4\uparrow_8\}] \\ &\quad + (M-I)[\{4\uparrow_4, 4\uparrow_5, 4\uparrow_6\}] \\ &= 16(\mathbf{u}_1+\mathbf{v}_1) + 12(\mathbf{u}_2+\mathbf{v}_2). \end{aligned} \tag{8.2.24}$$

It follows from (8.2.23)–(8.2.24) that the street-spreading matrix is given by

$$\mathbf{S} = \begin{pmatrix} 12 & 16 \\ 8 & 12 \end{pmatrix},$$

with eigenvalues $\tau_1 = 12+8\sqrt{2}$ and $\tau_2 = 12-8\sqrt{2}$. Using (7.2.38), the corresponding eigenvalues of M are

$$\lambda(12+8\sqrt{2};\pm) = 7+4\sqrt{2} \pm 2\Big(20+14\sqrt{2}\Big)^{1/2}$$

and

$$\lambda(12-8\sqrt{2};\pm) = 7-4\sqrt{2} \pm 2\Big(20-14\sqrt{2}\Big)^{1/2}.$$

The two largest eigenvalues are therefore

$$\lambda_1 = 7+4\sqrt{2}+2\Big(20+14\sqrt{2}\Big)^{1/2} \quad \text{and} \quad \lambda_2 = 7-4\sqrt{2}+2\Big(20-14\sqrt{2}\Big)^{1/2}.$$

Recall (8.2.16) and (8.2.17) that, for the branching parameter $k=1$, the two largest eigenvalues for the 1-step transition matrix are

$$\Lambda = (1+\sqrt{2}) + \Big((1+\sqrt{2})^2+1\Big)^{1/2} \quad \text{and} \quad \lambda = -(\sqrt{2}-1) - \Big((\sqrt{2}-1)^2+1\Big)^{1/2}.$$

Note that $\lambda_1 = \Lambda^2$ and $\lambda_2 = \lambda^2$.

8.3. **Regular octagon billiard.** We now switch to billiard flow on the regular octagon. This also leads to a street-rational polyrectangle surface with 1-direction geodesic flow, but the details are more complicated than in Section 8.1.

Clearly the method earlier of iterated reflection on a side, like in Figure 8.1.1, does not apply here, since we start with the regular octagon. In this case, we need a somewhat different, but ultimately equivalent, approach based on the construction of the "reflected net". The first step is illustrated by Figure 8.3.1 which shows a "reflected double-octagon net" of the regular octagon billiard surface, where the identified boundary edges are marked with the same letter. Using Euler's formula, it is easy to see that the Euler characteristic χ of the compact surface in Figure 8.3.1 is $\chi = 8-8+2 = 2$, so the genus g is $g = 1-(\chi/2) = 0$. Hence this double-octagon surface is homeomorphic to the sphere.

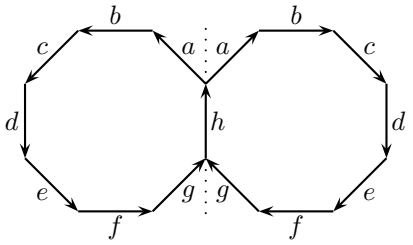

Figure 8.3.1: double-octagon net of the regular octagon billiard surface

Note the reflection symmetry of the boundary labelling, where the labelling on the right octagon is obtained from the labelling on the left octagon by a reflection across the vertical dotted line that we may call a "mirror".

Regular octagon billiard is a complicated flow. While the "double-octagon" net in Figure 8.3.1 is quite simple, the corresponding surface still exhibits a rather complicated geodesic flow. We illustrate how we construct this geodesic flow in Figure 8.3.2. We start with a short billiard orbit in the left octagon, labelled **1**, that hits the boundary edge a. Following the usual billiard rule, **1** bounces back as shown by the dashed arrow. We reflect this dashed arrow across the "mirror" in the middle, and obtain **2**. If **1** is considered an initial segment of a geodesic on the compact surface, then **2** is the continuation of the same geodesic on this compact surface. In this way, the process can be viewed as a partial unfolding of the 8-direction billiard flow in the left octagon into a 4-direction flow in the double-octagon, noting that a billiard orbit which starts horizontal or vertical or with slope ± 1 is not particularly interesting. Note that the two octagons are reflections of each other.

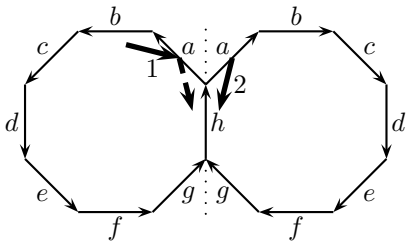

Figure 8.3.2: partial unfolding of the billiard in the left regular octagon

Next, we join up octagons in such a way that neighboring octagons are reflections of each other. We end up with a ring of 8 octagons, as shown in Figure 8.3.3. This is sometimes known as the translation surface for regular octagon billiard.

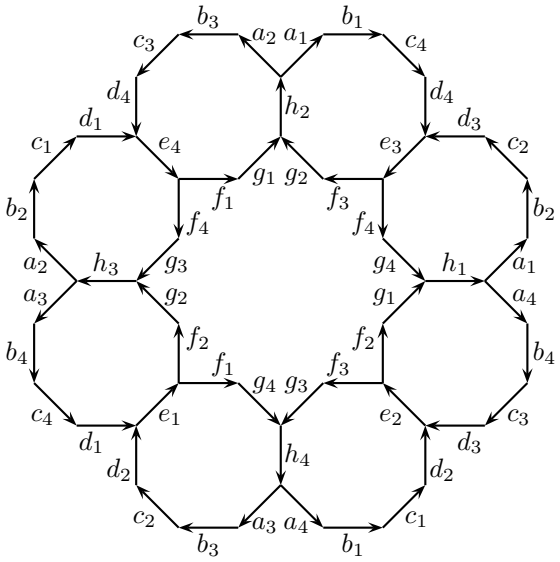

Figure 8.3.3: translation surface for regular octagon billiard with edge labellings

Remark. In general, for any even $k \geqslant 4$, we can glue k copies of a regular k-gon together in a perfect ring formation analogous to that in Figure 8.3.3 such that the midpoints of the common edges between neighboring k-gons all lie on a circle. For odd $k \geqslant 3$, we can do likewise with $2k$ copies of a regular k-gon.

The edge labellings in Figure 8.3.3 look very cumbersome at first sight. However, we can follow a simple convention. Start with one copy of the octagon, and label the directed edges of this octagon by a, b, c, d, e, f, g, h, initially without subscripts. The adjacent octagon has reflected labelling, and the next one in the ring has labelling that is a reflection of the labelling of the second one, and so on. When we complete this process, we have labellings a, b, c, d, e, f, g, h, still without subscripts, on each

octagon. The second step of the process is to look at all the edges labelled a, and they occur as 4 directed parallel pairs. We now identify such directed parallel pairs by labelling them a_1, a_2, a_3, a_4. In Figure 8.3.3, we have labelled them in increasing order of the angles they make with the positive horizontal direction. We then repeat this step with the other edges. Note that the edges e and h do not appear to come in pairs, but they actually do, but the identified edges overlap.

We clearly need more, as we need a corresponding net that exhibits a 1-direction geodesic flow and which shows the streets in a more transparent fashion. The impatient reader may jump ahead to the net in Figures 8.3.6 and 8.3.7 from which we can easily obtain the corresponding street-rational polyrectangle surface, adapt the shortline method in the proof of Theorems 6.1.1 and 6.4.1, and exhibit explicit slopes for which we can establish superdensity.

Remark. The remarkable result of Veech [18] on the *uniform-periodic dichotomy* in flat systems, particularly that every infinite billiard orbit in a regular polygon is either periodic or exhibits uniformity. His method is ergodic in nature, however, and does not give time-quantitative results. It is the purpose of our work here to make some quantitative statements.

The plan is quite straightforward, and the details are not too cumbersome. We shall proceed in steps and illustrate our ideas with pictures. Indeed, regular octagon billiard represents the whole difficulty. Once we fully understand the special case of regular octagon billiard, it is easy to visualize the general case of regular k-gon billiard, where $k \geqslant 8$ is any even integer.

We shall use the parallel decomposition of the regular polygon shown in the picture on the right in Figure 8.1.5. With the help of the edge labellings, we can easily work out some streets, as shown in Figure 8.3.4. We consider tilted streets in the direction shown.

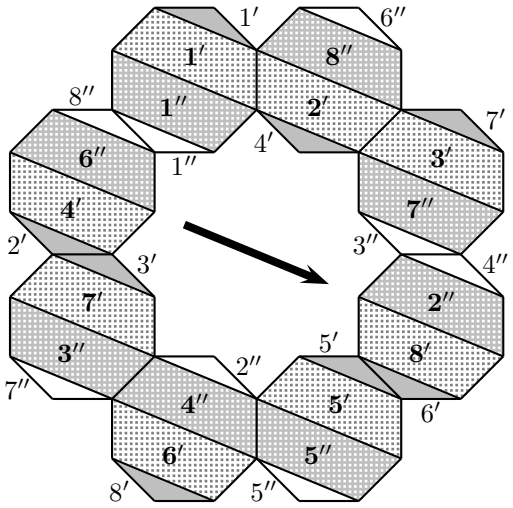

Figure 8.3.4: first set of tilted streets on the translation surface of regular octagon billiard

The first big street in this direction consists of 8 trapezoids labelled

$$\mathbf{1}', \mathbf{2}', \mathbf{3}', \mathbf{4}', \mathbf{5}', \mathbf{6}', \mathbf{7}', \mathbf{8}'.$$

Note the edge labellings in Figure 8.3.3. The right edge of the trapezoid $\mathbf{3}'$ is b_2, the same as the left edge of the trapezoid $\mathbf{4}'$. The right edge of the trapezoid $\mathbf{4}'$ is g_3, the same as the left edge of the trapezoid $\mathbf{5}'$. The right edge of the trapezoid $\mathbf{5}'$ is d_2, the same as the left edge of the trapezoid $\mathbf{6}'$. The right edge of the trapezoid $\mathbf{6}'$ is a_3, the same as the left edge of the trapezoid $\mathbf{7}'$. The right edge of the trapezoid

$\mathbf{7}'$ is f_2, the same as the left edge of the trapezoid $\mathbf{8}'$. The right edge of the trapezoid $\mathbf{8}'$ is c_3, the same as the left edge of the trapezoid $\mathbf{1}'$. This completes the street.

The second big street in this direction consists of 8 trapezoids labelled

$$\mathbf{1}'', \mathbf{2}'', \mathbf{3}'', \mathbf{4}'', \mathbf{5}'', \mathbf{6}'', \mathbf{7}'', \mathbf{8}''.$$

There are also two small streets in this direction, consisting of 8 triangles

$$1', 2', 3', 4', 5', 6', 7', 8' \quad \text{and} \quad 1'', 2'', 3'', 4'', 5'', 6'', 7'', 8''$$

each.

To use the shortline method, we need to consider streets in a second direction. Figure 8.3.5 is an analog of Figure 8.3.4 in this new direction. Again, we see that there are two big streets, each consisting of 8 trapezoids, and two small streets, each consisting of 8 triangles.

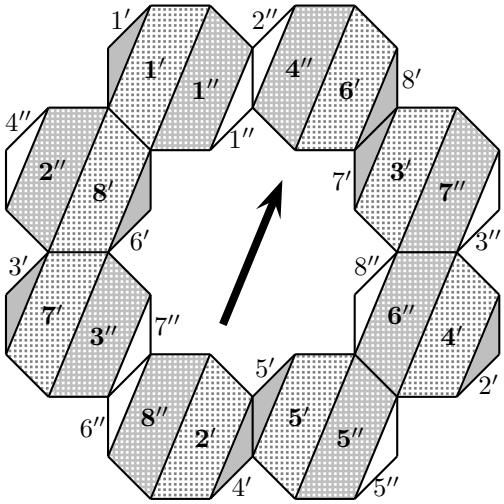

Figure 8.3.5: second set of tilted streets on the translation surface of regular octagon billiard

Having determined the streets in two perpendicular directions, we now attempt to visualize the translation surface of regular octagon billiard as a polyrectangle surface $\mathcal{P}$. To do so, we must be able to visualize the intersection of any two perpendicular streets in the translation surface of regular octagon billiard as one of the rectangle faces in $\mathcal{P}$. Figure 8.3.6 is a suitable modification of Figure 8.3.4.

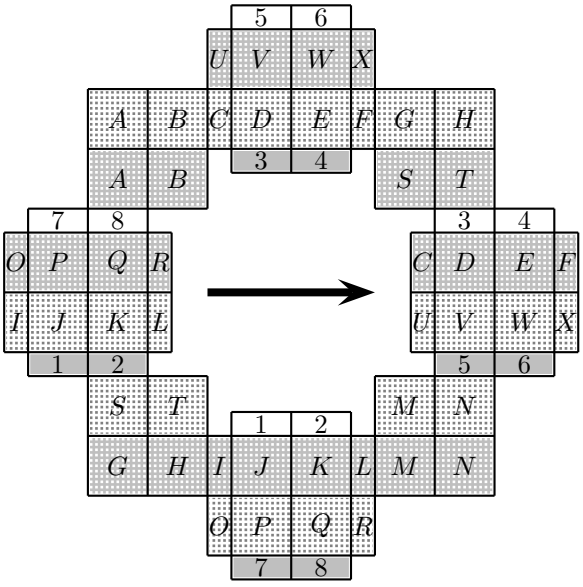

Figure 8.3.6: a modification of the streets in Figure 8.3.4

Note that in Figure 8.3.4, each big tilted street consists of 8 trapezoids, each the union of 2 squares and 2 $(\pi/8)$-right-triangles, while each small tilted street consists of 8 triangles, each the union of 2 $(\pi/8)$-right-triangles. This suggests that we attempt to visualize these $(\pi/8)$-right-triangles as pairs that combine to form $(\pi/8)$-rectangles. Here a $(\pi/8)$-right-triangle means a right triangle with an angle equal to $\pi/8$, whereas a $(\pi/8)$-rectangle means a rectangle that is the union of 2 $(\pi/8)$-right-triangles.

If we compare Figures 8.3.4 and 8.3.6, we see that A and B are the squares in the trapezoid $\mathbf{1}'$, while the $(\pi/8)$-rectangle C is made up of the $(\pi/8)$-right-triangle on the right hand end of the trapezoid $\mathbf{1}'$ and the $(\pi/8)$-right-triangle on the left hand end of the trapezoid $\mathbf{2}'$. On the other hand, the $(\pi/8)$-rectangle X is made up of the $(\pi/8)$-right-triangle on the right hand end of the trapezoid $\mathbf{8}'$ and the $(\pi/8)$-right-triangle on the left hand end of the trapezoid $\mathbf{1}'$.

Likewise, Figure 8.3.7 is a suitable modification of Figure 8.3.5.

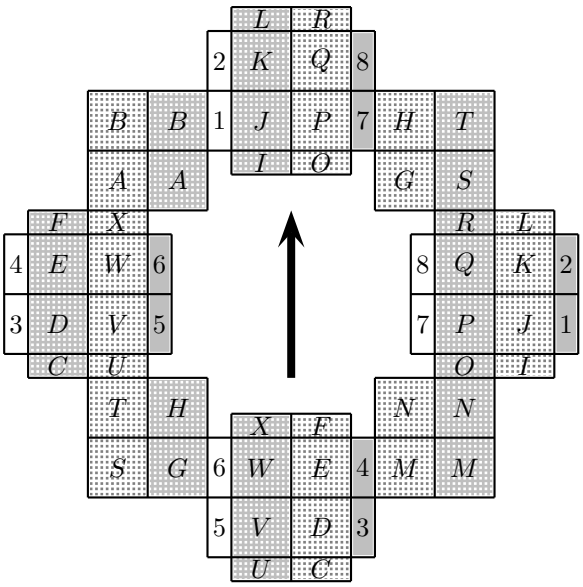

Figure 8.3.7: a modification of the streets in Figure 8.3.5

Figures 8.3.6 and 8.3.7 together clearly demonstrate that we can now visualize the translation surface of regular octagon billiard as a polyrectangle surface $\mathcal{P}$.

Figures 8.3.4–8.3.7 correspond to the decomposition of the regular octagon into 4 parts as shown in the picture on the right in Figure 8.1.5. If we repeat our argument in this section for the decomposition of the regular octagon into 3 parts as shown in the picture on the left in Figure 8.1.5, we obtain a different 8-octagon net which nevertheless has the same 1-direction geodesic flow.

Adapting the shortline method proof of Theorems 6.1.1 and 6.4.1 to any such concrete street-rational polyrectangle surface that arise, we then obtain the special case $k = 8$ of Theorem 8.3.1 below.

It is easy to see that the same method works for any regular k-gon, where $k \geqslant 6$ is even. Indeed, the first step is to have an analog of Figure 8.3.1. We simply need a regular k-gon with oriented boundary edges, and reflect it on a side. This gives a 2-copy version of the regular k-gon with boundary identification, which is a net of the corresponding billiard surface. To adapt the shortline method of Theorems 6.1.1 and 6.4.1, we need a flat surface with 1-direction geodesic flow. To construct such a surface we repeat the arguments illustrated by Figures 8.3.1–8.3.3. At the end we have the translation surface of regular k-gon billiard with boundary identification.

We have *street-rationality*, courtesy of the elementary geometric fact that the vertices of a regular polygon lie on a circle, so that we can use the "chord-angle

relation" on this circle. The last simple step is to rearrange this flat polygonal surface to a street-rational polyrectangle surface via translation of some corresponding parts, like converting Figures 8.3.4–8.3.5 to Figures 8.3.6–8.3.7.

To get a polyrectangle, we need two perpendicular decompositions into parallel strips like in Figure 8.1.5 for the regular octagon. And of course it can be done for every regular polygon of k sides, where $k \geqslant 6$ is even; see Figure 8.3.8 for the special case $k = 6$. In the picture on the left, the horizontal line divides the hexagon into 2 parts. In the picture on the right, the 2 vertical lines divide it into 3 parts.

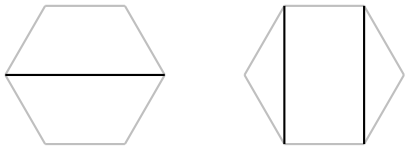

Figure 8.3.8: two perpendicular decompositions of the regular hexagon

Thus we obtain the following general result.

Theorem 8.3.1. *Let $k \geqslant 6$ be an even integer, and consider billiard in a regular polygon of k sides. There exist infinitely many explicit slopes, depending on k, such that any half-infinite billiard orbit having such an initial slope exhibits superdensity in the polygon.*

For infinitely many of these initial slopes that give rise to superdensity, we can explicitly compute the corresponding irregularity exponent.

Combining the irregularity exponent with the method of zigzagging introduced in Section 3.3 in [2]*, we can also describe, for billiard orbits having these initial slopes, the time-quantitative behavior of the edge-cutting and face-crossing numbers, as well as equidistribution relative to all convex sets.*

8.4. **More superdensity results.** Next we switch to the regular polygons of k sides, or k-gons for short, where $k \geqslant 5$ is odd.

The first example of this class comes from right triangle billiard with angle $\pi/5$. The standard trick of unfolding implies that the billiard can be described in terms of a 1-direction geodesic flow on the *regular double-pentagon surface*, as shown in Figure 8.4.1. Since we identify parallel edges, this surface has 1-direction geodesic flow.

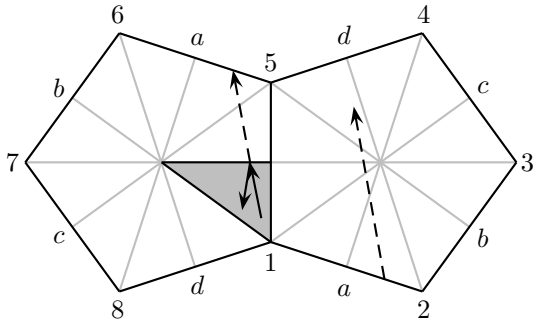

Figure 8.4.1: right triangle billiard with angle $\pi/5$, and geodesic flow on the regular double-pentagon surface via unfolding

Here the horizontal and vertical are no longer natural directions. However, viewed in the appropriate way, 1-direction geodesic flow on the regular double-pentagon surface can be shown to be equivalent to 1-direction geodesic flow on a street-rational *polyparallelogram* surface. By moving the two triangles on the bottom left to the top right, we end up with two rhombi and two other parallelograms, as shown in the picture on the left in Figure 8.4.2. Here street-rationality comes from the

geometric fact that the vertices of a regular polygon all lie on the same circle, and so we can use the "chord-angle relation" on this circle. Using this, we see that the angles 716 and 534 are the same. Hence these two other parallelograms are similar. Note from the picture on the right that we have two northwest-to-southeast streets, namely A, B, C and D, E. We also have two southwest-to-northeast streets, namely A, C, E and B, D. We shall return to this surface in the next section.

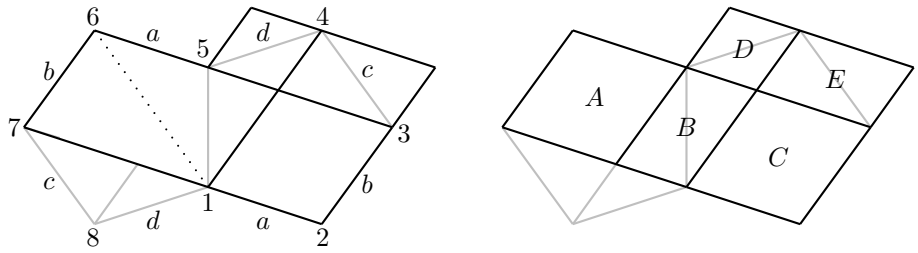

Figure 8.4.2: the double-pentagon surface as a polyparallelogram surface

Similar constructions show that 1-direction geodesic flow on every regular double-k-gon surface with odd $k \geqslant 5$ is equivalent to 1-direction geodesic flow on a street-rational polyparallelogram surface.

Regular pentagon billiard, on the other hand, is a complicated flow. While the "double-pentagon" net in Figure 8.4.3 is quite simple, the corresponding surface still exhibits a rather complicated geodesic flow. Note that the two pentagons are reflections of each other.

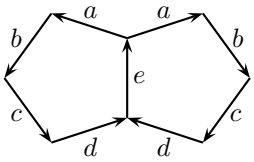

Figure 8.4.3: double-pentagon net of the regular pentagon billiard surface

As in the case for regular octagon billiard in Section 8.3, we join up pentagons in such a way that neighboring pentagons are reflections of each other. We end up with a ring of 10 pentagons, as shown in Figure 8.4.4. This is sometimes known as the translation surface of regular pentagon billiard. Note that the edge labellings in Figure 8.4.4 are obtained by following the convention discussed in the Remark after Figure 8.3.3.

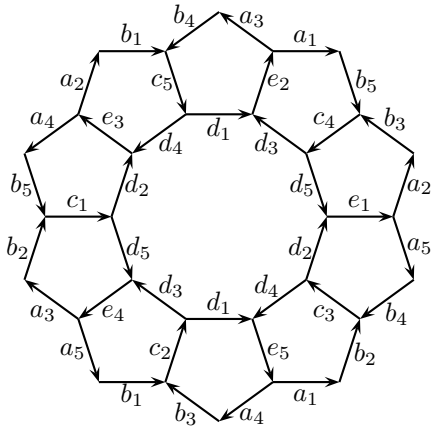

Figure 8.4.4: translation surface for regular pentagon billiard with edge labellings

We clearly need more, as we need a corresponding net that exhibits a 1-direction geodesic flow and which shows the streets in a more transparent fashion. The impatient reader may jump ahead to the nets in Figure 8.4.6 from which we can

easily obtain the corresponding street-rational polyparallelogram surface, adapt the shortline method in the proof of Theorems 6.1.1 and 6.4.1, and exhibit explicit slopes for which we can establish superdensity.

The plan is quite straightforward, and again the details are not too cumbersome. We shall proceed in steps and illustrate our ideas with pictures. Indeed, regular pentagon billiard represents the whole difficulty. Once we fully understand the special case of regular pentagon billiard, it is easy to visualize the general case of regular k-gon billiard, where $k \geqslant 5$ is any odd integer.

We shall use the decomposition of a regular pentagon into a trapezoid and a triangle. With the help of edge labellings, we can easily work out some streets, as shown in Figure 8.4.5. We first consider tilted streets in the direction shown in the picture on the left.

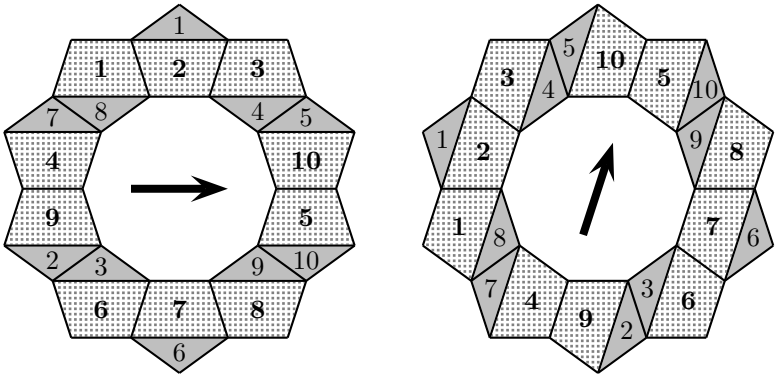

Figure 8.4.5: tilted streets on the translation surface of regular pentagon billiard

The big street in this direction consists of 10 trapezoids labelled

$$\mathbf{1}, \mathbf{2}, \mathbf{3}, \mathbf{4}, \mathbf{5}, \mathbf{6}, \mathbf{7}, \mathbf{8}, \mathbf{9}, \mathbf{10}.$$

There is also a small street in this direction, consisting of 10 triangles

$$1, 2, 3, 4, 5, 6, 7, 8, 9, 10.$$

To use the shortline method, we need to consider streets in a second direction, shown in the picture on the right in Figure 8.4.5. Again, we see that there are a big street, consisting of 10 trapezoids, and a small street, consisting of 10 triangles.

Having determined the streets in two different directions, we now attempt to visualize the translation surface of regular pentagon billiard as a polyparallelogram surface $\mathcal{P}$. To do so, we must be able to visualize the intersection of any two streets in different directions in the translation surface of regular pentagon billiard as one of the paralleogram faces in $\mathcal{P}$. Figure 8.4.6 is a suitable modification of Figure 8.4.5.

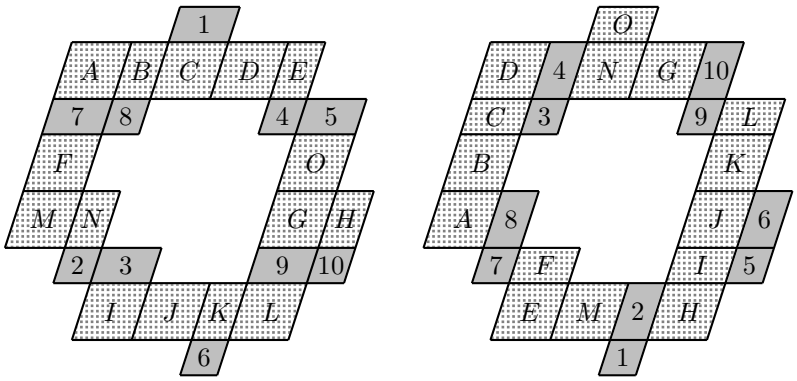

Figure 8.4.6: a modification of the streets in Figure 8.4.5 of regular pentagon billiard

Note that in Figure 8.4.5, each big tilted street consists of 10 trapezoids, each the union of a rhombus and a triangle. If we compare the pictures on the left in Figures 8.4.5 and 8.4.6, we see that A and C are the rhombi in the trapezoids **1** and **2**, while the parallelogram B is made up of the triangle on the right hand end of the trapezoid **1** and the triangle on the left hand end of the trapezoid **2**. On the other hand, the parallelogram E is made up of the triangle on the right hand end of the trapezoid **3** and the triangle on the left hand end of the trapezoid **4**.

Each small tilted street consists of 10 triangles, and each can be split into unequal parts by a segment parallel to the other direction and intersecting one of its vertices. If we compare the pictures on the left in Figures 8.4.5 and 8.4.6, we see that the parallelogram 1 is the union of the bigger half of the triangle 1 and the bigger half of the triangle 2, while the rhombus 2 is the union of the smaller half of the triangle 2 and the triangle 3.

Thus the resulting Figure 8.4.6 shows that we have a polyparallelogram surface.

We have already studied the superdensity of certain geodesic flow on the regular tetrahedron surface and on the cube surface. The next member of the famous list of the five platonic solids is the regular dodecahedron which has regular pentagon faces. Thus it is not surprising that a similar decomposition works for geodesic flow on the dodecahedron surface. The standard net of the dodecahedron surface consists of 12 pentagons. To construct the corresponding polygonal surface with 1-direction geodesic flow we have to glue together 10 copies of the 12-pentagon standard net. This means 120 copies of the pentagon, far too complicated to be explicitly included here. For illustration, Figure 8.4.7 shows one large street on the dodecahedron surface. We leave the complicated details of the explicit construction of the whole 120-copy version of the pentagon to the interested reader.

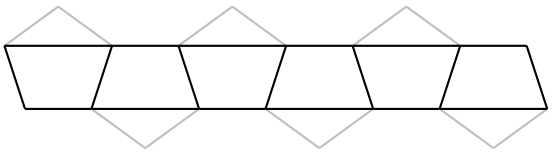

Figure 8.4.7: one large street on the dodecahedron surface

Note that the parity condition that $k \geqslant 5$ is odd requires us to have decomposition into street-rational parallelograms rather than street-rational polyrectangles for the case when $k \geqslant 6$ is even. This change is irrelevant, and does not prevent us from adapting the shortline method proof of Theorems 6.1.1 and 6.4.1. Thus we obtain the following analog of Theorems 8.1.1 and 8.3.1 for odd $k \geqslant 5$.

Theorem 8.4.1. *Let $k \geqslant 5$ be an odd integer.*

(i) *Consider the right-triangle with angle π/k. There exist infinitely many slopes, depending on k, such that any half-infinite billiard orbit with such an initial slope exhibits superdensity in the right-triangle with angle π/k.*

(ii) *Consider geodesic flow on the regular double-polygon of k sides. There exist infinitely many explicit slopes, depending on k, such that any half-infinite geodesic having such a slope exhibits superdensity in the double-polygon.*

(iii) *Consider billiard in a regular polygon of k sides. There exist infinitely many explicit slopes, depending on k, such that any half-infinite billiard orbit having such an initial slope exhibits superdensity in the polygon.*

(iv) *Consider geodesic flow on the dodecahedron surface. There exist infinitely many explicit slopes such that any half-infinite geodesic having such a slope exhibits superdensity on the surface.*

(v) *For infinitely many of these slopes in parts* (i), (ii), (iii) *and* (iv) *that give rise to superdensity, we can explicitly compute the corresponding irregularity exponent.*

Combining the irregularity exponent with the method of zigzagging introduced in Section 3.3 in [2]*, we can also describe, for trajectories having these initial slopes, the time-quantitative behavior of the edge-cutting and face-crossing numbers, as well as equidistribution relative to all convex sets.*

At this point, it is perhaps appropriate to mention the study of the remarkable *uniform-periodic dichotomy* in flat systems. This study essentially originates from the work of Veech [18], with the result that every infinite billiard orbit in a regular polygon is either periodic or exhibits uniformity.

As we have shown earlier, surfaces arising from regular polygons of k sides can be visualized as street-rational polyrectangle surfaces for even $k \geqslant 6$ and as street-rational polyparallelogram surfaces for odd $k \geqslant 5$.

Another flat system that exhibits the uniform-periodic dichotomy is billiard on a street-rational polyrectangle surface called the *golden L-surface*. As can be seen in the picture on the left in Figure 8.4.8, this surface exhibits 45-degree reflection symmetry, and it becomes a flat surface if we carry out the boundary identification indicated in the picture on the right in Figure 8.4.8.

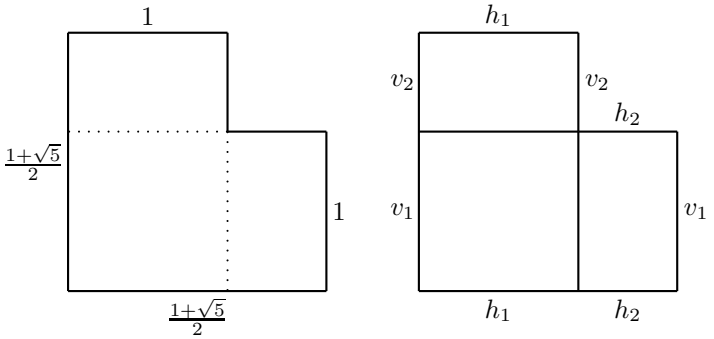

Figure 8.4.8: the golden L-surface

The street-rationality of the golden L-surface comes from a simple arithmetic property of the golden ratio, that

$$\frac{1+\sqrt{5}}{2} = \frac{1}{\frac{1+\sqrt{5}}{2} - 1}.$$

Of course the two special cases of square billiard and equilateral triangle billiard are well known classical results dating back to the 1920s. These classical results represent the "easy case" of integrable systems.

Billiard in a regular polygon of k sides, with $k \geqslant 5$, on the other hand, is a "non-integrable system", where the vertices represent split-singularities of the orbits.

A flat system exhibiting the uniform-periodic dichotomy is called *optimal*.

For a long time regular polygon billiard remains the only known infinite family of *primitive* optimal systems. Here *primitive* means that an elementary building block like an "atom" cannot be obtained from a simpler system by some covering space construction. We illustrate this concept on a familiar example.

Consider geodesic flow (or billiard) on the class of polysquare surfaces. By the Gutkin–Veech theorem, each member of this class is an optimal system, and together they exhibit every high genus. But there is only one *primitive* member, namely, geodesic flow (or billiard) on the unit torus $[0,1)^2$. In other words, the fractional part of geodesic flow on a polysquare surface, or *modulo one*, is the torus line flow on the flat torus. The inverse map of *modulo one* gives back the polysquare as a (branching) covering surface of the flat torus.

Similarly, we can glue together an arbitrary number of, for instance, *congruent* regular octagons in a natural horizontal or vertical way. The class of such *polyoctagon*

surfaces exhibits arbitrarily high genera. But there is only one primitive member, namely, the regular octagon surface itself.

Let us return to regular polygon billiard, the first infinite family of primitive optimal systems, discovered in the 1980s. A completely different infinite family of primitive optimal systems, discovered in the early 2000s independently by Calta [7] and McMullen [11], using different methods, consists of L-shaped tables for which the billiard is optimal. We shall refer to this as the Calta–McMullen family. Such billiard surfaces have genus 2, and the simplest member of this family is the golden L-surface. The L-shape has the special property that it is the same to consider geodesic flow or billiard flow, as they are equivalent systems.

The general member of the Calta–McMullen family is an L-shaped billiard table, with boundary identification given as in the picture on the right in Figure 8.4.9.

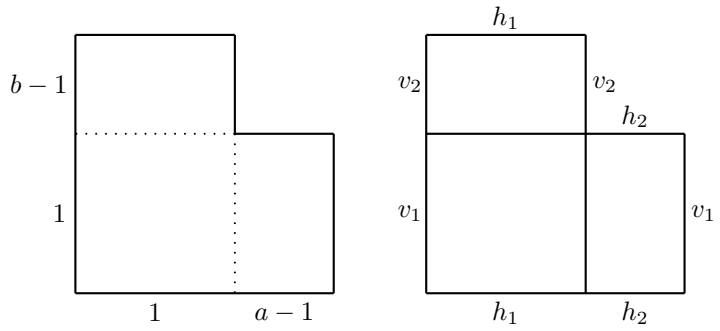

Figure 8.4.9: L-shaped billiard table

The bottom horizontal side has length a, the left-most vertical side has length b, the right-most vertical side has length 1, and the top-most horizontal side has length 1. The numbers

$$a = r_1\sqrt{d} + r_2 \quad \text{and} \quad b = r_1\sqrt{d} + 1 - r_2$$

are such that r_1, r_2 are rational numbers and $d \geqslant 2$ is a square-free integer. Here the choice of length 1 for two of the edges excludes equivalent systems, *i.e.*, it represents normalization.

It is easy to check that this is a street-rational polyrectangle surface. For the two horizontal streets, the width-height ratios of the two rectangle are

$$\frac{a}{1} \quad \text{and} \quad \frac{1}{b-1},$$

and their ratio is $a(b-1) = (r_1\sqrt{d} + r_2)(r_1\sqrt{d} - r_2) = r_1^2 d - r_2^2$, which is rational. For the two vertical streets, the width-height ratios of the two rectangle are

$$\frac{a-1}{1} \quad \text{and} \quad \frac{1}{b},$$

and their ratio is $(a-1)b = (r_1\sqrt{d} + r_2 - 1)(r_1\sqrt{d} + 1 - r_2) = r_1^2 d - (r_2 - 1)^2$, which is also rational.

The shortline method gives the following result.

Theorem 8.4.2. *Consider any surface in the Calta–McMullen family.*

(i) *There exist infinitely many explicit slopes, depending on the surface, such that any half-infinite geodesic on the surface having such a slope exhibits superdensity.*

(ii) *There exist infinitely many explicit slopes, depending on the surface, such that any billiard orbit on the surface having such an initial slope exhibits superdensity.*

(iii) *For infinitely many of these slopes in parts* (i) *and* (ii) *that give rise to superdensity, we can explicitly compute the corresponding irregularity exponents. Combining the irregularity exponent with the method of zigzagging introduced in*

Section 3.3 in [2]*, we can also describe, for trajectories having these initial slopes, the time-quantitative behavior of the edge-cutting and face-crossing numbers, as well as equidistribution relative to all convex sets.*

We shall justify part (iii) for the golden L-surface in Section 8.5.

Optimality and superdensity of some orbits are two different aspects concerning a dynamical system, both exhibiting "perfect" behavior. Optimality for these systems is established by Calta and McMullen via ergodicity, making use of Birkhoff's ergodic theorem. Since Birkhoff's ergodic theorem does not give any error term, these results do not say anything quantitative about the speed of convergence to uniformity, or even about time-quantitative density. Our superdensity results, on the other hand, establish a best possible form of time-quantitative density, at least for *some* slopes. And this is the best that we can hope for, since superdensity fails for almost every slope anyway.

Note next that every member of the Calta–McMullen family is what we may call a 1-*step L-staircase*, and the corresponding surface has the same genus 2. It is a 2-parameter family, since

$$a = \sqrt{q_1} + r_2 \quad \text{and} \quad b = \sqrt{q_1} + 1 - r_2$$

depend only on two rational parameters $q_1 = r_1^2 d$ and r_2.

We next describe a far-reaching extension of the Calta–McMullen family, leading to surfaces with arbitrarily large genus. For any integer $k \geqslant 1$, we construct an infinite family of street-rational polysquares that are *k-step L-staircases*, and each surface has genus $k + 1$.

The picture on the left in Figure 8.4.10 illustrates a typical street-rational 2-step L-staircase.

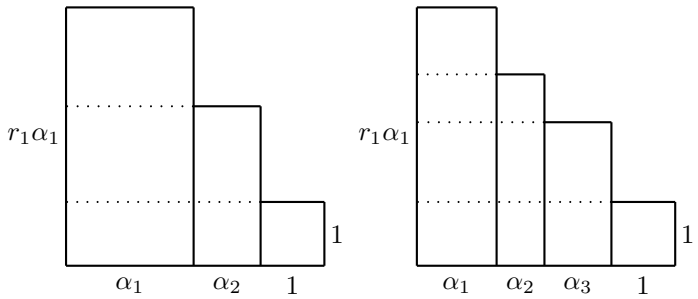

Figure 8.4.10: street-rational 2-step and 3-step L-staircases

The right-most vertical rectangle is a unit square, representing normalization to exclude equivalent systems. The left-most vertical rectangle has size $\alpha_1 \times r_1\alpha_1$, while the second vertical rectangle has size $\alpha_2 \times r_2\alpha_2$, where $r_1\alpha_1 > r_2\alpha_2 > 1$ and r_1, r_2 are positive rational numbers.

The top horizontal rectangle now has size $\alpha_1 \times (r_1\alpha_1 - r_2\alpha_2)$, the middle horizontal rectangle has size $(\alpha_1 + \alpha_2) \times (r_2\alpha_2 - 1)$, while the bottom horizontal rectangle has size $(\alpha_1 + \alpha_2 + 1) \times 1$. Thus the 2-step L-staircase is a street-rational polyrectangle surface precisely if we have the relations

$$\frac{\alpha_1}{r_1\alpha_1 - r_2\alpha_2} = r_3 \frac{\alpha_1 + \alpha_2}{r_2\alpha_2 - 1} = r_4(\alpha_1 + \alpha_2 + 1) \tag{8.4.1}$$

for the width-height ratios of the 3 horizontal rectangles, where r_3, r_4 are some positive rational numbers.

The analogous requirement for the 3 vertical rectangles is guaranteed by definition.

We wish to express the two positive real variables α_1, α_2 in (8.4.1) in terms of the given positive rational parameters r_1, r_2, r_3, r_4. Routine calculation shows that both

α_1, α_2 are algebraic numbers. Indeed, using the second equality in (8.4.1), we obtain

$$\alpha_1 = \frac{r_2 r_4 \alpha_2^2 + (r_2 r_4 - r_3 - r_4)\alpha_2 - r_4}{r_3 + r_4 - r_2 r_4 \alpha_2}. \tag{8.4.2}$$

Substituting this into the first equality in (8.4.1) eliminates the variable α_1, and gives rise to a polynomial equation of degree 4 in the variable α_2 with rational coefficients. Thus α_2 is algebraic. In view of (8.4.2), α_1 is also algebraic. Crucially, for the typical choice of the rational parameters r_1, r_2, r_3, r_4, this polynomial equation of degree 4 has a positive root which is not rational.

This completes the construction of the class of 2-step street-rational L-staircases. It is a 4-parameter family, depending on the rational parameters r_1, r_2, r_3, r_4, and each member of this family has genus 3.

The picture on the right in Figure 8.4.10 illustrates a typical street-rational 3-step L-staircase.

The right-most vertical rectangle is a unit square, representing normalization to exclude equivalent systems. The left-most vertical rectangle has size $\alpha_1 \times r_1\alpha_1$, the second vertical rectangle has size $\alpha_2 \times r_2\alpha_2$, while the third vertical rectangle has size $\alpha_3 \times r_3\alpha_3$, where $r_1\alpha_1 > r_2\alpha_2 > r_3\alpha_3 > 1$ and r_1, r_2, r_3 are positive rational numbers.

The top horizontal rectangle now has size $\alpha_1 \times (r_1\alpha_1 - r_2\alpha_2)$, the second horizontal rectangle has size $(\alpha_1 + \alpha_2) \times (r_2\alpha_2 - r_3\alpha_3)$, the third horizontal rectangle has size $(\alpha_1 + \alpha_2 + \alpha_3) \times (r_3\alpha_3 - 1)$, while the bottom horizontal rectangle has size $(\alpha_1 + \alpha_2 + \alpha_3 + 1) \times 1$. Thus the 3-step L-staircase is a street-rational polyrectangle surface precisely if we have the relations

$$\frac{\alpha_1}{r_1\alpha_1 - r_2\alpha_2} = r_4 \frac{\alpha_1 + \alpha_2}{r_2\alpha_2 - r_3\alpha_3} = r_5 \frac{\alpha_1 + \alpha_2 + \alpha_3}{r_3\alpha_3 - 1} = r_6(\alpha_1 + \alpha_2 + \alpha_3 + 1) \tag{8.4.3}$$

for the width-height ratios of the 4 horizontal rectangles, where r_4, r_5, r_6 are some positive rational numbers.

The analogous requirement for the 4 vertical rectangles is guaranteed by definition.

We wish to express the three positive real variables $\alpha_1, \alpha_2, \alpha_3$ in (8.4.3) in terms of the given positive rational parameters $r_1, r_2, r_3, r_4, r_5, r_6$. Routine calculation shows that $\alpha_1, \alpha_2, \alpha_3$ are all algebraic numbers. We leave the details to the reader.

This completes the construction of the class of 3-step street-rational L-staircases. It is a 6-parameter family, depending on the rational parameters $r_1, r_2, r_3, r_4, r_5, r_6$, and each member of this family has genus 4.

The construction of street-rational k-step L-staircases, where $k \geqslant 1$, goes in a similar way. This gives rise to a $2k$-parameter family, and each member of the family has genus $k + 1$.

The construction gives a street-rational polyrectangle with a 1-direction geodesic flow, and the corresponding billiard surface is also street-rational. Thus the shortline method works, and gives the following generalization of Theorem 8.4.2.

Theorem 8.4.3. *Let $k \geqslant 1$ be an integer, and consider a k-step street-rational L-staircase surface.*

(i) *There exist infinitely many explicit slopes, depending on the surface, such that any half-infinite geodesic on the surface having such a slope exhibits superdensity.*

(ii) *There exist infinitely many explicit slopes, depending on the surface, such that any billiard orbit on the surface having such an initial slope exhibits superdensity.*

(iii) *For infinitely many of these slopes in parts* (i) *and* (ii) *that give rise to superdensity, we can explicitly compute the corresponding irregularity exponents. Combining the irregularity exponent with the method of zigzagging introduced in Section 3.3 in* [2]*, we can also describe, for trajectories having these initial slopes,*

the time-quantitative behavior of the edge-cutting and face-crossing numbers, as well as equidistribution relative to all convex sets.

Remark. We are not aware whether these street-rational k-step L-staircases, where $k \geqslant 2$, in general are optimal. What we can prove is that they all have explicit superdense orbits. More precisely, our construction gives *primitive* street-rational L-staircase surfaces in *every* positive genus and which exhibit explicit superdense orbits. On the other hand, we are not aware of any infinite family of primitive optimal billiard systems in a fixed high genus.

To obtain new street-rational polyrectangle surfaces, there is a technique which is algebraic in nature. We shall describe this technique by first looking at a simple example.

Consider the polysquare surface which is a 3×3 square with a missing square in the middle, as shown in Figure 8.4.11 with boundary identification given by perpendicular translation.

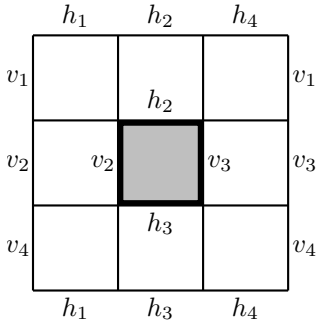

Figure 8.4.11: a polysquare surface

We can obtain a polyrectangle surface by varying the lengths of the edges of the square faces to change them to rectangle faces. To ensure that we obtain affine-different polyrectangles, we fix a horizontal side and a vertical side to have length 1. For simplicity, we have ensured that the bottom left square face does not get altered. As shown in Figure 8.4.12, we allow the other faces to have different lengths.

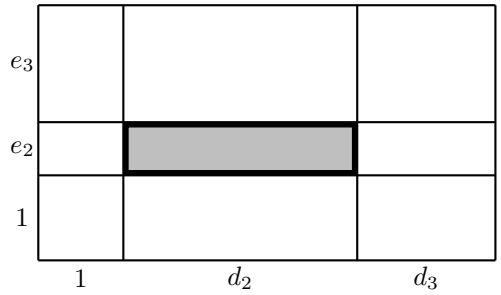

Figure 8.4.12: a polyrectangle surface corresponding to the polysquare surface in Figure 8.4.11

The original polysquare surface has 4 horizontal streets and 4 vertical streets, corresponding to the edge pairings v_1, v_2, v_3, v_4 and h_1, h_2, h_3, h_4. The 4 corresponding horizontal streets in the polyrectangle surface have normalized lengths, *i.e.* street lengths normalized by division by street widths, equal to

$$\frac{1 + d_2 + d_3}{e_3}, \quad \frac{1}{e_2}, \quad \frac{d_3}{e_2}, \quad \frac{1 + d_2 + d_3}{1}.$$

For horizontal street-rationality, we require positive rational numbers r_1, r_2, r_3 such that

$$e_3 = r_1, \quad d_3 = r_2, \quad e_2(1 + d_2 + d_3) = r_3. \tag{8.4.4}$$

On the other hand, the 4 corresponding verticalal streets in the polyrectangle surface have normalized lengths equal to

$$\frac{1+e_2+e_3}{1}, \quad \frac{e_3}{d_2}, \quad \frac{1}{d_2}, \quad \frac{1+e_2+e_3}{d_3}.$$

For vertical street-rationality, again we require e_3 and d_3 to be rational, already taken care of in (8.4.4), as well as another positive rational numbers r_4 such that

$$d_2(1+e_2+e_3) = r_4. \tag{8.4.5}$$

Combining (8.4.4) and (8.4.5), we obtain

$$e_2(d_2+1+r_2) = r_3 \quad \text{and} \quad d_2(e_2+1+r_1) = r_4,$$

leading to a linear equation in e_2 and d_2 with rational coefficients. On combining this linear equation with (8.4.5) and eliminating the variable e_2, say, we obtain a quadratic equation with rational coefficients in the variable d_2. One can check that for infinitely many choices of the rational numbers r_1, r_2, r_3, r_4, this quadratic equation has a positive irrational root d_2 with corresponding positive e_2, leading to a street-rational polyrectangle surface that is not a polysquare surface.

A similar argument seems to work if we start with a polysquare surface with perpendicular boundary identification. For illustration, we consider the slightly more complicated polysquare surafce shown in Figure 8.4.13.

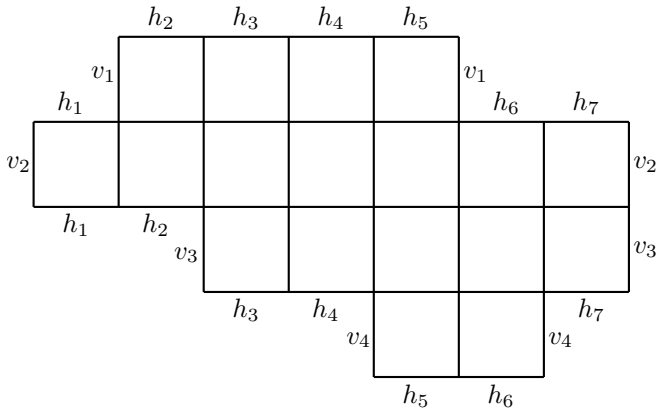

Figure 8.4.13: another polysquare surface

We can obtain a polyrectangle surface by varying the lengths of the edges of the square faces to change them to rectangle faces. To ensure that we obtain affine-different polyrectangles, we fix a horizontal side and a vertical side to have length 1. For simplicity, we have ensured that the left most square face does not get altered. As shown in Figure 8.4.14, we allow the other faces to have different lengths.

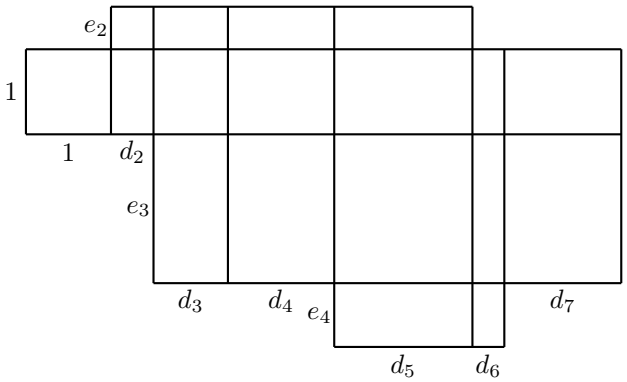

Figure 8.4.14: a polyrectangle surface corresponding to the polysquare surface in Figure 8.4.13

The original polysquare surface has 4 horizontal streets and 7 vertical streets. The 4 corresponding horizontal streets in the polyrectangle surface have normalized lengths equal to

$$\frac{d_2+\ldots+d_5}{e_2},\quad \frac{1+d_2+\ldots+d_7}{1},\quad \frac{d_3+\ldots+d_7}{e_3},\quad \frac{d_5+d_6}{e_4},$$

and horizontal street-rationality leads to 3 equations that involve 3 positive rational numbers r_1, r_2, r_3, say. On the other hand, the 7 corresponding vertical streets in the polyrectangle surface have normalized lengths equal to

$$\frac{1}{1},\ \frac{1+e_2}{d_2},\ \frac{1+e_2+e_3}{d_3},\ \frac{1+e_2+e_3}{d_4},\ \frac{1+e_2+e_3+e_4}{d_5},\ \frac{1+e_3+e_4}{d_6},\ \frac{1+e_3}{d_7},$$

and vertical street-rationality leads to 6 equations that involve 6 positive rational numbers $r_4, \ldots, r_9$, say. In other words, we have 9 equations in the 9 variables

$$d_2, d_3, d_4, d_5, d_6, d_7, e_2, e_3, e_4$$

that involve 9 positive rational parameters $r_1, \ldots, r_9$. And it is reasonable to expect that there are infinitely many choices of $r_1, \ldots, r_9$ that lead to positive solutions for all the variables and irrational solutions for some.

Indeed, we may generalize this to any arbitrary finite polysquare surface with m horizontal streets and n vertical streets. Street-rationality will give rise to $m+n-2$ equations in $m+n-2$ variables of the type d_i and e_j, and these equations involve $m+n-2$ positive rational parameters.

In sharp contrast, as far as we know, the current literature shows only 3 types of polysquare surfaces with the simplest perpendicular boundary identification that will lead to infinitely many primitive optimal translation surfaces. The L-surface on the left in Figure 8.4.15 leads to the Calta–McMullen family of L-shapes with genus 2. The second type, shown in the middle of Figure 8.4.15, has genus 3, while the third type, shown on the right in Figure 8.4.15, has genus 4.

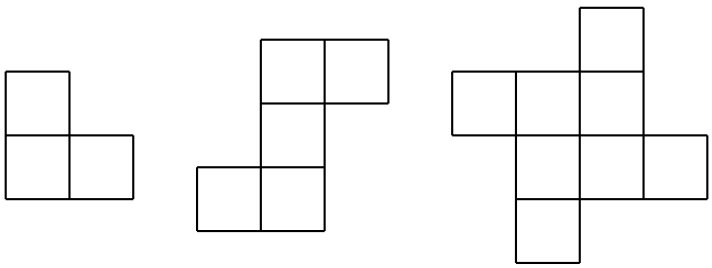

Figure 8.4.15: polysquare surfaces leading to infinitely many primitive optimal translation surfaces

For the details of the corresponding optimal families, we refer the reader to the paper of McMullen [14].

The simplest missing type of polysquare surfaces from this short list is the one shown in the picture on the left in Figure 8.4.16, with perpendicular boundary identification, and genus 2.

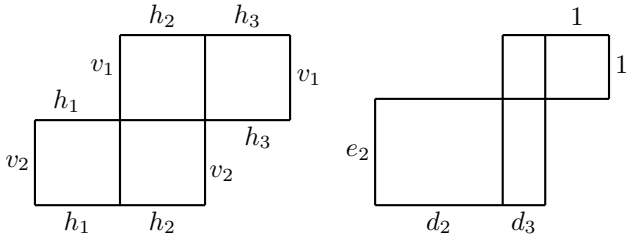

Figure 8.4.16: an infinite family of non-optimal street-rational polyrectangle surfaces

The polysquare surface has 2 horizontal streets and 3 vertical streets. Let us consider the corresponding polyrectangle surfaces shown in the picture on the right in Figure 8.4.16. The 3 vertical streets have normalized lengths equal to

$$\frac{e_2}{d_2}, \quad \frac{1+e_2}{d_3}, \quad \frac{1}{1},$$

and for vertical street-rationality, we need rational numbers $r_1, r_2 > 0$ such that

$$r_1 \frac{e_2}{d_2} = r_2 \frac{1+e_2}{d_3} = 1,$$

so we have the two conditions

$$d_2 = r_1 e_2 \quad \text{and} \quad d_3 = r_2(1+e_2). \tag{8.4.6}$$

On the other hand, the 2 horizontal streets have normalized lengths equal to

$$\frac{1+d_3}{1}, \quad \frac{d_2+d_3}{e_2},$$

and for horizontal street-rationality, we need a rational number $r_3 > 0$ such that

$$r_3 \frac{1+d_3}{1} = \frac{d_2+d_3}{e_2},$$

so we have the extra condition

$$d_2 + d_3 = r_3 e_2 (1+d_3). \tag{8.4.7}$$

The equations (8.4.6) and (8.4.7) have quadratic irrational solutions in d_2, d_3, e_2 that can be written in a simple explicit form, in sharp contrast to L-staircases where the corresponding requirements (8.4.1)–(8.4.3) lead to unpleasant higher degree equations, so we work out the details here.

Substituting (8.4.6) into (8.4.7), we obtain

$$r_1 e_2 + r_2(1+e_2) = r_3 e_2 (1 + r_2(1+e_2)). \tag{8.4.8}$$

This quadratic equation in the variable e_2 can be rewritten in the form

$$r_2 r_3 e_2^2 + (r_2 r_3 + r_3 - r_1 - r_2) e_2 - r_2 = 0.$$

Since $r_2, r_3 > 0$, such a typical quadratic equation has complex conjugate roots $e_2 = R_2 \pm R_1\sqrt{D}$, where R_1, R_2 are rational numbers and $D \geqslant 2$ is a positive squarefree integer. Furthermore,

$$R_1^2 D - R_2^2 = -(R_2 + R_1\sqrt{D})(R_2 - R_1\sqrt{D}) = \frac{1}{r_3} > 0. \tag{8.4.9}$$

For simplicity, let us assume that

$$e_2 = R_1\sqrt{D} + R_2 > 0. \tag{8.4.10}$$

Using (8.4.10), the left hand side of (8.4.8) becomes

$$r_1(R_1\sqrt{D} + R_2) + r_2(R_1\sqrt{D} + R_2 + 1),$$

and the right hand side of (8.4.8) becomes

$$r_3(R_1\sqrt{D} + R_2)(1 + r_2(R_1\sqrt{D} + R_2 + 1)).$$

The coefficient for $\sqrt{D}$ in (8.4.8) is equal to

$$(r_1 + r_2) R_1 = r_3(1+r_2) R_1 + 2 r_2 r_3 R_1 R_2, \tag{8.4.11}$$

while the rational term in (8.4.8) is equal to

$$(r_1 + r_2) R_2 + r_2 = r_3(1+r_2) R_2 + r_2 r_3 R_2^2 + r_2 r_3 R_1^2 D. \tag{8.4.12}$$

Combining (8.4.11) and (8.4.12) and eliminating r_3, we deduce that

$$\frac{(r_1+r_2)R_1}{(1+r_2)R_1+2r_2R_1R_2}=\frac{(r_1+r_2)R_2+r_2}{(1+r_2)R_2+r_2R_2^2+r_2R_1^2D},$$

which can be simplified to

$$\frac{r_1+r_2}{1+r_2+2r_2R_2}=\frac{(r_1+r_2)R_2+r_2}{(1+r_2)R_2+r_2R_2^2+r_2R_1^2D}.$$

For any given R_1, R_2, D and r_2, this is a linear equation in r_1, with solution

$$r_1=\frac{1+r_2(2R_2+1)}{R_1^2D-R_2^2}-r_2. \tag{8.4.13}$$

We require $r_1>0$, so we have to assume the *positivity condition*

$$\frac{1+r_2(2R_2+1)}{R_1^2D-R_2^2}-r_2>0.$$

In view of (8.4.9), this is equivalent to $1+r_2(2R_2+1)-(R_1^2D-R_2^2)r_2>0$, *i.e.*,

$$(R_1^2D-(R_2+1)^2)r_2<1. \tag{8.4.14}$$

Note that $R_1^2D-(R_2+1)^2$ is never zero, so there are only two possibilities:

(i) If $R_1^2D-(R_2+1)^2>0$, then r_2 is restricted to the range

$$0<r_2<\frac{1}{R_1^2D-(R_2+1)^2}.$$

(ii) If $R_1^2D-(R_2+1)^2<0$, then any $r_2>0$ is possible.

Combining (8.4.6) and (8.4.10), we now have

$$e_2=R_1\sqrt{D}+R_2,\quad d_2=r_1(R_1\sqrt{D}+R_2),\quad d_3=r_2(R_1\sqrt{D}+R_2+1). \tag{8.4.15}$$

Note that (8.4.13) and (8.4.14) become particularly simple if $R_1^2D-R_2^2=1$ and $R_2>0$. Then case (ii) applies. If we write $r=r_2$, then using (8.4.13), we can reduce (8.4.15) to

$$e_2=R_1\sqrt{D}+R_2,\quad d_2=(2rR_2+1)(R_1\sqrt{D}+R_2),\quad d_3=r(R_1\sqrt{D}+R_2+1).$$

It is a lucky coincidence that we know all the integral solutions of the Pell equation $R_1^2D-R_2^2=1$ and $R_2>0$. The simplest such choice is $D=2$ and $R_1=R_2=1$, leading to the solution

$$e_2=\sqrt{2}+1,\quad d_2=(2r+1)(\sqrt{2}+1),\quad d_3=r(\sqrt{2}+2),$$

where $r>0$ is any positive rational number.

We observe that neither geodesic flow on any of these street-rational polyrectangle surfaces nor billiard flow on any such polyrectangle billiard table is optimal. Our shortline method, nevertheless, does give time-quantitative results for infinitely many directions.

Next, we leave this algebraic approach and outline a completely different geometric way to construct primitive non-polysquare street-rational polyrectangle surfaces. We shall call this *double-rational gluing*. For a simple illustration of the ideas, we consider Figure 8.4.17, where we glue together two regular octagons with edge lengths that are rational multiples of each other.

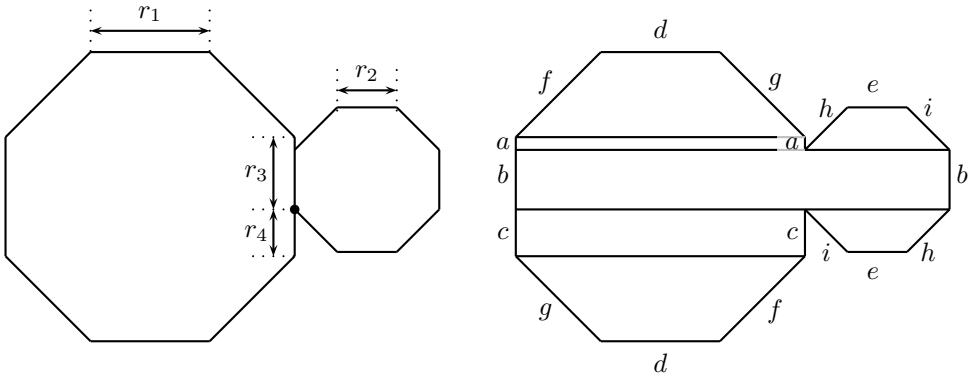

Figure 8.4.17: gluing together two regular octagons

Since the edge lengths of the two regular octagons are rational multiples of each other, we may assume, without loss of generality, that both edge lengths are rational numbers, equal to r_1 and r_2 as shown in the picture on the left in Figure 8.4.17. We glue the two octagons together in such a way that the vertex, indicated in the picture by the dot, of the octagon on the right lies on a point on the edge of the octagon on the left which has rational distances r_3 and r_4 from the two nearest vertices. With edge identification shown in the picture on the right in Figure 8.4.17, the union of the two regular octagons becomes a surface.

It is clear that the edge identification give rise to 4 vertical streets and 5 horizontal streets, as shown in Figure 8.4.18. To check for street-rationality, we need to look at the normalized lengths, *i.e.* street lengths normalized by division by street widths, of these streets.

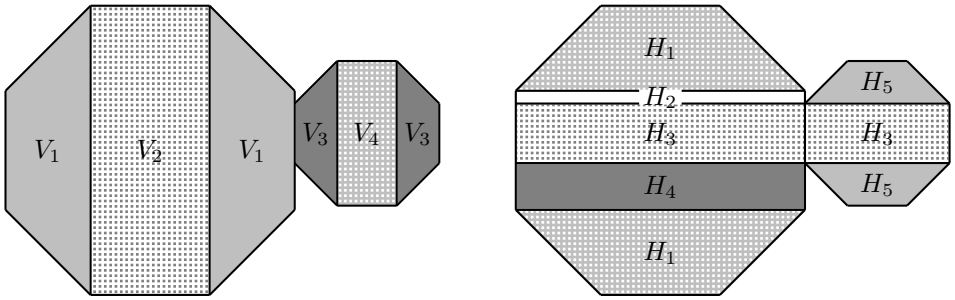

Figure 8.4.18: vertical and horizontal streets

The normalized lengths of the vertical streets V_1, V_2, V_3, V_4 are respectively

$$\frac{2+\sqrt{2}}{1/\sqrt{2}}, \quad \frac{1+\sqrt{2}}{1}, \quad \frac{2+\sqrt{2}}{1/\sqrt{2}}, \quad \frac{1+\sqrt{2}}{1},$$

and these are all rational multiples of $1+\sqrt{2}$. On the other hand, the normalized lengths of the horizontal streets H_1, H_2, H_3, H_4, H_5 are respectively

$$\frac{2+\sqrt{2}}{1/\sqrt{2}}, \quad \frac{r_1(1+\sqrt{2})}{r_3-r_2}, \quad \frac{(r_1+r_2)(1+\sqrt{2})}{r_2}, \quad \frac{r_1(1+\sqrt{2})}{r_4}, \quad \frac{2+\sqrt{2}}{1/\sqrt{2}},$$

and these are also all rational multiples of $1+\sqrt{2}$. Thus the surface comprising the two octagons is a street-rational polyrectangle surface which is not a polysquare surface.

Note that a bigger regular octagon is not a covering surface of a smaller regular octagon. Thus this street-rational polyrectangle surface is *primitive*, *i.e.* it cannot be obtained from a simpler surface via covering construction.

We need not stop at two regular octagons. In general, we can glue together, across horizontal or vertical edges, arbitrarily many regular octagons with edge lengths that are rational multiples of each other in a similar way. With a typical choice of rational edge length parameters, the resulting street-rational polyrectangle surface is primitive.

Of course, we can replace the regular octagon by any regular polygon of k sides, where $k \geqslant 8$ is divisible by 4, and obtain an analogous class of street-rational polyrectangle surfaces via double-rational gluing. The divisibility by 4 guarantees that each copy of the regular polygon has horizontal and vertical sides which play a special role in the gluing process.

We can also replace the regular octagon with the golden L-shape or, more precisely, the golden cross made up of 4 reflected copies of the golden L-shape, as shown in Figure 8.4.19. Then double-rational gluing gives rise to street-rational polyrectangle surfaces where the normalized length of any street is a rational multiple of the golden ratio $(1 + \sqrt{5})/2$.

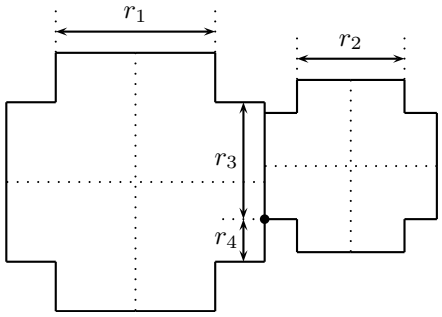

Figure 8.4.19: gluing together two golden crosses

In Figure 8.4.20, we have a street-rational polyrectangle surface made up of nine golden crosses, with six copies of the same size, two copies with double edge length, and one copy of triple edge length. Indeed, if we consider this figure as a billiard table, the the corresponding billiard surface is also a street-rational polyrectangle surface.

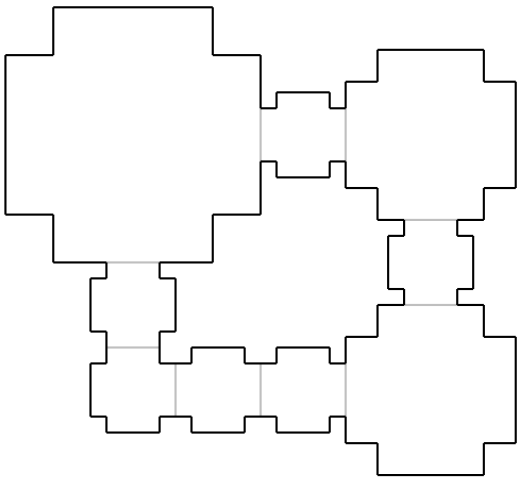

Figure 8.4.20: a street-rational polyrectangle surface consisting of nine golden crosses

A similar consideration arises if we start with a cross made up of 4 reflected copies of any member of the Calta–McMullen family, or a surface made up of 4 reflected copies of an street-rational k-step L-staircase.

Note that there is no analogous results for optimal systems. We are not aware of any construction using double-rational gluing that builds optimal systems from optimal components.

We conclude this section by considering surfaces of some rectangular boxes. This is a generalization of Example 7.2.4 concerning the surface of the unit cube.

One such example is what we may call the "golden brick", or a brick with golden ratio, as shown in Figure 8.4.21.

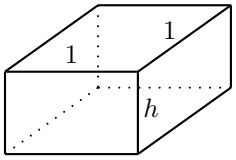

Figure 8.4.21: a brick with the golden ratio

This has two opposite faces that are unit squares, and the four parallel edges joining them have length $h = (\sqrt{5} - 1)/2$. It is easy to see that this gives rise to a street-rational polyrectangle surface. Indeed, it has 3 streets, each of length 4. One of these streets has size $h \times 4$, while the other two have common size $1 \times (2 + 2h)$. Street-rationality is now a consequence of the observation that

$$\frac{1}{2 + 2h} = 2 \cdot \frac{h}{4},$$

due to $h^2 + h = 1$. We shall return to this example in the next section where we shall determine some irregularity exponents.

Clearly, this example can be generalized. Starting with two opposite unit square faces, we now let z denote the length of the four parallel edges joining them. One of these streets has size $z \times 4$, while the other two have common size $1 \times (2 + 2z)$. Thus we have street-rationality if we can find coprime integers $a, b \geqslant 1$ such that

$$\frac{1}{2 + 2z} = \frac{a}{b} \cdot \frac{z}{4},$$

precisely when $az^2 + az - 2b = 0$. Thus

$$z = \frac{\sqrt{a^2 + 8ab} - a}{2a}.$$

Note that the choice $a = 2$ and $b = 1$ gives $z = h$.

Thus Theorem 8.4.3 can be extended to all of these special box-surfaces.

We can further generalize by starting with two opposite rectangle faces. We leave the details to the reader. Unfortunately the analogous problem for an *arbitrary* box-surface remains wide open.

8.5. **Computing more irregularity exponents.** In this section, we first return to the double-pentagon surface as shown in Figure 8.4.2. Our purpose is to find the eigenvalues of its 2-step transition matrix M.

This surface can be viewed as a polyparallelogram surface, and we shall use an analogy with a corresponding polyrectangle surface as shown in Figure 8.5.1.

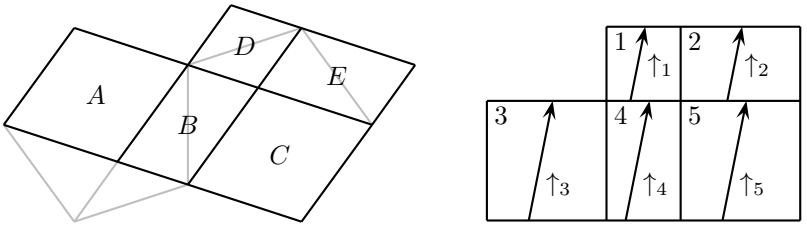

Figure 8.5.1: analogy of the double-pentagon surface with a polyrectangle surface

The rhombi A, C, D in the picture on the left become the squares $3, 5, 1$ respectively, while the parallelograms B, E become the rectangles $4, 2$ respectively. Here the horizontal streets are $1, 2$ and $3, 4, 5$, while the vertical streets are $1, 4$ and $2, 5, 3$. It is not difficult to check that both horizontal streets and both vertical streets have normalized lengths $(3 + \sqrt{5})/2$. Note here that the two distinct rectangle faces $3, 5$ can fall into the same horizontal street and the same vertical street, so we shall adapt our notation from Section 7.2 for the determination of the street-spreading matrix.

We also show in the picture on the right in Figure 8.5.1 the almost vertical units of type $\uparrow$ in the polyrectangle surface. We have not shown that almost vertical units of type $\nmid$ here.

Let

$$J_1 = \{1, 2\} \quad \text{and} \quad J_2 = \{3, 4, 5\}$$

denote the horizontal streets, and let

$$I_1 = I_4 = \{1, 4\} \quad \text{and} \quad I_2 = I_3 = I_5 = \{2, 3, 5\}$$

denote the vertical streets.

For the polyrectangle surface, we thus consider slopes of the form

$$\alpha_k = \frac{3 + \sqrt{5}}{2} k + \frac{1}{\frac{3+\sqrt{5}}{2} k + \frac{1}{\frac{3+\sqrt{5}}{2} k + \cdots}}.$$

For simplicity, however, we consider only the special case with branching parameter $k = 1$.

Corresponding to (7.2.14), we define the column matrices

$$\mathbf{u}_1 = [\{\uparrow_s : j \in J_1^*, s \in I_j^*\}] \quad \text{and} \quad \mathbf{u}_2 = [\{\uparrow_s : j \in J_2^*, s \in I_j^*\}]. \tag{8.5.1}$$

Here J_1^*, J_2^* and I_j^* denote that the edges are counted with multiplicity.

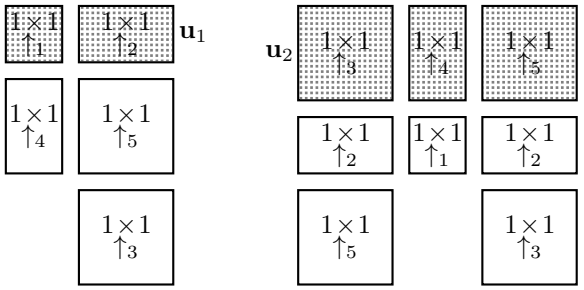

Figure 8.5.2: almost vertical units of type $\uparrow$ in $\mathbf{u}_1$ and $\mathbf{u}_2$

We also define the column matrices $\mathbf{v}_1$ and $\mathbf{v}_2$ analogous to (7.2.15), but their details are not important. Also, analogous to (7.2.17), we have

$$(M - I)[\{\uparrow_s\}] = \begin{cases} \mathbf{u}_1 + \mathbf{v}_1, & \text{if } s \in J_1, \\ \mathbf{u}_2 + \mathbf{v}_2, & \text{if } s \in J_2. \end{cases} \tag{8.5.2}$$

We now combine (8.5.1) and (8.5.2). For the horizontal street corresponding to $\mathbf{u}_1$, as highlighted in the picture on the left in Figure 8.5.2, we have

$$\begin{aligned}(M-I)\mathbf{u}_1 &= (M-I)[\{\uparrow_1,\uparrow_2\}] + (M-I)[\{\uparrow_3,\uparrow_4,\uparrow_5\}] \\ &= 2(\mathbf{u}_1+\mathbf{v}_1) + 3(\mathbf{u}_2+\mathbf{v}_2). \end{aligned} \tag{8.5.3}$$

For the horizontal street corresponding to $\mathbf{u}_2$, as highlighted in the picture on the right in Figure 8.5.2, we have

$$\begin{aligned}(M-I)\mathbf{u}_2 &= (M-I)[\{\uparrow_1,2\uparrow_2\}] + (M-I)[\{2\uparrow_3,\uparrow_4,2\uparrow_5\}] \\ &= 3(\mathbf{u}_1+\mathbf{v}_1) + 5(\mathbf{u}_2+\mathbf{v}_2). \end{aligned} \tag{8.5.4}$$

It follows from (8.5.3)–(8.5.4) that the street-spreading matrix is given by

$$\mathbf{S} = \begin{pmatrix} 2 & 3 \\ 3 & 5 \end{pmatrix},$$

with eigenvalues

$$\tau_1 = \frac{7+3\sqrt{5}}{2} \quad \text{and} \quad \tau_2 = \frac{7-3\sqrt{5}}{2}.$$

Using (7.2.38), the corresponding eigenvalues of M are

$$\lambda\left(\frac{7+3\sqrt{5}}{2};\pm\right) = \frac{11+3\sqrt{5}}{4} \pm \frac{1}{4}\left(150+66\sqrt{5}\right)^{1/2}$$

and

$$\lambda\left(\frac{7-3\sqrt{5}}{2};\pm\right) = \frac{11-3\sqrt{5}}{4} \pm \frac{1}{4}\left(150-66\sqrt{5}\right)^{1/2}.$$

The two largest eigenvalues are therefore

$$\lambda_1 = \frac{11+3\sqrt{5}}{4} + \frac{1}{4}\left(150+66\sqrt{5}\right)^{1/2}$$

and

$$\lambda_2 = \frac{11-3\sqrt{5}}{4} + \frac{1}{4}\left(150-66\sqrt{5}\right)^{1/2}.$$

Next, as promised earlier, we return to Theorem 8.4.2(iii) concerning the golden L-surface.

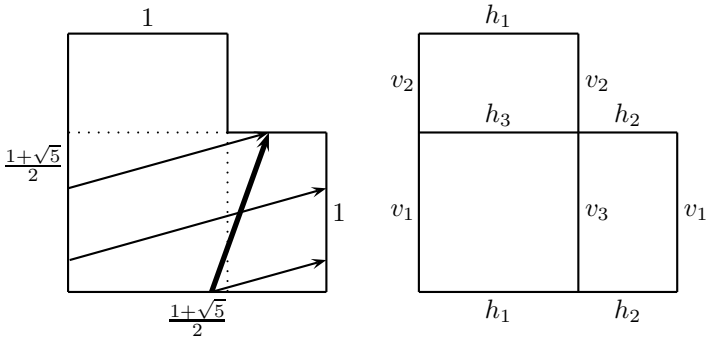

Figure 8.5.3: the golden L-surface, detour crossing and shortcut

As in Section 8.2, we shall apply the eigenvalue-based shortline method to compute the irregularity exponent for geodesic flow on this surface.

What makes the golden L-surface particularly simple is that its two horizontal streets are similar rectangles, and its two vertical streets are also similar rectangles; see Figure 8.5.3.

To apply the surplus shortline method, we consider slopes of the special form

$$\alpha = \frac{1+\sqrt{5}}{2}a_0 + \frac{1}{\frac{1+\sqrt{5}}{2}a_1 + \frac{1}{\frac{1+\sqrt{5}}{2}a_2+\cdots}}, \tag{8.5.5}$$

where $a_i \geqslant 1$, $i \geqslant 0$, are integers. Furthermore, to determine the irregularity exponent explicitly, we need eventual periodicity of the sequence $a_0, a_1, a_2, \ldots$.

The golden L-surface has 3 faces.

The almost vertical units $h_1h_2, h_1h_3, h_2h_2, h_2h_3, h_3h_1, h_3h_1^*$ can be defined in the same way as shown in Figure 7.1.6.

The almost horizontal units $v_1v_2, v_1v_3, v_2v_2, v_2v_3, v_3v_1, v_3v_1^*$ can be defined in a similar way.

The picture on the left in Figure 8.5.3 illustrates an almost horizontal detour crossing of a horizontal street and its almost vertical shortcut h_1h_2 in the special case when the branching parameter is equal to 2. Using the Delete-End Rule, for a general branching parameter $k \geqslant 1$, the ancestor process can be summarized by

$$h_1h_2 \rightharpoonup v_2v_3, k \times v_3v_1, k \times v_1v_3, \tag{8.5.6}$$

$$h_1h_3 \rightharpoonup v_2v_3, k \times v_3v_1, (k-1) \times v_1v_3, \tag{8.5.7}$$

$$h_2h_2 \rightharpoonup v_3v_1^*, k \times v_1v_3, (k-1) \times v_3v_1, \tag{8.5.8}$$

$$h_2h_3 \rightharpoonup v_3v_1^*, k \times v_1v_3, k \times v_3v_1, \tag{8.5.9}$$

$$h_3h_1 \rightharpoonup v_1v_2, (k-1) \times v_2v_2, \tag{8.5.10}$$

$$h_3h_1^* \rightharpoonup v_1v_2, k \times v_2v_2. \tag{8.5.11}$$

These lead to a 6×6 transition matrix

$$M(k) = \begin{array}{c} \\ h_1h_2 \\ h_1h_3 \\ h_2h_2 \\ h_2h_3 \\ h_3h_1 \\ h_3h_1^* \end{array} \begin{array}{c} \begin{array}{cccccc} v_1v_2 & v_1v_3 & v_2v_2 & v_2v_3 & v_3v_1 & v_3v_1^* \end{array} \\ \begin{pmatrix} 0 & k & 0 & 1 & k & 0 \\ 0 & k-1 & 0 & 1 & k & 0 \\ 0 & k & 0 & 0 & k-1 & 1 \\ 0 & k & 0 & 0 & k & 1 \\ 1 & 0 & k-1 & 0 & 0 & 0 \\ 1 & 0 & k & 0 & 0 & 0 \end{pmatrix} \end{array}.$$

Similarly, we can study the ancestor relation of each of the almost horizontal units, again using the Delete-End Rule, and obtain the analogs of (8.5.6)–(8.5.11). These will lead to another 6 transition matrix. Since we have listed the almost vertical units and almost horizontal units in lexicographical order, these two 6×6 transition matrices are the same.

The eigenvalues of $M(k)$ are two pairs of algebraic conjugates

$$\frac{1+\sqrt{5}}{4}k \pm \left(\left(\frac{1+\sqrt{5}}{4}k\right)^2 + 1\right)^{1/2},$$

$$\frac{1-\sqrt{5}}{4}k \pm \left(\left(\frac{1-\sqrt{5}}{4}k\right)^2 + 1\right)^{1/2},$$

and $(-1 \pm \sqrt{3}\mathrm{i})/2$ having absolute value 1. Of these, the eigenvalue with the largest absolute value is

$$\Lambda = \frac{1+\sqrt{5}}{4}k + \left(\left(\frac{1+\sqrt{5}}{4}k\right)^2 + 1\right)^{1/2} = \frac{1+\sqrt{5}}{2}k + \frac{1}{\frac{1+\sqrt{5}}{2}k + \frac{1}{\frac{1+\sqrt{5}}{2}k+\cdots}},$$

i.e., Λ is equal to the slope α in (8.5.5) in the special case $a_i = k$ for all $i \geqslant 0$. The eigenvalue with the second largest absolute value is

$$\lambda = \frac{1-\sqrt{5}}{4}k - \left(\left(\frac{1-\sqrt{5}}{4}k\right)^2 + 1\right)^{1/2}.$$

The remaining 4 eigenvalues are irrelevant.

We shall show that the transition matrix $M(k)$ has a conjugate with the form

$$P^{-1}M(k)P = \begin{pmatrix} T & ? \\ 0 & A(k) \end{pmatrix}, \tag{8.5.12}$$

where

$$T = \begin{pmatrix} \frac{-1-\sqrt{3}\mathrm{i}}{2} & ? \\ 0 & \frac{-1+\sqrt{3}\mathrm{i}}{2} \end{pmatrix}, \tag{8.5.13}$$

and

$$A(k) = \begin{pmatrix} \frac{(1+\sqrt{5})k}{2} & 1 & ? & ? \\ 1 & 0 & ? & ? \\ 0 & 0 & \frac{(1-\sqrt{5})k}{2} & 1 \\ 0 & 0 & 1 & 0 \end{pmatrix}. \tag{8.5.14}$$

The description of the matrix $M(k)$ by (8.5.12)–(8.5.14) is extremely convenient. It reduces the necessary eigenvalue computation of arbitrary products

$$\prod_{i=1}^{r} M(k_i)$$

of 6×6 matrices with different values of the branching parameter k_i to the much simpler eigenvalue computation of products

$$\prod_{i=1}^{r} \begin{pmatrix} \frac{(1+\sqrt{5})k_i}{2} & 1 \\ 1 & 0 \end{pmatrix} \quad \text{and} \quad \prod_{i=1}^{r} \begin{pmatrix} \frac{(1-\sqrt{5})k_i}{2} & 1 \\ 1 & 0 \end{pmatrix}$$

of 2×2 matrices, as the remaining eigenvalues $(-1 \pm \sqrt{3}\mathrm{i})/2$ are irrelevant.

We now outline the routine deduction of (8.5.12)–(8.5.14).

We first make use of the fact that $M(k)$ has 2 eigenvectors that are independent of the branching parameter k. Together with the eigenvalues, they are

$$\lambda_1 = \frac{-1-\sqrt{3}\mathrm{i}}{2}, \quad \mathbf{v}_1 = \left(\frac{-1-\sqrt{3}\mathrm{i}}{2}, -1, 0, \frac{-1+\sqrt{3}\mathrm{i}}{2}, 1, 1\right)^T,$$

$$\lambda_2 = \frac{-1+\sqrt{3}\mathrm{i}}{2}, \quad \mathbf{v}_2 = \left(\frac{-1+\sqrt{3}\mathrm{i}}{2}, -1, 0, \frac{-1-\sqrt{3}\mathrm{i}}{2}, 1, 1\right)^T.$$

This allows us to use a "partial diagonalization" trick first discussed in Lemma 4.1.1 in [3]. Let Q be a 6×6 invertible matrix such that the first 2 columns are $\mathbf{v}_1, \mathbf{v}_2$, and where the remaining columns are

$$\mathbf{v}_3 = (1, 0, -1, -1, -1, 0)^T,$$
$$\mathbf{v}_4 = (0, 1, 1, -1, 1, 0)^T,$$
$$\mathbf{v}_5 = (0, 0, 0, 0, 0, -1)^T,$$
$$\mathbf{v}_6 = (-1, 1, 1, 1, 0, 0)^T.$$

Then

$$Q^{-1}M(k)Q = \begin{pmatrix} T & ? \\ 0 & M_4(k) \end{pmatrix}, \tag{8.5.15}$$

where

$$M_4(k) = \begin{pmatrix} 3k-1 & 2-5k & 1 & 1-3k \\ -k & k-2 & 1 & k-2 \\ 4k & 3-6k & 0 & 2-4k \\ 3k & 3-4k & -1 & 3-3k \end{pmatrix}. \tag{8.5.16}$$

Let R be a 4×4 auxiliary matrix such that its first two columns are

$$\mathbf{w}_1 = \left(\frac{\sqrt{5}+1}{2}, \frac{\sqrt{5}-3}{2}, 2, \frac{5-\sqrt{5}}{2} \right),$$

$$\mathbf{w}_2 = \left(1, 0, \frac{\sqrt{5}+1}{2}, 1 \right).$$

Routine calculation shows that if R is invertible, then independently of the choice of its third and fourth columns, the conjugate $R^{-1}M_1(k)R$ has the simpler triangular form

$$R^{-1}M_4(k)R = \begin{pmatrix} A_1(k) & ? \\ 0 & A_2(k) \end{pmatrix}, \tag{8.5.17}$$

where

$$A_1(k) = \begin{pmatrix} \frac{(1+\sqrt{5})k}{2} & 1 \\ 1 & 0 \end{pmatrix}, \tag{8.5.18}$$

and $A_2(k)$ is a 2×2 matrix that depends on the third and fourth columns of R. Again with some routine calculation we can find suitable third and fourth columns of R which give

$$A_2(k) = \begin{pmatrix} \frac{(1-\sqrt{5})k}{2} & 1 \\ 1 & 0 \end{pmatrix}. \tag{8.5.19}$$

Clearly (8.5.12)–(8.5.14) follow on combining (8.5.15)–(8.5.19).

Consider now a geodesic on the golden L-surface with slope α of the form (8.5.5), where the sequence $a_i \geqslant 1$, $i \geqslant 0$, of integers is eventually periodic. Then the shortline of this geodesic has slope α_1^{-1}, where

$$\alpha_1 = \frac{1+\sqrt{5}}{2}a_1 + \frac{1}{\frac{1+\sqrt{5}}{2}a_2 + \frac{1}{\frac{1+\sqrt{5}}{2}a_3 + \cdots}},$$

and the shortline of this shortline has slope

$$\alpha_2 = \frac{1+\sqrt{5}}{2}a_2 + \frac{1}{\frac{1+\sqrt{5}}{2}a_3 + \frac{1}{\frac{1+\sqrt{5}}{2}a_4 + \cdots}},$$

and so on.

Theorem 8.5.1. (i) *Consider geodesic flow on the golden L-surface with slope α given by* (8.5.5). *If the sequence $a_0, a_1, a_2, \ldots$ has period $k_1, k_2, \ldots, k_r$ eventually, then the irregularity exponent of the geodesic with slope α is equal to*

$$\frac{\log|\lambda|}{\log|\Lambda|},$$

where λ is the eigenvalue with the larger absolute value of the product matrix

$$\prod_{i=1}^{r} \begin{pmatrix} \frac{(1-\sqrt{5})k_i}{2} & 1 \\ 1 & 0 \end{pmatrix}, \tag{8.5.20}$$

and Λ is the eigenvalue with the larger absolute value of the product matrix

$$\prod_{i=1}^{r} \begin{pmatrix} \frac{(1+\sqrt{5})k_i}{2} & 1 \\ 1 & 0 \end{pmatrix}. \tag{8.5.21}$$

Alternatively, we have the product formula

$$\Lambda = \prod_{i=1}^{r} \beta_i,$$

where for every $i = 1, \dots, r$,

$$\beta_i = \frac{1+\sqrt{5}}{2} k_i + \frac{1}{\frac{1+\sqrt{5}}{2} k_{i+1} + \frac{1}{\frac{1+\sqrt{5}}{2} k_{i+2} + \cdots}},$$

corresponding to the periodic sequence

$$k_i, k_{i+1}, k_{i+2}, \dots, k_r, k_1, k_2, \dots, k_r, \dots.$$

(ii) *Similarly, for every street-rational polyrectangle surface there are infinitely many explicit slopes for which any geodesic with such a slope exhibits superdensity, and we can also compute the corresponding irregularity exponent.*

(iii) *Combining the irregularity exponent with the method of zigzagging introduced in Section 3.3 in* [2]*, we can also describe, for any geodesic and special slopes in parts* (i) *and* (ii)*, the time-quantitative behavior of the edge-cutting and face-crossing numbers, as well as equidistribution relative to all convex sets.*

For the golden L-surface, let us now calculate the eigenvalues of 2-step transition matrix M by first finding the street-spreading matrix for the slope α given by (8.5.5) with $a_i = 1$ for every $i \geqslant 0$. We shall follow the notation in Section 7.2, and the details are shown in Figure 8.5.4.

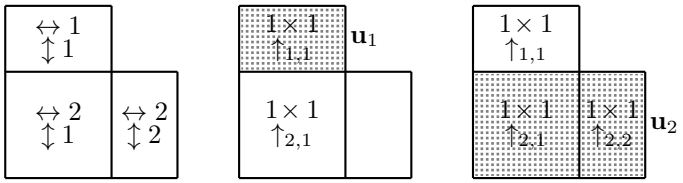

Figure 8.5.4: almost vertical units of type ↑ in $\mathbf{u}_1, \mathbf{u}_2$

Consider the horizontal street corresponding to $\mathbf{u}_1$, as highlighted in the picture in the middle in Figure 8.5.4. Using (7.2.17), we have

$$\begin{aligned} (M-I)\mathbf{u}_1 &= (M-I)[\{\uparrow_{1,1}\}] + (M-I)[\{\uparrow_{2,1}\}] \\ &= (\mathbf{u}_1 + \mathbf{v}_1) + (\mathbf{u}_2 + \mathbf{v}_2). \end{aligned} \tag{8.5.22}$$

For the horizontal street corresponding to $\mathbf{u}_2$, as highlighted in the picture on the right in Figure 8.5.4, a similar argument gives

$$\begin{aligned} (M-I)\mathbf{u}_2 &= (M-I)[\{\uparrow_{1,1}\}] + (M-I)[\{\uparrow_{2,1}, \uparrow_{2,2}\}] \\ &= (\mathbf{u}_1 + \mathbf{v}_1) + 2(\mathbf{u}_2 + \mathbf{v}_2). \end{aligned} \tag{8.5.23}$$

It follows from (8.5.22)–(8.5.23) that the street-spreading matrix is given by

$$\mathbf{S} = \begin{pmatrix} 1 & 1 \\ 1 & 2 \end{pmatrix},$$

with eigenvalues

$$\tau_1 = \frac{3+\sqrt{5}}{2} \quad \text{and} \quad \tau_2 = \frac{3-\sqrt{5}}{2}.$$

Using (7.2.38), the corresponding eigenvalues of M are

$$\lambda\left(\frac{3+\sqrt{5}}{2};\pm\right)=\frac{7+\sqrt{5}}{4}\pm\frac{1}{2}\left(\left(\frac{3+\sqrt{5}}{2}\right)^2+4\left(\frac{3+\sqrt{5}}{2}\right)\right)^{1/2}$$

and

$$\lambda\left(\frac{3-\sqrt{5}}{2};\pm\right)=\frac{7-\sqrt{5}}{4}\pm\frac{1}{2}\left(\left(\frac{3-\sqrt{5}}{2}\right)^2+4\left(\frac{3-\sqrt{5}}{2}\right)\right)^{1/2}.$$

The two largest eigenvalues are therefore

$$\lambda_1=\frac{7+\sqrt{5}}{4}+\frac{1}{2}\left(\left(\frac{3+\sqrt{5}}{2}\right)^2+4\left(\frac{3+\sqrt{5}}{2}\right)\right)^{1/2}$$

and

$$\lambda_2=\frac{7-\sqrt{5}}{4}+\frac{1}{2}\left(\left(\frac{3-\sqrt{5}}{2}\right)^2+4\left(\frac{3-\sqrt{5}}{2}\right)\right)^{1/2}.$$

For the corresponding 1-step transition matrix, we shall determine the eigenvalues Λ and λ by using (8.5.20) and (8.5.21) with $r=1$ and $k_1=1$. The eigenvalue with the larger absolute value of the matrices

$$\begin{pmatrix}\frac{1+\sqrt{5}}{2} & 1\\ 1 & 0\end{pmatrix}\quad\text{and}\quad\begin{pmatrix}\frac{1-\sqrt{5}}{2} & 1\\ 1 & 0\end{pmatrix}$$

are respectively

$$\Lambda=\frac{1+\sqrt{5}}{4}+\frac{1}{2}\left(\left(\frac{1+\sqrt{5}}{2}\right)^2+4\right)^{1/2}$$

and

$$\lambda=\frac{1-\sqrt{5}}{4}+\frac{1}{2}\left(\left(\frac{1-\sqrt{5}}{2}\right)^2+4\right)^{1/2}.$$

Note that $\lambda_1=\Lambda^2$ and $\lambda_2=\lambda^2$.

We complete this section by calculating the eigenvalues of the 2-step transition matrix M for the "golden brick", first introduced at the end of Section 8.4, for a geodesic with a suitable slope.

For the 4-copy surface of the golden brick, note that the streets of width 1 has length $2+2h$, and so normalized length $2+2h$, while the streets of width h has length 4, and so normalized length

$$\frac{4}{h}=2(2+2h),$$

so that $h^*=v^*=2(2+2h)$.

To visualize the 4-copy version of the golden brick, we refer the reader to Figures 7.2.12–7.2.14 which illustrate the 4-copy version of the surface of the unit cube. We obtain the 4-copy version of the golden brick if we shorten the edges a_1, a_2, a_3, a_4, and those in between, in Figure 7.2.12 from length 1 to length h. Then the horizontal streets $3, 6$ and vertical streets $2, 6$ in Figure 7.2.13 still have length 4 but now have width h instead of 1, and we can obtain an analog of Figure 7.2.14 with thinner rows $3, 6$ and columns $2, 6$.

For simplicity, we consider a geodesic with slope

$$\alpha = 2(2+2h) + \frac{1}{2(2+2h) + \frac{1}{2(2+2h)+\frac{1}{2(2+2h)+\cdots}}}.$$

As before, we define the matrices $\mathbf{u}_i, \mathbf{v}_i$, $i = 1, \ldots, 6$, according to (7.2.14) and (7.2.15).

Figures 8.5.5–8.5.7 below are the analogs of Figures 7.2.15–7.2.16 for the surface of the cube.

For the horizontal streets corresponding to $\mathbf{u}_1, \mathbf{u}_4$, as highlighted in Figure 8.5.5, we have, applying (7.2.17),

$$\begin{aligned}
(M-I)\mathbf{u}_1 &= (M-I)\mathbf{u}_4 \\
&= (M-I)[\{2\uparrow_{1,2}, 4\uparrow_{1,3}, 4\uparrow_{1,5}, 2\uparrow_{1,6}\}] + (M-I)[\{2\uparrow_{2,2}, 2\uparrow_{2,6}\}] \\
&\quad + (M-I)[\{4\uparrow_{3,3}, 4\uparrow_{3,5}\}] + (M-I)[\{2\uparrow_{4,2}, 4\uparrow_{4,3}, 4\uparrow_{4,5}, 2\uparrow_{4,6}\}] \\
&\quad + (M-I)[\{2\uparrow_{5,2}, 2\uparrow_{5,6}\}] + (M-I)[\{4\uparrow_{6,3}, 4\uparrow_{6,5}\}] \\
&= 12(\mathbf{u}_1+\mathbf{v}_1) + 4(\mathbf{u}_2+\mathbf{v}_2) + 8(\mathbf{u}_3+\mathbf{v}_3) \\
&\quad + 12(\mathbf{u}_4+\mathbf{v}_4) + 4(\mathbf{u}_5+\mathbf{v}_5) + 8(\mathbf{u}_6+\mathbf{v}_6). \qquad (8.5.24)
\end{aligned}$$

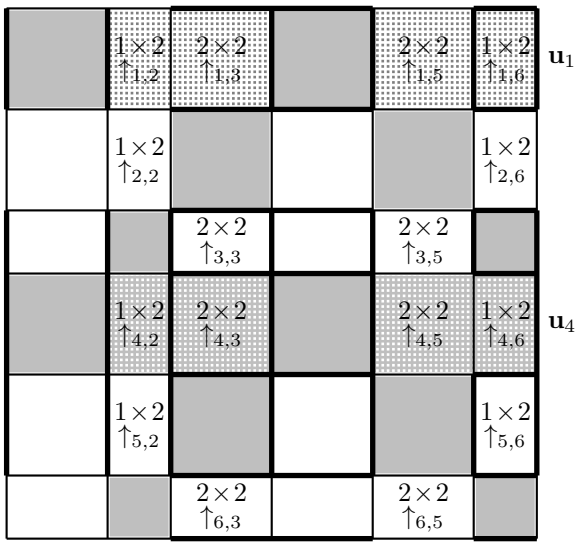

Figure 8.5.5: almost vertical units of type ↑ in $\mathbf{u}_1, \mathbf{u}_4$

For the horizontal streets corresponding to $\mathbf{u}_2, \mathbf{u}_5$, as highlighted in Figure 8.5.6, a similar argument gives

$$\begin{aligned}
(M-I)\mathbf{u}_2 &= (M-I)\mathbf{u}_5 \\
&= 4(\mathbf{u}_1+\mathbf{v}_1) + 12(\mathbf{u}_2+\mathbf{v}_2) + 8(\mathbf{u}_3+\mathbf{v}_3) \\
&\quad + 4(\mathbf{u}_4+\mathbf{v}_4) + 12(\mathbf{u}_5+\mathbf{v}_5) + 8(\mathbf{u}_6+\mathbf{v}_6). \qquad (8.5.25)
\end{aligned}$$

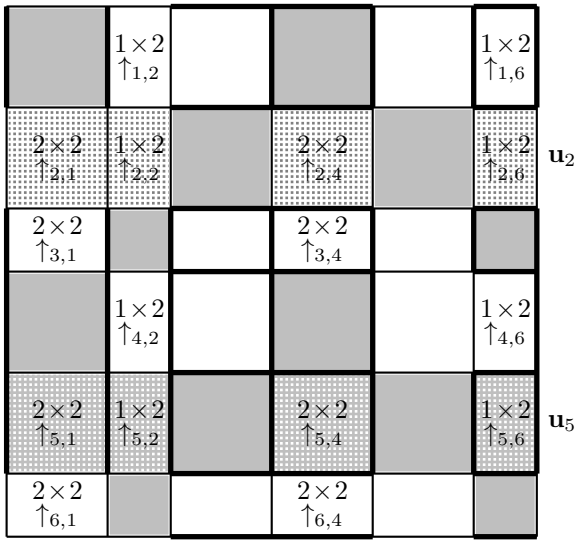

Figure 8.5.6: almost vertical units of type ↑ in $\mathbf{u}_2, \mathbf{u}_5$

For the horizontal streets corresponding to $\mathbf{u}_3, \mathbf{u}_6$, as highlighted in Figure 8.5.7, a similar argument gives

$$\begin{aligned}(M-I)\mathbf{u}_3 &= (M-I)\mathbf{u}_6 \\ &= 4(\mathbf{u}_1+\mathbf{v}_1)+4(\mathbf{u}_2+\mathbf{v}_2)+8(\mathbf{u}_3+\mathbf{v}_3) \\ &\quad +4(\mathbf{u}_4+\mathbf{v}_4)+4(\mathbf{u}_5+\mathbf{v}_5)+8(\mathbf{u}_6+\mathbf{v}_6). \end{aligned} \tag{8.5.26}$$

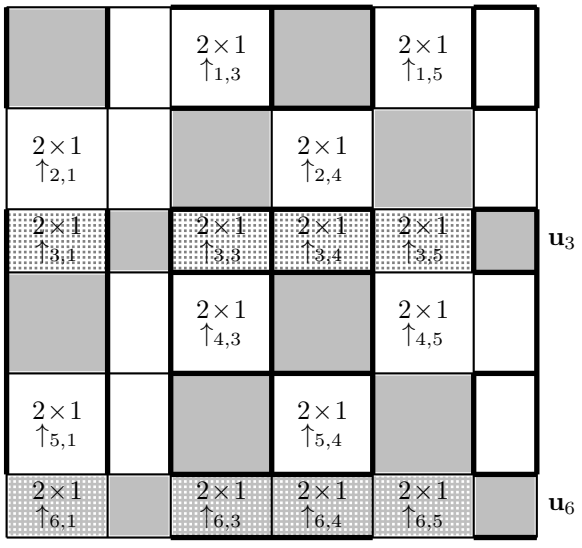

Figure 8.5.7: almost vertical units of type ↑ in $\mathbf{u}_3, \mathbf{u}_6$

It follows from (8.5.24)–(8.5.26) that the street-spreading matrix is given by

$$\mathbf{S} = \begin{pmatrix} 12 & 4 & 4 & 12 & 4 & 4 \\ 4 & 12 & 4 & 4 & 12 & 4 \\ 8 & 8 & 8 & 8 & 8 & 8 \\ 12 & 4 & 4 & 12 & 4 & 4 \\ 4 & 12 & 4 & 4 & 12 & 4 \\ 8 & 8 & 8 & 8 & 8 & 8 \end{pmatrix},$$

with non-zero eigenvalues $\tau_1 = 24+8\sqrt{5}$, $\tau_2 = 16$ and $\tau_3 = 24-8\sqrt{5}$. Using (7.2.38), the corresponding eigenvalues of M are

$$\begin{aligned}\lambda(24+8\sqrt{5};\pm) &= 13+4\sqrt{5} \pm \left(248+104\sqrt{5}\right)^{1/2},\\ \lambda(16;\pm) &= 9 \pm 4\sqrt{5},\\ \lambda(24-8\sqrt{5};\pm) &= 13-4\sqrt{5} \pm \left(248-104\sqrt{5}\right)^{1/2}.\end{aligned}$$

8.6. **Surfaces tiled with congruent equilateral triangles.** We wish to complete our study of geodesic flow on the surface of each of the 5 platonic solids.

We have already discussed in [2] the superdensity of geodesic flow on the regular tetrahedron surface which is integrable. Earlier in this paper, we have also discussed the superdensity of geodesic flow on the cube surface and the regular dodacahedron surface which are non-integrable.

The last two examples of the 5 platonic solids are the regular octahedron and the regular icosahedron. Both of these surfaces belong to the large class of flat surfaces where the faces are congruent equilateral triangles. We refer to such a surface as a *polytriangle surface*. Every polytriangle surface has the crucial property that the union of any two equilateral triangle faces sharing an edge forms a 60-degree rhombus, which turns out to be a perfect substitute for squares. Thus polytriangle surfaces are perfect analogs of polysquare surfaces, and both versions of the shortline method work for this class.

We give here a detailed discussion of geodesic flow on the regular octahedron surface, as shown in Figure 8.6.1. Geodesic flow on the icosahedron surface goes in a similar way, and we omit it.

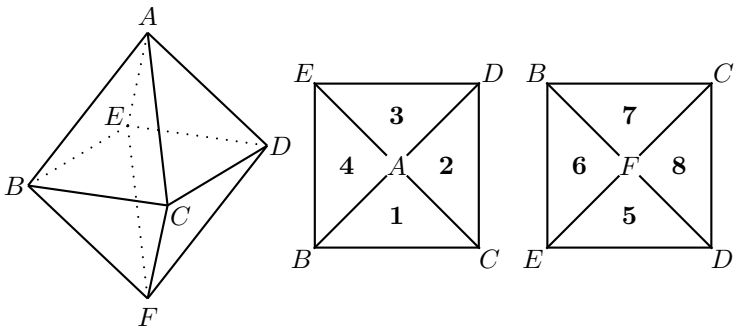

Figure 8.6.1: the regular octahedron, top view and bottom view

For our convenience, we shall label the faces as in Figure 8.6.1. Thus we have face and vertex pairings given by

$$\begin{aligned}&(\mathbf{1}, ABC), \quad (\mathbf{2}, ACD), \quad (\mathbf{3}, ADE), \quad (\mathbf{4}, AEB),\\ &(\mathbf{5}, FED), \quad (\mathbf{6}, FBE), \quad (\mathbf{7}, FCB), \quad (\mathbf{8}, FDC),\end{aligned}$$

where the three vertices of each triangle face are given in anticlockwise order. Note that we have four pairs of vertex-disjoint and parallel faces, given by

$$(\mathbf{1},\mathbf{5}), \quad (\mathbf{2},\mathbf{6}), \quad (\mathbf{3},\mathbf{7}), \quad (\mathbf{4},\mathbf{8}).$$

Between any vertex-disjoint pair of faces we have a *street* made up of 6 triangle faces. In Figure 8.6.2, we show 4 different nets of the regular octahedron, together with a surplus detour crossing of a geodesic in a given direction.

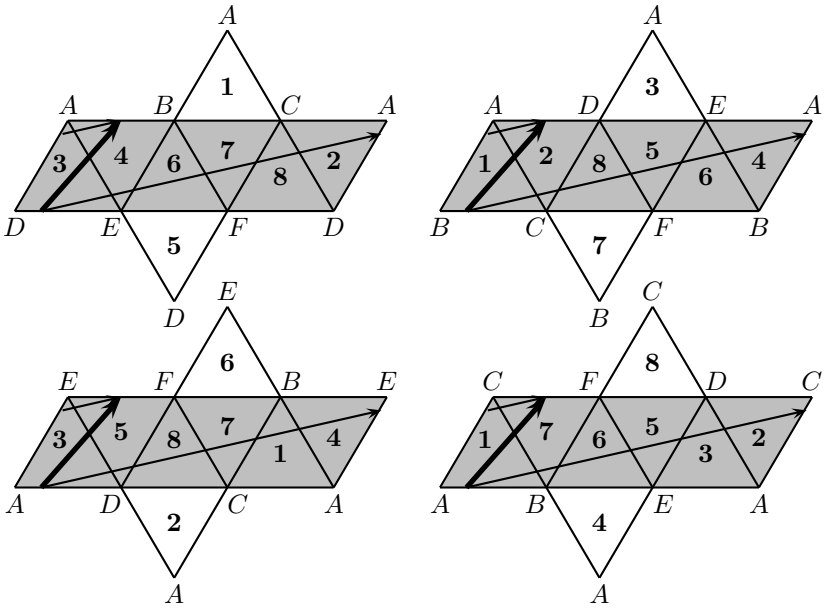

Figure 8.6.2: nets of the regular octagon surface, detour crossings and shortcuts

The picture on the top left of Figure 8.6.2 is a net of the regular octahedron surface. The long parallelogram in the middle is a street between faces **1** and **5**. More precisely, the cycle of triangle faces $\mathbf{3}, \mathbf{4}, \mathbf{6}, \mathbf{7}, \mathbf{8}, \mathbf{2}$ is the street, with the left and right edges of the parallelogram identified. This street also has a natural decomposition into 60-degree rhombi formed from the union of the pairs $(\mathbf{3}, \mathbf{4})$, $(\mathbf{6}, \mathbf{7})$ and $(\mathbf{8}, \mathbf{2})$.

The detour crossings in all 4 different nets can be thought of as all going in the same direction. The copies on the top left and bottom right have parallel edges AB, while the copies on the top right and bottom left have parallel edges AD. On the other hand, the two copies on the left have parallel edges CA, while the two copies on the right have parallel edges EA.

Note that each shaded triangle in Figure 8.6.2 has 2 more copies of itself rotated by 120 degrees and 240 degrees. We therefore conclude that a geodesic crosses every triangle face in 3 different directions, at 120 degrees to each other. Note also that every triangle face is complemented by 3 other triangle faces to form 60-degree rhombi. For instance, for the triangle face **3**, we have the pair $(\mathbf{3}, \mathbf{4})$ in the top left, the pair $(\mathbf{3}, \mathbf{5})$ in the bottom left, and the pair $(\mathbf{3}, \mathbf{2})$ in the bottom right.

Since a 60-degree rhombus is just a tilted analog of a square, and can be viewed as one, it is straightforward to adapt the shortline method. To obtain some special slopes, we consider the analogy illustrated in Figure 8.6.3.

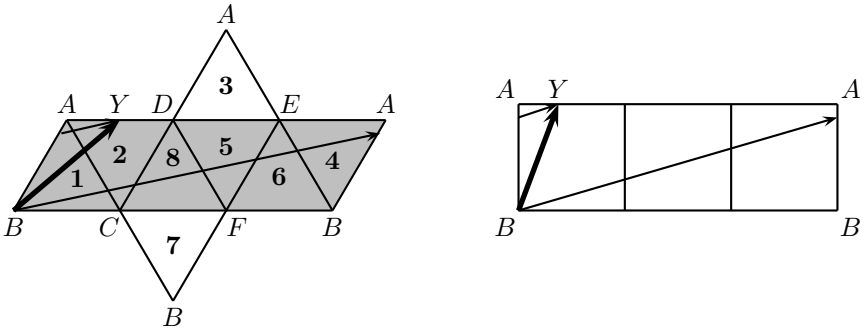

Figure 8.6.3: a particular geodesic and mutual shortlines

For the polysquare model in the picture on the right, it is clear that we consider an almost horizontal geodesic of slope α_k^{-1}, where

$$\alpha_k = [3k; 3k, 3k, 3k, \ldots] = \frac{\sqrt{9k^2+4}+3k}{2}. \tag{8.6.1}$$

Then the shortline has slope α_k. Returning to the original polytriangle surface, a suitable angle corresponding to α_k can be determined. In particular, if the length of the edge DE is equal to 1, then the length of the segment AY should be equal to α_k^{-1}. Elementary calculation shows that the detour crossing in the picture on the left in Figure 8.6.3 must have slope

$$\beta_k^{-1} = \frac{\sqrt{3}}{2\alpha_k + 1}, \tag{8.6.2}$$

which is $\sqrt{3}$ times a quadratic irrational.

Indeed, the case of the regular octahedron surface illustrates very well the whole class of polytriangle surfaces.

We next turn our attention to 60-degree rhombus billiard. We use the same idea as for the regular octagon billiard and regular pentagon billiard. We join up rhombi in such a way that neighboring rhombi are reflections of each other, and end up with a double ring of 6 rhombi, as shown in Figure 8.6.4. It is a double ring, as the third rhombus does not join up with the first, due to the edges a_1 and b_2 having different directions. This is sometimes known as the translation surface for 60-degree rhombus billiard. Note that the edge labellings in Figure 8.6.4 are obtained by following the convention discussed in the Remark after Figure 8.3.3. Identifying the boundary edges $a_1, b_2, b, c_1, c_2, c_3, d_1, d_2, d_3$, we obtain a polytriangle surface, which is intuitively a "double hexagon".

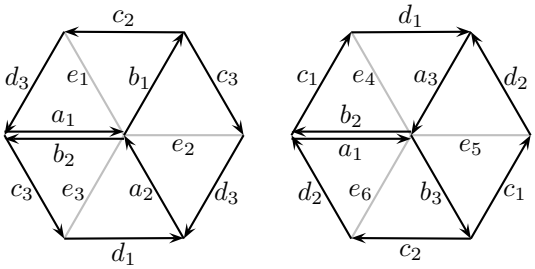

Figure 8.6.4: the translation surface of 60-degree rhombus billiard with edge labellings

Furthermore, we label the 6 rhombi as in Figure 8.6.5.

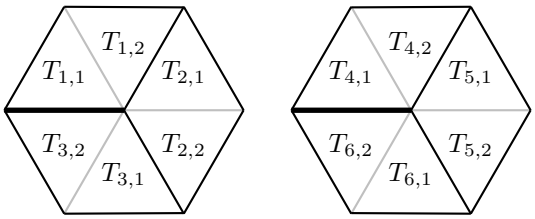

Figure 8.6.5: the faces of the translation surface of 60-degree rhombus billiard

It is not difficult to see that 60-degree rhombus billiard is equivalent to 1-direction geodesic flow on the polytriangle surface defined by the "double hexagon" shown in Figures 8.6.4 and 8.6.5. We refer to this polytriangle surface as the RB-surface, or the rhombus billiard surface.

We can list the streets of the RB-surface explicitly.

The long parallelogram in the middle of Figure 8.6.6 is a street of the RB-surface, comprising the cycle

$$T_{1,1}, T_{1,2}, T_{2,1}, T_{3,2}, T_{3,1}, T_{2,2} \tag{8.6.3}$$

of 6 equilateral triangles. The key fact is that this street has a natural decomposition into 60-degree rhombi

$$T_{1,1} \cup T_{1,2}, \quad T_{2,1} \cup T_{3,2}, \quad T_{3,1} \cup T_{2,2}.$$

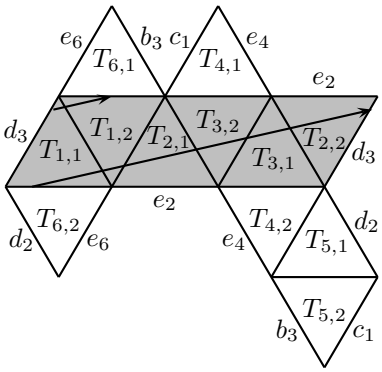

Figure 8.6.6: a net and a street with detour crossing of the RB-surface

Beside the street (8.6.3), there are 5 more streets of the RB-surface, made up of the cycles

$$T_{1,2}, T_{2,1}, T_{2,2}, T_{1,1}, T_{6,2}, T_{6,1}, \tag{8.6.4}$$

$$T_{2,1}, T_{2,2}, T_{3,1}, T_{4,2}, T_{4,1}, T_{3,2}, \tag{8.6.5}$$

$$T_{3,1}, T_{3,2}, T_{4,1}, T_{5,2}, T_{5,1}, T_{4,2}, \tag{8.6.6}$$

$$T_{4,1}, T_{4,2}, T_{5,1}, T_{6,2}, T_{6,1}, T_{5,2}, \tag{8.6.7}$$

$$T_{5,1}, T_{5,2}, T_{6,1}, T_{1,2}, T_{1,1}, T_{6,2}. \tag{8.6.8}$$

However, we only need some of these streets.

Figure 8.6.7 gives another description of the RB-surface as a polyrhombus surface.

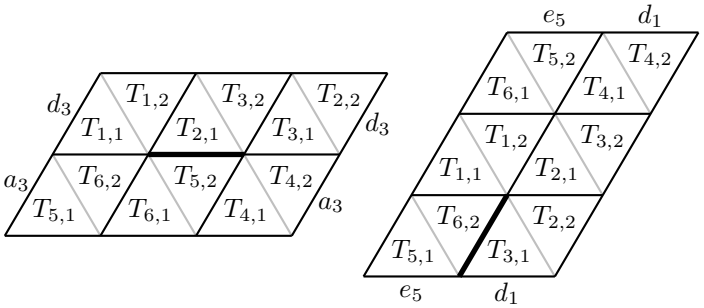

Figure 8.6.7: the RB-surface as a polyrhombus surface

In the picture on the left, we see 2 horizontal streets. The top horizontal street is (8.6.3), while the bottom horizontal street is (8.6.7). In the picture on the right, we see 2 tilted streets that are the analogs of vertical streets in polysquare surfaces. The left tilted street is (8.6.8), while the right tilted street is (8.6.5).

Noting the similarity between Figure 8.6.3 and Figure 8.6.6, we conclude that for the shortline method to work, the detour crossing in Figure 8.6.6 must have slope β_k^{-1}, given by (8.6.1) and (8.6.2).

We have the following analog of Theorem 8.5.1(ii).

Theorem 8.6.1. (i) *For any arbitrary polytriangle surface, there exist infinitely many explicit slopes, depending on the surface, such that any half-infinite geodesic with such a slope exhibits superdensity.*

(ii) *For any arbitrary table of polytriangle shape, there exist infinitely many explicit slopes, depending on the shape of the table, such that any half-infinite billiard orbit having such an initial slope exhibits superdensity.*

(iii) *For infinitely many of these slopes in parts* (i) *and* (ii) *that give rise to superdensity, we can explicitly compute the corresponding irregularity exponents which describe the time-quantitative aspects of equidistribution.*

For the RB-surface, we now attempt to find the eigenvalues of its 2-step transition matrix M. This surface can be viewed as a polyrhombus surface, and we shall use an analogy with a corresponding polysquare surface as shown in Figure 8.6.8.

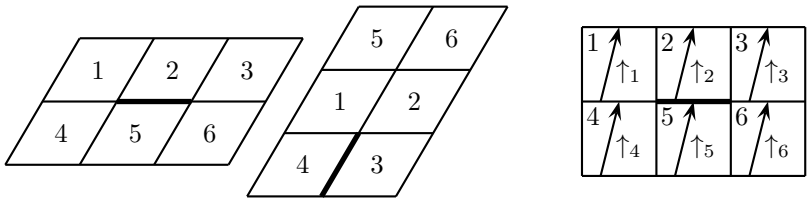

Figure 8.6.8: analogy of the double-pentagon surface with a polyrectangle surface

For simplicity of notation, the rhombi are renumbered $1, 2, 3, 4, 5, 6$, as shown in the picture on the left in Figure 8.6.8, and we consider the corresponding polysquare surface in the picture on the right. Here the horizontal streets are $1, 2, 3$ and $4, 5, 6$, while the vertical streets are $5, 1, 4$ and $6, 2, 3$. Both horizontal streets and both vertical streets have lengths 3. Note here that distinct square faces can fall into the same horizontal street and the same vertical street, so we shall adapt our notation from Section 7.2 for the determination of the street-spreading matrix.

We also show in the picture on the right in Figure 8.6.8 the almost vertical units of type $\uparrow$ in the polysquare surface. We have not shown that almost vertical units of type $\nmid$ here.

Let

$$J_1 = \{1, 2, 3\} \quad \text{and} \quad J_2 = \{4, 5, 6\}$$

denote the horizontal streets, and let

$$I_1 = I_4 = I_5 = \{1, 4, 5\} \quad \text{and} \quad I_2 = I_3 = I_6 = \{2, 3, 6\}$$

denote the vertical streets.

For the polysquare surface, we thus consider slopes of the form

$$\alpha_k = 3k + \frac{1}{3k + \frac{1}{3k+\cdots}}.$$

For simplicity, however, we consider only the special case with branching parameter $k = 1$.

Corresponding to (7.2.14), we define the column matrices

$$\mathbf{u}_1 = [\{\uparrow_s \colon j \in J_1^*, s \in I_j^*\}] \quad \text{and} \quad \mathbf{u}_2 = [\{\uparrow_s \colon j \in J_2^*, s \in I_j^*\}]. \tag{8.6.9}$$

Here J_1^*, J_2^* and I_j^* denotes that the edges are counted with multiplicity.

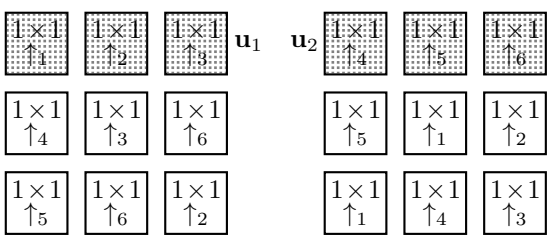

Figure 8.6.9: almost vertical units of type $\uparrow$ in $\mathbf{u}_1$ and $\mathbf{u}_2$

We also define the column matrices $\mathbf{v}_1$ and $\mathbf{v}_2$ analogous to (7.2.15), but their details are not important. Also, analogous to (7.2.17), we have

$$(M-I)[\{\uparrow_s\}] = \begin{cases} \mathbf{u}_1+\mathbf{v}_1, & \text{if } s\in J_1,\\ \mathbf{u}_2+\mathbf{v}_2, & \text{if } s\in J_2. \end{cases} \tag{8.6.10}$$

We now combine (8.6.9) and (8.6.10). For the horizontal street corresponding to $\mathbf{u}_1$, as highlighted in the picture on the left in Figure 8.6.9, we have

$$\begin{aligned}(M-I)\mathbf{u}_1 &= (M-I)[\{\uparrow_1, 2\uparrow_2, 2\uparrow_3\}] + (M-I)[\{\uparrow_4,\uparrow_5, 2\uparrow_6\}]\\ &= 5(\mathbf{u}_1+\mathbf{v}_1)+4(\mathbf{u}_2+\mathbf{v}_2).\end{aligned} \tag{8.6.11}$$

For the horizontal street corresponding to $\mathbf{u}_2$, as highlighted in the picture on the right in Figure 8.6.9, we have

$$\begin{aligned}(M-I)\mathbf{u}_2 &= (M-I)[\{2\uparrow_1,\uparrow_2,\uparrow_3\}] + (M-I)[\{2\uparrow_4, 2\uparrow_5,\uparrow_6\}]\\ &= 4(\mathbf{u}_1+\mathbf{v}_1)+5(\mathbf{u}_2+\mathbf{v}_2).\end{aligned} \tag{8.6.12}$$

It follows from (8.6.11)-(8.6.12) that the street-spreading matrix is given by

$$\mathbf{S} = \begin{pmatrix} 5 & 4\\ 4 & 5\end{pmatrix}.$$

The eigenvalues of $\mathbf{S}$ are $\tau_1 = 9$ and $\tau_2 = 1$. Using (7.2.38), the corresponding eigenvalues of M are

$$\lambda(9;\pm) = \frac{11}{2} \pm \frac{1}{2}\sqrt{117} \quad \text{and} \quad \lambda(1;\pm) = \frac{3}{2}\pm\frac{1}{2}\sqrt{5}.$$

The two largest eigenvalues are therefore

$$\lambda_1 = \frac{11}{2} + \frac{1}{2}\sqrt{117} \quad \text{and} \quad \lambda_2 = \frac{3}{2}+\frac{1}{2}\sqrt{5}.$$

We have studied geodesics and billiards on many flat surfaces, for which both versions of the shortline method work, and established many explicit slopes that yield superdensity and for which we can compute the irregularity exponents. Such surfaces include polysquares, street-rational polyrectangles and polyparallelograms which include regular polygons and L-staircases, and polytriangles. We may refer to them under the general name of *street-rational surfaces*.

8.7. **The shortline method works for all Veech surfaces, and beyond.** The title of this section summarizes Sections 8.1–8.6, that the surplus shortline method works for all Veech surfaces, providing time-quantitative results like superdensity and uniformity with explicit values of the irregularity exponents.

Note that we have not defined here the concept of *Veech surfaces*.

As motivation, consider an arbitrary polysquare surface P and 1-direction geodesic flow on it. We now consider the following two statements:

(1) The surface P has a street-rational decomposition in any arbitrary direction with rational slope.

(2) The surface P is optimal, *i.e.*, 1-direction geodesic flow on P exhibits uniform-periodic dichotomy.

Perhaps the best way to describe Veech surfaces is to say that they are translation surfaces that exhibit properties like (1) and (2). Unfortunately, the precise definition is a rather technical algebraic one, and we do not really need to know that here. The interested reader is referred to the introductory article [10].

Instead, our wish is to have a list of known examples of Veech surfaces, and some of the key properties of such surfaces. In particular, the following two properties established by Veech [17] are analogous to (1) and (2) respectively.

Theorem A. *Suppose that S is a Veech surface, and that* $\mathbf{v}$ *is an arbitrary direction such that there exists a non-empty finite geodesic segment on S that goes between two not necessarily distinct singularities. Then S has a street-rational decomposition in this direction.*

Theorem B. *Every Veech surface S is optimal, i.e.,* 1*-direction geodesic flow on S exhibits uniform-periodic dichotomy.*

Remark. Note that Veech and other authors use the term *cylinder* instead of the term *street*.

Classifying the class of Veech surfaces is a very difficult problem. Early examples are the translation surfaces of regular polygon billiards discovered by Veech, together with a few related examples. Progress has been slow, despite the effort of many. The subject is on the borderline of many fields, including ergodic theory, topology and algebraic geometry. The goal is to understand *optimal dynamics*, a time-qualitative property of the long-term behavior of orbits, and the existing methods do not seem to say anything about the time-quantitative aspects. Our goal here is to complement the time-qualitative work by making some time-quantitative statements on the long-term behavior of orbits.

Indeed, our surplus shortline method works for all Veech surfaces, and the reason is very simple. For the success of our method, we need a translation surface with street-rational decomposition in only *two* different directions, and Theorem A gives far more than that.

The class of Veech surfaces include the following:

(i) polysquare surfaces including the flat torus, and polytriangle surfaces;

(ii) translation surfaces of regular polygon billiards and some related systems such as infinitely many special triangle billiards, including the regular decagon surface and the Ward system;

(iii) Calta–McMullen L-staircases;

(iv) the class of *cathedral surfaces*;

(v) the Bouw–Möller family;

(vi) isolated triangle billiards with angles $(\pi/4, \pi/3, 5\pi/12)$, $(2\pi/9, \pi/3, 4\pi/9)$ and $(\pi/5, \pi/3, 7\pi/15)$;

(vii) and new Veech surfaces via the covering construction of some old ones.

This list is not exhaustive. There are a few more countable families of quadrilateral billiards, and so on, discovered very recently. Nevertheless, it does appear that the most elegant examples among these remain the regular polygon billiards discovered by Veech [17] in 1989.

In view of (vii) above, it suffices to know all the *primitive* Veech surfaces.

Here we do not say anything about the Ward system or the Bouw–Möller family. However, for illustration, we elaborate a little on the class of *cathedral surfaces*, first introduced by McMullen, Mukamel and Wright [15] in 2017.

Figure 8.7.1 shows two identical copies of the cathedral polygon $\mathrm{CP}(a, b)$. The polygon is symmetric across the horizontal axis, and each boundary edge either is horizontal or vertical, or has slope ± 1. The identification of boundary horizontal and vertical edges comes from perpendicular translation, while the identification of edges of slope ± 1 are indicated by the decomposition into horizontal streets $H_1, \ldots, H_5$ and the decomposition into vertical streets $V_1, \ldots, V_5$. Thus the cathedral surface is well defined. It has 5 horizontal streets and 5 vertical streets.

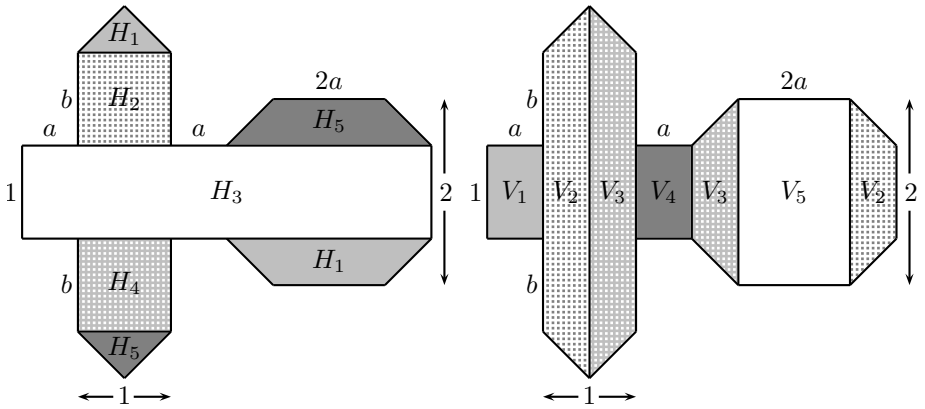

Figure 8.7.1: horizontal and vertical streets of $\mathrm{CP}(a, b)$

Let

$$a = r_1\sqrt{d} + r_2 > 0 \quad \text{and} \quad b = 3r_1\sqrt{d} - 3r_2 - \frac{3}{2} > 0, \tag{8.7.1}$$

where $d \geqslant 2$ is a square-free integer, and r_1, r_2 are rational numbers. Remarkably, as long as (8.7.1) is satisfied, geodesic flow on the cathedral surface $\mathrm{CP}(a, b)$ is optimal, as shown by McMullen, Mukamel and Wright.

We now verify that under the condition (8.7.1), the cathedral surface $\mathrm{CP}(a, b)$ is a street-rational polyrectangle surface.

Consider first the horizontal streets $H_1, \ldots, H_5$ as indicated in the picture on the left in Figure 8.7.1. Here the ratio of the (horizontal) lengths and (vertical) widths of these streets are respectively

$$\frac{1+2a}{1/2}, \quad \frac{1}{b}, \quad \frac{2+4a}{1}, \quad \frac{1}{b}, \quad \frac{1+2a}{1/2},$$

so these streets have only two different shapes, with ratio

$$2b(1+2a) = 3(2r_1\sqrt{d} - 2r_2 - 1)(2r_1\sqrt{d} + 2r_2 + 1) = 3(4r_1^2 d - (2r_2+1)^2),$$

which is clearly rational.

Consider next the vertical streets $V_1, \ldots, V_5$ as indicated in the picture on the right in Figure 8.7.1. Here the ratio of the (vertical) lengths and (horizontal) widths of these streets are respectively

$$\frac{1}{a}, \quad \frac{3+2b}{1/2}, \quad \frac{3+2b}{1/2}, \quad \frac{1}{a}, \quad \frac{2}{2a},$$

so these streets have only two different shapes, with ratio

$$2a(3+2b) = 12(r_1\sqrt{d} + r_2)(r_1\sqrt{d} - r_2) = 12(r_1^2 d - r_2^2),$$

which is also clearly rational.

Thus the surplus shortline method works for any cathedral surface $\mathrm{CP}(a, b)$ that satisfies (8.7.1). We therefore conclude that geodesic flow on such surfaces exhibits *time-qualitative* optimality, and also exhibits *time-quantitative* behavior in the sense that there are infinitely many explicit slopes such that geodesics with such slopes are superdense and we can also compute the irregularity exponents.

It is easy to see that the class of cathedral surfaces $\mathrm{CP}(a, b)$ depends only on two rational parameters $q_1 = r_1^2 d$ and r_2, so this is a 2-parameter class.

While we remain very far from the complete classification of all primitive Veech surfaces, we now know all the primitive Veech surfaces that have genus 2, through the breakthrough of McMullen [12, 13].

Theorem C. *The affine-different primitive Veech surfaces in genus* 2 *are precisely the following:*

(i) *the infinite class of Calta–McMullen L-staircases; and*

(ii) *the regular decagon surface with parallel edge identification.*

The following partial converse to Theorem B is also due to McMullen [12].

Theorem D. *Suppose that a translation surface S in genus* 2 *is not a Veech surface. Then there exist geodesics on S which are neither dense nor periodic.*

A different sort of partial converse to Theorem B is due to Cheung and Masur [8], building on the work of McMullen.

Theorem E. *Suppose that a translation surface S in genus* 2 *is not a Veech surface. Then there exist geodesics on S which are dense but not uniformly distributed.*

Recall that the surplus shortline method works for all Veech surfaces, as we need only street-rational decomposition in two different directions, while Veech surfaces exhibit street-rational decomposition in infinitely many different directions. This makes it plausible to expect that there are many surfaces that are not Veech surfaces, or not optimal, but nevertheless have sufficient street-rationality for the surplus shortline method to work, giving rise to time-quantitative results. Thus the surplus shortline method goes beyond the class of optimal systems.

We next give an example of a 3-parameter family of non-optimal systems that have sufficient street-rationality for the surplus shortline method to work. Figure 8.7.2 shows a family of decagons which are affine-different, due to the fixed height 2 and fixed width 2. These decagons are also symmetric across the horizontal axis and the vertical axis as shown. Identifying the parallel edges of every such decagon, we obtain a translation surface $S_{10}(a, b, c)$ in genus 2.

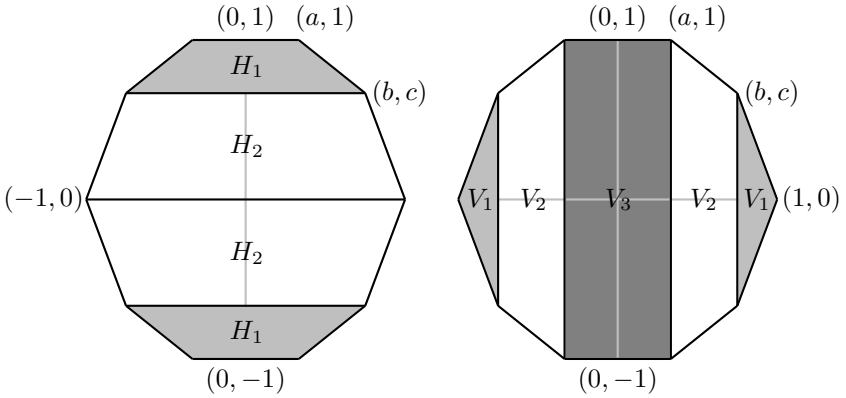

Figure 8.7.2: $S_{10}(a, b, c)$ and its horizontal and vertical streets

Note first that $S_{10}(a, b, c)$ has 2 horizontal streets H_1, H_2, as shown in the picture on the left in Figure 8.7.2. Here the ratio of the (horizontal) lengths and (vertical) widths of these streets are respectively

$$\frac{2a + 2b}{1 - c}, \quad \frac{2 + 2b}{c},$$

so we have street rationality if there exists a positive rational number r_1 such that

$$\frac{a + b}{1 - c} = r_1 \frac{1 + b}{c}. \tag{8.7.2}$$

Note next that $S_{10}(a, b, c)$ has 3 vertical streets V_1, V_2, V_3, as shown in the picture on the right in Figure 8.7.2. Here the ratio of the (vertical) lengths and (horizontal)

widths of these streets are respectively

$$\frac{2c}{1-b}, \quad \frac{2+2c}{b-a}, \quad \frac{2}{2a},$$

so we have street rationality if there exist positive rational numbers r_2, r_3 such that

$$a = r_2\frac{1-b}{c} \quad \text{and} \quad a = r_3\frac{b-a}{1+c}. \tag{8.7.3}$$

Given positive rational numbers r_1, r_2, r_3, we have 3 equations (8.7.2)–(8.7.3) in the 3 variables a, b, c. It follows that there exist infinitely many affine-different non-regular decagons $S_{10}(a, b, c)$ that have street-rational decompositions in the horizontal and vertical directions. Every one of these non-regular decagons is primitive and has genus 2, differs from the Veech surfaces listed in Theorem C, and is therefore not optimal. It then follows from Theorem D that each has geodesics which are neither dense nor periodic. It also follows from Theorem E that each has geodesics which are dense but not uniformly distributed. However, it also follows from the surplus shortline method that each has geodesics that exhibit superdensity and quantitative equidistribution with explicit irregularity exponents. These vastly different types of orbits that can arise demonstrate the intriguing fact that we have a wide spectrum of possibilities.

Unfortunately, we currently do not have analogs of Theorems C and D when the genus exceeds 2, and this prevents us from proving plausible conjectures about more infinite families of surfaces that are not optimal but have sufficient street-rationality for the surplus shortline method to work. Nevertheless, we are of the opinion that the class of surfaces that have sufficient street-rationality for the surplus shortline method to work is *much*, *much* larger than the class of surfaces with optimal dynamics.

8.8. **Density in generalized mazes.** In this section, we switch to infinite flat surfaces, and begin by generalizing the concept of *square-maze* first introduced in Section 6.5 in [4].

It is natural to start the discussion here with arguably the simplest example of generalized square-mazes, the so-called *infinite halving staircase surface* $S(\infty; 1/2)$, arising from the *infinite halving staircase region* $R(\infty; 1/2)$ shown in Figure 8.8.1.

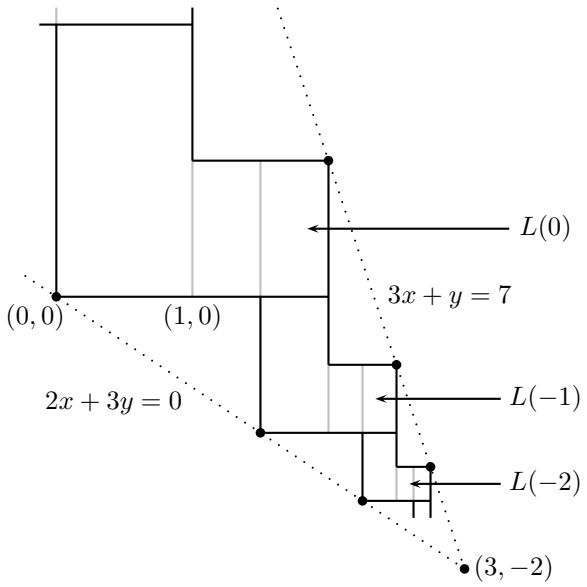

Figure 8.8.1: three halving L-shapes $L(0), L(-1), L(-2)$ of $R(\infty; 1/2)$

The building blocks of $R(\infty; 1/2)$ are L-shapes $L(n)$, $n \in \mathbb{Z}$, that consist of three squares of the same size $2^n \times 2^n$. These L-shapes of different sizes are glued together as shown. Thus

$$R(\infty; 1/2) = \bigcup_{-\infty<n<\infty} L(n).$$

For reference, we take the bottom left vertex of $L(0)$ to be the origin $(0, 0)$.

Note that as we move from $L(i)$ to $L(i+1)$, we move up and there is doubling, and that as we move from $L(i)$ to $L(i-1)$, we move down and there is halving.

Moving towards the bottom right of the staircase region $R(\infty; 1/2)$, we converge to the limit point $(3, -2)$. On the other hand, moving towards the top left of the staircase region $R(\infty; 1/2)$, we approach $(-\infty, \infty)$, and the region is bounded between the two lines $3x + y = 7$ and $2x + 3y = 0$.

To obtain the desired closed surface $S(\infty; 1/2)$ from the infinite region $R(\infty; 1/2)$, we have to identify pairs of boundary edges of $R(\infty; 1/2)$. The edge identification comes from the simplest perpendicular translation, both horizontal and vertical, as shown in Figure 8.8.2. We have indicated all the horizontal and vertical boundary edges of $L(i)$. The vertical boundary edge identification is simple, and comprises a pair of identified edges v_i' on the top square of $L(i)$ and a pair of identified edges v_i'' on the two bottom squares of $L(i)$. The horizontal edge identification is a little less straightforward. First of all, there is a pair of identified edges h_i' on the left half of the right square of $L(i)$. Then there are two further horizontal boundary edges. The edge h_i'' on the top of the right half of the right square of $L(i)$ is identified with a horizontal edge of the L-shape $L(i-1)$ below, while the edge h_{i+1}'' on the bottom of the bottom left square of $L(i)$ is identified with a horizontal edge of the L-shape $L(i+1)$ above.

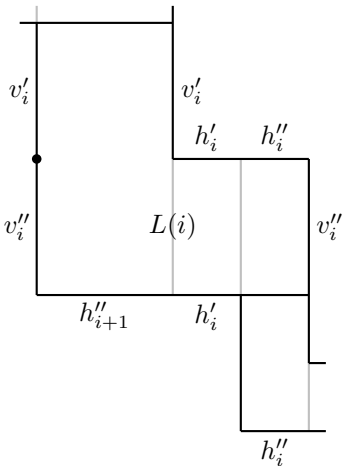

Figure 8.8.2: identifying pairs of boundary edges of $R(\infty; 1/2)$

Carrying out this boundary edge identification pattern throughout on $R(\infty; 1/2)$, we obtain a closed surface. If it is equipped with a flat metric, *i.e.*, every square has zero curvature, then it becomes the desired flat infinite closed surface $S(\infty; 1/2)$.

Recall that in a finite or infinite polysquare surface, we have building blocks that are congruent unit size squares. This property is clearly violated in $S(\infty; 1/2)$, since the building blocks can be arbitrarily large and arbitrarily small. This is why we refer to $S(\infty; 1/2)$ as a *generalized maze* – more about this later.

The infinite surface $S(\infty; 1/2)$ can be interpreted as a limit of a sequence of compact surfaces $S(n; 1/2)$, $n = 0, 1, 2, 3, \ldots$. For an arbitrary integer $n \geqslant 0$, the surface $S(n; 1/2)$ is defined by "closing" the open surface

$$\bigcup_{-n\leqslant i\leqslant n} L(i),$$

which is a union of $2n+1$ L-shapes. Here "closing" means setting up an appropriate pattern for identifying pairs of parallel boundary edges.

We illustrate the pattern in the special cases $n = 0$ and $n = 1$ in Figure 8.8.3. The general case goes in a similar way.

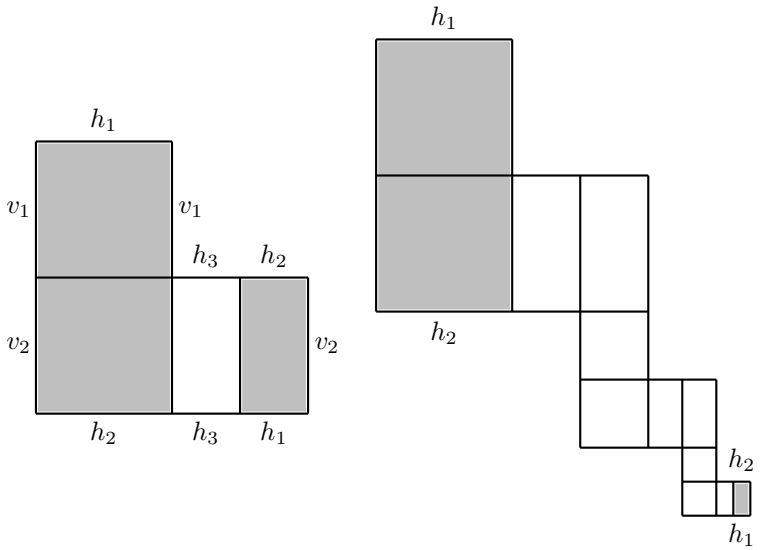

Figure 8.8.3: $S(0;1/2)$ and $S(1;1/2)$ (not to scale)

In the picture of $S(0;1/2)$ on the left, the edges v_1, v_2 and h_3 correspond respectively to v_0', v_0'' and h_0' in Figure 8.8.2. The only novelty comes from the two copies of h_1 and the two copies of h_2, as these identified edges do *not* have the same length. The edge h_1 on the left has twice the length of the edge h_1 on the right, and the edge h_2 on the left has twice the length of the edge h_2 on the right. Thus the identification comes from a translation combined with a dilation or contraction with factor 2.

In the picture of $S(1;1/2)$ on the right, we have only indicated the edge pairings h_1 and h_2. The remaining edge pairings follow the pattern set in Figure 8.8.2. Again, the pairs of edges h_1 and h_2 do not have the same length. The edge h_1 on the left has 8 times the length of the edge h_1 on the right, and the edge h_2 on the left has 8 times the length of the edge h_2 on the right. Thus the identification comes from a translation combined with a dilation or contraction with factor 8.

It is easy to see that for an arbitrary integer $n \geqslant 0$, the identification of the special edges h_1 and h_2 comes from a translation combined with a dilation or contraction with factor 2^{2n+1}.

In view of this dilation or contraction, the bounded surfaces $S(n;1/2)$, $n \geqslant 0$, fall outside of the class of polysquare surfaces. We say that $S(n;1/2)$, $n \geqslant 0$, belong to the class of *d-c-polysquare surfaces*, where *d-c* refers to the *dilation* and *contraction* of some boundary edges of the polysquare.

It is easy to see that $S(\infty;1/2)$ has infinite genus which, intuitively, represents "infinite complexity of the geodesic flow". Actually, all square-mazes have infinite genus. We have already mentioned this simple fact several times without proof. For the sake of completeness, we include here a sketch of the proof in the special case of $S(\infty;1/2)$. It is a routine application of Euler's formula, which gives

$$2 - 2g_i = V_i - E_i + R_i,$$

where g_i denotes the genus of $S(i;1/2)$, whereas V_i, E_i, R_i denote respectively the numbers of vertices, edges and regions of $S(i;1/2)$ after boundary edge identification.

Using Figure 8.8.3, we see that

$$2 - 2g_0 = V_0 - E_0 + R_0 = 2 - 8 + 4 = -2,$$
$$2 - 2g_1 = V_1 - E_1 + R_1 = 2 - 24 + 12 = -10.$$

Hence the genus of $S(0; 1/2)$ is 2, and the genus of $S(1; 1/2)$ is 6. Similarly, one can show that for an arbitrary integer $n \geqslant 0$, the genus of $S(n; 1/2)$ is $4n + 2$. Since $S(\infty; 1/2)$ is a limit of $S(n; 1/2)$ as $n \to \infty$, we conclude that $S(\infty; 1/2)$ has infinite genus.

Since $S(\infty; 1/2)$ is a flat surface, its geodesics consist of parallel straight line segments, and we have a 1-direction flow. We may call $S(0; 1/2)$, shown in the picture on the left in Figure 8.8.3, the *period-surface* of $S(\infty; 1/2)$. Clearly it is a d-c-polysquare surface.

Figure 8.8.4 shows the horizontal and vertical streets of the surface $S(\infty; 1/2)$.

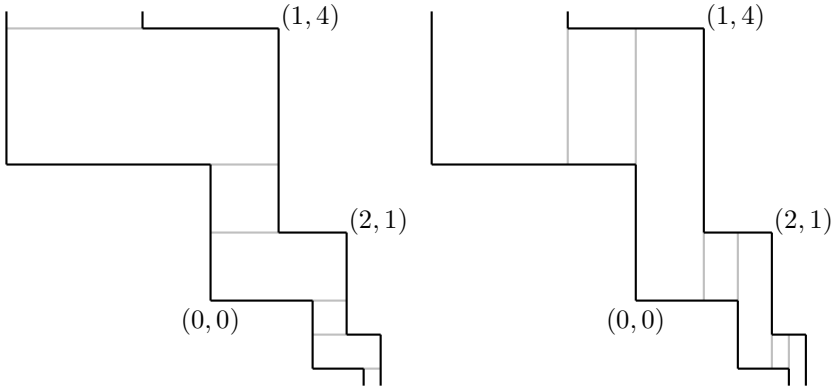

Figure 8.8.4: the horizontal and vertical streets of $S(\infty; 1/2)$

It is clear that the normalized lengths of horizontal streets are 1 and 2, while the normalized lengths of vertical streets are 2 and 4. Thus the normalized horizontal street-LCM is equal to 2, while the normalized vertical street-LCM is equal to 4.

With a view to using the surplus shortline method on $S(\infty; 1/2)$, we now focus on two particular geodesics $V_*(t)$ and $H_*(t)$ on $S(\infty; 1/2)$, shown in Figure 8.8.5.

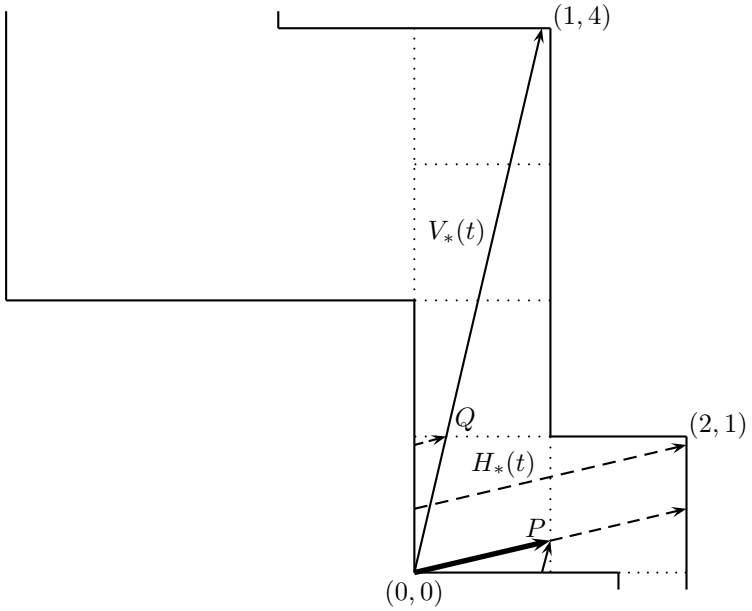

Figure 8.8.5: two particular geodesics of $S(\infty; 1/2)$

The almost vertical geodesic $V_*(t)$, $t \geqslant 0$, starts from the origin and has special slope

$$\alpha = 2 + \sqrt{5} = 4 + \frac{1}{4 + \frac{1}{4+\cdots}}, \tag{8.8.1}$$

where the continued fraction digits are all equal to 4. The almost horizontal geodesic $H_*(t)$, $t \geqslant 0$, starts from the origin and has the reciprocal slope $\alpha^{-1} = \sqrt{5} - 2$. Note that $V_*(0) = H_*(0)$ is the origin and, as usual, the parameter t denotes time; in other words, for both $V_*(t)$ and $H_*(t)$, we use the arc-length parametrization, which represents unit-speed motion of a particle. The key fact is that $V_*(t)$ and $H_*(t)$ are shortlines of each other. Indeed, the initial segment of $V_*(t)$, $t \geqslant 0$, between the origin and the point P is a detour crossing of a vertical street of 4 building block squares, and the initial segment of $H_*(t)$, $t \geqslant 0$, between the origin and the point P is the shortcut. Similarly, the initial segment of $H_*(t)$, $t \geqslant 0$, between the origin and the point Q is a detour crossing of a horizontal street of 2 building block squares, and the initial segment of $V_*(t)$, $t \geqslant 0$, between the origin and the point Q is the shortcut.

The "mutual shortcut" property of the special geodesics $V_*(t)$, $t > 0$, and $H_*(t)$, $t > 0$, means that for every vertical street of $S(\infty; 1/2)$, the detour crossing points of $V_*(t)$ coincides with the shortcut crossing points of $H_*(t)$. Similarly, for every horizontal street of $S(\infty; 1/2)$, the detour crossing points of $H_*(t)$ coincides with the shortcut crossing points of $V_*(t)$.

As a consequence of an intrinsic symmetry within $S(\infty; 1/2)$, we can easily list all the different types of shortcuts or units. While the surface $S(\infty; 1/2)$ is infinite; this symmetry makes it sufficient to distinguish only 8 different types of almost vertical shortcuts or units of slope α, where the prototypes are a_i, $1 \leqslant i \leqslant 8$, in the picture on the left in Figure 8.8.6. Similarly, it is sufficient to distinguish only 8 different types of almost horizontal shortcuts of slope α^{-1}, where the prototypes are b_j, $1 \leqslant j \leqslant 8$, in the picture on the right in Figure 8.8.6.

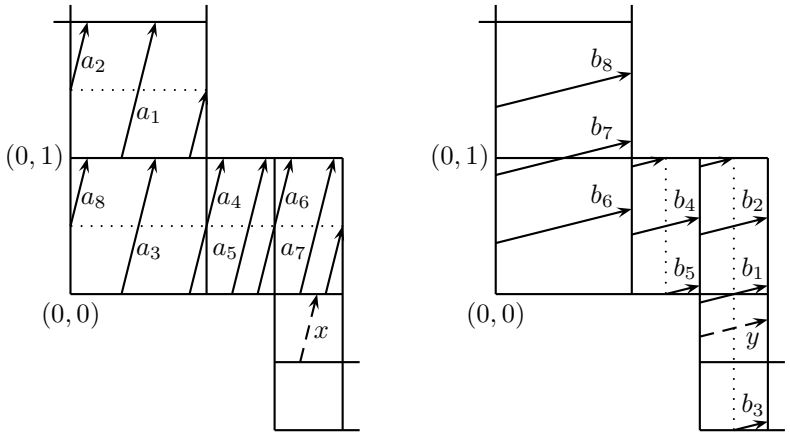

Figure 8.8.6: almost vertical and almost horizontal units of $S(\infty; 1/2)$

We recall that the infinite halving staircase region $R(\infty; 1/2)$ is built from similar L-shapes $L(i)$, $i \in \mathbb{Z}$, where $L(i+1)$ and $L(i-1)$ are respectively obtained from $L(i)$ by doubling and halving. This gives rise to a transformation $\mathbf{U}$, which represents "up and doubling", as well as an inverse transformation $\mathbf{D}$, which represents "down and halving".

Consider a prototype almost vertical unit a_1 and another almost vertical unit x in the picture on the left in Figure 8.8.6, where x is the same type of unit as a_1. The transformation $\mathbf{U}$ maps x to a_1, which we denote formally by $a_1 = \mathbf{U}x$. The transformation $\mathbf{D}$ maps a_1 to x, which we denote formally by $x = \mathbf{D}a_1$.

Consider a prototype almost horizontal unit b_8 and another almost horizontal unit y in the picture on the right in Figure 8.8.6, where y is the same type of unit as b_8. The transformation $\mathbf{U}$ maps y to b_8, which we denote formally by $b_8 = \mathbf{U}y$. The transformation $\mathbf{D}$ maps b_8 to y, which we denote formally by $y = \mathbf{D}b_8$.

There are analogs for the remaining prototypes a_i, $2 \leqslant i \leqslant 8$, and b_j, $1 \leqslant j \leqslant 7$. Moreover, we can take any power of the transformation $\mathbf{U}$, and the symmetry group of $S(\infty; 1/2)$ contains the infinite cyclic group $\{\mathbf{U}^k : k \in \mathbb{Z}\}$.

It is straightforward to determine the ancestor units of the almost vertical units a_i, $1 \leqslant i \leqslant 8$. These include a fractional unit at the beginning and a fractional unit at the end, with whole units in the middle. We have

$$a_1 \hookrightarrow \{b_7\}, 3b_8, \{\mathbf{U}b_1\}, \tag{8.8.2}$$

$$a_2 \hookrightarrow \{b_7\}, 4b_8, \{\mathbf{U}b_1\}, \tag{8.8.3}$$

$$a_3 \hookrightarrow \{\mathbf{U}b_3\}, 2b_2, 2b_4, b_6, \{b_7\}, \tag{8.8.4}$$

$$a_4 \hookrightarrow \{\mathbf{U}b_3\}, 2b_2, 2b_4, 2b_6, \{b_5\}, \tag{8.8.5}$$

$$a_5 \hookrightarrow \{b_5\}, 2b_2, b_4, 2b_6, \{b_5\}, \tag{8.8.6}$$

$$a_6 \hookrightarrow \{b_5\}, 2b_2, 2b_4, 2b_6, \{b_3\}, \tag{8.8.7}$$

$$a_7 \hookrightarrow \{b_1\}, b_2, 2b_4, 2b_6, \{b_3\}, \tag{8.8.8}$$

$$a_8 \hookrightarrow \{b_1\}, 2b_2, 2b_4, 2b_6, \{b_7\}, \tag{8.8.9}$$

where fractional units are indicated by $\{\ldots\}$, and the whole units in the middle are listed lexicographically.

We also determine the ancestor units of the almost horizontal units b_j, $1 \leqslant j \leqslant 8$. We have

$$b_1 \hookrightarrow \{\mathbf{D}a_2\}, \mathbf{D}a_1, \mathbf{D}a_3, a_7, \{a_8\}, \tag{8.8.10}$$

$$b_2 \hookrightarrow \{a_6\}, \mathbf{D}a_1, \mathbf{D}a_3, \{a_8\}, \tag{8.8.11}$$

$$b_3 \hookrightarrow \{a_6\}, \mathbf{D}a_1, \mathbf{D}a_3, a_7, \{\mathbf{D}a_2\}, \tag{8.8.12}$$

$$b_4 \hookrightarrow \{a_4\}, a_5, \{a_6\}, \tag{8.8.13}$$

$$b_5 \hookrightarrow \{a_4\}, 2a_5, \{a_6\}, \tag{8.8.14}$$

$$b_6 \hookrightarrow \{a_8\}, a_1, \mathbf{U}a_7, \{a_4\}, \tag{8.8.15}$$

$$b_7 \hookrightarrow \{a_8\}, a_1, a_3, \mathbf{U}a_7, \{a_2\}, \tag{8.8.16}$$

$$b_8 \hookrightarrow \{a_2\}, a_3, \mathbf{U}a_7, \{a_2\}. \tag{8.8.17}$$

The symmetry group of $S(\infty; 1/2)$ contains the infinite cyclic group $\{\mathbf{U}^k : k \in \mathbb{Z}\}$. It follows that by applying arbitrary integer powers of the transformation $\mathbf{U}$ to (8.8.2)–(8.8.17), we obtain their analogs over the whole infinite surface.

The infinite halving staircase surface $S(\infty; 1/2)$ is *not* a square-maze. However, as Figure 8.8.6, the relations (8.8.2)–(8.8.17) and their analogs illustrate, the key concept of *shortline* is well defined for some explicit slopes including the particular slope given by (8.8.1). We can therefore easily adapt the proof of Theorem 6.5.1 in [4] and obtain density of some explicit geodesics on this infinite surface.

We may say, intuitively speaking, that $S(\infty; 1/2)$ is an infinite polysquare surface "with bounded-ratio streets formed from squares with side lengths equal to integer powers of 2". We now make this intuition precise with the following definition, which includes the infinite halving staircase surface as a special case.

Definition of the 2-power square-maze. An infinite closed flat surface S is called a 2-power square-maze if it satisfies the following four requirements:

(1) The building blocks of S are axis-parallel squares with possibly different side lengths 2^k, where $k \in \mathbb{Z}$.

(2) Any two building block squares that have a common edge have a common vertex, and either they have the same side length, or the side length of one is half the side length of the other.

(3) S does not contain an infinite horizontal or vertical line. Furthermore, there is an integer r such that any horizontal or vertical line segment fully inside S can be covered by at most r congruent squares fully inside S.

(4) We apply the simplest boundary identification via perpendicular translation, giving rise to 1-direction geodesic flow in S.

The requirement (3) expresses the analogous "maze property" that the surface S has "bounded-ratio streets", where the ratio of the long side and the short side of any street is less than an absolute constant.

If the minimum value of r in (3) is r_0, then we call this a 2-*power* r_0-*square-maze*. The infinite halving staircase surface $S(\infty; 1/2)$ is a an example of a 2-power 4-square-maze.

In a similar way, we can define the class of k-*power* r-*square-mazes* for every fixed integers $k \geqslant 2$ and $r \geqslant 2$.

It is easy to see that the special symmetry of the infinite halving staircase surface $S(\infty; 1/2)$ provided by **U** and **D** is not really important. What is important is that the concept of shortline is well defined for any k-power r-square-maze at least for some explicit slopes. Moreover, the requirement (3) on "bounded-ratio streets" guarantees that, despite the different sizes of the squares, the magnification process in the shortline method still works. Thus we can adapt the proof of Theorem 6.5.1 in [4] and obtain density of some explicit geodesics on these generalized maze surfaces.

Next we return to the ordinary square-maze of congruent unit square building blocks. We can obtain a different kind of generalization by replacing the "unit square" in the definition of the square-maze with, say, any other fixed regular n-gon, where $n \geqslant 8$ is divisible by 4. From a supply of infinitely many congruent copies of such a fixed regular n-gon, we can form a horizontal-vertical $\mathbb{Z}^2$-like grid. Making infinitely many appropriate "holes" in the grid, we can easily enforce the "maze property" that the lengths of the horizontal and vertical streets are uniformly bounded. The "maze property" then guarantees that we can adapt the proof of Theorem 6.5.1 in [4] and obtain density of some explicit geodesics on these n-*gon-maze surfaces*.

8.9. **When the flow does not preserve the area.** We now return to the infinite halving staircase surface $S(\infty; 1/2)$, with the period-surface $S(0; 1/2)$ shown in the picture on the left in Figure 8.8.3, and recall that $S(0; 1/2)$ is not a polysquare surface, but belongs to the class of d-c-polysquare surfaces, where there is boundary edge identification involving dilation or contraction.

We study 1-*direction line-flow* on the period-surface $S(0; 1/2)$, which comes from the *projection* of 1-direction geodesic flow on the infinite halving staircase surface $S(\infty; 1/2)$.

In our investigation on flat systems in [2, 3, 4] and up to Section 8.6 in this paper, we have been studying 2-dimensional flow that preserves the 2-dimensional Lebesgue measure. Since area is homogeneous, it is natural to study whether or not an infinite orbit exhibits uniform distribution on the surface. What therefore makes the period-surface $S(0; 1/2)$ particularly interesting is that it is our first example of a flat system with a natural 1-direction line-flow that is *not* area-preserving, a consequence of the dilation or contraction at the boundary. Thus we cannot expect uniform distribution of the orbits. Our purpose in this section is therefore to examine what we can still say about the distribution of an orbit.

Let us return to the picture on the left in Figure 8.8.6. Since every almost vertical unit a_i, $1 \leqslant i \leqslant 8$, has the same length, it is fairly easy to compute asymptotically the relative time a 1-direction line-flow with slope α spends in the top square of $S(0;1/2)$. Indeed, the visiting time mainly depends on the ratio of the coordinates of an eigenvector corresponding to the largest eigenvalue Λ of the 2-step transition matrix M of the shortcut-ancestor process, assuming of course that the shortline method works for the slope α.

More precisely, the relative time a 1-direction line-flow with slope α spends in the top square of $S(0;1/2)$ is asymptotically the ratio

$$\frac{v(1)+v(2)}{v(1)+\ldots+v(8)}, \tag{8.9.1}$$

where $(v(1),\ldots,v(8))^T$ is an eigenvector corresponding to the largest eigenvalue Λ of M where, for $j=1,\ldots,8$, $v(j)$ denotes the coefficient of the almost vertical unit a_j. Here we make the usual assumption that the 1-direction line-flow moves with constant speed.

We can generalize the slope α given by (8.8.1) to any slope of the form

$$\alpha = [n;m,n,m,\ldots] = n + \frac{1}{m+\frac{1}{n+\frac{1}{m+\cdots}}} = \frac{n}{2}\left(1+\sqrt{1+\frac{4}{mn}}\right), \tag{8.9.2}$$

where both $n, m \geqslant 4$ are divisible by 4. This is motivated by the observation that for $S(\infty;1/2)$ and the period-surface $S(0;1/2)$, the normalized lengths of horizontal streets are 1 and 2, while the normalized lengths of vertical streets are 2 and 4. Thus the surplus shortline method works for these slopes.

Indeed, it is clear from the picture on the left in Figure 8.8.3 that $S(0;1/2)$ has 2 horizontal streets, where the top street consists of 1 square, and the bottom street consists of 2 squares. It also has 2 vertical streets. One of these is the white rectangle with top and bottom edges h_3. The more complicated one is shaded, with the left part consisting of 2 squares with side length 1, and the right part consisting of 2 squares with side length 1/2.

The good news is that, despite the fact that $S(0;1/2)$ is not a polysquare surface, we can still apply Theorem 7.2.2. The pessimistic reader may verify that this result can indeed be extended to d-c-polysquare surfaces.

Using this, we now attempt to find the eigenvalues of the 2-step transition matrix M. For simplicity of notation, we number various parts of $S(0;1/2)$ as in Figure 8.9.1.

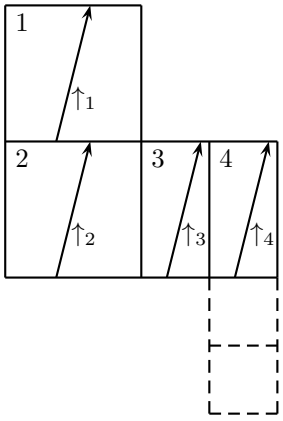

Figure 8.9.1: $S(0;1/2)$ and almost vertical units of type $\uparrow$

Here the horizontal streets are 1 and $2,3,4$, while the vertical streets are $1,2,4$ and 3. We also show the almost vertical units of type $\uparrow$, so that $\uparrow_1,\uparrow_2,\uparrow_3,\uparrow_4$ are

respectively a_1, a_3, a_5, a_7 in Figure 8.8.6. We have not shown the almost vertical units of type $\updownarrow$, but $\updownarrow_1, \updownarrow_2, \updownarrow_3, \updownarrow_4$ are respectively a_2, a_4, a_6, a_8.

Let

$$J_1 = \{1\} \quad \text{and} \quad J_2 = \{2, 3, 4\}$$

denote the horizontal streets, and let

$$I_1 = I_2 = I_4 = \{1, 2, 4\} \quad \text{and} \quad I_3 = \{3\}$$

denote the vertical streets.

We consider slopes of the form (8.9.2).

Corresponding to (7.2.14), we define the column matrices

$$\mathbf{u}_1 = [\{\uparrow_s\colon j \in J_1^*, s \in I_j^*\}] \quad \text{and} \quad \mathbf{u}_2 = [\{\uparrow_s\colon j \in J_2^*, s \in I_j^*\}]. \tag{8.9.3}$$

Here J_1^*, J_2^* and I_j^* denote that the edges are counted with multiplicity.

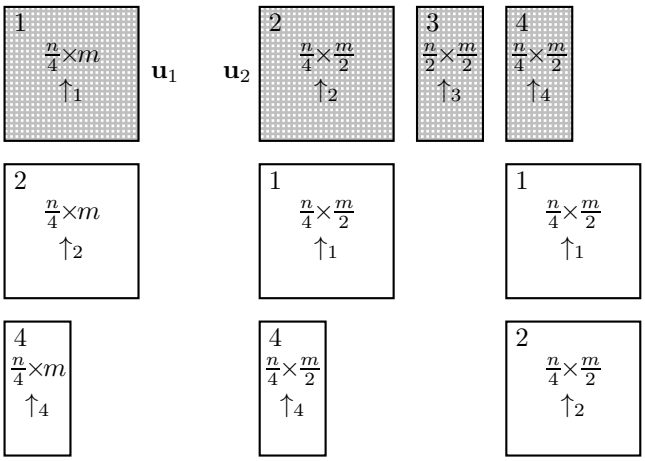

Figure 8.9.2: almost vertical units of type $\uparrow$ in $\mathbf{u}_1$ and $\mathbf{u}_2$

Corresponding to (7.2.15), we also define the column matrices

$$\mathbf{v}_1 = [\{\updownarrow_j : j \in J_1^*\}] - [\{\uparrow_j\colon j \in J_1^*\}], \tag{8.9.4}$$

$$\mathbf{v}_2 = [\{\updownarrow_j : j \in J_2^*\}] - [\{\uparrow_j\colon j \in J_2^*\}]. \tag{8.9.5}$$

Also, analogous to (7.2.17), we have

$$(M - I)[\{\uparrow_s\}] = \begin{cases} \mathbf{u}_1 + \mathbf{v}_1, & \text{if } s \in J_1, \\ \mathbf{u}_2 + \mathbf{v}_2, & \text{if } s \in J_2. \end{cases} \tag{8.9.6}$$

We now combine (8.9.3) and (8.9.6). For the horizontal street corresponding to $\mathbf{u}_1$, as highlighted in the picture on the left in Figure 8.9.2, we have

$$\begin{aligned}(M - I)\mathbf{u}_1 &= (M - I)\left[\left\{\frac{mn}{4}\uparrow_1\right\}\right] + (M - I)\left[\left\{\frac{mn}{4}\uparrow_2, \frac{mn}{4}\uparrow_4\right\}\right] \\ &= \frac{mn}{4}(\mathbf{u}_1 + \mathbf{v}_1) + \frac{mn}{2}(\mathbf{u}_2 + \mathbf{v}_2).\end{aligned} \tag{8.9.7}$$

For the horizontal street corresponding to $\mathbf{u}_2$, as highlighted in the picture on the right in Figure 8.9.2, we have

$$\begin{aligned}(M - I)\mathbf{u}_2 &= (M - I)\left[\left\{\frac{mn}{4}\uparrow_1\right\}\right] + (M - I)\left[\left\{\frac{mn}{4}\uparrow_2, \frac{mn}{4}\uparrow_3, \frac{mn}{4}\uparrow_4\right\}\right] \\ &= \frac{mn}{4}(\mathbf{u}_1 + \mathbf{v}_1) + \frac{3mn}{4}(\mathbf{u}_2 + \mathbf{v}_2).\end{aligned} \tag{8.9.8}$$

It follows from (8.9.7)–(8.9.8) that the street-spreading matrix is given by

$$\mathbf{S} = \frac{mn}{4}\begin{pmatrix} 1 & 1 \\ 2 & 3 \end{pmatrix},$$

with eigenvalues

$$\tau_1 = \frac{(2+\sqrt{3})mn}{4} \quad \text{and} \quad \tau_2 = \frac{(2-\sqrt{3})mn}{4}, \tag{8.9.9}$$

and eigenvector

$$\psi_1 = \left(\frac{\sqrt{3}-1}{2}, 1\right)^T$$

corresponding to τ_1. By (7.2.38) and (7.2.39), the largest eigenvalue of $M|_{\mathcal{V}}$ is

$$\Lambda = 1 + \frac{\tau_1 + \sqrt{\tau_1^2 + 4\tau_1}}{2},$$

with eigenvector

$$\Psi = (y, 1, xy, x)^T,$$

where

$$y = \frac{\sqrt{3}-1}{2} \quad \text{and} \quad x = \frac{-\tau_1 + \sqrt{\tau_1^2 + 4\tau_1}}{2}. \tag{8.9.10}$$

We know that Λ is the largest eigenvalue of M.

Suppose that a corresponding eigenvector is given by

$$\mathbf{V} = (v(1), \ldots, v(8))^T, \tag{8.9.11}$$

where $v(i)$, $i = 1, \ldots, 8$, denote respectively the coefficients of a_i, $i = 1, \ldots, 8$, also represented in alternative form respectively by

$$\uparrow_1, \updownarrow_1, \uparrow_2, \updownarrow_2, \uparrow_3, \updownarrow_3, \uparrow_4, \updownarrow_4.$$

Then

$$\mathbf{V} = y\mathbf{u}_1 + \mathbf{u}_2 + xy\mathbf{v}_1 + x\mathbf{v}_2. \tag{8.9.12}$$

From (8.9.3)–(8.9.5), we have

$$\begin{aligned}
\mathbf{u}_1 &= \left[\left\{\frac{mn}{4}\uparrow_1, \frac{mn}{4}\uparrow_2, \frac{mn}{4}\uparrow_4\right\}\right], \\
\mathbf{u}_2 &= \left[\left\{\frac{mn}{4}\uparrow_1, \frac{mn}{4}\uparrow_2, \frac{mn}{4}\uparrow_3, \frac{mn}{4}\uparrow_4\right\}\right], \\
\mathbf{v}_1 &= [\{m\updownarrow_1\}] - [\{m\uparrow_1\}], \\
\mathbf{v}_2 &= \left[\left\{\frac{m}{2}\updownarrow_2, \frac{m}{2}\updownarrow_3, \frac{m}{2}\updownarrow_4\right\}\right] - \left[\left\{\frac{m}{2}\uparrow_2, \frac{m}{2}\uparrow_3, \frac{m}{2}\uparrow_4\right\}\right],
\end{aligned}$$

so that

$$\mathbf{u}_1 = \left(\frac{mn}{4}, 0, \frac{mn}{4}, 0, 0, 0, \frac{mn}{4}, 0\right)^T, \tag{8.9.13}$$

$$\mathbf{u}_2 = \left(\frac{mn}{4}, 0, \frac{mn}{4}, 0, \frac{mn}{4}, 0, \frac{mn}{4}, 0\right)^T, \tag{8.9.14}$$

$$\mathbf{v}_1 = (-m, m, 0, 0, 0, 0, 0, 0)^T, \tag{8.9.15}$$

$$\mathbf{v}_2 = \left(0, 0, -\frac{m}{2}, \frac{m}{2}, -\frac{m}{2}, \frac{m}{2}, -\frac{m}{2}, \frac{m}{2}\right)^T. \tag{8.9.16}$$

Combining (8.9.11)–(8.9.16), we conclude that

$$v(1) = \frac{(y+1)mn}{4} - xym, \quad v(2) = xym, \tag{8.9.17}$$

$$v(3) = v(7) = \frac{(y+1)mn}{4} - \frac{xm}{2}, \tag{8.9.18}$$

$$v(5) = \frac{mn}{4} - \frac{xm}{2}, \quad v(4) = v(6) = v(8) = \frac{xm}{2}. \tag{8.9.19}$$

It follows from (8.9.17)–(8.9.19) that

$$v(1)+v(2)=\frac{(y+1)mn}{4} \quad \text{and} \quad v(1)+\ldots+v(8)=\frac{(3y+4)mn}{4}, \tag{8.9.20}$$

so that the ratio (8.9.1) is equal to

$$\frac{v(1)+v(2)}{v(1)+\ldots+v(8)}=\frac{y+1}{3y+4}=2-\sqrt{3}, \tag{8.9.21}$$

in view of (8.9.10).

Recall that the ratio (8.9.21) is asymptotically the relative time a 1-direction line-flow in $S(0;1/2)$ with slope α given by (8.9.2) spends in the top square. Its value of $2-\sqrt{3}\approx 0.268$ is independent of the choice of the integer parameters m and n, and crucially it is less than $1/3$. Thus any such 1-direction line-flow cannot be uniform in $S(0;1/2)$, and the top square is *under-visited*.

Consider next the left half-square of the right square of $S(0;1/2)$, denoted by the label 3 in Figure 8.9.1. We wish to study the relative time a 1-direction line-flow in $S(0;1/2)$ with slope α given by (8.9.2) spends in this half-square.

Note first of all from the edge identification given in the picture on the left in Figure 8.8.3 that every time a 1-direction line-flow enters this half-square, it spends a constant time t_1 in it before leaving. On the other hand, it is clear from the picture on the left in Figure 8.8.6 that the only way that such 1-direction line-flow can enter this half-square is along an almost vertical unit of type a_4. Thus the total time the line-flow spends in this half-square is equal to $t_1 v(4)$.

To evaluate t_1, we note that from the edge identification given in the picture on the left in Figure 8.8.3 that every time a 1-direction line-flow enters the top square, it spends a constant time t_2 in it before leaving. Furthermore, t_2 is equal to the length of an almost vertical unit. Simple geometric consideration now shows that $t_1/t_2=\alpha/2$.

Finally, note that the total time of the line-flow is equal to $t_2(v(1)+\ldots+v(8))$, which is the product of the total number of almost vertical units and the length of such a unit. Thus the relative time a 1-direction line-flow in $S(0;1/2)$ with slope α given by (8.9.2) spends in the half-square under consideration is equal to

$$\frac{t_1 v(4)}{t_2(v(1)+\ldots+v(8))}=\frac{\alpha x}{(3y+4)n}=(3\sqrt{3}-5)\frac{1+\sqrt{1+\frac{4}{mn}}}{1+\sqrt{1+\frac{16}{(2+\sqrt{3})mn}}}, \tag{8.9.22}$$

in view of (8.9.2), (8.9.9), (8.9.10), (8.9.19) and (8.9.20).

Taking the limit $m,n\to\infty$ in (8.9.22), the relative time a 1-direction line-flow in $S(0;1/2)$ with slope α given by (8.9.2) spends in the half-square under consideration converges to $3\sqrt{3}-5\approx 0.196$. In fact, easy computation shows that the value of (8.9.22) is greater than 0.195 for every choice $m,n\geqslant 4$ of the parameters. Crucially, it is greater than $1/6$. Thus this half-square is *over-visited*.

We summarize our observations in the form of a theorem.

Theorem 8.9.1. *Let $m,n\geqslant 4$ be arbitrary integers such that both are divisible by 4, and let $\alpha=\alpha(m,n)$ be the slope given by (8.9.2). Let $L_\alpha(t)$, $t\geqslant 0$, be any half-infinite line-flow with slope α on the d-c-polysquare surface $S(0;1/2)$.*

(i) *The relative visiting time of L_α to the top square of $S(0;1/2)$ is asymptotically equal to $2-\sqrt{3}\approx 0.268$, which is independent of the choice of the integer parameters m and n. In particular, the top square is under-visited. Furthermore, in an arbitrary time interval $0\leqslant t\leqslant T$ with $T\geqslant 1$, the actual visiting time of the line-flow to the*

top square is equal to

$$(2-\sqrt{3})T+O(T^{\kappa_0}),\quad \textit{where}\quad \kappa_0=\frac{\log|\Lambda_2|}{\log|\Lambda_1|}.$$

Here Λ_1 and Λ_2 are respectively the eigenvalues of the 2-step transition matrix of the line-flow with the largest and second largest absolute value.

(ii) *The relative visiting time of L_α to the left half of the right square of $S(0;1/2)$ is asymptotically equal to* (8.9.22) *which depends on the choice of the integer parameters m and n. In particular, this part of $S(0;1/2)$ is over-visited. The error term of the actual visiting time remains the same $O(T^{\kappa_0})$.*

References

[1] A. Avila, V. Delecroix. Weak mixing directions in non-arithmetic Veech surfaces. *J. Amer. Math. Soc.* **29** (2016), 1167–1208.

[2] J. Beck, M. Donders, Y. Yang. Quantitative behavior of non-integrable systems (I). *Acta Math. Hungar.* **161** (2020), 66–184.

[3] J. Beck, M. Donders, Y. Yang. Quantitative behavior of non-integrable systems (II). *Acta Math. Hungar.* **162** (2020), 220–324.

[4] J. Beck, W.W.L. Chen, Y. Yang. Quantitative behavior of non-integrable systems (III). *Discrete Anal.* (submitted).

[5] M. Boshernitzan. A condition for minimal interval exchange maps to be uniquely ergodic. *Duke Math. J.* **52** (1985), 723–752.

[6] M. Boshernitzan. A condition for unique ergodicity of minimal symbolic flows. *Ergodic Theory Dynam. Systems* **12** (1992), 425–428.

[7] K. Calta. Veech surfaces and complete periodicity in genus two. *J. Amer. Math. Soc.* **17** (2004), 871–908.

[8] Y. Cheung, H. Masur. Minimal non-ergodic directions on genus-2 translation surfaces. *Ergodic Theory Dynam. Systems* **26** (2006), 341–351.

[9] E. Gutkin. Billiards on almost integrable polyhedral surfaces. *Ergodic Theory Dynam. Systems* **4** (1984), 569–584.

[10] P. Hubert, T.A. Schmidt. An introduction to Veech surfaces. *Handbook of Dynamical Systems* (B. Hasselblatt, A. Katok, eds.), volume 1B, pp. 501–526 (Elsevier, 2006).

[11] C.T. McMullen. Billiards and Teichmüller curves on Hilbert modular surfaces. *J. Amer. Math. Soc.* **16** (2003), 857–885.

[12] C.T. McMullen. Teichmüller curves in genus two: the decagon and beyond. *J. Reine Angew. Math.* **582** (2005), 173–199.

[13] C.T. McMullen. Teichmüller curves in genus two: torsion divisors and ratios of sines. *Invent. Math.* **165** (2006), 651–672.

[14] C.T. McMullen. Prym varieties and Teichmüller curves. *Duke Math. J.* **133** (2006), 569–590.

[15] C.T. McMullen, R.E. Mukamel, A. Wright. Cubic curves and totally geodesic subvarieties of moduli space. *Ann. of Math.* **185** (2017), 957–990.

[16] W.A. Veech. Boshernitzan's criterion for unique ergodicity of an interval exchange transformation. *Ergodic Theory Dynam. Systems* **7** (1987), 149–153.

[17] W.A. Veech. Teichmüller curves in moduli space, Eisenstein series and an application to triangle billiards. *Invent. Math.* **97** (1989), 553–583.

[18] W.A. Veech. The billiard in a regular polygon. *Geom. Funct. Anal.* **2** (1992), 341–379.

Department of Mathematics, Rutgers University, Hill Center for the Mathematical Sciences, Piscataway NJ 08854, USA

E-mail address: jbeck@math.rutgers.edu

Department of Mathematics and Statistics, Macquarie University, Sydney NSW 2109, Australia

E-mail address: william.chen@mq.edu.au

Department of Mathematics, Rutgers University, Hill Center for the Mathematical Sciences, Piscataway NJ 08854, USA

E-mail address: yy458@math.rutgers.edu